

SQSTM1 MUTATIONS AND PAGET'S DISEASE OF BONE

by

Dereen Najat, BSc

Thesis submitted to the University of Nottingham for
the degree of Doctor of Philosophy

September 2009

To my parents and my aunt Nasiha

Acknowledgements

“No act of kindness however small is ever wasted” *Aesop*.

I would like to express my deepest gratitude and appreciation to all the people who helped me through out my PhD; I have tried to remember every one.

Firstly, I would not have been able to complete my project without the insight, tremendous and constant support, of my supervisor, Dr. Robert Layfield. I hope that in this small space I would be able to show my sincere gratitude. Working with Dr. Layfield was a journey full of experiences; his ideas and suggestions to my project made my work very interesting and challenged my way of thinking. I loved what I did and learnt, regardless of the difficulties and occasional setbacks of the work. Every day felt like a bonus. One of my valuable skills I learnt from Dr. Layfield can be summarised perfectly from a quote by Elbert Hubbard - “The greatest mistake a man can ever make is to be afraid of making one” - which was impossible to achieve and understand without the advice given by Dr. Layfield to learn from mistakes, his generosity and forgiveness, it had the greatest impact on my perspective at work and in life in general; in my view an experience like this is what defines a great education from a standard one.

Big thanks go to Prof. John Mayer, for his kindness, also for his interesting and enlightening tea break conversations, I enjoyed every one of them. I’m in his debt forever.

Dr. Ian Kerr, thank you very much for your patient, tolerance and understanding, words can’t express my gratitude.

Many thanks go to Dr. Leonidas Karagounis, for being an exceptionally supportive friend and helping me with statistics and IT problems.

Dr. Andrew Bennett for helping me during a difficult time and providing support.

Maureen Mee, for her kindness, technical lab advice and making my transition to lab D43 an easy one. Special thanks go to those who provided practical and

technical support through out the project, including members of D45 lab, Barry Shaw, especially at the start of the project for his patience with my limited lab experience and unfamiliarity with the English language.

Dr. Tyson Sharp, Pierre Zhang for helping me to learn cell culture techniques and providing reagents for the assays at the start of the cell culture experiments. My deepest thanks go to Dr. Slavko Čeru from the Jožef Stefan Institute, Slovenia, for his technical support on confocal imaging, valuable scientific advice and tips.

Thanks to Thomas Garner from the School of Chemistry at the University of Nottingham for his contribution to the NMR experiments.

Thanks also to Dr. Thilo Hagen from the Wolfson Digestive Disease Centre at the University of Nottingham, for his advice on luciferase reporter assays, and providing plasmids for the assay.

To Dr. Linda Morgan from the Division of Clinical Chemistry at the University of Nottingham, for generous guidance on statistical analyses; the D43 lab, Dr. Simon Paine, Dr. Lynn Bedford for preparing tea; and third year project students (Alex Larder, Lisa Bradley, Kathryne Brownless, and Sarah Martin), for their contribution to the project.

I would also like to thank Miss Harriet day at the International office of the University of Nottingham, for facilitating my admission to the University and helping me to get a Nottingham-Iraq scholarship. In addition, I would like to thank Sulaimani University for providing half of my tuition fees.

Finally my gratitude and thanks go to my family, including my parents and two sisters, for their tolerance, patience, financial support and endless phone calls, it helped a lot. I would also like to thank my cousin, Ali Mukhtar, for providing "postal services" for university application documents.

Abbreviations

A381V	Alanine to valine change at amino acid 381 of p62 protein
AD	Alzheimer's disease
AMPS	Ammonium persulfate
ALP	Serum alkaline phosphatase
ANOVA	Analysis of variance
Asn	Asparagine
ATCC	American type cell culture collection
Atg	Autophagy specific genes
ATP	Adenosine tri phosphate
aPKC	a Protein kinase C
BSA	Bovine serum albumin
CATK	Cathepsin K
cDNA	Complementary DNA
CDV	Canine distemper virus
CMA	Chaperone mediated autophagy
CSP	Chemical shift perturbation
CSF	Colony stimulating factor
CYLD	Cylindromatosis
D335E	Aspartic acid to glutamic acid change at amino acid 335 of p62 protein
dATP	2'-deoxyadenosine 5'-triphosphate
DMSO	Dimethyl Sulfoxide
DTT	Dithiothreitol
DNA	Deoxyribonucleic acid
dNTP	Deoxyribonucleotide triphosphate
E396X	Truncating mutation as amino acid 396 of p62 protein
E1	Ubiquitin-activating enzymes
E2	Ubiquitin-conjugating enzyme
E3	Ubiquitin ligase enzymes
<i>E. coli</i>	Escherichia coli
EDTA	Ethylenediaminetetraacetic
EGFP	Enhanced Green Fluorescent Proteins
ESH	Expansile skeletal hyperphosphatase
ERK	Extracellular signal-regulated kinase
FEO	Familial expansile osteolysis
FRET	Fluorescence Resonance Energy Transfer
FSG	Fish skin gelatine
FCS	Foetal calf serum
G425R	Glycine to Arginine change at amino acid 425 of p62 protein
Gln	Glutamine
GST	Glutathione S-transferase
HA	Hemagglutinin epitope
HEK293	Human Embryonic Kidney 293 cells
HSC	Haematopoietic stem cells
I κ B	I-kappa-B
IKK	IkappaB kinase
IKK γ	IKK gamma

IL	Interleukin
IL-1	Interleukin 1
IL-8	Interleukin 8
IPTG	Isopropyl β -D-1-thiogalactopyranoside
IRAK	Interleukin-1 receptor-associated kinase
ISH	In Situ Hybridization
JNK	c-Jun N-terminal kinase (JNK)
K	Lysine
K378X	Truncating mutation at amino acid 378 of p62 protein
K_a	Association constant
Kb	kilo base
K_d	Dissociation constant
LC3	Light chain 3
LIR	LC3 interacting region
M	Molarity
Min	Minute
mM	Millimolar
μ M	Micro molar
mmol/L	Millimol per litre
mRNA	Messenger Ribonucleic Acid
MVNP	Measles virus nucleocapsid
NGF	Nerve growth factor
NF- κ B	Nuclear Factor kappa B
Nm	Nanometre
OCL	Osteoclasts
OD	Optical density
OPG	Osteoprotegerin
OLC	Osteoclasts like cell
P392L	Proline to leucine change at amino acid 392 of p62 protein
P392L/S399P	a p62 construct with two mutations (P392L,S399P) on the same allele
PAGE	Polyacrylamide gel electrophoresis
PBS	Phosphate buffered saline
PCR	Polymerase chain reaction
PDB	Paget's disease of bone
PDB1	Paget's disease of bone
PDB2	Paget's disease of bone
PKC	Protein kinase C
PE	Phosphatidylethanolamine
pI	Isoelectric point
PPM	Part per million
PTHrP	Parathyroid hormone-related protein
RANK	Receptor activator of NF- κ B
RANKL	Receptor activator of NF- κ B Ligand
RNA	Ribonucleic Acid
RIP	Receptor interacting protein
RPM	Round per minute
S399P	Serine to proline change at amino acid 399 of p62 protein
SD	Standard deviation
SDS	Sodium dodecyl sulfate
SEC	Seconds

SQSTM1	Sequestosome 1
SNP	Single-nucleotide polymorphism
TBS	Tris Buffered Saline
TBST	Tris-buffered saline-Triton X-100
TEMED	N,N,N',N'-Tetramethylethylenediamine
TNF	Tumor necrosis factor
TRAP	Tartrate-resistant acid phosphatase
TRAF6	Tumour-necrosis factor (TNF) receptor-associated factor 6
U2OS	Human osteosarcoma cell line
UBA	Ubiquitin-associated domain
UB	Ubiquitin
UPS	Ubiquitin proteasome system
UV	Ultraviolet
VCP	Valosine-containing proteins
WT	Wild type
W/V	Weight per volume
W/W	Weight per weight
2D HSQC	Two dimensional Heteronuclear Single Quantum Coherence
Δ351-388	Product of a splice site mutation resulting in the deletion of amino acids 351-388 of p62

Standard amino acid abbreviations

Amino acid	3-letter	1-letter
Alanine	Ala	A
Arginine	Arg	R
Asparagine	Asn	N
Aspartic acid	Asp	D
Cysteine	Cys	C
Glutamic acid	Glu	E
Glutamine	Gln	Q
Glycine	Gly	G
Histidine	His	H
Isoleucine	Ile	I
Leucine	Leu	L
Lysine	Lys	K
Methionine	Met	M
Phenylalanine	Phe	F
Proline	Pro	P
Serine	Ser	S
Threonine	Thr	T
Tryptophan	Trp	W
Tyrosine	Tyr	Y
Valine	Val	V

Contents

Acknowledgements.....	i
Abbreviations	iii
Abstract	xi
CHAPTER 1.....	1
1.1 Introduction.....	2
1.2 Bone	9
1.2.1 Bone structure and cell types	9
1.2.2 Osteoclasts in PDB.....	10
1.2.3 Signalling in osteoclasts	11
1.2.4 Role of the NF- κ B transcription factor in osteoclasts	14
1.2.5 Bone remodelling	15
1.3 Paget's disease of bone (PDB).....	17
1.3.1 Diagnostic metabolic markers for PDB.....	20
1.3.2 Genetics of PDB	21
1.4 SQSTM1 and PDB	26
1.4.1 Structure of the p62 protein	29
1.4.1.1 The ZZ domain.....	29
1.4.1.2 TRAF6-binding domain	30
1.4.1.3 PEST sequences	30
1.4.1.4 The UBA domain	30
1.4.1.4.1 Ubiquitin	31
1.5 Relationship between PDB severity and ubiquitin-binding properties of p62	35
1.6 p62's role in RANK-L-NF- κ B signalling	35
1.6.1 IKK γ (NEMO)	39
1.6.1.1 Characteristics of IKK γ	39
1.6.1.2 Role of IKK γ in RANK-L-NF- κ B signalling	40
1.6.2.2 Role of CYLD in RANK-L-NF- κ B signalling	41
1.7 Emerging functions of p62	42
1.7.1 General overview of autophagy	42
1.7.2 Role of p62 in autophagy.....	47
1.8 Role of viral factors in PDB pathogenesis.....	49
1.9 Role of environmental factors in PDB pathogenesis	52
1.10 PDB mouse models	53
1.10.1 P392L knock in mice	53
1.10.2 S409X mouse model	54
1.10.3 p62 knockout mice	54
1.10.4 MVNP mouse models	55
1.11 Aims and objectives	57
CHAPTER 2.....	60
Materials and methods.....	61
2.1 DNA techniques	61
2.1.1 Plasmids.....	61
2.1.2 Plasmid DNA preparation	61
2.1.3 DNA electrophoresis.....	62
2.1.4 Measurement of DNA concentration	63
2.1.5 Storage of plasmid DNA	63
2.1.6 DNA Sequencing	63
2.2 Mammalian cell culture methods	64
2.2.1 Cell handling.....	64

2.2.2	Passaging cells	64
2.2.3	Thawing cells.....	64
2.2.4	Cell freezing and storage	64
2.2.5	Counting cells with a haemocytometer	65
2.2.6	Transient co-transfection based on non lipid based transfection reagent.....	65
2.3	Indirect immunofluorescence confocal microscopy.....	66
2.3.1	Confocal microscopy	67
2.4	NF- κ B reporter assays	67
2.4.1	Preparation of NF- κ B reporter construct	67
2.4.2	Transient co-transfection of p62 and NF- κ B reporter constructs using polyamine based transfection reagent.....	67
2.5	Western blotting and immunodetection techniques	68
2.5.1	Sodium dodecyl sulphate polyacrylamide-gel electrophoresis (SDS PAGE)	68
2.5.2	Coomassie blue staining of SDS-PAGE gels.....	69
2.5.3	Western blotting.....	69
2.5.4	Ponceau S staining of nitrocellulose membranes.....	69
2.5.5	Immunodetection	70
2.5.6	Detection of expression levels of overexpressed plasmids in cells using immunoblotting	71
2.6	General laboratory methods	71
2.6.1	Preparation of chemically competent bacterial cells.....	71
2.6.2	Oligonucleotide mutagenic primer preparation.....	72
2.6.3	Site-directed mutagenesis.....	72
2.6.4	Transformation of Plasmid DNA to XL10-Gold® competent cells.....	74
2.6.5	GST-fusion protein expression.....	74
2.6.6	Bacterial storage	74
2.6.7	Preparation of ubiquitin-Sepharose	74
2.6.8	Measurement of protein concentration using the Bradford assay	75
2.6.9	Ubiquitin-Sepharose binding assay.....	76
2.6.10	Large scale protein purification	76
2.7	Buffers and reagents	78
2.7.1	Reagents	78
2.7.2	Antibodies	79
2.7.3	Buffers.....	80
2.7.4	Buffers used in preparation of ubiquitin-Sepharose beads ...	83
2.7.5	Plasmid DNA purification solutions:.....	84
2.8	List of software	84
CHAPTER 3.....		85
Chapter 3: Interaction of PDB mutant p62 proteins with ubiquitin <i>in vitro</i>.....		86
3.1	Introduction	86
3.2	Clinical features associated with the 'new' PDB-associated p62 mutations	87
3.3	Generation of prokaryotic expression constructs for PDB mutant p62 proteins	90
3.4	Investigation of the relative expression levels of GST tagged wild type and PDB mutant p62 proteins	92
3.5	Effects of 'new' PDB mutations on ubiquitin-binding function of p62	94
3.5.1	Effects of the PDB-associated A381V mutation on the ubiquitin-binding function of p62.....	96

3.5.2 Effects of the PDB-associated Δ351-388 mutation on the ubiquitin-binding function of p62.....	98
3.5.3 Effects of the PDB-associated D335E mutation on ubiquitin-binding function of p62.....	100
3.5.4 Effects of the PDB-associated P392L/S399P mutation on the ubiquitin-binding function of p62.....	102
3.6 Investigation of the interaction of p62 and ubiquitin using 2D protein NMR.....	104
3.6.1 Introduction.....	104
3.6.2 Basic theoretical background of NMR.....	106
3.7 Generation of a prokaryotic expression constructs for GST-p62 (341-440) containing the P392L mutation.....	111
3.8 Large scale purification p62 (P392L; 341-440) for protein NMR.....	113
3.9 NMR analysis of the interaction of ¹⁵ N-ubiquitin with p62 (P392L; 341-440).....	116
3.10 Discussion.....	128
CHAPTER 4.....	137
Chapter 4: Cellular phenotypes of PDB mutant p62 proteins.....	138
4.1 Introduction.....	138
4.2 Generation of eukaryotic expression constructs for PDB mutant p62 proteins.....	140
4.3 Method development.....	143
4.3.1 Localisation of endogenous p62 and ubiquitin in U2OS cells.....	143
4.3.2 Comparison between different chemical fixatives.....	146
4.3.3 Optimisation of polyHis-FLAG-tagged p62 plasmid concentration for transfections.....	148
4.3.4 Optimisation of time of transfection.....	150
4.3.5 Co-transfection of polyHis-FLAG-p62 and HA-ubiquitin, and comparison of staining of different primary antibodies.....	152
4.3.6 Comparison of different staining colours for p62 and ubiquitin.....	154
4.3.7 Specificity of secondary antibodies.....	156
4.3.8 Cellular phenotypes of transfected wild type polyHis-FLAG-p62 and selected PDB mutants in U2OS cells.....	158
4.3.9 Cellular phenotypes of transfected HA-ubiquitin in U2OS cells.....	162
4.4 Co-localisation of wild type and PDB mutant polyHis-FLAG-p62 with HA-ubiquitin.....	164
4.5 Quantification of the size of p62-positive and ubiquitin-positive cytoplasmic bodies.....	180
4.6 Further analysis of polyHis-FLAG-p62 cytoplasmic bodies.....	184
4.6.1 Co-localisation studies of D335E mutant polyHis-FLAG-p62 with tdTomato-LC3 in U2OS cells.....	190
4.7 Discussion.....	192
4.7.1 Limitations of indirect immunofluorescence and 2D confocal laser scanning microscopy.....	196
CHAPTER 5.....	198
Chapter 5: Effects of PDB-mutant p62 proteins on NF-κB signalling.....	199
5.1 Overview.....	199
Chapter 5 - Part I.....	205
5.2 Investigation of regulation of NF-κB activation by PDB-mutant p62 proteins using luciferase reporter assays.....	206
5.2.1 Introduction.....	206

5.2.2 Measurements of basal NF- κ B activation using luciferase reporter assays	208
5.2.3 Measurements of TNF- α induced NF- κ B activation using luciferase reporter assays	211
Chapter 5 - Part II	215
5.3 Interaction of PDB-mutant p62 proteins and CYLD.....	216
5.3.1 Introduction	216
5.3.2 Co-localisation studies of wild type and PDB mutant polyHis-FLAG-p62 with HA-CYLD.....	217
Chapter 5 - Part III.....	223
5.4 Interaction of PDB-mutant p62 proteins and NEMO.....	224
5.4.1 Introduction	224
5.4.2 Effects of expression of polyHis-FLAG-p62 on levels of endogenous NEMO in U20S cells	226
5.4.3 Co-localisation studies of wild type and PDB mutant polyHis-FLAG-p62 with endogenous NEMO	228
5.5 Discussion.....	232
5.5.1 p62 positively and negatively regulates RANK-NF- κ B signalling.....	235
5.5.2 Limitations of the luciferase reporter assay	239
 CHAPTER 6.....	 241
Chapter 6: General Discussion	242
6.1 General Discussion	242
 References.....	 250
List of publications resulted from the thesis	267
Appendix.....	268
Appendix: vector maps	269

Abstract

Mutations affecting the p62 signalling adapter protein are commonly found in patients with the skeletal disorder Paget's disease of bone (PDB). We have extended previous *in vitro* functional analyses of PDB-mutant p62 proteins (Cavey *et al.*, 2006) to study the effects of several uncharacterised PDB-associated mutations on the ubiquitin-binding properties of p62. These include mutations which affect regions of p62 outside of the ubiquitin-binding UBA domain (A381V, D335E and a mutant equivalent to a predicted product of the G1205C splice-site mutation which lacks amino acids 351-388), as well as a double mutation involving the P392L and S399P changes on the same allele. In accordance with previous findings, both of the non-UBA domain mutations (A381V, Δ 351-388) showed deleterious effects on ubiquitin-binding by p62 in pull-down assays, further emphasising the important role of non-UBA domain sequences in mediating ubiquitin-recognition, as well as in PDB aetiology. The D335E mutant retained its ubiquitin-binding function *in vitro*. The P392L/S399P double mutant showed a more severe effect on ubiquitin-binding than either of the single P392L or S399P missense mutations alone; as this double mutation is associated with a particularly severe phenotype, our findings are supportive of the proposal that disease severity in PDB with p62 mutations may be directly related to the effects of the mutations on the ubiquitin-binding function of the p62 protein.

Since the *in vitro* pull-down assays are semi-quantitative at best, we sought to investigate if a more quantitative biophysical approach, two dimensional Heteronuclear Single Quantum Coherence (2D-HSQC) protein NMR, might be applied to investigate the effects of PDB-associated mutations on protein (ubiquitin-binding) function. Our results showed that protein NMR was not optimal to quantitatively assess the effects of the mutations on the interaction between p62 and ubiquitin *in vitro*.

Using confocal microscopy, co-transfection of U20S cells showed that the selected PDB-associated p62 mutants (A381V, P392L, G425R) co-localised with ubiquitin with a cellular phenotype indistinguishable from wild type, as each PDB mutant formed cytoplasmic bodies with an area ranging from the detection limit of the microscope to $40\mu\text{m}^2$ or higher; in contrast the E396X truncating mutant did not form cytoplasmic bodies nor co-localise with ubiquitin.

In addition to interacting with ubiquitin, p62 also interacts with the LC3 (an autophagic marker) through its LC3 interacting region (LIR) to mediate the formation of autophagosomes. By co-transfecting p62 constructs with LC3 We found that some of the p62-positive cytoplasmic bodies were autophagosomes, and that the D335E mutation of p62 (which lies within the LIR) did not appear to affect the formation of autophagosomes.

The effects of the wild type and PDB-mutant p62 proteins on NF- κ B signalling were assessed in HEK293 cells co-transfected with an NF- κ B luciferase reporter construct. A381V mutant p62 produced a level of activation of NF- κ B signalling greater than wildtype and similar to that of UBA domain mutants, indicating that non-UBA and UBA domain mutations may exert their effects through a common mechanism involving dysregulated NF- κ B signalling. To further examine the function of p62 in the regulation of NF- κ B signalling, we went on to determine possible effects of PDB-associated mutations on p62-CYLD (a DUB enzyme) interactions. Unexpectedly we found that CYLD expression appears to abrogate the formation of the p62 cytoplasmic bodies previously shown to be ubiquitin-positive.

Finally, we went on to study the interaction of p62 (and its PDB mutants) with another important regulator of NF- κ B signalling, IKK γ /NEMO. We concluded that wild type and PDB-mutant p62 proteins are capable of recruiting NEMO to cytoplasmic bodies which may represent autophagosomes, but do not appear to accelerate its degradation.

CHAPTER 1

Introduction

1.1 Introduction

Paget's disease of bone (PDB) is the second most common metabolic bone disease in the UK after osteoporosis. The disease is asymptomatic in the majority of patients, however about 30% of those affected may show symptoms (Cooper *et al.*, 1999), with bone pain being the most common. In addition, bone deformity, increased bone vascularity and other variable signs and complications might accompany PDB depending on the stage of the disease (Kanis *et al.*, 1992).

PDB has an interesting prevalence, as it is common in Europe, America, New Zealand and Australia, and not found or very rare in Asia, and Africa (Figure 1.1). Intriguingly, the incidence of PDB appears to be declining in Europe over the last few years (Poor *et al.*, 2006), suggesting environmental factors such as diet and viruses (which themselves might be in decline) might contribute to the disease development, although there might be other declining unknown factors might contribute to the decline in PDB. However, increasing evidence supports the important contribution of genetic factors to the disease aetiology. To date seven susceptibility loci have been identified (although not all confirmed) in PDB patients. The most common genetic mutations found in PDB affect the *SQSTM1* gene (encodes the p62 protein), which is located on chromosome 5 at the PDB3 locus (Watts *et al.*, 2004) with the P392L missense mutation being the most common p62 mutation (Laurin *et al.*, 2002).

At the cellular level, ongoing research shows that disruption of the osteoclast RANK-NF- κ B signalling pathway contributes to the development of PDB and related syndromes (Layfield *et al.*, 2007; Duran *et al.*, 2004). For example, mutations in the *RANK* (Receptor Activator for Nuclear Factor κ B) gene which encodes the receptor in this pathway have been found in several Pagetic-like

syndromes such as familial expansile osteolysis (FEO), expansile skeletal hyperphosphatasia (ESH) and early-onset familial PDB. Also, mutations affecting the osteoprotegerin (OPG) protein (a decoy receptor in the pathway) which inhibits binding of Receptor Activator for Nuclear Factor κ B Ligand (RANK-L) to RANK (Figure 1.8) have been associated with juvenile PDB.

NF- κ B signalling is regulated through complicated pathways composed of different proteins, and a considerable number of these proteins require ubiquitylation (post-translational modification with ubiquitin) at different stages of the pathway (Chen *et al.*, 2005, Layfield *et al.*, 2007). Many adaptor proteins in the NF- κ B pathways contain ubiquitin-binding domains; these adaptors interact with other ubiquitylated signalling proteins noncovalently and function as scaffolds to mediate signal induced interactions between the two new proteins (Layfield *et al.*, 2007) (Figure 1.8). For example, the adaptor proteins TAB2-TAB3 through their ubiquitin-binding regions recognize the Lys63-linked polyubiquitin chain assembled on TRAF6 following receptor activation. This step facilitates phosphorylation and activation of another complex which includes IKK β ; the latter activated complex finally causes phosphorylation and subsequent degradation of I- κ B (which normally sequesters NF- κ B in the cytoplasm), releasing NF- κ B to the nucleus to activate gene expression.

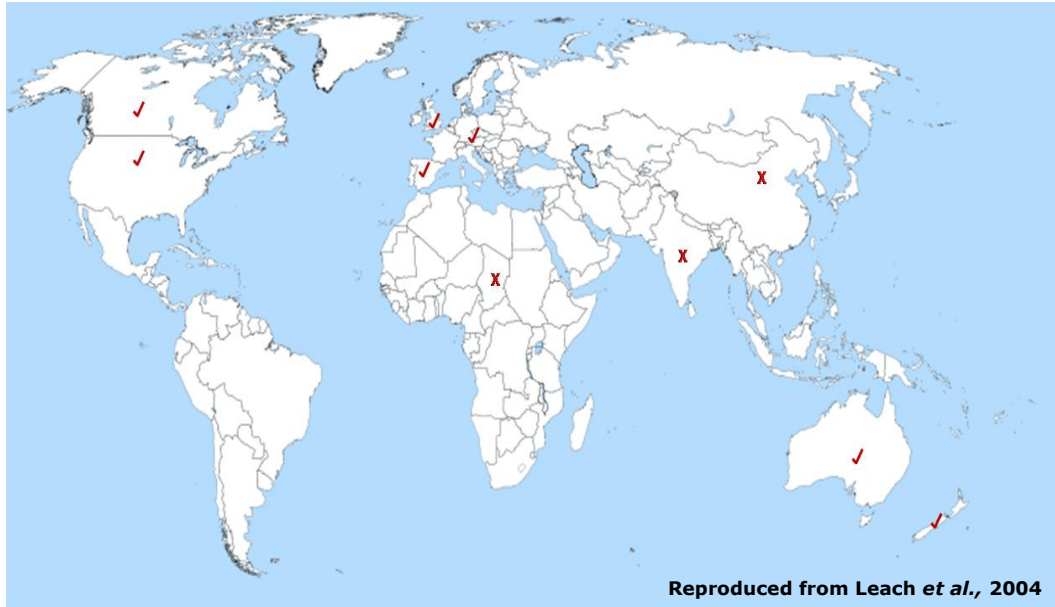


Figure 1.1: Prevalence of PDB worldwide

PDB is common in the USA, Canada, Australia and most of Europe (indicated by ticks), but is rare in Africa, India, and Asia (crosses).

The p62 protein (encoded by the *SQSTM1* gene) is a further example of a scaffold protein which regulates a variety of NF- κ B signalling pathways, including RANK-L-NF- κ B signalling in osteoclasts (Layfield *et al.* 2007). In particular, p62 through its ubiquitin-associated (UBA) domain interacts with ubiquitin and is proposed to facilitate the autoubiquitylation of TRAF6 in response to activation of the signalling pathway. This ubiquitylation step ultimately leads to further activation of other signalling complexes in the pathway with subsequent activation of NF- κ B (Layfield *et al.*, 2004a) (Figure 1.8).

Interestingly, all the PDB-associated *SQSTM1* mutations studied prior to this study commencing affected the ubiquitin-binding UBA domain of p62. Obviously therefore, investigating the ubiquitin-binding properties of p62 is important to understand the (dys) regulation of the NF- κ B pathway in PDB. In 2005, Cavey *et al.* proposed that all PDB-associated p62 mutations impair ubiquitin-binding *in vitro*, subsequently leading to a proposal that *SQSTM1* mutations predispose to PDB by a unifying mechanism which involves this loss of function of the p62 protein (Cavey *et al.*, 2005; Cavey *et al.*, 2006).

These findings were the starting point of our project, as we wanted to further extend these studies and investigate the ubiquitin-binding properties of several recently discovered p62 mutations, of note several of which were located outside the UBA domain of p62 (Figure 1.2). Prior to this study, the ubiquitin-binding properties of p62 had been only studied through semi-quantitative techniques (*in vitro* protein pull-down assays), and it was deemed desirable to investigate the interaction between p62 and ubiquitin using more quantitative protein interaction methods.

In addition, several other experimental approaches have been used in recent years to investigate the role of p62 and the effects of its mutation on NF- κ B

signalling and bone cell function. For example, the functional roles of p62 and effects of selected PDB-associated mutants (e.g. P392L, K378X and E396X) in NF- κ B signalling have been investigated using luciferase reporter assays. These mutations were found to cause an increase in NF- κ B activation relative to empty vector controls (Rea *et al.*, 2006).

Further to the functional role of p62, the subcellular localisation of wild type p62 and several PDB mutants was previously investigated using confocal microscopy (Leach *et al.*, 2006; Biørkøy *et al.*, 2005). Transfected wild type p62 was found to form vesicle-like cytoplasmic bodies in a wide variety of cell lines, and interestingly p62 truncating mutants, which lack the UBA domain, showed a distinct diffused cytoplasmic pattern which could be easily distinguished from wild type p62. The subcellular localisation of two other PDB-associated p62 missense mutants (P392L, P387L) was also investigated and it was concluded that these changes were associated with larger cytoplasmic bodies than wild type p62 (Leach *et al.*, 2006). These observations can potentially be used as a diagnostic tool to study the impact of the PDB-associated mutations on cellular functions of p62, although further research is needed to draw absolute conclusions and it should be noted that the functional characterisation of p62 cytoplasmic bodies is incomplete.

Another group showed that wild type p62 formed cytoplasmic bodies also contain ubiquitin when co-transfected in HeLa cells, and later it was shown that these cytoplasmic bodies were autophagosomes (Biørkøy *et al.*, 2005). An alternative way to degrade proteins other than via the ubiquitin-proteasome system (UPS) is through autophagy, in which ubiquitylated proteins (through p62 binding) are directed for degradation in the lysosome, although the exact mechanism for the degradation is still unknown. In general autophagy is thought of as a bulk degradation mechanism during cell starvation and cellular

stress (Pankiv *et al.*, 2007; Komatsu *et al.*, 2007), although recently it has been shown that p62 regulates the selective degradation of proteins by autophagy and is selectively degraded itself as part of the process (Ichimura *et al.*, 2008). Therefore it will be particularly interesting to examine the role of autophagy in PDB and the implications of p62 dysfunction in autophagy and PDB development.

Interaction of p62 with other proteins in the RANK-L-NF- κ B signalling pathway may be relevant to understanding the molecular mechanisms by which p62 controls osteoclastogenesis and bone remodelling, and how PDB-associated mutations exert their effects. p62 interacts with several proteins downstream of TRAF6 upon stimulation of RANK (Xu *et al.*, 2008). For example, p62 interacts with NEMO (IKK γ) and regulates its ubiquitylation through TRAF6. NEMO is a regulatory subunit of the IKK complex (Scheidereit *et al.*, 2006); this complex is activated following activation of the RANK receptor by RANK-L, and activation of the complex leads further to NF- κ B activation (Layfield *et al.*, 2007).

As noted earlier, p62 through its ubiquitylation of TRAF6 appears to positively regulate NF- κ B activity; however it has also been shown that NF- κ B is negatively regulated by a deubiquitylating enzyme CYLD (Kovalenco *et al.*, 2003). Through interaction of CYLD with IKK γ , CYLD negatively regulates NF- κ B signalling by controlling deubiquitylation of TRAF6 (Jin *et al.*, 2008). Interestingly, p62 facilitates this interaction between CYLD and TRAF6, suggesting that p62 also might negatively regulate NF- κ B signalling.

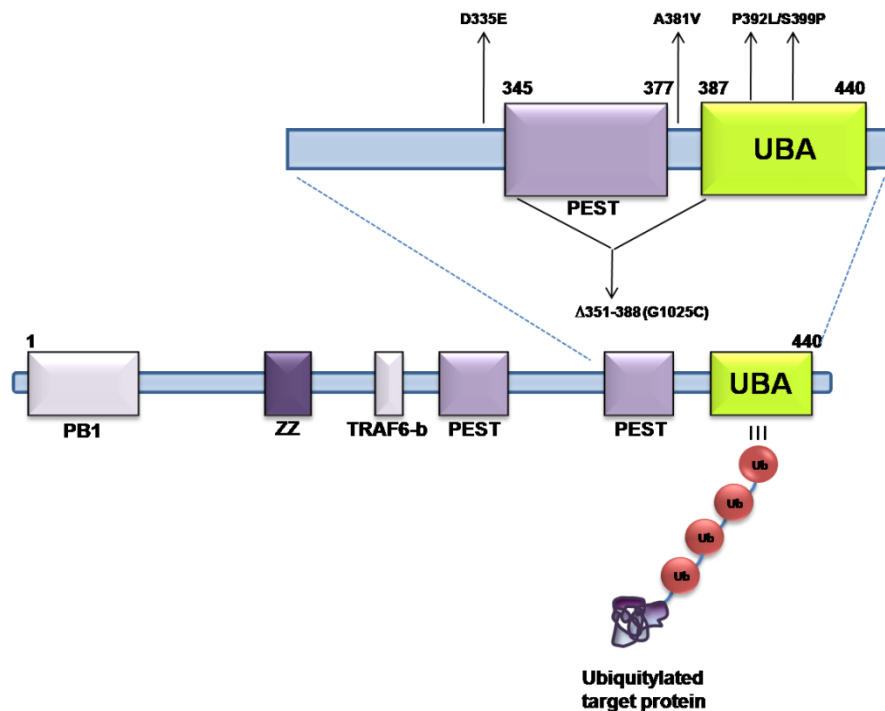


Figure 1.2: Schematic representation of the domain structure of p62 indicating sites of 'new' PDB mutations analysed in this study

The PDB mutations analysed in this study can be classified into those within the UBA domain (double mutation P392L/S399P) and those outside the UBA domain (D335E, A381V and Δ 351-388). A381V is located within a linker region between the UBA domain and second PEST sequence; D335E is located at N-terminal of the second PEST sequence; and Δ 351-388 results in a p62 protein that lacks almost the entire second PEST sequence. The double mutation (P392L/S399P) is located within the UBA domain. p62 binds to ubiquitylated protein substrates through non-covalent interactions involving its UBA domain and to LC3 through its LIR (see 1.7.2). Numbering relates to the position within the 440 amino acid sequence of the human p62 protein.

UBA, ubiquitin-associated domain; PEST sequence is rich in Proline (P), Glutamic acid (E), Serine (S), and Threonine (T); PB1 (Phox and Bem1) allows polymerisation of p62 with itself and other proteins containing PB1 domain; ZZ (zinc finger motif) mediates binding with RIP (receptor-interacting protein), which is necessary for NF- κ B activation; TRAF6-b is the TRAF6-binding domain.

1.2 Bone

1.2.1 Bone structure and cell types

Bone is a specialised tissue with multiple functions; it serves as a mechanical support, protects other softer organs such as the brain, and functions as a reservoir for minerals such as calcium. Bone marrow is responsible for producing red blood cells, certain white blood cells and blood platelets.

Bone is mainly composed of an extra-cellular matrix, which comprises a non-mineral matrix composed of collagen and glycosaminoglycans (osteoid), inorganic mineral salts deposited within the matrix, and a variety of cell types. Bone cells include osteoprogenitor cells, resorbing cells (osteoclasts), bone forming cells (osteoblasts) and support cells (osteocytes). The components of the extra-cellular matrix and bone cells are discussed in more detail below (Rubin's Pathology 5th Ed).

The osteoid is the organic part of bone tissue and is synthesised by osteoblasts. Osteoid is mainly composed of type I collagen embedded in a glycosaminoglycan gel. Osteoprogenitor cells are precursors of osteoblasts which give rise to osteoblasts; these are essentially derived from the mesenchymal lineage which can synthesise and secrete osteoid collagen and other organic components to bone matrix, then mineralise it by depositing calcium and phosphate hydroxides (hydroxyapatite)(Rubin's Pathology 5th Ed).

Osteoblasts are active when there is need for osteoid deposition, and when they are inactive they can be found lying on the bone surface (bone lining cells). Osteocytes are mature osteoblasts that have been trapped in the mineralised bone (Rubin's Pathology 5th Ed).

In contrast, osteoclasts are large cells with multiple nuclei (usually 3 to 5), and are originated from monocyte-macrophage lineage (Layfield *et al.*, 2007). Osteoclasts are highly mobile cells which have the ability to erode mineralised bone. At the end of the resorption process osteoclasts undergo apoptosis (Hughes *et al.*, 1996). Osteoclasts are distinguished by the presence of extended Golgi complexes around each nucleus, and also have large number of mitochondria and transport vesicles and lysosomes (Mundy *et al.*, 1999). Osteoclasts are characterised by a folded plasma membrane at a location facing bone matrix termed the ruffled border. Through this border osteoclasts secrete digestive enzymes and pump hydrogen ions to dissolve bone matrix; the area between the ruffled border of the osteoclasts and bone matrix is termed Howship's lacuna, which is the cavity where bone resorption occurs (Rubin's Pathology 5th Ed).

1.2.2 Osteoclasts in PDB

Osteoclasts in PDB are characterised by increased numbers of nuclei (up to 100), are larger in their size compared to normal counterparts (Reddy *et al.*, 1999). In addition, osteoclasts in PDB are hyperactive, being hyperresponsive to $1,25(\text{OH})_2\text{D}_3$, RANK-L and TNF- α , and also showing increased expression of TAF(11)-17 (Kurihara *et al.*, 2000) and *SQSTM1* (Collet *et al.*, 2007).

Frequently, nuclear (and sometimes cytoplasmic) inclusions that resemble paramyxovirus nucleocapsids are found in Pagetic osteoclasts.

Notably, PDB osteoblasts have similar morphology to normal osteoblasts, implying that the condition is principally a disease of the osteoclasts.

Although osteoblasts cultured from Pagetic bone lesions showed increased expression of IL-1, IL-6 and DKK1 and alkaline phosphatase (Naot *et al.*, 2007), the role of osteoblasts in PDB has not been investigated extensively and more research is needed to draw definitive conclusions about their contributions (Layfield *et al.*, 2007).

1.2.3 Signalling in osteoclasts

Osteoclasts originate from haematopoietic stem cells (HSC), and through a series of steps they differentiate to preosteoclasts before maturing to active osteoclasts. Osteoclastogenesis is a complicated process which is regulated negatively and positively by at least 24 genes (Boyle *et al.*, 2003). Several signalling pathways and transcription factors regulate each step of osteoclastogenesis. Each of these genes functions at different stages of osteoclastogenesis. For example, some genes such as *PU.1* and *op/CSF-1* are responsible for formation and or survival of the osteoclast precursor cells, whilst other genes such as *RANK*, *NF-κB1/NF-κB2* *rel* and *fos* help in the differentiation of the precursor cells. Genes such as *src*, *oc/Tc1rg* and *CATK* mediate the adherence and lytic function of mature osteoclasts (Boyle *et al.*, 2003).

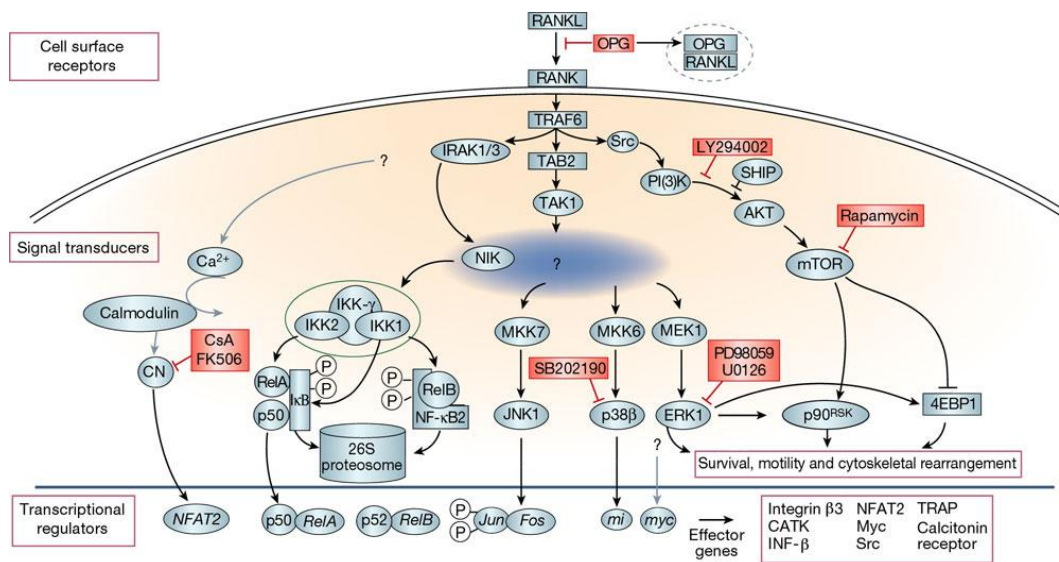
Together colony stimulating factor (CSF)-1 and RANK-L are required to induce expression of osteoclast specific genes, such as a lytic enzyme tartrate-resistant acid phosphatase (TRAP), osteoclast specific protease cathepsin K (CATK), calcitonin receptor and β3-integrin. The latter proteins are secreted to the resorption pit of the osteoclasts (Howship's lacunae), in which the osteoclasts resorb the underlying bones (Boyle *et al.*, 2003). Upon interaction of RANK-L with RANK at least five signalling pathways are activated, which are mediated by protein kinases, such as inhibitor of NF-κB kinase (IKK), c-Jun N-terminal kinase (JNK), p38, extracellular signal-regulated kinase (ERK) and Src pathways (Figure 1.3). The osteoclastogenic pathways activated by RANK-L are also activated by other cytokines such as TNF-α and IL-1, which both play important roles in osteoclast differentiation and function (Pfeilschifter *et al.*, 1989; Roodman *et al.*, 2005). However, RANK-L is considered the main cytokine in osteoclastogenesis and other cytokines are not as central as RANK-L in regulating osteoclastogenesis. The marginal role of these two cytokines

was proven by generating mice with disrupted receptors of TNF- α and IL-1, which had minimal bone phenotypes compared to RANK or RANK-L knockout mice (Erickson *et al.*, 1994; Roodman *et al.*, 2005).

The most important regulator of osteoclastogenesis is the regulatory axis known as RANK-L/RANK/OPG signalling axis. The amount of bone resorption depends on the balance between RANK-L and OPG; as RANK-L increases bone resorption increases and if OPG increases bone resorption decreases. RANK-L is a cytokine expressed by preosteoblastic cells and interacts with RANK on the surface of osteoclasts (Khosla *et al.*, 2001). RANK-L is the key cytokine required for differentiation, activation and survival of osteoclastic cells (Khosla *et al.*, 2001). This is evidenced by analysis of RANK-L knockout mice, which show severe osteopetrosis, defective tooth formation, and impaired osteoclastogenesis causing complete deficiency of osteoclasts (Kong *et al.*, 1999).

OPG is a soluble decoy receptor expressed by osteoblasts which prevents RANK-L from interacting with RANK, thereby deactivating the RANK-L-NF- κ B signalling (Figure 1.3). OPG over-expression inhibits osteoclast formation and causes osteopetrosis in mice. On the other hand, OPG deletion causes enhanced remodelling of bone and osteoporosis (Boyle *et al.*, 2003).

There are other regulators which are important in osteoclasts, such as *c-fos* and *c-src*. Knockout mouse models of these two genes developed osteopetrosis, which is believed to result from impaired osteoclast function in *c-src* knockout mice and the inability of *c-fos* mice to form osteoclasts (Roodman *et al.*, 2005).



Reproduced from Boyle *et al.*, 2003

Figure 1.3: RANK signalling in osteoclasts

RANK-L interaction with RANK triggers several signalling cascades. The most important cascade in osteoclast includes the RANKL/OPG/NF-κB proteins. NF-κB causes activation of osteoclast specific genes such as TRAP, calcitonin receptor, CATK and other effector genes.

1.2.4 Role of the NF- κ B transcription factor in osteoclasts

NF- κ B is a transcription factor that functions in all eukaryotic cell types and regulates various genes. NF- κ B activity is activated by cytokines, bacterial and viral factors and various other inducers (Karin *et al.*, 2005). Interestingly, defective NF- κ B signalling is correlated with several diseases including those with osteolytic conditions such as PDB, arthritis and periodontitis (Xu *et al.*, 2008). Recent studies show that NF- κ B activates osteoclast-specific genes, and in particular NF- κ B's role lies within the differentiation and survival of osteoclasts, with defective NF- κ B activation in osteoclasts causing excessive osteoclastic activity (Xu *et al.*, 2008).

The important role of NF- κ B in osteoclasts was demonstrated by generating double knockout mice of NF- κ B p50/p52 (p50 and p52 are class I NF- κ B member proteins formed after processing of their larger inactive precursors p105 and p100 respectively); these mice had defective osteoclast differentiation, which caused them to develop osteopetrosis (Iotsova *et al.*, 1997; Xu *et al.*, 2008). As noted earlier, NF- κ B signalling pathways are specifically regulated by several cytokines, such as TNF- α and IL1 (Xu *et al.*, 2008).

In osteoclasts, NF- κ B activation is regulated by the signalling axis composed of RANK-L, OPG and RANK (Wada *et al.*, 2006) with important downstream molecules in this axis include TRAF6, aPKC, p62 and the deubiquitylating enzyme CYLD. Not surprisingly mouse models with gene knock out of several of these proteins show defective NF- κ B signalling and various pathological bone phenotypes. For example, TRAF6 knockout mice exhibit osteopetrosis, which is due to defective NF- κ B signalling (Wada *et al.*, 2006).

1.2.5 Bone remodelling

In adult vertebrates about 10% of bone is regenerated every year through a process called bone remodelling, which is a coupled process, in which osteoblast formation will be triggered when osteoclasts first digest old bone (Roodman *et al.*, 1996). In healthy bones, bone remodelling is maintained at a homeostatic state (Figure 1.4) but, in PDB the rate of osteoclastogenesis increases focally, causing a disorganized secondary increase in osteoblast formation. This secondary increase in osteoblast activity produces denser bones, which are weaker than normal bone, and susceptible to fractures and mechanical deformities.

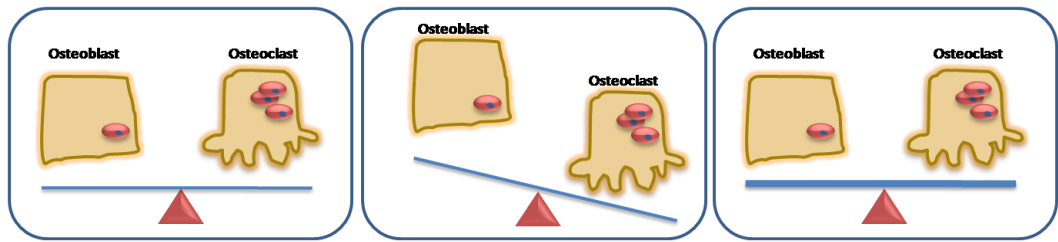


Figure 1.4: Bone remodelling

The first cartoon image shows the skeleton in balance, in which the rate of bone deposition is equivalent to the rate of bone resorption. The second image shows the state of bone remodelling during osteoporosis, in which the rate of bone resorbed is more than bone deposited, resulting from increased osteoclastic activity or osteoclastogenesis. The third image shows the state of bone remodelling in PDB, in which the rate of bone deposition is equivalent to bone resorption however, bone remodelling increases causing increased osteoclastic activity and/or osteoclastogenesis at focal regions of bone, leading to secondary increase in osteoblast activity.

1.3 Paget's disease of bone (PDB)

PDB is a common skeletal disorder, which is characterised by focal abnormalities and increased bone turnover affecting one or more sites throughout the skeleton (Ralston *et al.*, 2008a).

It is thought that PDB is resulting from abnormal bone remodelling, in which excess osteoblasts (bone-forming cells) are produced to compensate for increased osteoclast (bone-resorbing cells) activity, which lead to the formation of disordered (Pagetic) bone that is fragile and susceptible to fractures (Layfield *et al.*, 2007).

The disease is characterised by deformed bone formation in various parts of the skeleton with various frequencies, often affecting the pelvis, vertebral bodies, skull, femur and tibia (Kanis *et al.*, 1992) (Figure 1.5).

PDB is asymptomatic in the majority of patients, however about 30% of those affected may show features such as: bone pain; increase in bone vascularity; expanding lytic lesions; and bowing which leads to restriction in bone movement (Van Staa *et al.*, 2002). Bone fractures often occur at later stages of the disease, and PDB can develop to osteosarcoma in rare cases (less than 1%) (Huvos *et al.*, 1983). In addition, although it is rare, cardiovascular complications occasionally accompany PDB, in particular if the patient is suffering from high frequencies (15-35%) of bone deformities (Harrison, 16th Ed.). With respect to clinical investigation of PDB, the disease is often diagnosed through investigations for other diseases (since the disease is asymptomatic in majority of the cases) but it is known to be accompanied by increased level of serum alkaline phosphatase ALP (Harinck *et al.*, 1986); in addition, radiograms can be used to uncover enlarged bone formation in various parts of the skeleton.

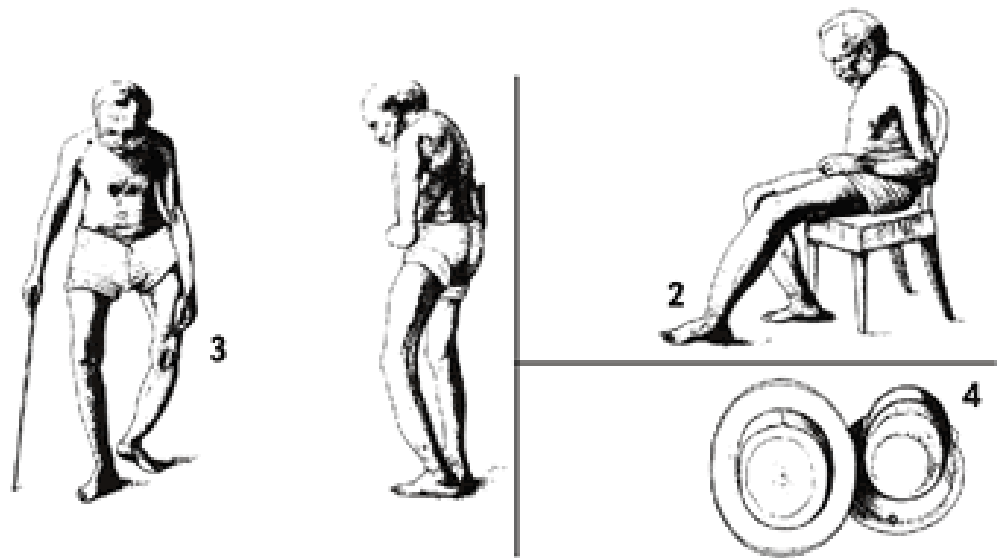


Figure 1.5: Drawings of Sir James Paget's first patient published in his original paper (1877)

1) Curvature of the spine; 2) tibial thickening and bowing; 3) bowing of the femur and tibia in the leg; 4) increase in hat size indicative of skull enlargement.

Source: www.surgeongeneral.gov/library/bonehealth/chapter_3.html

Paget J, On a form of chronic inflammation of bones (osteitis deformans), *Trans Med-Chir Soc*, 1877, 60, 37:63.

PDB is more common in people over 55 years old of age, and occurs more frequently in males (2.5%) than females (1.6%) (Cooper *et al.*, 1999). PDB is most common in Caucasian populations with a prevalence of about 3% (PDB is found in France, Germany, and within English speaking countries such as USA, Australia, New Zealand, with Great Britain having the highest prevalence up to 1,000,000 of the population (Van Staa *et al.*, 2002; source: [www.paget.org.co.uk]). However, PDB is uncommon in Scandinavia, Switzerland and Asia, indicating a genetic background (Barker *et al.*, 1984; Takata 2006; Joshi *et al.*, 2006).

Although there are some theories suggesting a role for viruses in PDB pathogenesis, the precise cause(s) of the disease is still unknown. As noted earlier, p62 mutations are commonly found in PDB patients and interestingly, all of the PDB-associated p62 mutations identified prior to this study directly affect the UBA domain or sequences very close to it (Cavey *et al.*, 2006). Since p62 is a scaffold protein in the RANK-TRAF6-NF- κ B signalling pathway in osteoclasts, it is likely that the PDB mutations cause altered function of p62 within this signalling axis (Cavey *et al.*, 2006).

In these cases (presumably as in the sporadic cases) the increase in osteoclast activity is believed to result from hyper-activation or hyper-responsiveness of the osteoclast-specific signalling pathway stimulated by RANK-L, which leads to activation of NF- κ B (Duran *et al.*, 2004).

Clinical treatments of the disease are still relatively ineffective, and several treatments (including surgical) have been used to treat the disease. Drug treatments include bisphosphonates (such as Etidronate, Tiludronate, Pamidronate) or calcitonin, although these do not allow complete recovery from the disease, and Pamidronate was the only bisphosphonates

approved for treatment of PDB (Miller *et al.*, 1999; Reid *et al.*, 2005, Ralston *et al.*, 2008a).

Another study showed that Zoledronate (another type of bisphosphonates) is the most effective treatment for PDB (Hosking *et al.*, 2007), as in 90% of the patients treated with Zoledronate total ALP levels remained in the normal range, in addition the quality of life of the patients were also improved.

Previous observations suggested treatment of asymptomatic patients with bisphosphonates might help in preventing further progression of PDB or even suppressing the disease, however a recent clinical trial showed that although bisphosphonates help in maintaining low levels of ALP, they are ineffective in preventing the disease complications or improving quality of life of patients who were treated with bisphosphonates irrespective of their symptoms (Langston *et al.*, 2009).

1.3.1 Diagnostic metabolic markers for PDB

PDB is largely asymptomatic in the majority of patients. Although bone pain is regarded as the most common symptom of PDB, generally patients are diagnosed with PDB when they are referred for investigation for other possible diseases. Currently, a combination of biochemical markers and radiographic imaging are used to confirm the diagnosis of PDB. Focal disruption in the balance of bone remodelling in PDB i.e. acceleration in the rate bone resorption and formation and osteoblasts formation, increases respective bone markers in blood and urine (Fukunaga *et al.*, 2001).

ALP is a hydrolase enzyme, which dephosphorylates several targets and it reaches its optimum activity at alkaline pH (Harris *et al.*, 1990). There are several isoenzymes of ALP and the skeletal isoform of ALP is a glycoprotein

(Harris *et al.*, 1990). ALP is used as a marker for osteoblastic activity (Leunge *et al.*, 1993), as this enzyme is required for mineralization of bone matrix in osteoblasts (Whyte, 3rd Ed.). Since bone remodelling is coupled, the amount of ALP produced from osteoblasts can be used as indirect measurement of osteoclastic activity.

ALP usually is elevated in active PDB, and patients with PDB should be referred to test for their ALP levels regularly to monitor disease extent (Schneider *et al.*, 2002). ALP can be used as a good marker to observe the metabolic state of bone turnover, also to monitor the response to antiresorptive therapy (Shankar *et al.*, 2006).

As ALP measurements have some limitations, for example interfering results from hepatic ALP may affect the assessment of PDB severity, measurement of bone specific ALP was developed to avoid false results (Farley *et al.*, 1994).

1.3.2 Genetics of PDB

Several observations suggested a genetic predisposition to PDB. For example, 15-40% of PDB patients have a positive family history (Morales-Piga *et al.*, 1995; Sofaer *et al.*, 1983; Siris *et al.*, 1991) and PDB relatives also have 7-10 times higher risks of developing PDB than control patients (Sofaer *et al.*, 1983; Siris *et al.*, 1991). Notably, relatives of PDB patients have severe disease phenotypes, earlier age of onset with bone deformity and polyostotic involvement (Daroszevska *et al.*, 2005).

A number of other observations support the genetic predisposition to PDB. For example, PDB prevalence varies between countries, as it is most common in Caucasian populations and rare in Asia and Africa, although there is evidence for involvement of environmental factors in PDB

development as well (Gardner *et al.*, 1978; Daroszewska *et al.*, 2005) (see section 1.9).

Although *SQSTM1* is the only gene identified which predisposes to classical PDB, recent research confirmed the importance of several susceptibility loci for PDB, including the PDB1 locus on chromosome 6 (Fotino *et al.*, 1977); the PDB2 locus on chromosome 18q21 (Hughes *et al.*, 1994; Cody *et al.*, 1997; Haslam *et al.*, 1998); the PDB3 locus on chromosome 5q35 (contains the *SQSTM1* gene, see section 1.4) (Hocking *et al.*, 2001; Laurin *et al.*, 2001); the PDB4 locus on chromosome 5q31 (Laurin *et al.*, 2001); the PDB5 locus on chromosome 2q36 (Hocking *et al.*, 2001); the PDB6 locus on chromosome 10p13 (Hocking *et al.*, 2001); and the PDB7 locus on chromosome 18q23 (Good *et al.*, 2002); although some of these candidate loci have been reported as being false positives, such as PDB1 (Ralston *et al.*, 2008). Given the role of p62 in the RANK-L-NF- κ B pathway, it will be interesting to find if the specified new genes at these loci encode proteins which function in this same signalling pathway.

Another association of the genetic predisposition to PDB originates from the notion that several PDB-like syndromes are all caused by genetic defect. Notably, mutated genes are all located in the signalling pathway downstream of RANK-L (Layfield *et al.*, 2007). PDB-like syndromes share several features with classical PDB such as high concentrations of serum ALP, but these syndromes are distinguished from classical PDB by having earlier age of onset, often accompanied with deafness and premature tooth loss rather than bone lesions (Ralston *et al.*, 2008b).

Common PDB-like syndromes include Familial expansile osteolysis (FEO), Expansile skeletal hyperphosphatasia (ESH) and early-onset familial PDB, which are all caused by different mutations in the *TNFRSF11A* gene, which

encodes the RANK receptor. All three diseases are caused by insertion mutations between 15-27 bp in exon 1 of *TNFRSF11A* gene, affecting the signal peptide and causing abnormal localisation of RANK in cells (Crockett *et al.*, 2007; Hughes *et al.*, 2000). Interestingly, similar to classical PDB, FEO, ESH and early-onset familial Paget's disease is inherited in an autosomal dominant manner (Ralston *et al.*, 2008b).

Juvenile Paget disease (also known as juvenile hyperphosphatasia) is caused by mutations affecting the *TNFRSF11B* gene encoding OPG. OPG is a protein secreted by osteoblasts and acts as decoy receptor for RANK-L (Simonet *et al.*, 1997). OPG negatively regulates RANK-mediated signalling (Menna *et al.*, 2000) therefore, inactivating mutations in OPG are believed to increase levels of free RANK-L and hence increase NF- κ B activation.

A further condition also associated with a PDB phenotype, inclusion body myopathy associated with PDB and frontotemporal dementia (IBMPFD) is caused by variations in *VCP* gene (also known as p97). VCP is a member of type II AAA (ATPases Associated with a variety of Activities) proteins, which serves as basic molecular chaperone in the UPS (Daroszewska *et al.*, 2005; Li *et al.*, 2002). VCP, like p62, is an ubiquitin-binding protein, and one of its roles is believed to involve to delivery of polyubiquitylated I- κ B for degradation by the 26S proteasome (Dai *et al.*, 1998).

The majority of classical PDB patients carry heterozygous mutations, in which one of the alleles is a variant form of *SQSTM1* (Helfrich *et al.*, 2008). Some researchers (including our own group) have proposed that the severity of PDB phenotype may correlate with the ability of the mutant form of the p62 protein to bind ubiquitin (Hocking *et al.*, 2004; Layfield *et*

et al., 2006). Further, on comparison of *SQSTM1* and *VCP* mutations, both mutations appear to affect the ubiquitin-binding region of the respective proteins (Layfield *et al.*, 2007), implying that disruption of ubiquitin-binding function may play a critical role in the development of these diseases (Layfield *et al.*, 2001).

Some of the mutant genes associated with PDB-like syndromes were investigated as possible candidates for classical PDB and investigations showed that *TNFRSF11A*, *TNFRSF11B* and *VCP* mutations did not cause classical late onset PDB (Wuyts *et al.*, 2001; Lucas *et al.*, 2006). However, it was suggested that a genetic polymorphism found in *TNFRSF11A* and *TNFRSF11B* genes might predispose to PDB development (Daroszewska *et al.*, 2005). For example, single-nucleotide polymorphism (SNP) variation at exon 1 of *TNFRSF11B* (G1181C) predisposed to both sporadic and familial PDB. This SNP is a common variant causing a change of lysine to asparagine at codon 3 of OPG; although the exact role for this variation is not clear, it might subtly alter OPG functions (Daroszewska *et al.*, 2004; Daroszewska *et al.*, 2005).

PDB phenotypes vary in severity, and several genetic effects or a combination of genetic and environmental factors might account for this spectrum; alternatively, the spectrum of phenotypes might originate from genetic mutations affecting different interacting proteins in the RANK-NF- κ B signalling pathway (Johnson-Pais *et al.*, 2003). For example, the contribution from a polymorphism of the *TNFRSF11B* gene, which is found in association with PDB, may cause moderate additional effects on PDB phenotypes (Daroszewska *et al.*, 2004; Helfrich *et al.*, 2008).

Interestingly, these effects appear to be entirely gender specific, as it was associated significantly with females (Beyens *et al.*, 2007). Although the exact reason for this gender difference is unclear, the difference in gender

prevalence might occur because of protective effects (such as estrogen hormones) in females (Helfrich *et al.*, 2008).

Genetic heterogeneity is a common feature of many diseases, and is a feature of PDB as well, as heterogeneity was found between different families and within the same families. For example, members (with PDB) of the same families carried *SQSTM1* mutation, whilst other members were not carriers (Good *et al.*, 2004). Offspring who inherited *SQSTM1* mutations had milder PDB phenotypes (Bolland *et al.*, 2007), which might be because combinations of factors are necessary to cause the disease (Bolland *et al.*, 2007). Genetic variation, or/and any environmental factors, or all of the above factors might account for the variation in the disease phenotypes between affected PDB patients (Helfrich *et al.*, 2008).

Finally, the overlap between major susceptibility loci within families affected with PDB suggests the possibility that two separate genetic variants might be necessary to cross some "threshold" rate to cause PDB phenotypes (Helfrich *et al.*, 2008). For example in a large family with PDB some individuals had linkage to locus (PDB7) on chromosome 18q23 also had mutations in *SQSTM1* (although not all family members had *SQSTM1* mutations) (Helfrich *et al.*, 2008). Of note, those patients with the PDB7 linkage had earlier onset of disease phenotype, indicating that this locus might have the necessary factors to cause the occurrence of PDB phenotypes at an earlier age (Good *et al.*, 2002).

1.4 SQSTM1 and PDB

The *SQSTM1* gene, encoding the p62 protein, is located on chromosome 5q35, the PDB3 locus (Laurin *et al.*, 2004) and the disease has as high as an 80% penetrance for *SQSTM1* mutations carriers (Morissette *et al.*, 2006). *SQSTM1* mutations are found in PDB to a varying extent between different populations ranging from 5-30% in sporadic cases and 10-50% of familial PDB (Collet *et al.*, 2007; Eekhoff *et al.*, 2004; Hocking *et al.*, 2004; Laurin *et al.*, 2002; Rhodes *et al.*, 2008). In addition to PDB, *SQSTM1* has been associated with other diseases such as Alzheimer's disease (AD) Parkinson's disease and Huntington's disease (Kuusisto *et al.*, 2001 & 2002; Zatloukal *et al.*, 2002; Nagaoka *et al.*, 2004). p62 knockout mice have a greater susceptibility to late onset obesity accompanied by diabetic phenotypes such as insulin resistance (Rodriguez *et al.*, 2006). Interestingly p62 knockout mice and wild type mice had similar bone phenotypes, however upon challenge with osteoclastogenic stimuli such as the calciotropic hormone parathyroid hormone-related protein (PTHrP), p62 knockout mice showed different bone phenotypes to the wild type mice (see section 1.10.3). The p62 protein is also found to be over-expressed in some cancers, such as prostate (Kitamura *et al.*, 2006) and breast cancer (Thompson *et al.*, 2003) and p62 is also necessary for asthma development (Martin *et al.*, 2006).

The C-terminus of the p62 protein contains the UBA domain which harbours most of the mutations linked to PDB, and as noted earlier these mutations result in loss or impairment of ubiquitin-binding function and defective NF- κ B signalling (Cavey *et al.*, 2006). In addition being the most common PDB-associated *SQSTM1* mutation (first recognized by Laurin *et al.*, 2004) in French Canadian families, P392L is also the most common PDB-associated mutation in Great Britain, New Zealand and Australia and

haplotype analysis indicated that P392L is a founder mutation (Lucas *et al.*, 2005) although in the French-Canadian population two founder effects are proposed and founder effects were not detected for other common PDB mutations (Helfrich *et al.*, 2008). In total more than 20 different *SQSTM1* mutations have now been identified in PDB patients (Table 1.1).

No. of mutation	p62-PDB associated mutations	References
1	P392L	Laurin <i>et al.</i> , 2002
2	S399P	Eekhoff <i>et al.</i> , 2004
3	G425E	Falchetti <i>et al.</i> , 2009
4	A426V	E. Corral Moro <i>et al.</i> , 2005
5	E396X	Hocking <i>et al.</i> , 2002
6	K378X	Rea <i>et al.</i> , 2006
7	P392L/S399P	Eekhoff <i>et al.</i> , 2004
8	Δ351-388	Beyens <i>et al.</i> , 2006
9	A381V	Falchetti <i>et al.</i> , 2009
10	D335E	Falchetti <i>et al.</i> , 2009
11	P364S	Rea <i>et al.</i> , 2009
12	P387L	Johanson-pais <i>et al.</i> , 2003
13	G411S	Hocking <i>et al.</i> , 2004
14	M404V	Eekhoff <i>et al.</i> , 2004; Falchetti <i>et al.</i> , 2004
15	A390X	Hocking <i>et al.</i> , 2002
16	Y383X	Falchetti <i>et al.</i> , 2009
17	D423X	Falchetti <i>et al.</i> , 2009
18	S397A	Falchetti <i>et al.</i> , 2009
19	M404T	Eekhoff <i>et al.</i> , 2004
20	A381V/P392L	Collet <i>et al.</i> , 2007
21	L413F	Collet <i>et al.</i> , 2007
22	A390X/P392L	Collet <i>et al.</i> , 2007
23	G425R	Eekhoff <i>et al.</i> , 2004; Falchetti <i>et al.</i> , 2004; Hocking <i>et al.</i> , 2004
24	L394X	Good <i>et al.</i> , 2004; Hocking <i>et al.</i> , 2004; Johanson pais <i>et al.</i> , 2003

Table 1.1: p62-PDB associated mutations identified todate

1.4.1 Structure of the p62 protein

In humans the *SQSTM1* gene encodes the 440 amino acid p62 protein. This gene consists of eight exons which range in size from 81bp to 872bp, and seven introns ranging in size from 8kb to 200kb (Vadlamudi *et al.*, 1998). The p62 protein has several homologs with approximately 90% conserved amino acid sequences, such as zeta atypical protein kinase (aPKC- ζ)-interacting protein (ZIP) (Puls *et al.*, 1997), the murine homologs A170 (Ishii *et al.*, 1996) and signal transduction and adaptor protein (STAP) (Okazaki *et al.*, 1999).

The p62 protein has several domains (see Figure 1.2), with the N-terminal region of the protein containing a PB1 domain, through which it can interact with other p62 monomers producing polymers structured in a 'back to front' manner (Wilson *et al.*, 2003). The C-terminal region contains a UBA domain between residues 387-440; through this domain p62 is able to bind to monoubiquitin or polyubiquitin chains (linked either through Lys48, -63 or -29 of ubiquitin) (Vadlamudi *et al.*, 1998; Shin *et al.*, 1998). ZZ, TRAF6-binding and two PEST domains are located between the N and C termini of p62, allowing p62 to interact with various other proteins mediating intracellular signalling. These domains are discussed in more detail below.

1.4.1.1 The ZZ domain

The ZZ domain is a domain that is found in diverse cellular proteins: in p62 the ZZ domain mediates binding with RIP, which is necessary for the activation of certain NF- κ B signalling pathways (Sanz *et al.*, 1999). Because of the presence of the ZZ domain, p62 has been classified as member of zinc finger proteins (ZZ & TAZ; zinc finger proteins are

composed of putative finger structure which cluster around a Zn²⁺ ion which is tetrahedrally coordinated by cysteine and histidines residues, stabilising the folded structure of zinc finger peptide (Ponting *et al.*, 1996).

1.4.1.2 TRAF6-binding domain

This region of p62 mediates interactions with a range of proteins (including TRAF6) which, in general leads to the phosphorylation of IKK and the subsequent release of NF-κB to the nucleus (Sanz *et al.*, 2000). Through these pathways TRAF6 is stimulated by various signals for example when cells are stimulated by IL-1, TRAF6 binds with IRAK protein (Geetha *et al.*, 2002); upon activation of the RANK receptor by RANK-L in osteoclasts, TRAF6 directly binds to RANK stimulating the Lys63-linked autoubiquitylation of TRAF6 (Layfield *et al.*, 2004a).

1.4.1.3 PEST sequences

PEST is the abbreviation of Proline (P), Glutamic acid (E), Serine (S), and Threonine (T). Two regions of p62 contain sequences rich in these amino acids; proteins containing PEST domains are often degraded by the ubiquitin-dependent proteolysis pathway (Rechsteiner *et al.*, 1996).

1.4.1.4 The UBA domain

The UBA domain is a small domain located at the C-terminus of the p62 protein. NMR studies showed that the p62 UBA domain has a stable hydrophobic three helix structure (Ciani *et al.*, 2003), through which it binds to ubiquitin by non-covalent hydrophobic interactions (Long *et al.*, 2008). The UBA domain is thought to play important roles in the functions of p62, including in the control of protein degradation (Chau *et al.*, 1989; Thrower *et al.*, 2000), endocytosis (Galan *et al.*, 1997; Haglund *et al.*, 2003), and NF-κB signalling (Deng *et al.*, 2000; Wang *et al.*, 2001; Layfield *et al.*,

2004a). Binding of the UBA domain to monoubiquitin is apparently weaker to that observed for polyubiquitin, and its precise functional role (in particular in osteoclasts) requires further investigation.

1.4.1.4.1 Ubiquitin

Ubiquitin is a small protein which has a pear-drop like structure (Doherty *et al.*, 2002), that it is composed of 76 amino acids (Schlesinger *et al.*, 1975). In man ubiquitin is composed of 19 polar (CNQSTY) amino acids, 24 hydrophobic (AILFWV) amino acids, 11 acidic (DE) amino acids, 11 basic (KR) amino acids, in addition these amino acids include 24 charged amino acids (DEHKR). Ubiquitin's molecular weight in total is ~8.5kDa (Schlesinger *et al.*, 1975) and its primary sequence being highly conserved between species (Schlesinger *et al.*, 1975). For example, the human ubiquitin sequence (Figure 1.6) only differs from yeast ubiquitin by three amino acids.

(1)MQIFVKLTGKTITLEVEPSDTIENVKAKIQDKEGIPPDQQLIFAGKQLEDGRT
DYNIQKESTLHLVLRGG (76)

Figure 1.6: Primary sequence of human ubiquitin

Ubiquitin is a highly stable protein, due to presence of stabilizing residues (A,C,G,M,P,S,V,T) with a half life ($t_{1/2}$)>20 hours; it is not denatured by temperature, pH (Lenkinski *et al.*, 1977) or proteases (Schlesinger *et al.*, 1975), although often ubiquitin loses its C-terminal glycine residues during proteolysis upon purification. The general stability of ubiquitin is attributed to the prevalence of extensive hydrogen bonding in its structure.

Ubiquitin serves as a tag for non-lysosomal degradation, by recruiting damaged proteins (or normal short-lived proteins destined for degradation) to the 26S proteasome; in this case an isopeptide bond is formed between glycine residue (Gly-76) at the C-terminus of ubiquitin and specific ϵ -amino groups in lysine residues of the target protein (Hershko *et al.*, 1998). Ubiquitin itself contains seven lysine residues, and multiple ubiquitins can be linked together through all seven of these lysines to form polyubiquitin chains (Haglund *et al.*, 2005). Depending on the lysine residues used in these chains, the ubiquitylated proteins have differing fates. For example, polyubiquitin chains linked via Lys48 (or Lys29) generally target the protein for degradation by the 26S proteasome complex (Thrower *et al.*, 2000; as is the case for I- κ B). Polyubiquitin chains linked via Lys63 have important non-degradative roles in processes such as DNA repair, apoptosis, and activation of NF- κ B signalling pathways (Chan *et al.*, 2001) as is the case for TRAF6. Monoubiquitylation regulates processes such as endocytosis (Haglund *et al.*, 2003).

Ubiquitin is first activated by an ubiquitin-activating enzyme (E1), through the formation of a thioester bond between Gly76 of ubiquitin and a cysteine residue of E1, in an ATP-dependent reaction, releasing AMP and the E1-ubiquitin complex. The E1-ubiquitin complex is then recognised by another group of enzymes called ubiquitin conjugating enzymes (E2s) replacing E1 by E2, through the formation of another thioester bond with a cysteine residue of E2, producing a new complex E2-ubiquitin. The last step in the ubiquitylation cascade is mediated by E3 (ubiquitin ligase) enzymes which can bind to both of the substrate and the E2-ubiquitin complex, producing a bridge between the two, hence recruiting ubiquitin for its conjugation to the substrate (Hershko *et al.*, 1998; Doherty *et al.*, 2002). After degradation of the substrates, ubiquitin is detached from the

complex by Deubiquitylating enzymes (DUBs) (Figure 1.7) which also play important regulatory roles in other ubiquitin-mediated processes.

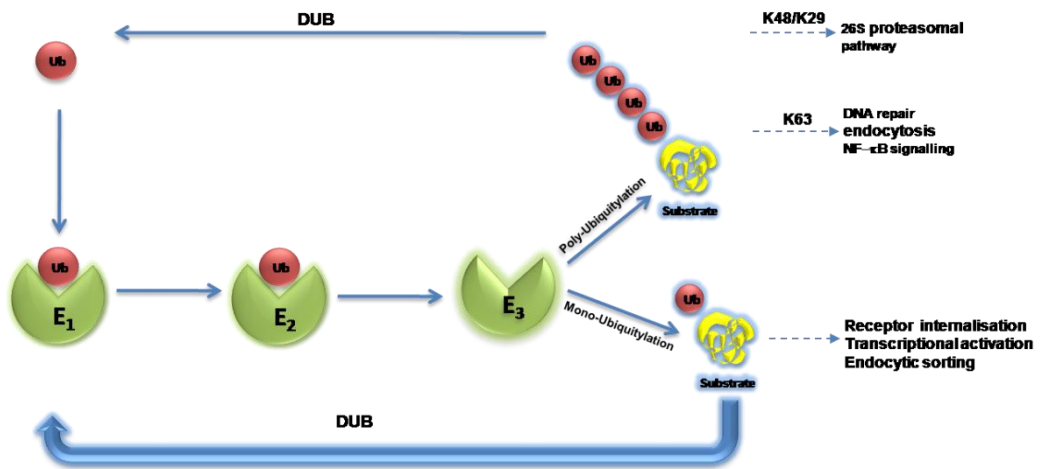


Figure 1.7: Outline of the ubiquitylation pathway

Ubiquitin-activating enzyme (E1) binds to ubiquitin, then activated ubiquitin is transferred to an ubiquitin conjugating enzyme (E2). Finally, the substrate protein is transferred to the E2-ubiquitin complex by an E3 enzyme. Substrate can either be monoubiquitylated or polyubiquitylated. DUBs detach ubiquitin from the complex, after degradation or to reverse the modification.

1.5 Relationship between PDB severity and ubiquitin-binding properties of p62

The exact role of *SQSTM1* mutations in PDB is still unclear, but recent research highlights a possible correlation between impaired protein function of p62 mutants and PDB (Layfield *et al.*, 2007). For example, individuals who have *SQSTM1* mutations are on average diagnosed 10 years younger than those without *SQSTM1* mutations (Hocking *et al.*, 2004) and PDB patients (not healthy controls) are the only carriers of *SQSTM1* mutations. Also, *SQSTM1* mutation effects on the ubiquitin-binding function of p62 proteins were found to be variable depending on the type of mutation (Cavey *et al.*, 2005; Cavey *et al.*, 2006), and the severity of PDB may be directly correlated to effects on ubiquitin-binding function of p62. For example, patient carriers of truncating mutations have more severe disease phenotype than those with missense mutations (Hocking *et al.*, 2004) and interestingly these truncating mutations have the most severe effect on the ubiquitin-binding function of the p62 protein (Cavey *et al.*, 2006).

1.6 p62's role in RANK-L-NF-κB signalling

p62 is an important protein in multiple signalling pathways that control osteoclastogenesis (Figure 1.8) (Roodman *et al.*, 2005). For example, as noted earlier p62 functions as a scaffold protein that regulates NF-κB signalling downstream of the RANK receptor (Moscat *et al.*, 2002).

In RANKL-NF-κB signalling, RANK-L interacts with RANK and the cytoplasmic tail of RANK binds to TRAF6 (Galibert *et al.*, 1998). Notably, p62 binds through its UBA domain to ubiquitin and mediate Lys63-linked polyubiquitylation of

TRAF6, and also p62 acts as a scaffold in bridging aPKC and forming a complex with TRAF6. Ultimately this complex leads to phosphorylation and degradation of I- κ B by the UPS; I- κ B degradation is followed by the release of NF- κ B transcription factor and its translocation to the nucleus, in which NF- κ B induces appropriate gene expression (Layfield *et al.*, 2007).

The important role of p62 in NF- κ B signalling and osteoclastogenesis has been investigated by several groups. For example, to elucidate the role of p62 in bone remodelling, Duran *et al.* conducted an investigation on p62 knockout mice. Although, wild type mice and p62 knockout mice had similar phenotypes, which implies that basal osteoclastogenesis was unaffected, osteoclastic stimuli uncovered different results; p62 knockout mice showed impaired osteoclastogenesis upon stimulation with both RANK-L *in vitro* and PTHrP *in vivo* indicating a requirement of p62 in induced osteoclastogenesis (Duran *et al.*, 2004).

The importance of p62 in NF- κ B signalling is also illustrated by luciferase reporter assays, in which PDB-associated mutants were found to be associated with increased NF- κ B activation and osteoclast activity *in vitro* (Yip *et al.*, 2006; Rea *et al.*, 2006).

Further, a PDB-associated p62 mutant (P392L) resulted in an increase in osteoclast activity in a mouse model with progressive bone loss, but without affecting osteoblast numbers (Kurihara *et al.*, 2007), possibly by increasing RANK signalling and increased NF- κ B activation. The exact role of p62 in osteoclastogenesis is still not clear but, it was suggested by earlier investigators that it could involve ubiquitin-dependent proteolysis (Roodman *et al.*, 2005).

Furthermore, osteoclasts expressing a p62 UBA domain deletion mutant showed increased osteoclastogenesis. The osteoclasts had higher number of nuclei than control osteoclasts, and the osteoclasts were larger, similar to the phenotypes of pagetic osteoclasts. This observation leads to a hypothesis that p62 may normally serve to negatively regulate osteoclastogenesis, and that UBA domain is an important factor in this negative regulation (Yip *et al.*, 2006; Rea *et al.*, 2006).

p62 also regulates NF- κ B pathways through its interaction with other equally important regulators of the pathway, such as NF- κ B Essential Modulator (NEMO) and the DUB enzyme CYLD (see sections 1.6.1 and 1.6.2).

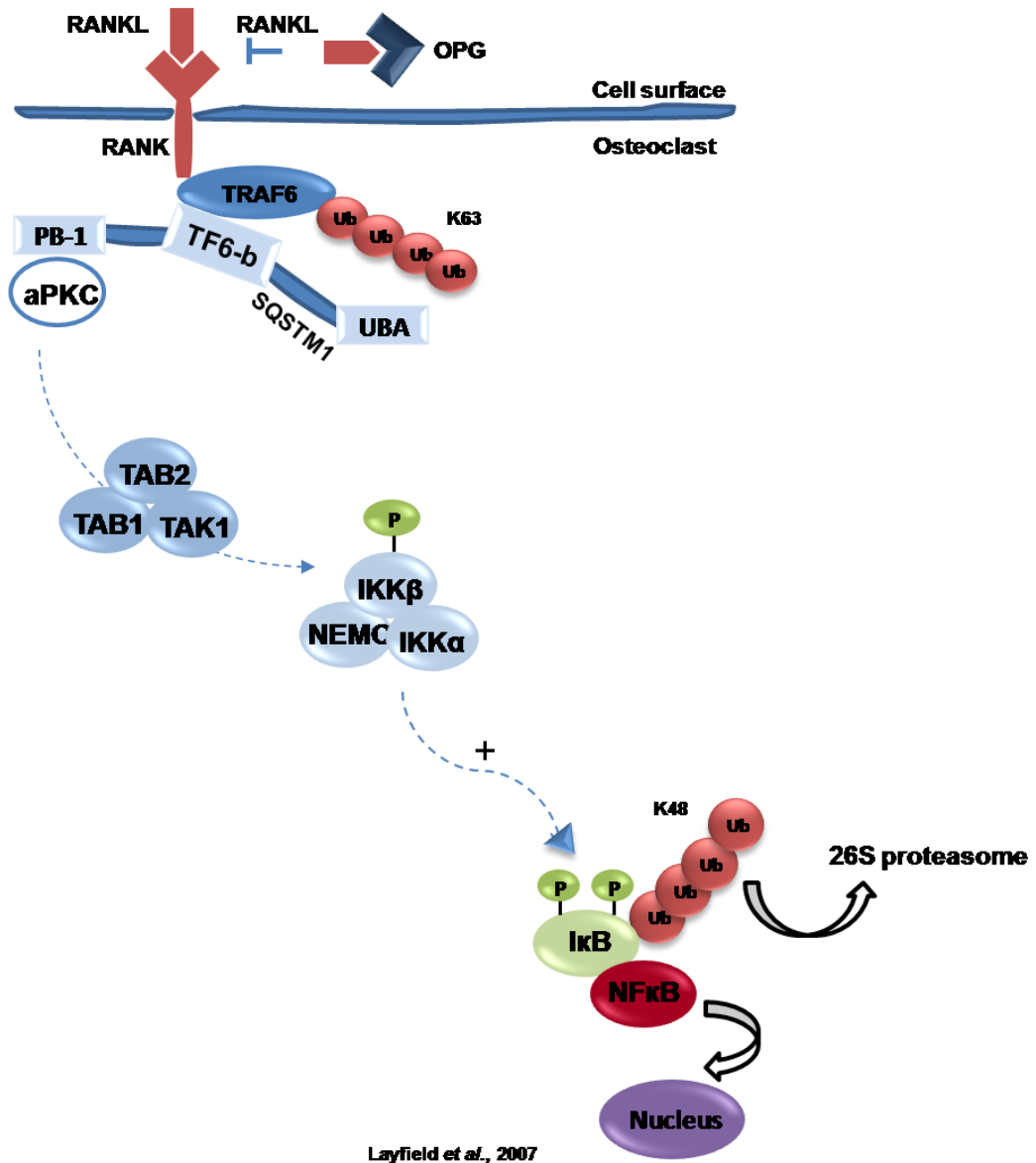


Figure 1.8: The RANK-L-NF-κB signalling pathway

Upon interaction of RANK-L with RANK, TRAF6 directly interacts with RANK and undergoes autoubiquitylation by its intrinsic ubiquitin ligase activity. Also, TRAF6 interacts with SQSTM1 (p62) through its TF6-b, and it is believed that p62 facilitates the K63-linked polyubiquitylation of TRAF6. p62 recruits aPKC to the signalling complex, and polyubiquitylation of TRAF6 leads to activation of TAK1, which in turn leads to phosphorylation and activation of the IKK complex (IKK α , IKK β , IKK γ); the activated IKK complex ultimately leads to phosphorylation of I- κ B and its degradation by the 26S proteasome, followed by the release of NF- κ B to the nucleus.

1.6.1 IKK γ (NEMO)

1.6.1.1 Characteristics of IKK γ

IKK γ , sometimes known as NEMO (NF- κ B essential modulator), is a 48kDa protein, composed of 419 amino acids and located on chromosome Xq28 (Jin *et al.*, 1999). The IKK γ protein is acidic (pI 5.66), and unusually rich in glutamic acid and glutamine (13% each). IKK γ is composed of a two coiled-coil regions (CC1 and CC2), a leucine zipper, a zing finger C-terminal structure and a CC1 region N-terminal, which interacts with the C-terminal tails of IKK kinase (Rushi *et al.*, 2008; Ghosh *et al.*, 2002; Leonardi *et al.*, 2000).

IKK γ is the regulatory subunit of IKK complex, which is composed of two other catalytic subunits IKK α and IKK β (Scheidereit *et al.*, 2006). IKK γ interacts with IKK α and IKK β through a short sequence at the extreme C-terminal of these two subunits (May *et al.*, 2000). IKK γ interacts mainly with IKK β through the N-terminal of IKK γ (Prajapati *et al.*, 2002), but IKK γ has a weaker interaction with IKK α (Yamaoka *et al.*, 1999).

IKK γ phosphorylation is mediated by IKK β (Prajapati *et al.*, 2002).

Interestingly, p62 is involved in phosphorylation of the IKK complex and probably favours the phosphorylation of IKK β through interaction with the aPKCs (Lallena *et al.*, 1999). Previously, it was shown that IKK γ binds to Lys63-linked polyubiquitin chains, but not Lys48-linked polyubiquitin chains (Wu *et al.*, 2006) consistent with the notion that IKK γ ubiquitylation is not for its degradation (Zhou *et al.*, 2004). Interestingly, recent studies showed that NEMO also binds selectively to linear polyubiquitin chains and this interaction is required for NF- κ B activation; studies showed that the UBAN (ubiquitin binding in ABIN and NEMO) motif of NEMO binds stronger

to linear diubiquitin chains than both Lys63 and Lys48 linked polyubiquitin chains (Rahighi *et al.*, 2009).

1.6.1.2 Role of IKK γ in RANK-L-NF- κ B signalling

IKK γ is required for the activation of the IKK complex in the canonical NF- κ B signalling pathway (Bonizzi *et al.*, 2004). IKK activation leads to phosphorylation of I- κ B and its degradation by the proteasome, thereby releasing NF- κ B from the cytoplasm to the nucleus (Zhang *et al.*, 2005). Activation of IKK is mediated by formation of a complex between TRAF6, p62 and α PKC, the formation of this complex is stimulated by IL-1, RANK-L and other signals (Zhang *et al.*, 2005).

p62 interacts with TRAF6 and regulates Lys63-linked polyubiquitylation of TRAF6 (Wooten *et al.*, 2005) and TRAF6 in turn acts as an ubiquitin ligase E3 by attaching Lys63-linked polyubiquitin chains to IKK; this ubiquitylation is important for IKK activation (Ruefli-Brasse *et al.*, 2003; Ruland *et al.*, 2003; Sun *et al.*, 2004; Zhou *et al.*, 2004). Specifically, p62 induces TRAF6 to ubiquitylate IKK γ , as without TRAF6, p62 was unable to ubiquitylate IKK γ (Martin *et al.*, 2006).

1.6.2 CYLD

1.6.2.1 Characteristics of CYLD

CYLD is a deubiquitylating enzyme (one of \sim 70 or so in man) which deubiquitylates Lys63-linked polyubiquitylated substrates, but not Lys48-linked targets. CYLD deubiquitylates several proteins associated with NF- κ B signalling, such as NEMO, TRAF6 and TRAF2 (Kovalenco *et al.*, 2003). CYLD also functions as a tumour suppressor gene (Courtois *et al.*, 2008). At the sequence level CYLD is an approximately 120 kDa protein, composed

of 956 amino acids and its gene is located on chromosome 16q12–13 (Courtois *et al.*, 2008).

CYLD was first discovered in a genetic analysis of a rare cancer, cylindromatosis (turban tumour syndrome); the tumours of this disease are benign and called cylndromas, occurring mostly in the scalp or other skin appendages (Bignell *et al.*, 2000). In addition to its tumour suppression activity, CYLD has diverse roles in other cellular activities, such as apoptosis, cell proliferation (Jono *et al.*, 2004), and is involved in immunity, infection and tumorigenesis (Courtois *et al.*, 2008).

CYLD functions in a cell type specific manner, for example it is inactive in macrophages but, on the other hand CYLD negatively regulates lymphocytes and preosteoclasts (Jin *et al.*, 2008).

1.6.2.2 Role of CYLD in RANK-L-NF- κ B signalling

In addition to the positive role of p62 in NF- κ B signalling, p62 also has a negative role in regulating signalling; although this regulation is poorly understood it is likely to involve interaction of p62 with the negative regulators of NF- κ B activity (Jin *et al.*, 2008).

Recently, it has been shown that p62 mediates the interaction between CYLD and TRAF6 (this interaction requires the C-terminal of p62). Notably, the interaction between p62 and TRAF6 is unaffected by expression levels of CYLD. CYLD mediates deubiquitylation of Lys63-linked polyubiquitin chains from TRAF6, thereby deactivating NF- κ B signalling (Trompouki *et al.*, 2003). On the other hand CYLD itself seems also to be induced by NF- κ B (Jono *et al.*, 2004). CYLD was defined as the first DUB enzyme that has a negative role in osteoclastogenesis (Jin *et al.*, 2008). This negative regulation is believed to be through its interactions with TRAF6 and TRAF2

and IKK γ (Kovalenco *et al.*, 2003). When CYLD interacts with NEMO (Kovalenco *et al.*, 2003), NEMO facilitates the phosphorylation of CYLD but the exact reason for this phosphorylation is not obvious (Courtois *et al.*, 2008). Interestingly, as CYLD prefers Lys63-linked polyubiquitylated substrates, in addition to TRAF6 it is also able to deubiquitylate IKK γ (Kovalenco *et al.*, 2003; Sebban-Benin *et al.*, 2007).

Using mouse models, *in vitro* studies showed CYLD specifically acts as a negative regulator for osteoclast development through suppression of RANK signalling. The expression of CYLD is induced specifically by RANK-L although, the mechanism is still unknown (Jin *et al.*, 2008). Further, CYLD knockout mice had increased activation of osteoclastogenesis and had large and multinucleated osteoclasts, although osteoblast activities were not affected considerably (Jin *et al.*, 2008).

1.7 Emerging functions of p62

The role of p62 in autophagy will be described. Although there is no direct evidence for the role of autophagy in PDB development, emerging research point to the direction of an important role of p62 and autophagy in PDB pathogenesis.

1.7.1 General overview of autophagy

Autophagy is a process by which a cell's long lived proteins and organelles are degraded in the lysosomes. Autophagy was first recognised by Christian de Duve in 1963, when he was observing cytoplasmic structures using electron microscopy (Cecconi *et al.*, 2008).

Defective autophagy has many complications. For example, impairment of autophagy is linked to cancer development (Gozuacik *et al.*, 2004), neurodegenerative diseases, cardiomyopathies and several other diseases (Cuervo *et al.*, 2004). In addition, autophagy is involved in tissue remodelling, cellular differentiation and removal of bacterial infections (Bjørkøy *et al.*, 2005).

Generally, autophagy is thought to be a non-selective degradation process, but recent studies highlight the possible selective degradation of individual proteins through autophagy in an ubiquitin-dependent manner, including selective degradation of organelles by autophagy such as pexophagy (Bellu *et al.*, 2001) and mitophagy (Lemasters *et al.*, 2005), which represent selective degradation of peroxisomes and mitochondria, respectively. More evidence of selective degradation is emerging, for example the IKK complex is selectively degraded by autophagy (Li *et al.*, 2006), and most recently p62-associated ubiquitylated protein aggregates were shown to be selectively degraded by autophagy (Ichimura *et al.*, 2008).

During inhibition of the UPS, autophagy serves as an alternative mechanism to degrade ubiquitylated proteins and aggregates. This coordination between the UPS and autophagy requires further research to understand these molecular processes completely (Ding *et al.*, 2007).

Autophagy occurs in all eukaryotes (Komatsu *et al.*, 2007) and it has two basic physiological roles. Firstly, autophagy functions as basic survival process in eukaryotes, as it supplies amino acids by degrading cell constituents; this process is defined as adaptive autophagy. In contrast, basal or constitutive autophagy is a process which is activated irrespective of cells nutritional conditions, as basal autophagy is responsible for the

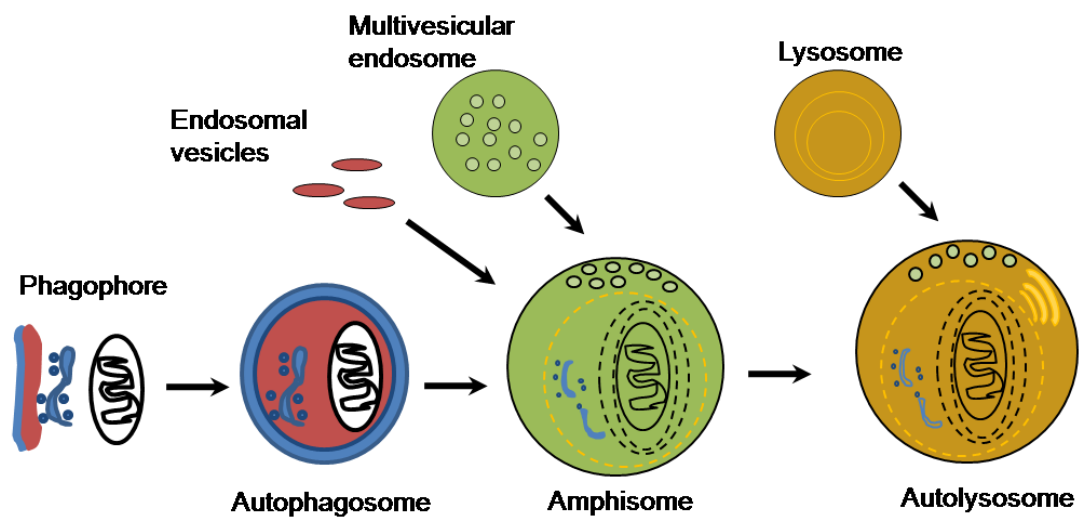
degradation of long lived proteins (Iwata *et al.*, 2006), damaged and non-functional organelles (Elmore *et al.*, 2001) and toxic aggregated proteins (Komatsu *et al.*, 2007).

In addition, autophagy serves as a substitute to apoptosis when cell death through apoptosis is dysfunctional (Levine *et al.*, 2005); as a result autophagy was classified as type II cell death (Levine *et al.*, 2005). Despite the ongoing extensive research in autophagy, the paradoxical function of autophagy in cell survival and cell death is not clearly understood.

Autophagy can be classified into three basic types based on the way cytoplasmic materials are shuttled to the lysosomes: macroautophagy, microautophagy and chaperone-mediated autophagy (Pankiv *et al.*, 2007). Macroautophagy (commonly denoted as autophagy) is a multi-step process, which is initiated by the formation of a separation membrane around the materials which need to be degraded, sequestering the materials inside a structure called phagophore or isolation membrane (Kroemer *et al.*, 2005); this structure is a flat organelle like Golgi cisterna (Mizushima *et al.*, 2007) (Figure 1.9). The phagophore then elongates to enclose the cytoplasmic materials completely, forming autophagosomes. Autophagosomes fuse with endosomes to produce amphisomes; this step is followed by further fusion step with the lysosome, in which the structures will be called autolysosomes. These autophagic structures are classified based on their function not their morphology, and are difficult to recognise under electron microscopy (Mizushima *et al.*, 2007).

The second type of autophagy is microautophagy, which is characterised by sequestration of cytoplasmic materials by lysosomal membrane directly.

The third type of autophagy, chaperone mediated autophagy (CMA), as the name implies requires specific set of molecular chaperones, which recognise peptide sequences in the proteins which needed to be degraded. In this process a complex will form between the unwanted proteins and the molecular chaperones, the complex is then imported to the lysosomes (Kroemer *et al.*, 2005).



Reproduced from Kroemer *et al.*, 2005

Figure 1.9: Autophagy

Macroautophagy is a multi step process which starts with the enclosure of the cytoplasmic materials by phagophore (isolating membrane) and a cisterna. The next step is the formation of autophagosomes, in which the cytoplasmic materials will be sequestered. Autophagosomes are double membrane structures and p62 is required for their formation. The final step of autophagy is characterised by fusion of the autophagosomes with endosomes and/or lysosomes, thereby forming autolysosomes (also known as autophagolysosomes), in which the inner membrane together with the luminal content of the autophagosomes will be degraded by the active lysosomal enzymes in the acidic environment of the autolysosomes.

Microautophagy is similar to macroautophagy, as microautophagy starts with sequestration of cytoplasmic materials, but the lysosomal membrane itself engulf the cytoplasmic materials to be degraded. CMA is characterised by cytosolic chaperones which interact with soluble cytosolic proteins, forming a complex that will be engulfed to the lysosomal lumen through interaction of the complex with a receptor on the membrane of lysosomes.

Each step in autophagy is controlled by specific autophagy-related genes. To date 27 autophagy genes (Atg) have been identified (Ding *et al.*, 2007). One of the important genes in autophagy is Atg8-phosphatidylethanolamine (PE), which mediates the formation of autophagosomes. LC3 (light chain3) is the best characterised mammalian Atg8 homologue, and LC3 is used commonly as an autophagic marker (Mizushima *et al.*, 2004).

LC3 is classified into two types, depending on its structure, LC3I and LC3-II. LC3I is the cytoplasmic form, which is the backbone structure for formation of LC3-II. A series of steps convert LC3I to LC3-II: Atg4B cleaves pro-LC3 and exposes its C-terminal glycine residue, then LC3-II will form by conjugation of phosphatidylethanolamine (PE) to the exposed glycine residue of LC3I and the association of LC3-II to the autophagosomal membrane (Pankiv *et al.*, 2007). LC3-II is PE conjugated and it is localised in the inner and outer membrane of autophagosomes; LC3-II in the inner membrane is degraded together with the materials inside the autophagosomes after the fusion step of the autophagosomes with the lysosomes (Kabeya *et al.*, 2000).

1.7.2 Role of p62 in autophagy

Recent studies highlighted the important role of p62 in autophagy. LC3 interacts with p62 through a region of p62 known as LC3 interacting region (LIR), which is encoded by amino acids 321-342 of human p62 (Pankiv *et al.*, 2007).

The role of p62 in autophagy is evident by the notion that large portion of cellular p62-containing ubiquitylated aggregates are degraded by

autophagy (Biørkøy *et al.*, 2005). Interestingly, autophagic degradation of p62 is present in a wide range of cell types, such as HEK293 cells, HeLa cells and mouse embryonic fibroblasts (Biørkøy *et al.*, 2005).

Furthermore, other studies showed the importance of p62 in autophagy. p62 is required for LC3 accumulation in HeLa cells, as when HeLa cells were depleted of endogenous p62 and starved of amino acids, LC3 did not accumulate in HeLa cells. Further, LC3 did not accumulate in cells expressing mutant forms of p62 (Biørkøy *et al.*, 2005).

To test the role of p62 in autophagy in a more physiological environment, autophagy deficient mice models were generated. When hepatocytes of mice were depleted of two important genes in autophagy (*Atg7* and *Atg5*), p62 accumulated in hepatocytes of the autophagy-deficient livers; in addition p62 accumulated in the neurons of autophagy deficient neurons. p62 accumulation formed inclusion bodies which co-localised with ubiquitin (Komatsu *et al.*, 2007). These results are indicative that p62-ubiquitin positive inclusion bodies are degraded by autophagy.

In addition, in contrast to single *Atg7* knockout mice, ubiquitin-positive inclusion bodies were absent in hepatocytes of a double knockout mice (*Atg7* and *p62*), showing the importance of p62 in the formation of the ubiquitin inclusion bodies (Komatsu *et al.*, 2007).

Recent studies suggest that p62 is regulated by autophagy in osteoclasts and more research is ongoing to establish the regulation mechanism (Helfrich *et al.*, 2008). Preliminary results showed that Autophagy-Linked FYVE-domain containing protein (ALFY) co-localised with p62 in osteoclasts (unpublished data by Hocking *et al.*). Interestingly, inhibition of autophagy

leads to accumulation of aggregates containing p62, ubiquitylated proteins and ALFY (Filimonenko, *et al.*, 2007), consistent with the inclusion bodies in the hepatocytes and neurons of autophagy-deficient mice.

1.8 Role of viral factors in PDB pathogenesis

Some thirty years ago a viral aetiology was proposed for PDB, as inclusion bodies similar in structure, morphology, and size to nucleocapsid of paramyxovirus were observed in pagetic osteoclasts (Mills *et al.*, 1976; Harvey *et al.*, 1982). These inclusion bodies were commonly located in the nucleus and occasionally in the cytoplasm of osteoclasts, without any appearance in any other types of bone cells (Helfrich *et al.*, 2000). Nevertheless, detection of viruses in PDB gave contradicting results (Ralston *et al.*, 2007), and since the first proposal of viral aetiology in PDB extensive research is ongoing to determine the viral contribution to PDB pathogenesis.

In support of the role of viruses in PDB, several groups attempted to test the viral hypothesis using common detection techniques. As a result, measles virus nucleocapsid (MVNP) sequence was detected in pagetic osteoclasts using reverse transcriptase PCR (RT-PCR) (Reddy *et al.*, 1999a; Friedrichs *et al.*, 2002). Another study showed that expression of the *MVNP* gene in normal OCL precursors stimulated OCL formation and induced the formation of OCLs with pagetic phenotypes (Kurihara *et al.*, 2000).

In addition, transgenic mouse models were made by targeting MVNP to the osteoclast lineage. The mice developed pagetic phenotypes and sometimes pagetic lesions (Kurihara *et al.*, 2006).

Another virus, Canine distemper virus (CDV) has also been linked with PDB. In support of this notion, studies in Spain and Italy suggest that there is higher risk of PDB development in rural areas, which might be because of zoonotic origins (Gennari *et al.*, 2006; Lopez-Abente *et al.*, 2003) and dog owners were reported to have a higher prevalence of PDB (O'Driscoll *et al.*, 1985). Osteoclasts infected with CDV showed high expression levels of p62 and ubiquitin (Selby *et al.*, 2006), implying that the virus might disturb RANK–NF- κ B signalling (Layfield *et al.*, 2007).

Previous techniques to robustly detect viral transcripts in pagetic osteoclasts may not have been sensitive enough to be conclusive and the role of virus in PDB is still subject to conflicting views. In an attempt to resolve this issue, a comparison study between several groups in UK was conducted by Ralston *et al.* in 2007, which found a 1000-fold difference in the sensitivity of RT-PCR for detection of measles virus, emphasising the unreliability of the techniques used. Several experimental variables were suggested to explain the variability of the results. One of these explanations was lab contamination, as one of the groups has been working with this virus for a long time and all of the transcripts were from the same strain without detection of other common measles virus strains. However, Ralston *et al.* argued that the difference arising between the laboratories cannot simply be explained by sensitivity of the techniques or experimental errors; therefore, research is still ongoing to clarify the role of viruses in PDB (Ralston *et al.*, 2007).

Despite the notion that viruses might have a role in PDB development, several pieces of evidence oppose the viral aetiology of PDB, and these can be summarised as follows:

- Using more sensitive assays such as *in situ* hybridization (ISH), one group showed that samples of peripheral blood from PDB patients were positive for measles virus (Reddy *et al.*, 1999a), whilst other groups failed to detect the same virus using ISH-RT-PCR or ISH in bone samples (Helfrich *et al.*, 2000)
- The prevalence of these viruses is fairly equal worldwide and they infect humans at a young age, which does not explain the geographic differences in PDB prevalence (Cooper *et al.*, 2006).
- The inclusion bodies are not exclusive for PDB, for example similar inclusions are found in FEO (Wallace *et al.*, 1989).
- The characteristics of osteoclasts in PDB accompanied by IBMPFD have high similarity with classical PDB; and it should be noted that this type of syndrome results from mutations in *VCP* rather than *SQSTM1* and without contribution of virological factors (Hübbers, *et al.*, 2007; Watts *et al.*, 2007; Bersano *et al.*, 2007; Helfrich *et al.*, 2008)
- Some viruses can hijack microtubule routes used by autophagy machinery to deliver aggregates for degradation, by mimicking the normal functions of dynein (Helfrich *et al.*, 2008; Wileman *et al.*, 2007)
- Importantly, these structures 'viral' inclusions might be simply aggregates of proteins which have not been degraded by normal cellular degradation mechanisms, such as the proteasome system and autophagy (Ralston *et al.*, 2008).
- Some patients showed viral antigens without detection of inclusion bodies (Mills *et al.*, 1988).

- The location of these inclusions in the nucleus is also intriguing, since usually virus replication and transcription occur in the cytoplasm rather than in the nucleus (Helfrich *et al.*, 2000).
- No intact virus has yet been fully isolated from Pagetic osteoclasts.
- Finally, the most recent research (Ralston *et al.*, 2007; Matthews *et al.*, 2008) showed no evidence of paramyxovirus protein or nucleic acids in Pagetic bone samples or peripheral blood using a wide range of techniques, including nested RT/PCR, immunohistochemistry, and ISH.

1.9 Role of environmental factors in PDB pathogenesis

In the last 30 years, strong evidence for a decline in PDB was noted in some countries such as Great Britain, New Zealand and Spain. In support of this decline, offspring who inherit the *SQSTM1* mutation have less extensive phenotypes than their parents, being diagnosed at later age and with reduced penetrance (Bolland *et al.*, 2007).

Interestingly, PDB decline is so rapid that it negates the possibility of genetic dilution (Cundy *et al.*, 2006); therefore it is proposed that environmental factors are causing this decline (Van Staa *et al.*, 2002; Cundy *et al.*, 1997; Morales-Piga *et al.*, 2002). However, the specific environmental factors are still unknown and several suggestions have been made to explain the possible causes of PDB decline including changes in diet, physical activity, oral bacteria, zoonotic infections and viruses (Cundy *et al.*, 2006).

An interesting study in Lancashire linked arsenic, which was used in the cotton mill industry, to PDB development. Lancashire historically had a

high rate of PDB in Britain (Lever *et al.*, 2002) and *in vitro* studies showed osteoblasts treated with arsenic had high levels of p62 expression and ubiquitylation (Aono *et al.*, 2003).

Moreover, studies in Italy and Spain showed that people living in rural areas were more susceptible to develop PDB, supporting the role of zoonotic factors, also in some studies ownership of dogs and cats are linked to PDB (Gennari *et al.*, 2006; Lopez-Abente *et al.*, 2003).

Nevertheless, it should be noted that vaccines developed against canine distemper virus (~1955) and measles virus (~1970) precede the decline in PDB in New Zealand (Cundy *et al.*, 2006), therefore these observations might indicate that vaccine introduction did not cause PDB decline.

Obviously, it is difficult to prove which factor(s) might be a possible trigger of PDB and further research is still needed in this area.

1.10 PDB mouse models

Several PDB mouse models (involving p62 mutation) have been generated by different groups in recent years, in an attempt to understand the role of p62 in bone physiology *in vivo* and *in vitro*. The phenotypes of the models are discussed in detail below

1.10.1 P392L knock-in mice

P392L knockin mice were generated by targeting cells of the osteoclast lineage (Kurihara *et al.*, 2007). P392L mice did not exhibit full development of pagetic phenotypes, which strengthens the idea that other factors are necessary for full PDB development. Although the mice did not

develop full pagetic phenotypes, they did however show progressive bone loss, increased number of osteoclasts, but without parallel increase in osteoblast activity (Kurihara *et al.*, 2007). Osteoclast precursors from P392L transgenic mice had some phenotypic similarity to pagetic cells, such as hyper-responsivity to RANK-L, TNF- α and increased NF- κ B signalling. Nevertheless, the cells were not hyper-responsive to 1,25-(OH) $_2$ D $_3$, didn't have increased expression of TAF(II)-17, and did not show increased numbers of nuclei (Kurihara *et al.*, 2007).

1.10.2 S409X mouse model

A truncating p62 mutant mouse model (S409X), which is a mutation that has not been found in humans, was generated (Rojas *et al.*, 2007).

In contrast to the P392L mice, S409X animals developed focal osteolytic lesions and other features of pagetic phenotype. This difference in the mice phenotypes between the two mutations might be due to the fact that the truncating mutations S409X inhibit normal functions of p62 more effectively than the missense P392L mutation. Another reason for the difference might lie in the cell lines which the mutations were introduced to, as P392L was introduced to mature osteoclasts, whilst S409X was germ line, more closely resembling the origin of the mutations in humans (Ralston *et al.*, 2008).

1.10.3 p62 knockout mice

Although p62 knockout mice have a similar phenotype properties to wild type mice (Duran *et al.*, 2004) and do not show signs of osteopetrosis, the animals do show impaired osteoclastogenesis upon stimulation with both RANK-L *in vitro* and PTHrP *in vivo* (Duran *et al.*, 2004). p62 knockout mice also have greater susceptibility for late onset obesity, accompanied by diabetic phenotypes, such as insulin resistance (Rodriguez *et al.*, 2006).

p62 knockout mice had normal liver and neurons, the mice neither developed neurodegeneration nor formed inclusion bodies in neurons (Komatsu *et al.*, 2007). In p62 knockout mice basal osteoclastogenesis was unaffected, while stimulated osteoclastogenesis was defective, in which bone cells were challenged by PTHrP, which makes the osteoclasts hyper-responsive to PTHrP *in vivo* (Li *et al.*, 2000). The mice induced with PTHrP had larger bone volume and some other phenotypic differences when compared to wild type mice (Duran *et al.*, 2004). Upon stimulation with PTHrP, IL-6 expression was shown to be decreased in p62 knockout mice, although RANK-L expression was not affected by PTHrP stimulation, consistent with increased IL-6 expression in pagetic patients (Roodman *et al.*, 1996). p62 knockout mice showed impaired autophagy, as the mice suppressed inclusion bodies in hepatocytes and neurons (Komatsu *et al.*, 2007).

1.10.4 MVNP mouse models

Two different *MVNP* genes [one of the sequences was from the Edmonston strain (E-MVNP), the second one isolated from a PDB patient (P-MVNP)] were targeted independently to OCL lineage of mice, using the TRACP promoter, which is highly expressed in OCLs and OCL precursors (Kurihara *et al.*, 2006). OCL precursors from the two variants had common characteristics of Pagetic OCL precursors, which can be summarized as: increased levels of OCL formation; large OCL size; multinucleation; and hyper-responsivity to $1,25(\text{OH})_2\text{D}_3$. Noticeably, the OCLs were not hyper responsive to RANK-L, suggesting that other factors might contribute to the response of Pagetic OCLs toward RANK-L.

The OCL from the P-MVNP animals also expressed high levels of IL-6, consistent with Pagetic bone phenotypes. The mice had increased bone

volume and thickened trabeculae and these phenotypes developed in older mice, which might indicate that slow development of PDB may result from virus infection. In addition, bones from the two strains had bone lesions similar to Pagetic bone lesions, some monostotic in their nature. The fact that the two strains were associated with similar phenotypes was taken to imply that MVNP is directly linked to PDB (Kurihara *et al.*, 2006).

1.11 Aims and objectives

To further test the hypothesis that all PDB-associated p62 mutations cause impaired or loss of ubiquitin-binding (Cavey *et al.*, 2005; Cavey *et al.*, 2006), this study investigated in detail several newly-identified p62 mutations found in PDB patients. Different approaches were used to examine the ubiquitin-binding properties of the new PDB-associated mutants. The initial investigations were extended to examine the role of p62 in autophagy, as well as the functional roles of wild type p62 and PDB-associated mutant p62 in NF- κ B signalling.

The 'new' mutations analysed in the study are summarised below (Figure 1.2):

- a double missense mutation located within the UBA domain (P392L/S399P) (Eekhoff *et al.*, 2004)
- two missense mutations located outside of the UBA domain (D335E, A381V)
- a predicted product of G1205C splice-site mutation, which produces a p62 sequence lacking amino acids 351-388 (Δ 351-388) (Beyens *et al.*, 2006); this region is also outside the UBA domain and includes the site of the non-UBA domain A381V mutation.

Specific aims:

1) Effects of PDB mutations on the ubiquitin-binding properties of p62:

- to determine the effects of each of the mutations on ubiquitin-binding by p62 using *in vitro* protein pull-down assays at 37°C. To further examine the correlation between the ubiquitin-binding properties of p62 mutants and PDB disease severity, from analysis of the P392L/S399P double mutation (since patients with individual mutants

were reported to show a milder phenotype than those with the double mutations).

- to assess the ubiquitin-binding function of p62 using two dimensional Heteronuclear Single Quantum Coherence (2D-HSQC) protein NMR, a biophysical method that allows quantitative measurements of the association constant (K_a) between two proteins to be determined.
- to study the interaction of p62 and certain PDB mutants in a cellular context using confocal microscopy analysis of transfected U2OS cells.

2) Role of p62 in autophagy and effects of PDB-associated mutations

- to investigate the interaction properties of wild type p62 with LC3 (an autophagic marker) using confocal microscopy analysis of co-transfected U2OS cells.
- to determine the role of p62 in autophagosome formation; since autophagosome formation requires both p62 and LC3 (Bjørkøy *et al.*, 2005; Pankiv *et al.*, 2007) and the PDB-associated D335E mutant of p62 is located within the LC3-binding region of p62 (Pankiv *et al.*, 2007), we also investigated the effect of this missense mutation on the autophagosome formation using confocal microscopy.

3) Functional roles of wild type p62 and PDB-associated mutants on NF- κ B signalling

- initially, to use luciferase reporter assays to assess the effect of wild type and mutant p62 on signalling in HEK293 cells co-transfected with an NF- κ B luciferase reporter construct.
- to determine the interaction properties of wild type p62 and PDB-associated p62 mutations with CYLD using confocal microscopy analysis of co-transfected U2OS cells.

- to investigate of the interaction properties of wild type p62 and PDB-associated p62 mutants with NEMO using confocal microscopy analysis of transfected U2OS cells.

CHAPTER 2

Materials and Methods

2 Materials and methods

2.1 DNA techniques

2.1.1 Plasmids

[Note: for vector maps see appendix]

A starting point for this study was the provision of plasmids pGEX-4T1-WT-p62 and pcDNA3.1-WT-p62, previously produced in the lab, which allow the expression of wild type sequence human p62 (440 residues) in prokaryotic and eukaryotic host cells, respectively. pGEX-4T1-WT-p62 encodes a GST-p62 fusion protein and pcDNA3.1-WT-p62 a polyHis-FLAG-p62 fusion protein. Both were provided as frozen (15% glycerol) stocks, stored at -80°C.

- The pcDNA3.1 construct for expression of LC3 as a fusion with tdTomato (tdTomato-LC3), a red fluorescent protein (Bjørkøy *et al.*, 2005), was kindly provided by T. Johansen, University of Tromsø, Norway.

- The pcDNA3.1 construct for expression of CYLD as a fusion with a HA tag, was kindly provided by Dr. S.C. Sun, University of Houston.

- The NF-κB reporter construct was provided by Dr. Thilo Hagen, Wolfson Digestive Diseases Centre, University of Nottingham.

- The pcDNA3.1 construct for expression of ubiquitin as a fusion with a HA tag, was also kindly provided by Dr. Thilo Hagen.

2.1.2 Plasmid DNA preparation

[Note: for buffers and reagents see 2.7.5]

The method is based on alkaline lysis of bacteria, followed by adsorption of DNA

on a silica gel membrane in the presence of high salt (www.biocompare.com). Bacteria were grown overnight in 10ml of LB/ampicillin (see 2.7.1) and cell pellets were collected by centrifugation. After removing the supernatant, the pellets were re-suspended using 250µl of buffer P1, then the suspension was transferred to a microcentrifuge tube (at this step no cell clumps should be visible). The suspension was lysed using 250µl of P2 with the tube being inverted six times, resulting in a viscous and slightly clear solution. After a maximum of five minutes, 350µl of neutralization buffer (N3) was added, followed by mixing immediately by inverting the tube 10 times until the solution become cloudy (to avoid localized precipitation). Following centrifugation for 10 minutes at 13,000 RPM the supernatants were transferred to QIAprep spin columns, which were centrifuged for 60 seconds at 13,000 RPM. The flow through was discarded and the column was washed using 500µl PB buffer, followed by centrifugation for a further 60 seconds. The flow through was again discarded, and columns were washed using 750µl of buffer PE with centrifugation for 60 seconds. The flow through was discarded and a final 60 second centrifugation was performed to remove residual wash buffer. The last step to collect the DNA involved placing the QIAprep spin columns in clean 1.5ml microcentrifuge tubes, followed by addition of 50µl of nuclease-free deionised water. After 1 minute, centrifugation of the columns for 1 minute was carried out and the eluant which contains the purified plasmid DNA was collected, and stored at -20°C.

2.1.3 DNA electrophoresis

1% (agarose in TAE) gels were prepared by melting the agarose using a microwave for approximately two minutes. After cooling and mixing, 1µl of ethidium bromide (which binds DNA and emits light upon UV excitation) was added to the mixture, followed by pouring the gel in horizontal gel tank, with the insertion of an appropriate comb and leaving to set for at least 20 minutes. After loading the samples, the tank was filled with TAE buffer and electrophoresed at a

constant voltage of 150V (for approximately one hour). Bands were visualised on a UV Transilluminator.

2.1.4 Measurement of DNA concentration

DNA concentration was measured using a NanoDrop (ND-1000) spectrophotometer (NanoDrop Technologies). The spectrophotometer is blanked twice using 1 μ l sterile deionised water, then 1 μ l sample is introduced directly without dilution to the spectrophotometer. The purity of the sample is monitored by observing the numerical outcome of $A_{260/280}$ ratio on the spectrophotometer ($A_{260/280} \geq 1.8$ indicates pure DNA, $A_{260/280} \leq 1.8$ indicates presence of impurities, such as proteins and aromatic compounds (for example, phenol), while $A_{260/280} \geq 2$ indicates possible RNA impurities).

2.1.5 Storage of plasmid DNA

DNA samples prepared using the Qiagen miniprep purification kit (see 2.1.2), were kept at -20°C .

2.1.6 DNA Sequencing

All DNA sequencing was performed by the Biopolymer Synthesis and Analysis Unit (BSAU), School of Biomedical Sciences, D95, D floor, Medical School, The University of Nottingham. The sequencing was performed with the use of an ABI PRISM® 3130 Genetic Analyzer, using dye terminator chemistry (Big Dye version 3.1). The sequences were analysed using the ebi.ac.uk/clustalw alignment tool, and ChromasLite software (version 2.01) was used for chromatogram analysis.

2.2 Mammalian cell culture methods

2.2.1 Cell handling

U2OS or HEK293 cells (obtained from ATCC) were grown in DMEM growth medium (see 2.7.1), which contains the nutrients necessary for cell culture. The cells were kept humidified in 75 cm² Corning cell culture flasks in a 5% CO₂ 37°C incubator. The cells were split every 48 hours or when they reached approximately 90% confluency, with regular inspection for contamination.

2.2.2 Passaging cells

When the cells reached ~90% confluency they were subcultured. Prior to splitting, EDTA-Trypsin enzyme (see 2.7.1) and the DMEM media were equilibrated to room temperature. After discarding the old DMEM media, the cells were washed with 5ml DPBS (see 2.7.3), followed by introducing 3ml of Trypsin solution for 10-15 minutes to cells in the humidified 5% CO₂ 37°C incubator, then the detached cells were diluted at a ratio 1:20 with DMEM growth media, and kept humidified in the 5% CO₂ 37°C incubator.

2.2.3 Thawing cells

Frozen cells stored in liquid nitrogen were thawed in a 37°C water bath, and transferred to 10ml of DMEM growth medium followed by centrifugation at 1000 RPM for 5 minutes. The pellets were re-suspended in a fresh 5 ml of DMEM growth medium and grown as usual in the humidified 5% CO₂ 37°C incubator.

2.2.4 Cell freezing and storage

Cells were subcultured as above (2.2.2) then centrifuged at 1000 RPM for 5 minutes. After decanting the supernatant, the pellets were re-suspended in 1ml cell freezing media (see 2.7.1), which helps maintain the cells in a cryopreserved

state. Before storing them in liquid nitrogen, the cells were first stored at -80°C for one or two days.

2.2.5 Counting cells with a haemocytometer

Prior to performing this procedure, the cover slip and the counting chamber were cleaned carefully with ethanol and properly dried. The cells were washed with DPBS, then were detached from the flask using trypsin enzyme and diluted with DMEM to an appropriate dilution volume to avoid overloading the chambers. Then the cover slip was placed on the haemocytometer followed by introducing $5\mu\text{l}$ of the suspension carefully to both chambers of the haemocytometer, the rest of the suspension were left to cover the whole chamber through capillary force. Average numbers of cells were counted using a light microscope as indicated below.

The haemocytometer is divided to several squares; since each square is equal to a volume of 0.1mm^3 (10^{-4}cm^3), and 1ml is equal to 1cm^3 , hence the total cell number per 1ml solution was determined according to the following equation:

$$\text{Cells/ml} = (\text{Average count}) \times 10^4 (\text{chamber conversion factor})$$

$$\text{Total cells} = (\text{cells/ml}) \times (\text{original volume of solution})$$

2.2.6 Transient co-transfection based on non lipid based transfection reagent

$\sim 60\%$ confluent cells (U2OS) were split and left to grow on 19mm cover slips (VWR International) in 12 well plates. 1ml DMEM growth medium was added to the wells. The cells were left to grow at least for 24 hours before performing transient co-transfection of the exogenous plasmids. This was achieved by mixing $0.25\mu\text{g}$ of each of the plasmids in separate eppendorfs; then a mixture of $50\mu\text{l}$ serum free medium (Opti-MEM; see 2.7.1) and $1.5\mu\text{l}$ transfection reagent, GeneJuice (Novagen; composed of non-toxic cellular protein and a small amount of novel polyamine), was incubated at room temperature for five minutes,

followed by introducing the plasmids to the latter mixture with gentle mixing and incubating for 20-30 minutes at room temperature. To avoid sudden pH changes, the final mixture was added drop wise to the U2OS cells and the cells were incubated in the humidified 5% CO₂ 37°C incubator for ~ 48hours.

2.3 Indirect immunofluorescence confocal microscopy

Before starting the procedure, PBS buffer (see 2.7.3) was sterilised in an autoclave, left to equilibrate to room temperature and kept at 4°C.

DMEM media was discarded from cells and the cover slips were washed 3X with PBS. The cells were fixed by incubating with 1ml of fresh cold 4% formaldehyde for five minutes at room temperature, and then the cells were washed with 3X PBS and quenched for 5 minutes with 3X 100mM glycine. Later the cells were washed 3X for 5 minutes with PBS, followed by permeabilising with 0.2% (v/v) Triton-X100 for 10 minutes at room temperature. Blocking of non-specific sites was performed by incubating the cells with a PBS solution containing 0.5% (w/v) fish skin gelatin and 0.2% (w/v) BSA (99.9% purity; Sigma-Aldrich) at room temperature, for 1 hour.

After the blocking step, primary and secondary antibodies were introduced to the cells as follows:

- the cells were washed 3X with PBS and the primary antibody mixture (mouse anti-p62 and rabbit anti-HA; see 2.7.2) were introduced to the cells with a dilution ratio of 1:500 in PBS and incubated for one hour at room temperature.
- cells were washed with PBS 3X, and the secondary antibody mixture (AlexaFluor488 anti-mouse and AlexaFluor 568 anti-rabbit; see 2.7.2) was diluted in PBS (1:1000) and incubated for 1 hour at room temperature.
- 1 ml Hoechst 33258 (1:20,000) in PBS was used to stain the nuclei for five minutes and cells were washed 3X with PBS; 50µl mounting media

(Glycerol/PBS) was applied to the cover slips, followed by sealing the cover slips to microscopic slides with toluene and formaldehyde free nail polish.

- finally, slides were kept at 4°C in the dark until visualized with a Leica TCS SPII confocal microscope.

2.3.1 Confocal microscopy

All images were collected using a Leica TCS SPII confocal microscope, with a 63X objective lens, with 20 averaged sequential scanning images collected. The images were analysed and processed using LCS Lite software.

2.4 NF-κB reporter assays

2.4.1 Preparation of NF-κB reporter construct

An NF-κB luciferase reporter construct was generated by Dr. Thilo Hagen. The reporter gene is composed of a fusion in which an IL-8 promoter (with an NF-κB consensus sequence) is ligated in to a luciferase pGL2 vector (Promega). The expression of the luciferase enzyme is under control of the IL-8 promoter (which has the NF-κB response element), therefore the amount of luciferase enzyme activity is proportional to the activity of the promoter in the fused gene.

2.4.2 Transient co-transfection of p62 and NF-κB reporter constructs using polyamine based (non lipid based) transfection reagent

This assay is based on transiently co-transfecting the polyHis-FLAG-p62 constructs with the NF-κB reporter in HEK293 cells, followed by measuring the NF-κB activity through the amount of the light detected from the luciferase enzyme using a luminometer; the assay was performed with the Steady Glo kit from Promega.

Before starting the transfection procedure, HEK293 cells were grown in 12 well

plates, in DMEM growth media, in a humidified 5% CO₂ 37°C incubator until they reached 70% confluency. Cells were transfected as follows: 0.3 µg of NF-κB reporter construct was mixed with 0.2 µg of wild type or mutant polyHis-FLAG-p62 pcDNA3.1 (or empty pcDNA3 vector for the control) at room temperature, then a mixture of 100µl of serum free medium (Opti-MEM) and 2.1µl of genejuice transfection reagent (Novagen) was prepared and incubated at room temperature for five minutes, followed by addition of the two plasmids to the transfection mixture and incubating for 15 minutes at room temperature. The final mixture was added drop wise to the 70% confluent HEK293 cells. After 24 hours, the cells were equilibrated to room temperature, then the old media was discarded and 80µl of the luciferase reagent (prepared by mixing one bottle of Steady Glo buffer with one bottle of Steady Glo substrate, provided with the kit) was added to each well, and the cells were incubated for 5 minutes at room temperature with rocking. Then the cells were re-suspended, and the lysates were added to a luminometer tube; the amount of the light emitted were measured quickly. Each measurement was performed in duplicate, and each assay was performed in triplicates, with the mean values of the results analysed statistically using PRISM4 software.

2.5 Western blotting and immunodetection techniques

2.5.1 Sodium dodecyl sulphate polyacrylamide-gel electrophoresis (SDS PAGE)

A mixture of 5% (10ml) acrylamide resolving gel and 20% (10ml) acrylamide resolving gel, with the addition of 100µl AMPS and 10µl TEMED (added at the last step; since they are the catalysers of gel polymerization) was poured using gradient caster to generate a 5-20% gradient gel. Water-saturated butanol was immediately over-layered on to the gel, which was left for at least 30 minutes until polymerisation had taken place. The butanol was then removed using deionised

water. The stacking gel was poured (5ml stacking gel buffer, and 1ml of 30% acrylamide, with the addition of 100 μ l AMPS and 10 μ l TEMED), and a correct sized comb was inserted to form the loading wells. The gel was left for at least 20 minutes to polymerize, followed by the careful removal of the comb. The gel was then transferred to an ATTO electrophoresis unit (GRI), in which SDS-PAGE running buffer is poured, and used to wash the lanes of the gel to remove any debris. After setting up the electrophoresis unit appropriately and loading the samples, gels were run at a constant current of 40mA until the bromophenol blue dye reached the bottom of the gel.

2.5.2 Coomassie blue staining of SDS-PAGE gels

When protein staining was required, the SDS-PAGE gel was shaken carefully for one hour in Coomassie blue staining solution (see 2.7.1), then to remove background staining the gel was de-stained by incubation overnight with de-staining solution (see 2.7.1).

2.5.3 Western blotting

When required, proteins resolved by SDS-PAGE were transferred to nitrocellulose membrane (Hybond-C extra, GE Healthcare), by laying the gel on to the nitrocellulose membrane and layering between two western buffer-soaked filter papers. After elimination of the bubbles produced during the sandwiching of gel, the nitrocellulose membrane was directed to the positive anode of the western blotting unit (Fisher Scientific) then the sandwich was left over night to be transferred using a constant current of 40mA. The proteins on the membrane were reversibly visualized with Ponceau staining (see 2.5.4).

2.5.4 Ponceau S staining of nitrocellulose membranes

The proteins on the nitrocellulose membrane were visualized by shaking the membrane slowly in Ponceau S (see 2.7.1) solution for approximately two

minutes, followed by washing the membrane in deionised water, to eliminate background staining. For complete de-staining, the membrane washed several times with TBS (see 2.7.3).

2.5.5 Immunodetection

[For ubiquitin-Sepharose binding assays (anti-p62 immunodetection)]

The nitrocellulose membrane was blocked in blocking buffer for one hour, in order to block non-specific binding sites. After incubation of the nitrocellulose membrane in the primary antibody (anti-p62), the membrane was washed at least four times in TBS for approximately 30 minutes to eliminate non-specific binding, then the membrane was incubated with the secondary antibody (Peroxidase-Conjugated Rabbit Anti-Guinea Pig immunoglobulins (PRAG) for one hour, and washed again in TBS for 4X. Immunoreactive bands were visualised using high performance chemiluminescence film (Hyperfilm™, GE Healthcare), and the film developed by an automatic developing system (Curix 60 processor, Agfa Gevaert Ltd.). Before exposure to the films, the nitrocellulose membrane was agitated gently for one minute in Enhanced Chemiluminescence Reagent (Western lightning™, PerkinElmer Life Sciences) and sealed in cling-film. The emitted light from the membrane was left to react with the film for one minute or more depending on the sensitivity of the antibodies.

[For anti-ubiquitin immunodetection]

Before blocking the nitrocellulose membrane it was first autoclaved; this was done by sandwiching the membrane between two filter papers soaked in TBS, then holding them between two glass plates, followed by autoclaving the plate for approximately one hour. This step is to increase the sensitivity of the ubiquitin antibodies. The rest of the method is identical to that for detecting p62, with the use of appropriate anti-ubiquitin primary and PSAR secondary

antibodies (see 2.7.2). The same protocol was applied to detect other proteins through out the thesis, but simply changing the antibodies as appropriate (see 2.7.2).

2.5.6 Detection of expression levels of overexpressed plasmids in cells using immunoblotting

The transfected cells were introduced to 1ml gel application buffer (GAB; see 2.7.3) and incubated for 5 minutes at room temperature. Then 50µl of the lysates were subjected to SDS-PAGE (see 2.5.1) and further immunodetection (see 2.5.5) using mouse anti-p62 diluted 1:1000 (or other antibodies depending on the experiment) as a primary antibody, and peroxidase-conjugated swine anti-mouse (PSAR) immunoglobulins diluted 1:2000 as secondary antibody (see 2.7.2). To detect the amount of expressed HA-ubiquitin, the blot was stripped using 10ml stripping reagent for 15 minutes, then the same steps for immunodetection were repeated to detect the bound proteins with the use of 1:1000 rabbit anti-HA antibody and 1:2000 peroxidase-conjugated swine anti-rabbit (PSAR) immunoglobulins (see 2.7.2).

2.6 General laboratory methods

2.6.1 Preparation of chemically competent bacterial cells

XL10-Gold *E. coli* bacterial cells were treated with (CaCl₂) to make them competent for plasmid transformation. 300 ml of autoclaved LB was inoculated with 10ml overnight cultures of XL10-Gold cells (obtained originally from Stratagene) and incubated at 37°C in a shaking incubator until the OD₆₀₀ of the culture reached 0.4-0.5 (this range is critical to obtain high quality competent cells), then the cells were cooled on ice for 20 minutes (it is necessary to keep all the solutions at 4°C and on ice during mixing steps). The culture was

centrifuged, using a Beckman Avanti J-25 centrifuge, at 4000 RPM for 20 minutes at 4°C and the supernatant was discarded, while the pellets were suspended with cold sterile MgCl₂ (0.1M). The suspension was centrifuged again at 4000 RPM for 20 minutes at 4°C, followed by discarding the filtrate and incubating the cells with cold sterile CaCl₂ (0.1M) at 4°C for 20 minutes. The cells were harvested by centrifugation at 4000RPM, 4°C for 20 minutes. Finally, the cells were stored in 400µl aliquots in a mixture of 86% cold CaCl₂ and 14% glycerol at -80°C.

2.6.2 Oligonucleotide mutagenic primer preparation

Mutagenic primers were synthesised by the BSAU, School of Biomedical Sciences, D95, D Floor, Medical School, The University of Nottingham using an Applied Biosystems model 394 DNA Synthesizer; the preparation is based on solid phase synthesis methodology.

2.6.3 Site-directed mutagenesis

The procedure follows the instructions in the QuikChange® Site-Directed Mutagenesis Kit (Stratagene). For every mutation created a control reaction were carried out in which the same protocol were performed, but without the addition of PfuTurbo DNA polymerase to the reaction mixture. A mixture of the following solutions was prepared in a thin-walled PCR tube, giving a final volume of 50µl.

For full-length p62 and 341-440 constructs:

5 µl 10×Pfu reaction buffer

1 µl (final concentration 40 ng/µl) of the template (plasmid)

3 µl (final concentration 125 ng/µl) of oligonucleotide forward primer

3 µl (final concentration 125 ng/µl) of oligonucleotide reverse primer

3 µl DMSO

1 µl (10mM) of dNTP mixture

33.5µl Autoclaved sterile dH₂O to a final volume of 50µl

0.5 µl PfuTurbo DNA polymerase (2.5 U/µl)

The mixture (without polymerase) was placed in a thermocycler and the lid heated until it reached 95°C, then the reaction mixture were left to cool for two minutes on ice, prior to introducing the DNA polymerase (quickly with gentle mixing). After this time the PCR mutagenesis program was continued according to the following cycling programme:

Segment	Cycles	Temperature	Time
1	1	95°C (initial denaturation step)	30sec
2	18	95°C (denaturation step)	30sec
		55°C (annealing step)	1min
		68°C (extension step)	7min
3	cooling reaction	4°C	-

At the end of the last cycle, 1µl of the restriction enzyme *DpnI* was added to the mixture on ice, followed by incubation at 37°C for one hour, to allow the complete digestion of the non-mutated template. Finally, the mutated plasmid was transformed in to XL10-Gold bacterial cells (see 2.6.4).

2.6.4 Transformation of Plasmid DNA to XL10-Gold® competent cells

200µl of XL10-Gold competent cells were mixed with 5µl of the digested plasmid and left on ice for 30 minutes, followed by heat shocking the mixture at 42°C, for 30 seconds and incubating on ice again for five minutes. The cells were inoculated into 800µl sterile LB, and incubated at 37°C in a shaking incubator for one hour. The culture was spun down at 5000 RPM for two minutes, and the pellets were re-suspended in 50 µl of LB. Suspensions were plated out on agar/LB plates (see 2.7.1) and spread with a sterile spreader over the plate, followed by incubation overnight at 37°C.

2.6.5 GST-fusion protein expression

The pGEX-4T1 plasmid allows expression of the cloned protein (in this case p62) fused with GST in *E. coli* and confers ampicillin-resistance to the host cells (allows the replication only of the bacteria that contain the plasmid). Cells were grown overnight with shaking at 37°C in 10ml of LB, with the addition of ampicillin (see 2.7.1) (1:1000). The next day, cells were diluted (1/50) in ampicillin/LB and grown for three hours at 37°C (1:1000); to induce recombinant gene expression IPTG (see 2.7.1) to a final concentration of 200µM was added, then the bacterial cells were grown for a further four hours at 37 °C. The pellets were collected by centrifugation and stored at -20 °C.

2.6.6 Bacterial storage

500µl of 10 ml overnight cultures were made up to 500µl with filter sterilised glycerol (Sigma) and stored in a cryovial tube at -80°C.

2.6.7 Preparation of ubiquitin-Sepharose

[Note: Control Sepharose was prepared in parallel without the addition of ubiquitin].

Cyanogen bromide-activated-Sepharose 4B (Sigma) was swollen for 15 minutes in 0.1M HCl solution, transferred to a polyprep column (BioRad) and washed further in HCl. The Sepharose was then washed with 5 bed volumes of coupling buffer (see 2.7.4). The polyprep column was capped and the Sepharose incubated on a rotary mixer for 2 hours at 4°C in a solution of ubiquitin (10 mg of purified bovine ubiquitin (Sigma) per 1 ml of Sepharose) in coupling buffer. The Sepharose was washed extensively with coupling buffer and then incubated in ethanolamine solution on a rotary mixer overnight at 4°C. The Sepharose was then washed alternatively (4 times with 10 bed volumes) with acetate and Tris buffer (see 2.7.4) and then in column storage buffer (see 2.7.4). The Sepharose was stored at 4°C as 50% slurry in column storage buffer.

2.6.8 Measurement of protein concentration using the Bradford assay

This assay was first described by Bradford *et al.*, 1976. Its basic principle depends on the binding between Coomassie brilliant blue dye G-250 with arginyl and lysyl residues of proteins. 8 diluted standards (0, 5, 10, 20, 25, 30, 40 and 50µg), which were prepared from a stock solution (1 mg/ml of BSA in H₂O or a buffer used to prepare the protein under study) were used to generate a calibration curve. The final volume of each of the standards was 50µl. The unknown proteins were diluted to a final volume of 50µl, and the assay was performed by mixing 150µl of Bradford reagent (see 2.7.1) to both of the standards and the unknowns, followed by incubation for 2 minutes at room temperature. The standards and the unknowns were measured in duplicate by introducing the samples to a microplate spectrophotometer (SpectraMax 340PC384) in 96 well plates (Falcon) and reading the absorbance at a wavelength of 630nm.

2.6.9 Ubiquitin-Sepharose binding assay

50µl aliquots of glutathione-Sepharose (GE healthcare), control-Sepharose and ubiquitin-Sepharose beads (see 2.6.7) were washed once in 1ml TBSTr (see 2.7.3). Bacterial supernatants (100µl; derived by sonicating a 10ml culture prepared as in section 2.6.5 in 1ml TBSTr, and centrifugation at 13,000 RPM in a microfuge) containing the wild type and mutant GST-p62 proteins were incubated for 30 minutes at 37°C with the three types of beads, with mixing every few minutes to ensure complete binding. To eliminate unbound and non-specific binding proteins the beads were washed three times in TBSTr (1ml) and the bound protein were eluted using GAB, by heating at 95°C for five minutes. The eluted proteins were analyzed using SDS-PAGE (see 2.5.1), and the bound GST-p62 was detected by immunodetection (see 2.5.5) with anti-p62 antibodies (see 2.7.2).

2.6.10 Large scale protein purification

20 ml overnight cultures of XL10 Gold cells transformed with the GST-p62 plasmid (residues 341-440 including the P392L change) were inoculated to 1000ml sterile medium (Amp/LB 1:1000µl) and left to grow for three hours at 37°C in a shaking incubator. Recombinant protein was expressed by the addition of 2ml IPTG (1:500) followed by incubation for 10 hours at 30°C in a shaking incubator, then the cells were collected in 1 litre centrifuge tubes and were centrifuged at 4000 RPM, 4°C, for 10 minutes. The pellets were washed in TBS (10ml/4°C), and the suspension were transferred to 50ml Falcon tubes and re-centrifuged at 4000 RPM, 4°C, for 10 minutes. The pellets were stored at -80°C. The next day, the pellets were re-suspended in a mixture of 10ml TBS and 10µl of Benzonase® Nuclease (Novagen) and sonicated on ice at 6 microns for 5x30seconds, with 30 second breaks to allow cooling of the mixture. 10µl of protease inhibitor (Sigma-Aldrich) was added to the mixture and the sonication

step was repeated as before. The mixture was centrifuged using a Beckman Avanti J-25 at 4°C, 17010 RPM (35000g) for 35 minutes.

If the filtrate had visible impurities, the filtrate was transferred to a new set of centrifuge tubes and the centrifugation step was repeated with the same conditions. Then the supernatant was bound for 6 hours at 4°C on a mixing rotator to 0.5ml of glutathione-Sepharose beads, which has been previously introduced to a poly prep chromatography column (Biorad) and washed twice in TBS, then glutathione-Sepharose beads were washed extensively with TBS (6X) and 1X TCB (see 2.7.3). At this stage 20µl of the beads were kept for further analysis using SDS-PAGE and Coomassie blue staining to check the purification of the fusion proteins. 10 µl (5 units/ml) of thrombin enzyme (Sigma-Aldrich) was introduced to the beads in a final volume of 1ml TCB and rotated overnight at 10°C. The 1ml digested protein was eluted and kept on ice, then the beads were washed with 3x 0.5ml TCB, and the eluted washes were pooled with the previous 1ml eluted protein, giving a final volume of 2.5ml. Finally, 20 µl EDTA (1M; pH 8) was added to the proteins, in order to stabilise the proteins. Since Ca^{+2} is necessary for enzymatic activities, EDTA is added to chelate the Ca^{+2} . The protein was kept at -20°C. 20µl of the cleaved proteins were subjected to SDS-PAGE analysis for Coomassie blue staining (see 2.5.2). Protein concentration was calculated using the Bradford assay (see 2.6.8). Thomas Garner in the School of Chemistry performed protein gel filtration as a final preparation step prior to protein NMR analysis.

2.7 Buffers and reagents

2.7.1 Reagents:

IPTG solution (Melford): (200mM, filter sterilised)

LB: Luria broth (25g/L)

Ampicillin (Fischer): (100µg/ml, filter sterilised)

Coomassie blue stain:

50% (v/v) methanol

20% (v/v) glacial acetic acid

0.12% (w/v) Coomassie Brilliant Blue R-250

Coomassie blue destain:

10% (v/v) methanol

10% (v/v) glacial acetic acid

Ponceau S staining solution:

0.1% (w/v) Ponceau S

5% (v/v) acetic acid

Bradford reagent (10X):

0.05% (w/v) Coomassie brilliant blue G250

50% (v/v) perchloric acid (HClO₄)

25% (v/v) Ethanol

25% H₂O

DMEM growth medium:

Dulbecco's Modified Eagle medium (DMEM)

10% (v/v) FCS

1% (v/v) penicillin/streptomycin

Trypsin:

0.5 g porcine trypsin (Sigma-Aldrich)

0.2 g EDTA·4Na per litre of Hanks' Balanced Salt Solution, plus phenol red

Opti-MEM (GIBCO™):

Reduced-serum medium (1X) liquid (Invitrogen), contains A GlutaMAX™-I medium. This includes the dipeptide L-alanyl-L-glutamine substituted on a molar equivalent basis for L-glutamine

Cell freezing medium:

90% (v/v) FCS

10% (v/v) DMSO

Agar/ampicillin plates:

(1.5% agar in LB (W/v), 100 µg/ml ampicillin)

Glutathione Sepharose beads 4B:

purchased from GE Healthcare.

2.7.2 Antibodies

- rabbit anti-ubiquitin antibody was prepared *in house* in the School of Biomedical Sciences, University of Nottingham.

- mouse anti-IKK γ was purchased from Abcam/UK.
- mouse anti-p62 was purchased from BD-Biosciences/UK.
- rabbit anti-HA was purchased from Sigma-Aldrich/UK.
- peroxidase-conjugated swine anti-mouse (PSAR) immunoglobulins was purchased from DAKO/UK.
- peroxidase-conjugated swine anti-rabbit (PSAR) immunoglobulins were purchased from DAKO/UK.
- Alexaflour488 anti-mouse and AlexaFluor 568 anti-rabbit were purchased from Invitrogen/UK.
- mouse anti- β -actin was purchased from Abcam/UK.
- mouse anti-FLAG was purchased from Sigma-Aldrich/UK.

2.7.3 Buffers

TAE (Tris acetic acid EDTA) buffer:

40 mM Tris (hydroxymethyl) methylamine

1 mM EDTA

pH 8 with 1.14ml glacial acetic acid

Blocking buffer:

5% (w/v) Marvel milk powder in TBS

TCB (Thrombin cleavage buffer):

50mm Tris (hydroxymethyl) methylamine

150mm Sodium Chloride

2mm Calcium Chloride

pH 8.3 with HCl

Ammonium acetate buffer:

25 mM Ammonium acetate

pH 7 with acetic acid

TBS (Tris buffered saline):

10mM Tris (hydroxymethyl) methylamine

150mM NaCl

pH7.5 with HCl

TBSTr:

0.1% (v/v) Triton X-100 in TBS

GAB (Gel application buffer):

150mM Tris (hydroxymethyl) methylamine

8 M urea

2.5% (w/v) SDS

20% (v/v) glycerol

10% (v/v) 2- β mercaptoethanol

3% (w/v) DTT (dithiothreitol)

0.1% (w/v) bromophenol blue

pH 6.8 with HCl

5% acrylamide resolving gel mixture:

5% (v/v) acrylamide

367mM Tris (hydroxymethyl) methylamine

0.13% (w/v) SDS

pH 8.8 with HCl

20% acrylamide resolving gel mixture:

20% (v/v) acrylamide

367mM Tris (hydroxymethyl) methylamine

0.13% (w/v) SDS

10% (v/v) glycerol

pH 8.8 with HCl

Stacking gel buffer:

0.14M Tris (hydroxymethyl) methylamine

0.1% (w/v) SDS

pH 6.8 with HCl

SDS-PAGE running buffer:

25mM Tris (hydroxymethyl) methylamine

0.1% (w/v) SDS

186mM glycine

Western transfer buffer:

25mM Tris (hydroxymethyl) methylamine

129mM glycine

20% (v/v) methanol

PBS: Phosphate buffered saline (Dulbecco A) Oxid, each tablet was dissolved in 100ml d H₂O, autoclaved and left to cool down. The solution has a pH of 7.3 at 25°C. Each tablet's typical formula is:

Component	(g/L)
NaCl	8
KCl	0.2
Na ₂ HPO ₄	1.15
KH ₂ PO ₄	0.2

DPBS: Dulbecco's Phosphate buffered saline (Sigma), liquid, sterile-filtered, cell culture tested. It has additional $\text{CaCl}_2 \cdot 2\text{H}_2\text{O}$, and $\text{MgCl}_2 \cdot 6\text{H}_2\text{O}$ the solution's typical formula is:

Component	(g/L)
$\text{CaCl}_2 \cdot 2\text{H}_2\text{O}$	0.113
$\text{MgCl}_2 \cdot 6\text{H}_2\text{O}$	0.1
NaCl	8
KCl	0.2
Na_2HPO_4	1.15
KH_2PO_4	0.2

2.7.4 Buffers used in preparation of ubiquitin-Sepharose beads

Coupling buffer:

100mM Sodium bicarbonate

500mM Sodium chloride, pH 8.3 with HCl

1M Ethanolamine, pH 8 with HCl

Acetate buffer:

100mM Sodium Acetate

500mM NaCl

pH 4 with acetic acid

Tris buffer:

100mM Tris (hydroxymethyl) methylamine

pH8 with HCl

Column storage buffer:

25 mM Tris (hydroxymethyl) methylamine

1mM sodium azide

pH 7.4 with HCl

2.7.5 Plasmid DNA purification solutions:

P1: re-suspension buffer (Tris-EDTA, RNAase added at the time of the experiment)

P2: sodium hydroxide (should be closed immediately after use, to prevent reaction with CO₂ in the air, which leads to pH change)

PE: guanidine hydrochloride/isopropanol (ethanol added at the time of the experiment)

N3: neutralization buffer, guanidine hydrochloride/acetic acid

PB: wash buffer (ethanol added at the time of the experiment)

2.8 List of software:

- **Igor Pro 5.0.5.7:** scientific graphing, data analysis, image processing and programming software tool from WaveMetrics.
- **Clustlaw2:** is a general purpose multiple sequence alignment programme for DNA from European bioinformatics institute (EBI).
- **PRISM 4:** is a combination of basic biostatistical, curve fitting and scientific graphing software from GraphPad.
- **Leica confocal software II:** is an imaging software from Leica.

CHAPTER 3

Interaction of PDB mutant p62 proteins with ubiquitin *in vitro*

Chapter 3: Interaction of PDB mutant p62 proteins with ubiquitin *in vitro*

3.1 Introduction

PDB has been linked to numerous mutations affecting the *SQSTM1* gene, to date several of which have been investigated at the level of protein function. The majority of these mutations are located within exon 8 of the *SQSTM1* gene and affect the UBA domain (residues 387-440) of the p62 protein. Since this region of p62 mediates its ubiquitin-binding properties, the functional effects of a number of PDB mutations were previously analysed using *in vitro* ubiquitin-binding (pull-down) assays. In summary the mutations were classified into those which showed complete loss of ubiquitin-binding in these assays, and those which showed reduced ubiquitin-binding, under the 'physiological' conditions used i.e. at pH7.5 and 37°C (Cavey *et al.*, 2005; Cavey *et al.*, 2006). These observations led to the proposal of a unifying hypothesis that all PDB-associated mutations of p62 cause loss or impairment of ubiquitin-binding, and this altered function is related to disease aetiology (Cavey *et al.*, 2006).

Subsequent to these initial analyses, several 'new' mutations have been identified in patients with PDB, including some outside of the UBA domain (located within exon 7 of the *SQSTM1* gene). In order to further test the above hypothesis, and in particular to determine if non-UBA domain mutations exert their effects *via* the same mechanism as UBA domain mutations, four 'new' PDB-associated PDB mutations (Figure 3.1) were selected, including three outside the UBA region, and initially analysed in the same *in vitro* ubiquitin-binding assays.

3.2 Clinical features associated with the 'new' PDB-associated p62 mutations

Two of the new mutations are non-UBA domain missense mutations, D335E and A381V, both of Italian origin that were first presented by our collaborators (Dr. ML Brandi and co-workers, University of Florence) at the International Symposium on Paget's Disease, 8-9th July 2005, Oxford UK, and subsequent to this work being completed published in a full paper (Falchetti *et al.*, 2009). The A381V mutation was identified in an Italian patient in 2000; the patient was diagnosed by scintigraphy with a positive scan in the sacrum and bilateral iliac regions. Alkaline phosphatase (ALP) levels were already increased in 1999 (577 I.U.) and sequencing of DNA samples showed the patient (and her son) harboured a heterozygous C to T transversion at position 1182 of exon 7, resulting in an alanine to valine substitution at codon 381. In the same individual exon 8 of the *SQSTM1* gene was sequenced to confirm the absence of any other associated p62 mutations. Whilst this work was in progress, the A381V mutation was also described by another group but only in combination with the P392L mutation (Collet *et al.*, 2007).

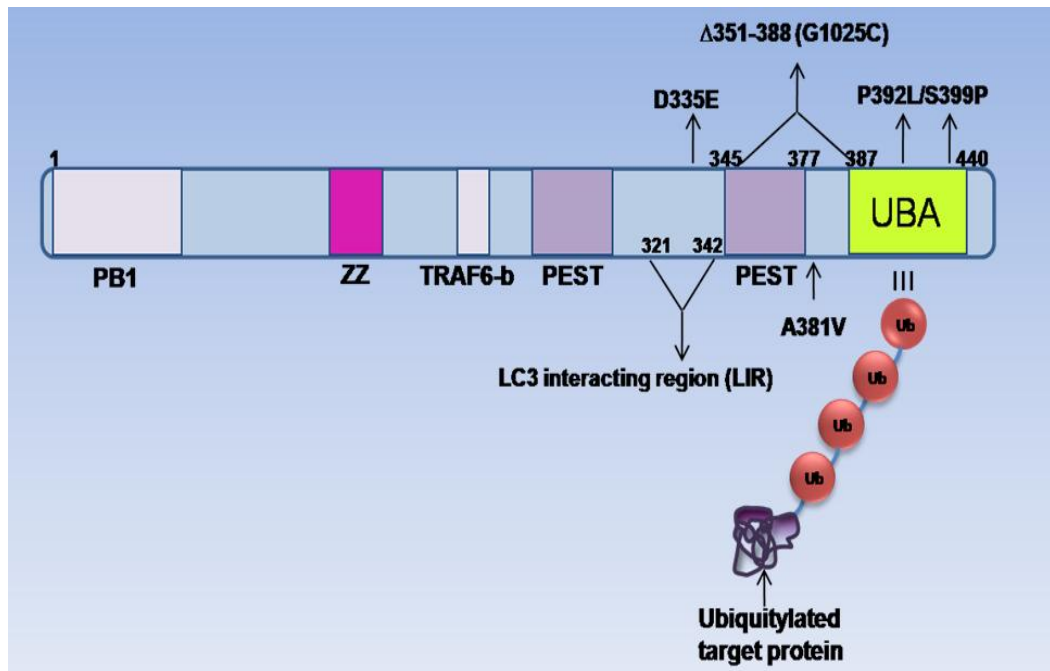


Figure 3.1: Schematic representation of the domain structure of p62 indicating sites of 'new' PDB mutations analysed in this study

The PDB mutations analysed in this study can be classified into those within the UBA domain (double mutation P392L/S399P) and those outside the UBA domain (D335E, A381V and Δ 351-388). A381V is located within a linker region between the UBA domain and second PEST sequence; D335E is located at N-terminal of the second PEST sequence; and Δ 351-388 results in a p62 protein that lacks almost the entire second PEST sequence. The double mutation (P392L/S399P) is located within the UBA domain. p62 binds to ubiquitylated protein substrates through non-covalent interactions involving its UBA domain and to LC3 through its LIR. Numbering relates to the position within the 440 amino acid sequence of the human p62 protein.

UBA, ubiquitin-associated domain; PEST sequence is rich in Proline (P), Glutamic acid (E), Serine (S), and Threonine (T); PB1 (Phox and Bem1) allows polymerisation of p62 with itself and other proteins containing PB1 domain; ZZ (zinc finger motif) mediates binding with RIP (receptor-interacting protein), which is necessary for NF- κ B activation; TRAF-b is the TRAF6-binding domain; LIR is the LC3-interacting region.

The D335E mutation was identified in an Italian patient in 1992 with no family history of PDB; the patient was diagnosed by scintigraphy with a positive scan exhibiting a monostotic lesion in the left femur. ALP levels were 129 I.U. before therapy and sequencing of DNA samples showed the patient harboured a heterozygous transversion of T to A at position 1047 of exon 7 (Falchetti *et al.*, 2004), resulting in an aspartate to glutamate substitution at codon 335. Again, exon 8 of the *SQSTM1* gene was sequenced to confirm the absence of any other associated p62 mutations.

The final non-UBA domain mutant analysed is equivalent to a predicted product of a splice donor site mutation, which lacks amino acids 351-388 of p62, found in American family (Beyens *et al.*, 2006). This results from a G1205C intron 7 mutation that gives rise to two abnormal mRNA transcripts, translation of which would result in the formation of a truncated p62 protein lacking most of the UBA domain (390X) as well as the p62 sequence analysed in this study (Δ 351-388). Patients carrying this mutation were reported to have a severe phenotype, with a very early age of onset and high levels of ALP, but the disease symptoms varied from none to hearing loss and cranial nerve palsies due to compression of nerves (Beyens *et al.*, 2006).

In addition we also analysed a 'double' UBA domain mutation, P392L/S399P, which involves two changes on the same allele, identified in a PDB patient from a Dutch colony in Suriname (Eekhoff *et al.*, 2004). Since previous work has proposed that there may be a relationship between the magnitude of the effects of different mutations on the ubiquitin-binding function of p62 and disease severity, and the carrier of the P392L/S399P double mutation had a more severe phenotype than individuals with the single missense mutations (nearly all of the skeleton was reported to be affected with pronounced deformities of the extremities, spine and skull), we used this double mutation

to further examine the correlation between the ubiquitin-binding properties of p62 mutants and PDB disease severity. Specifically, we wished to assess whether this double mutation had an additive negative effect on the ubiquitin-binding function of p62, compared to the effects exerted by individual missense mutations P392L and S399P.

3.3 Generation of prokaryotic expression constructs for PDB mutant p62 proteins

Previously in the lab, a construct which allows wild type human p62 to be expressed as a GST-fusion protein in *E. coli* was generated by introducing a p62 cDNA into the multiple cloning site of the pGEX-4T-1 plasmid (Cavey *et al.*, 2005). The D335E, A381V and Δ 351-388 mutations were each separately introduced into this wild type GST-p62 sequence by site directed mutagenesis following the instructions of QuikChange® Site-Directed Mutagenesis kit (Stratagene). The same protocol was used to generate a GST-p62 (P392L/S399P) double mutant, by introducing the P392L change in to a GST-p62 (S399P) construct generated in a previous study (Cavey *et al.*, 2006); a separate GST-p62 (P392L) mutant, as well as a GST-p62 (G425R) mutant, was also available in the lab (from (Cavey *et al.*, 2005)). Each mutant plasmid was analysed by DNA sequencing and resulting chromatograms were viewed using ChromasLite2 software (Figure 3.2). The presence of the mutations was confirmed by sequence alignment with the wild type p62 sequence using ClustalW2.

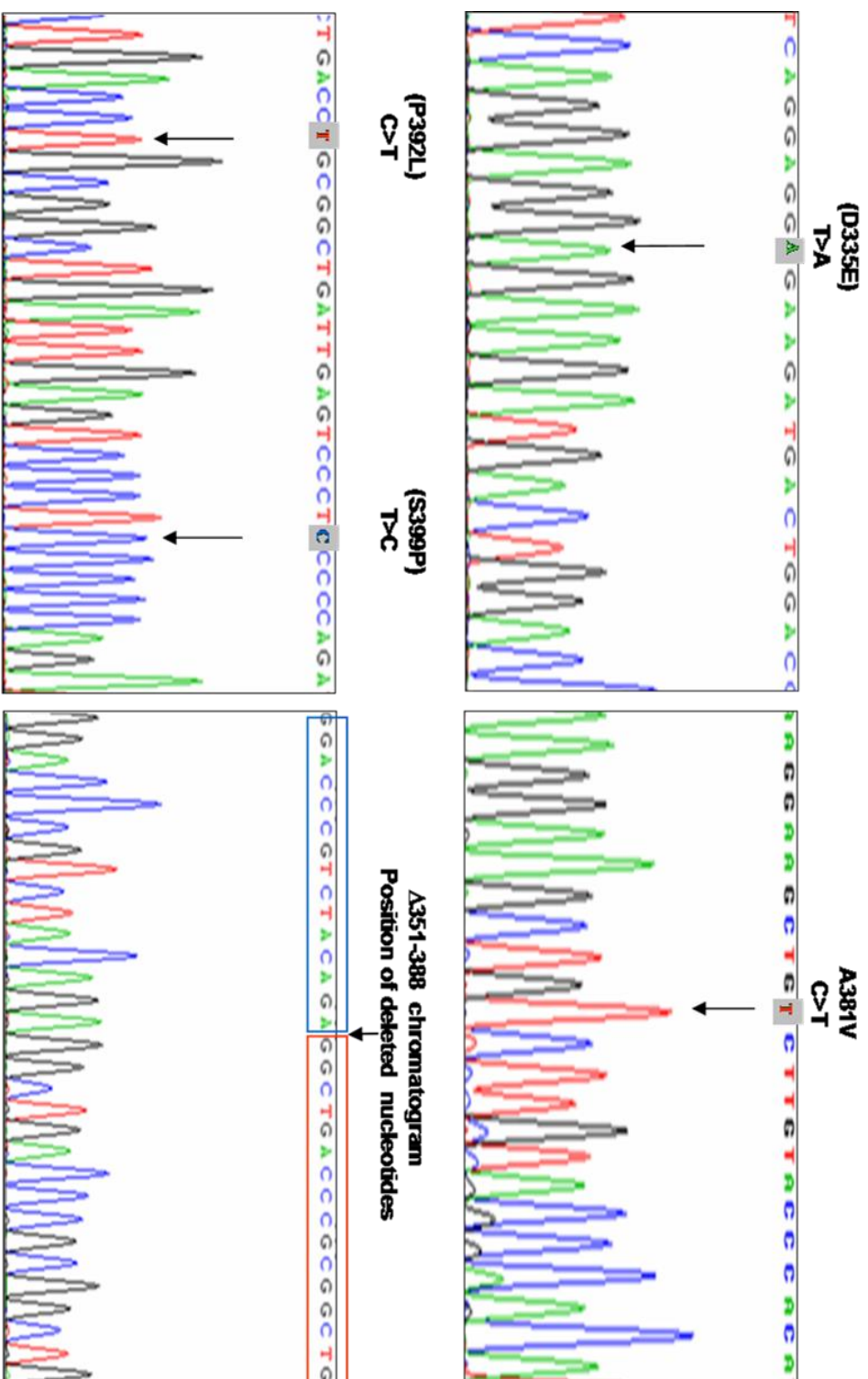


Figure 3.2: DNA sequencing of GST-p62 PDB mutants: D335E, A381V, P392L/S399P and A351-388. All the mutations were introduced to the wild type GST-p62 sequence by site directed mutagenesis. Arrows indicate the sites of each mutation.

3.4 Investigation of the relative expression levels of GST tagged wild type and PDB mutant p62 proteins

In order to first confirm that the 'new' PDB mutations did not adversely affect expression levels of GST-p62 in *E. coli*, protein expression was induced in bacterial cultures of equal volume (10ml) grown in parallel, and recombinant proteins were purified by affinity chromatography using glutathione-Sepharose beads. Briefly, cells were pelleted, lysed by sonication, and centrifuged, then samples of supernatant (equivalent to 1/200th the volume of the original culture) containing soluble proteins were incubated with an excess of glutathione-Sepharose beads with continuous mixing for 30 minutes at room temperature. Non-specific protein binding was removed by washing the beads with TBST (TBS containing Triton X-100), then with TBSA (TBS containing albumin). Proteins bound to glutathione-Sepharose were eluted with gel loading buffer and the eluted proteins were analysed by SDS PAGE and visualised with Coomassie staining. Analysis of the gel indicated comparable expression levels of GST-p62 (wild type), GST-p62 (D335E), GST-p62 (A381V), GST-p62 (P392L/S399P) and GST-p62 (Δ 351-388) proteins (Figure 3.3). Note the GST-p62 (Δ 351-388) protein migrated with a lower denatured molecular weight than the other fusion proteins, consistent with the internal deletion of 38 amino acids.

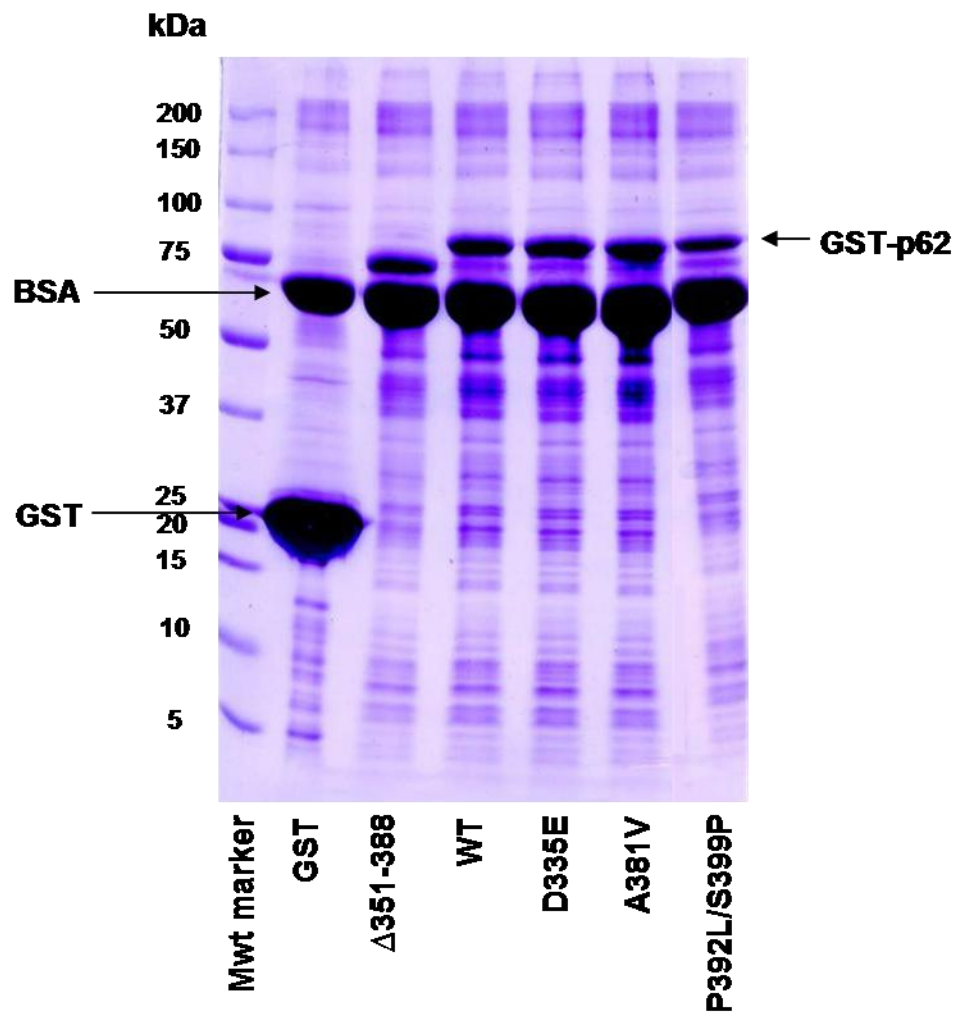


Figure 3.3: Investigation of the relative expression levels of GST tagged wild type and PDB mutant p62 proteins

GST tagged wild type and PDB mutant p62 proteins (as indicated) were expressed in *E. coli*. GST-tagged proteins (or GST control) were purified from bacterial supernatants by incubation at room temperature with glutathione-Sepharose beads. Beads were washed with TBST (TBS containing Triton X-100), then with TBSA (TBS containing albumin). Proteins bound to glutathione-Sepharose were eluted with gel loading buffer and the eluted proteins were analysed by SDS PAGE and visualisation with Coomassie staining. Residual BSA is highlighted.

3.5 Effects of 'new' PDB mutations on ubiquitin-binding function of p62

The effects of the 'new' PDB-associated mutations on the interaction of p62 with monoubiquitin were assessed using *in vitro* pull-down assays (Cavey *et al.*, 2005). In this assay, the GST-tagged p62 proteins are expressed in *E. coli* (10ml cultures), then bacterial supernatants (equivalent to 1/20th the volume of the original culture) containing the recombinant proteins are precipitated with an excess of three types of beads: glutathione-Sepharose; monoubiquitin-Sepharose; or control-Sepharose (Figure 3.4). The monoubiquitin-Sepharose beads have purified bovine ubiquitin (10 mg/ml) covalently attached, and the control-Sepharose beads are prepared in parallel without the addition of protein.

Binding to glutathione-Sepharose (*via* GST) indicates the total GST-p62 protein available, and to ubiquitin-Sepharose the fraction of GST-p62 protein able to bind ubiquitin *via* its UBA domain. Non-specific binding is controlled for using the control-Sepharose beads. Bound proteins are eluted with gel loading buffer and detected by SDS-PAGE followed by western blotting (anti-p62). Loss of ubiquitin-binding function associated with any of the PDB mutants is indicated by a reduced immunoreactivity to GST-p62 proteins precipitated by the ubiquitin-Sepharose, relative to wild type.

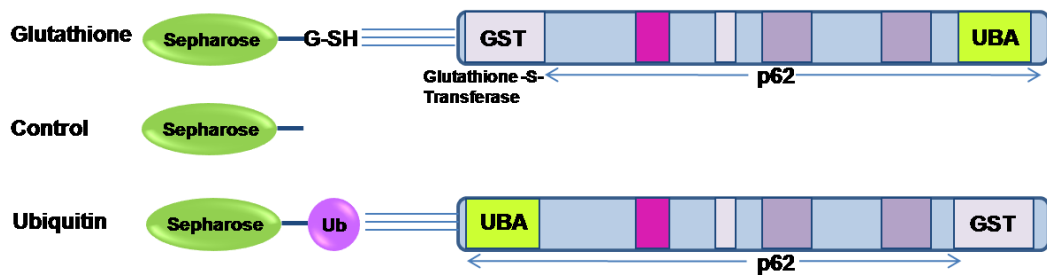


Figure 3.4: Schematic representation of monoubiquitin-binding assay for GST-p62 fusion proteins

The affinity of the p62-ubiquitin interaction depends on the non-covalent interaction of the UBA domain of p62 for the covalently immobilised ubiquitin. When glutathione-Sepharose beads are used, the GST-tag binds non-covalently with immobilised glutathione. Control-Sepharose is used to control for non-specific binding to the beads. Bound GST-p62 protein is detected by western blotting (anti-p62).

The assay was first performed at pH7.5 (and subsequently at pH6.5) and throughout the experiment, all the reagents (including beads, binding and washing buffers) were maintained at the required temperature (37°C or 21°C). The assays were independently repeated several times for each of the mutations.

3.5.1 Effects of the PDB-associated A381V mutation on the ubiquitin-binding function of p62

The ubiquitin-binding properties of GST-p62 (A381V) compared to GST-p62 (wild type) and GST-p62 (G425R) was first assessed at 37°C and pH7.5; the latter PDB mutation acts as a control as it has previously been shown to be associated with complete loss of ubiquitin-binding under these conditions (Cavey *et al.*, 2005). In these experiments, the A381V mutant was initially found to show a comparable level of binding to ubiquitin as wild type p62, whereas the control mutation G425R showed loss of ubiquitin-binding (for a representative example see Figure 3.5).

The binding assay was repeated under several experimental conditions, including at different temperatures and with variations in the time used to lyse the GST-p62-expressing *E. coli* by sonication; none of these changes affected the binding of GST-p62 (A381V) to ubiquitin, relative to wild type GST-p62 (not shown). However, on mild acidification of the binding buffer (pH6.5), we noted a small but reproducible reduction in the amount of GST-p62 (A381V) mutant p62 binding to ubiquitin-Sepharose, relative to the wild type sequence (Figure 3.5). Again, under these conditions GST-p62 (G425R) showed complete loss of ubiquitin-binding.

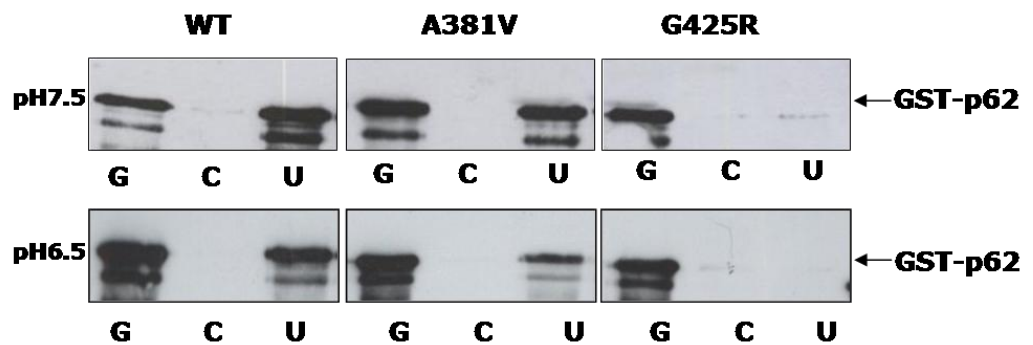


Figure 3.5: Effects of the PDB-associated A381V p62 mutation on ubiquitin-binding *in vitro*; at two different pHs (pH7.5, pH6.5)

The mutations as indicated were introduced into the full length p62 sequence, and the GST-tagged proteins used in pull-down assays at 37°C. Bacterial lysates containing the GST-p62 fusions were precipitated with glutathione-Sepharose (G), control-Sepharose (C) and ubiquitin-Sepharose (U) beads. Precipitated proteins were detected by western blotting (anti-p62 antibodies). Proteins in the (G) lanes are precipitated *via* the GST-glutathione interaction, and (U) lanes *via* the UBA-ubiquitin interaction. At pH7.5 the A381V mutant did not show any reproducible loss of binding compared to the wild type protein, whereas at lower pH (pH6.5) the A381V mutant exhibited a slightly reduced ubiquitin-binding ability, relative to wild type. The control G425R mutant showed complete loss of ubiquitin-binding at both pHs.

3.5.2 Effects of the PDB-associated Δ 351-388 mutation on the ubiquitin-binding function of p62

With the exception of the P387L missense mutation which has already been shown to cause a partial loss of p62 ubiquitin-binding function *in vitro* at pH7.5 (Cavey *et al.*, 2006), the only other (non-truncating) non-UBA domain mutants are that equivalent to a predicted product of the G1205C splice-site mutation, which lacks amino acids 351–388 (Beyens *et al.*, 2006), and a D335E missense mutation (see 3.2 and 3.5.3). The former retains the region of p62 that was previously defined as the minimum (poly)ubiquitin-binding sequence, namely residues 392–436 (Cavey *et al.*, 2006) but loses A381. The deleted 38 amino acids also include the first two amino acids of the UBA domain and a large part of the second PEST domain of p62, as well as the flexible linker region between UBA domain and second PEST domain (the PEST domain being encoded by amino acids 345–377 of p62; Figure 3.1).

Residues 351–388 were deleted from the GST-p62 (wild type) sequence and the effects of this gross change on ubiquitin-binding function were assessed. As for the A381V mutation, these ubiquitin-binding assays were performed at 37°C and at two different pHs (7.5 and 6.5). In this case, it was noted that the mutant protein showed significantly reduced binding to ubiquitin-Sepharose at pH7.5 (for a representative example see Figure 3.6). In addition, the effects of this mutation on ubiquitin-binding function of p62 were even more pronounced at pH6.5 (Figure 3.6).

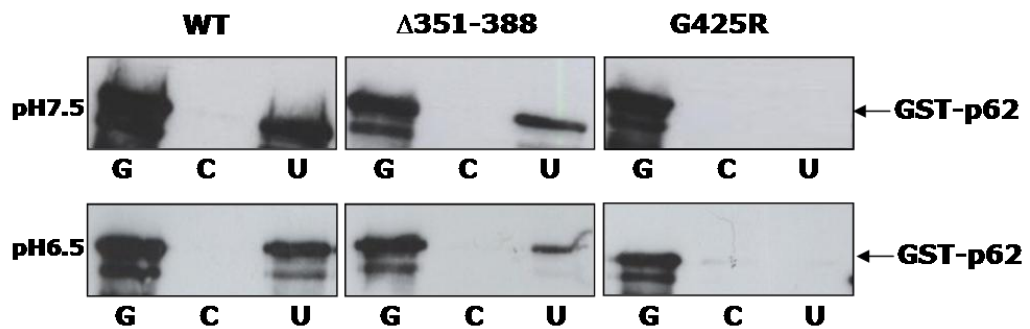


Figure 3.6: Effects of the PDB-associated $\Delta 351-388$ p62 mutation on ubiquitin-binding *in vitro*; at two different pHs (pH7.5, pH6.5)

The mutations as indicated were introduced into the full length p62 sequence, and the GST-tagged proteins used in pull-down assays at 37°C. Bacterial lysates containing the GST-p62 fusions were precipitated with glutathione-Sepharose (G), control-Sepharose (C) and ubiquitin-Sepharose (U) beads. Precipitated proteins were detected by western blotting (anti-p62 antibodies). Proteins in the (G) lanes are precipitated *via* the GST-glutathione interaction, and (U) lanes *via* the UBA-ubiquitin interaction. At both pHs (7.5, 6.5) the $\Delta 351-388$ mutant showed reduced ubiquitin-binding compared to the wild type protein. The control G425R mutant also showed loss of binding at both pHs.

3.5.3 Effects of the PDB-associated D335E mutation on ubiquitin-binding function of p62

This mutation was found in a single PDB patient in Italy with mild phenotype compared to other p62 common mutations, and it is the final example (in addition to P387L, A381V and Δ 351-388) of a non-UBA domain mutation of p62. Notably, this mutation does however map to an unstructured region of p62 involved in the direct interaction with LC3 (Pankiv *et al.*, 2007) which is required to mediate p62's role in the regulation of autophagy.

The ubiquitin-binding properties of GST-p62 (D335E) compared to GST-p62 (wild type) and GST-p62 (G425R) was assessed at 37°C and at pH7.5 and pH6.5. In contrast to the A381V and Δ 351-388 mutants, under both conditions the D335E mutation retained ubiquitin-binding function comparable to the wild type sequence (for a representative example see Figure 3.7), indicating potentially a different disease mechanism for this mutation.

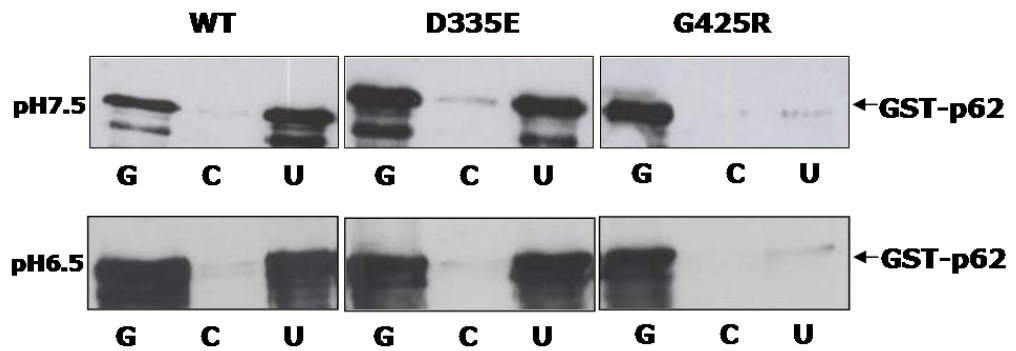


Figure 3.7: Effects of the PDB-associated D335E p62 mutation on ubiquitin-binding *in vitro*; at two different pHs (pH7.5, pH6.5)

The mutations as indicated were introduced into the full length p62 sequence, and the GST-tagged proteins used in pull-down assays at 37°C. Bacterial lysates containing the GST-p62 fusions were precipitated with glutathione-Sepharose (G), control-Sepharose (C) and ubiquitin-Sepharose (U) beads. Precipitated proteins were detected by western blotting (anti-p62 antibodies). Proteins in the (G) lanes are precipitated *via* the GST-glutathione interaction, and (U) lanes *via* the UBA-ubiquitin interaction. At both pHs (7.5, 6.5) the D335E retained ubiquitin-binding similar to the wild type protein. The control G425R mutant showed loss of binding at both pHs.

3.5.4 Effects of the PDB-associated P392L/S399P mutation on the ubiquitin-binding function of p62

The effects of the individual P392L and S399P missense mutations on the ubiquitin-binding function of p62 have been analysed previously using the *in vitro* mono ubiquitin-binding assay at 37°C, pH7.5 (Cavey *et al.* 2005; Cavey *et al.* 2006). Both of the mutations showed complete loss of binding under these conditions. Interestingly, when assays were performed at a lower temperature (room temperature; ~21°C) it was noted that P392L retained its ubiquitin-binding function, whilst S399P showed only reduced binding relative to wild type. Hence, since neither of the mutations showed a complete loss of binding under these conditions, any additive effects of the mutations on ubiquitin-binding by p62 could be assessed.

From assessments of representative western blots (Figure 3.8) the relative effects of the double mutation on the p62-ubiquitin interaction with ubiquitin were estimated; indeed it was concluded that the P392L/S399P double mutation causes a complete loss of ubiquitin-binding under conditions (~21°C) where the individual mutants retained at least some ubiquitin-binding function.



Figure 3.8: Effects of the PDB-associated double P392L/S399P p62 mutation on ubiquitin-binding *in vitro*; at room temperature (~21°C)

The mutations as indicated were introduced into the full length p62 sequence, and the GST-tagged proteins used in pull-down assays at room temperature (~21°C). Bacterial lysates containing the GST-p62 fusions were precipitated with glutathione-Sepharose (G), control-Sepharose (C) and ubiquitin-Sepharose (U) beads. Precipitated proteins were detected by western blotting (anti-p62 antibody). Proteins in the (G) lanes are precipitated *via* the GST-glutathione interaction, and (U) lanes *via* the UBA-ubiquitin interaction. As indicated the S399P/P392L double mutation caused a complete loss in ubiquitin-binding function. Both individual S399P and P392L mutations retained at least partial binding function under the same experimental conditions. Thus, effects of the mutations on protein function appear to be additive, and the double mutation has a more severe effect than the individual mutations.

3.6 Investigation of the interaction of p62 and ubiquitin using 2D protein NMR

3.6.1 Introduction

Analysis of the PDB-associated 'double' P392L/S399P UBA domain missense mutation using *in vitro* binding assays (3.5.4) further supported the hypothesis that the ubiquitin-binding function of p62 may in some cases correlate with disease severity in patients. In addition, we noted a small but reduced ubiquitin-binding function of A381V mutant p62 (3.5.1), relative to wild type, but only under certain *in vitro* conditions. These observations highlight the need for more quantitative measures of p62 ubiquitin-binding function; not least because the *in vitro* pull-down assays described in the earlier part of this chapter are at best only semi-quantitative in nature.

Consequently, we sought to investigate if a more quantitative biophysical approach, two dimensional Heteronuclear Single Quantum Coherence (2D-HSQC) protein NMR, might be applied to investigate the effects of PDB-associated mutations on protein (ubiquitin-binding) function. Indeed this technique has previously been used to estimate the dissociation constant (K_d) for the interaction of the p62-UBA (residues 387-436) with monoubiquitin at 298K as $540 \pm 45\mu\text{M}$ (Long *et al.*, 2008), although the effects of PDB mutations were not reported, and more recent analyses (*in house*) indicated a refined value for this K_d of this interaction of $710 \pm 10\mu\text{M}$ (Tom Gallagher, School of chemistry, University of Nottingham, personal communication).

This particular NMR technique involves measuring chemical shift perturbations (CSP) of unbound and UBA-bound isotopically-labelled ubiquitin; these CSP changes are used as a sensitive tool to monitor the weak interactions between

ubiquitin and p62. With this approach one can quantify interactions by determining a K_d , or alternatively an association constant (K_a), where K_a can be defined as an equilibrium constant of a reversible reaction, which measures the affinity of two molecules to each other at equilibrium state, and K_d is an equilibrium constant defining the tendency of the products of a reversible reaction to dissociate to its reactants. These two constants are used to show how tight two proteins bind to each other, as the smaller the K_d (the higher the K_a) the tighter the proteins are binding.

Prior to this work, the interaction of a longer p62 construct containing the UBA domain and additional N-terminal residues (341-440) with ubiquitin was also investigated using 2D-HSQC NMR (by Tom Gallagher, personal communication). In this case ^{15}N -ubiquitin (prepared by growing *E coli* expressing the protein in a medium in which the only source for nitrogen was its isotope ^{15}N) was titrated with unlabelled p62 (341-440) up to a 1:6 molar ratio (ubiquitin:UBA). The K_d for the p62 (341-440) binding to ubiquitin was estimated as $501\mu\text{M} \pm 34\mu\text{M}$, notably indicating that the longer p62 protein is associated with a tighter binding, and supporting the idea that non-UBA sequences (and by extension mutations) can influence ubiquitin-binding affinity.

One of the downsides of the method is difficulty in studying full-length p62, which is 440 amino acids in total, because full-length p62 exhibits relatively low protein expression levels and the NMR technique requires a large amount of protein (typically >40mg). Therefore, a compromise of using the shorter p62 (341-440) construct was accepted; notably however this sequence does contain A381, the site of one of the 'new' PDB mutations analysed in this study.

Initially we sought to make quantitative analyses of the effects of the well characterised P392L mutation, associated with complete loss of ubiquitin-binding function in full-length p62 in pull-down assays at 37°C, pH7.5 (Cavey *et al.*, 2005) – with the intention of extending these analyses to other PDB-associated mutations. In particular it would be desirable to investigate more fully the A381V mutation which we noted appeared to be associated with a minor reduction in ubiquitin-binding function (3.5.1).

3.6.2 Basic theoretical background of NMR

NMR depends on the magnetic moment of nuclei, in other words their spin, which is a characteristic of atoms with a total odd number of protons and neutrons (Alberty's Physical Chemistry, 2th Ed.). When a strong magnetic field is applied to atoms the nucleus spin can exist at two energy states: E1 (which is the lower (ground) energy state and the magnetic spin is in alignment with the applied field), or the nucleus can be excited to a higher energy state E2 (in which the magnetic spin is in opposite direction of the applied field); the amount of energy needed to excite the nucleus from E1 to E2 is called resonance (Figure 3.12). The energy needed to cause the resonance is in the radio frequency range. As the nucleus return to the ground state it emits energy which is recorded by the NMR spectrometer as chemical shift, which is measured in Parts Per Million (PPM). Notably the amount of energy needed to cause the resonance and hence the chemical shift depends on the chemical (magnetic) environment around each nuclus. The reason that chemical shift is affected by the environment is that each nuclus and electron are moving charges, so they tend to have their own local magnetic field, which will reduce the applied field by the amount of the local magnetic field of the atoms; this leads to a distinct chemical shift for every nuclus. In practice a reference

compound will be regarded as zero PPM chemical shift and the chemical shift of other compounds will be measured relative to this reference compound.

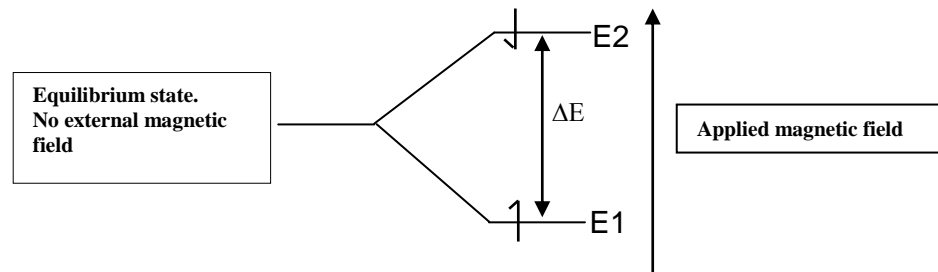


Figure 3.12: Energy level diagram of spin states of a nucleus.

E1 is the lower energy state, E2 is the higher energy state, ΔE represents the energy difference between the two states, which is proportional to the radio frequency necessary to excite the nucleus from the lower energy state to the higher energy state.

↑ : Denotes to the spin state of the nucleus when it is in alignment to the direction of applied field.

↓ : Denotes to the spin state of the nucleus when it is aligned in the opposite direction of the applied field.

To study the interactions between p62 and ubiquitin, a two dimensional NMR approach was used. In our study we used ^{15}N - ^1H HSQC, in which the chemical shift of ^{15}N is directly correlated to the chemical shift of ^1H , and the correlated chemical shift is detected as a cross peak on the resulting spectrum (Vaynberg *et al.*, 2006). This technique facilitates the detection of a chemical shift for every N-H bond across a protein. Since every residue of a protein (except proline) has an N-H derived from the α -amino group of the amino acid, the number of peaks on the 2D spectrum represents number of the residues of the proteins (Branden and Tooze 2nd Ed.) and since the N-H of each amino acid has a different environment when contained in different proteins, each protein produces a characteristic cross-peak fingerprint. In addition, N-H of side chain residues (Asn, Gln) can be distinguished from the back bone N-H as an additional cross peak on the spectrum (Figure 3.13).

In our experiment, first a separate ^{15}N - ^1H HSQC spectrum is collected for the ^{15}N labelled protein (in this case ubiquitin), then another spectrum is collected after adding an unlabelled protein (p62 (341-440 containing the P392L mutation)) to the ^{15}N labelled ubiquitin using a range of molar ratios. Since the chemical shifts of both N and H are sensitive to the chemical environment around them, the effects of protein binding on the chemical shifts can be used to study the interaction of the two proteins.

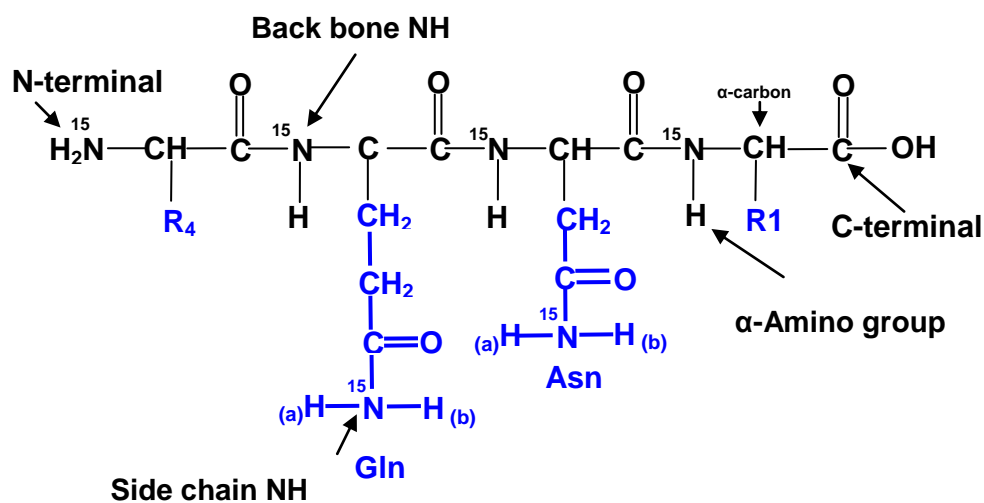


Figure 3.13: A polypeptide chain of a ^{15}N -labelled protein, showing the ^{15}N and ^1H at the back bone and selected side chains

R represents amino acids side chain, blue groups are representative side chains (Gln, Asn). These two side chains have an NH_2 group which has two hydrogen atoms attached to the same ^{15}N , therefore there will be two ^1H signals for each ^{15}N signal. These two hydrogen atoms are denoted as a, b.

3.7 Generation of a prokaryotic expression constructs for GST-p62 (341-440) containing the P392L mutation

Previously in the lab, a pGEX-4T-1 plasmid which allows p62 residues (341-440) to be expressed as a GST-fusion protein in *E. coli* was generated. The P392L mutation was introduced in to this sequence by site-directed mutagenesis following the instructions of QuikChange® Site-Directed Mutagenesis kit (Stratagene) (Materials and Methods). The resulting protein will be denoted GST-p62 (P392L; 341-440).

The GST-p62 (P392L; 341-440) plasmid was analysed by DNA sequencing and the resulting chromatogram was viewed using ChromasLite2 software (Figure 3.14). The mutation was confirmed by sequence alignment with the wild type sequence using ClustalW2.

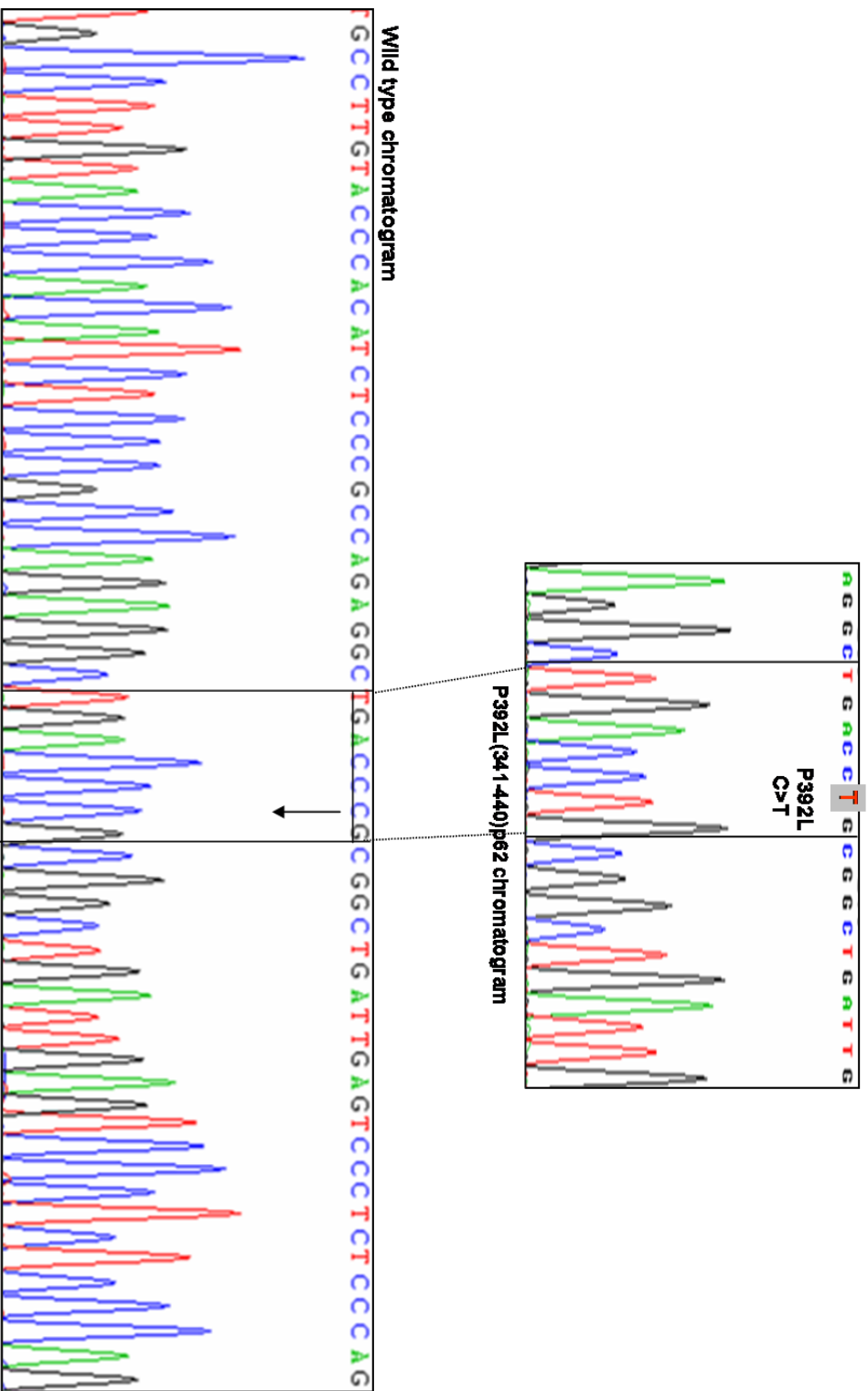


Figure 3.14: DNA sequencing of p62 (P392L; 341-440); the main chromatogram shows part of the wild type sequence of p62 (the arrow indicates mutation site). The smaller chromatogram highlights the PDB mutation introduced into p62 by site-directed mutagenesis.

3.8 Large scale purification p62 (P392L; 341-440) for protein NMR

Bacterial lysates obtained from multiple one litre cultures of *E. coli* expressing GST-p62 (P392L; 341-440) were incubated at 4°C for 6 hours with glutathione-Sepharose beads in chromatography columns, producing a complex between GST tagged proteins with the glutathione-Sepharose beads. As the GST tagged p62 (P392L; 341-440) includes a thrombin enzyme recognition site, LeuValProArgGlySer, between the GST and p62 sequences, the beads were incubated with thrombin enzyme overnight, at room temperature resulting in proteolysis between Arg and Gly residues, eluting the p62 (P392L; 341-440) protein with additional Gly and Ser residues at the N-terminus. The beads retain the GST tag (Figure 3.15). Fractions were analysed with SDS-PAGE followed by staining the gel with Coomassie brilliant blue dye (Figure 3.16). In total ~40 separate 1 litre cultures were processed in this way. The eluted p62 (P392L; 341-440) protein was stored at 4°C and subjected to further purification step by gel filtration. Final protein concentration was measured using Bradford assay (See Materials and Methods) and was equivalent to ~40mg of total recombinant protein.

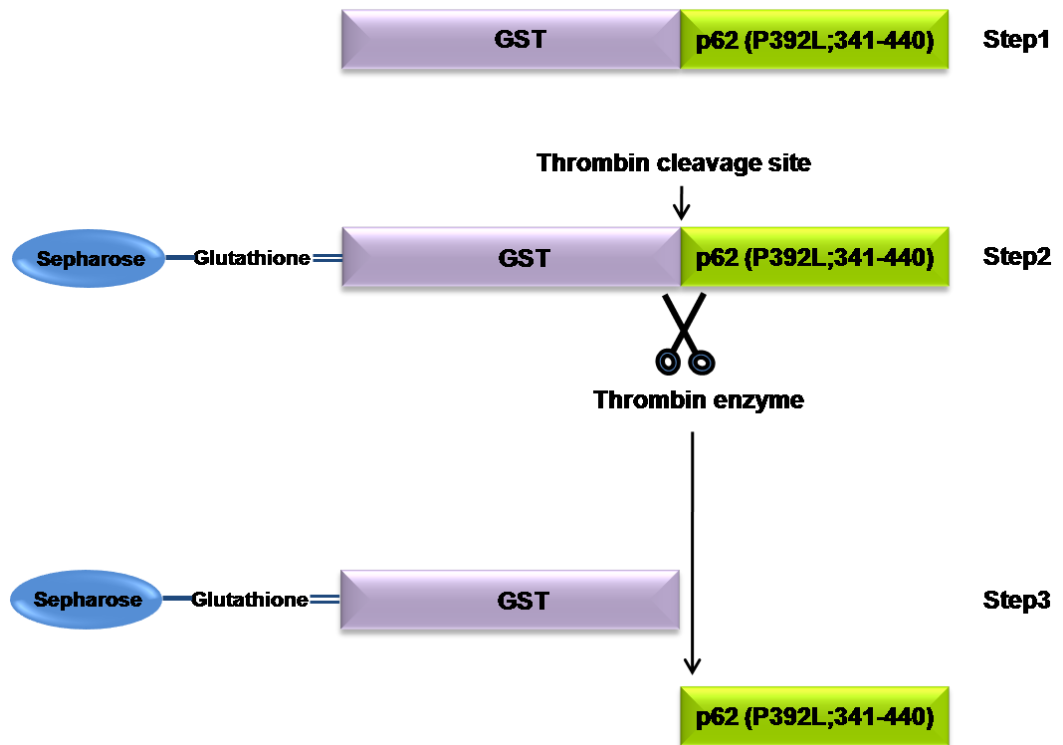


Figure 3.15: Large scale purification of the recombinant p62 (P392L; 341-440)

Bacterial lysates containing GST-p62 (P392L; 341-440) were incubated with glutathione-Sepharose beads, which leads to formation of a complex between the GST-p62 (P392L; 341-440) and glutathione beads. Beads are incubated with thrombin enzyme, which proteolyzes GST-p62 (P392L; 341-440) at its thrombin cleavage sequence, thus eluting p62 (P392L; 341-440) protein and leaving the rest of the tag sequence on the beads.

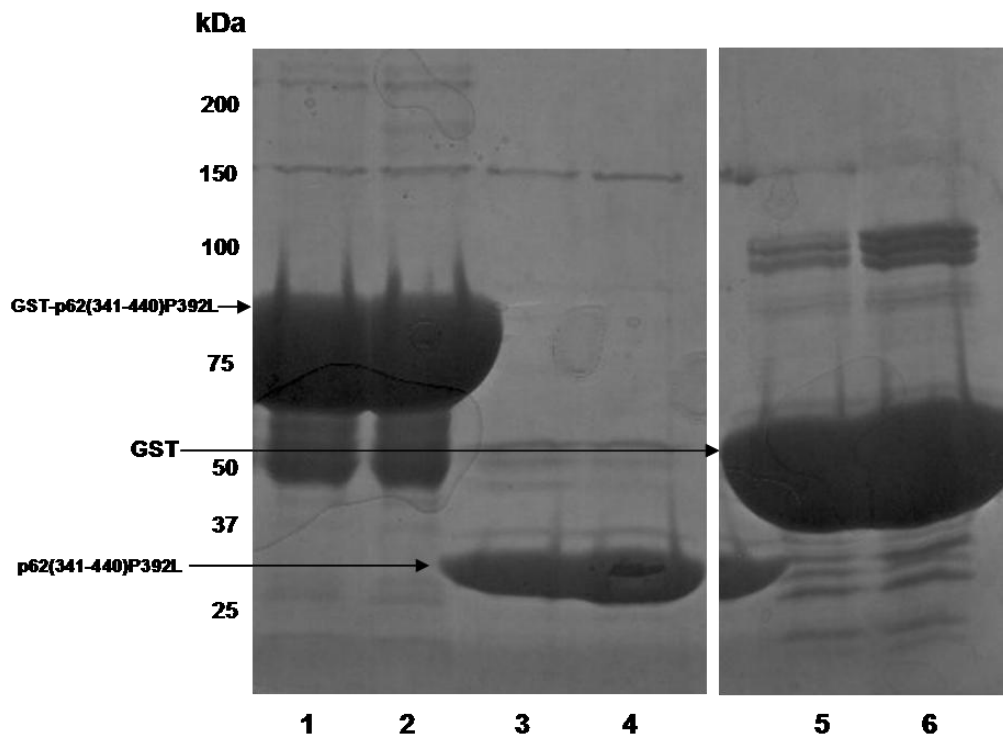


Figure 3.16: Large scale purification of GST-p62 (P392L; 341-440)

GST-p62 (P392L; 341-440) was expressed in *E. coli*, and the bacterial lysates were bound to glutathione-Sepharose beads at 4°C for 6 hours, followed by incubating the resulting complex (lanes 1, 2) overnight and at room temperature with thrombin enzyme. Thrombin enzyme cleaves the complex and p62 (P392L; 341-440) is eluted (lanes 3, 4) leaving GST bound to the beads (lanes 5, 6). Aliquots of protein fractions were subjected to SDS PAGE and the gel stained with Coomassie blue.

3.9 NMR analysis of the interaction of ¹⁵N-ubiquitin with p62 (P392L; 341-440)

After purifying p62 (P392L; 341-440), NMR titration experiments were performed between the purified protein and ¹⁵N-ubiquitin (in collaboration with Tom Gallagher, School of Chemistry). A fixed concentration of ¹⁵N-ubiquitin (1mM) was titrated with a range of concentrations of unlabelled p62 (P392L; 341-440) (Table 3.1), both prepared in NMR buffer pH7 at 298K, with analysis using a Bruker Avance 600MHz NMR spectrometer. The NMR spectra were collected at each titration step. The CSP was recorded for each ¹⁵N and ¹H of ubiquitin as it interacted with p62 (P392L; 341-440). The same analyses were previously performed for p62 (WT; 341-440) by Tom Gallagher.

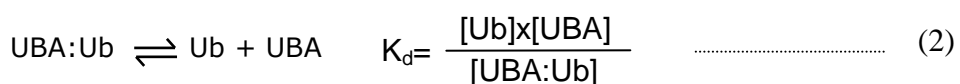
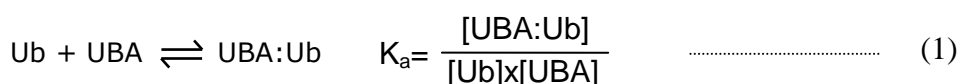
Sample number	1	2	3	4	5	6	7	8	9	10	11	12	13	14
¹⁵ N- Ubiquitin (mM)	1	1	1	1	1	1	1	1	1	1	1	1	1	1
p62 (P392L; 341-440) (mM)	0.0	0.1	0.2	0.3	0.4	0.5	0.6	0.8	1.0	1.2	1.5	2	4	6

Table 3.1: Molar ratios of p62 (P392L; 341-440) and ¹⁵N-Ubiquitin

Changes in the chemical shifts of some of ubiquitin's residues obtained from the analyses were used to calculate the K_d for the interaction between p62 (P392L; 341-440) and ubiquitin.

To illustrate how the K_d s were obtained from the chemical shift data, we first need to consider basic theoretical concepts for K_d calculations: the interaction

between ubiquitin and p62 (P392L; 341-440) can be represented by reaction 1, in which the reactants bind in a 1:1 model to form a complex; at equilibrium the reaction follows equation (1), in which K_a defines the association constant of the interactions, or alternatively K_d can be used to define the binding equilibrium. K_a or K_d ($K_a=1/K_d$) are calculated from equation (3). Equation (3) is derived from equations (1), (2) and the state of bound and unbound proteins in the solution; this equation is applied to draw a graph (Figure 3.17) by assigning p62 (P392L; 341-440) concentration to the X axis and the CSP of a ubiquitin residue (CSP is measured from the NMR spectrometer) to the Y axis; a curve will form which shows that the complex will form a steady state, i.e. addition of more p62 (P392L; 341-440) will no longer lead to any observable CSP and this state is represented by the plateau. CSPmax is calculated from the point when the interactions reach the plateau. At this stage, $1/K_a$ (K_d) is the only unknown in equation (3), and by applying the equation using Igor Pro 5.0.5.7 software the K_d s can be calculated for each of ubiquitin's residues.



[UBA:Ub] is the concentration of the complex between ubiquitin and p62 (P392L; 341-440) at equilibrium

[Ub] is the concentration of ubiquitin at equilibrium

[UBA] is the concentration of p62 (P392L; 341-440) at equilibrium

$$\text{CSP} = \text{CSP}_{\text{Max}} * ([\text{UBA}] / ((1/K_a) + [\text{UBA}])) \quad \dots\dots\dots (3)$$

CSP: chemical shift perturbation measured by the NMR spectrometer.

CSP_{Max} is CSP at saturation.

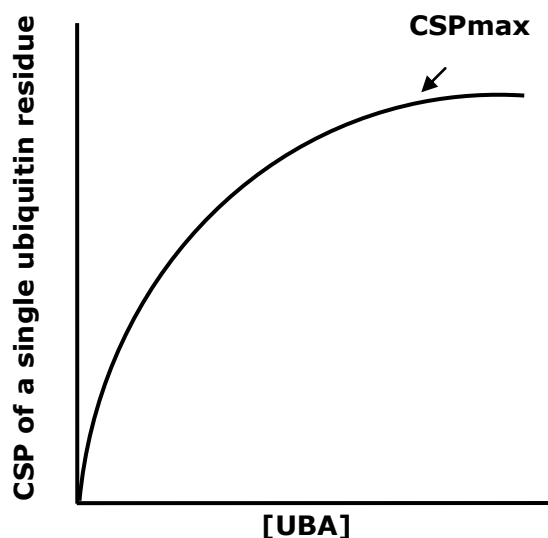


Figure 3.17: A typical rectangular hyperbola, plotted from CSP of ubiquitin as a function of p62 (P392L; 341-440) (denoted UBA) concentration.

Figures 3.18-3.21 demonstrate the necessary steps for K_d calculations; the chemical shift of one residue of ubiquitin (K11) is shown in Figure 3.18. The chemical shifts of each residue of ubiquitin were first recorded without addition of p62 (P392L; 341-440) and marked as red, while the CSPs of ubiquitin after addition of p62 (P392L; 341-440) were marked as black. The cross peak of K11 changes its position, indicating changes in the chemical environment of K11 after the addition of p62 (P392L; 341-440), which indicates possible direct interaction between K11 of ubiquitin and p62 (P392L; 341-440).

The chemical shifts of all of ubiquitin's residues are shown in Figure 3.19, and to obtain a clearer graph the crosses on the residues were deleted (Figure

3.20). From the CSP values obtained from Figure 3.19, binding curves for each ubiquitin residue were produced (Figure 3.21), and from these curves the K_d s were calculated by applying equation (3) using the Igor Pro 5.0.5.7 computer software.

Table 3.2 shows the CSP values of p62 (P392L; 341-440) compared to CSP values of p62 (WT; 341-440), the latter data provided by Tom Gallagher. The table shows that not all residues in ubiquitin undergo large variations in their CSPs, indicating that the binding surface between p62 (P392L; 341-440) and ubiquitin is a defined region. The CSP values were used as an indicator to gauge the areas in the UBA domain where most changes occur, and the CSP values indicated broadly that the changes in the CSP are roughly similar in both constructs with some variation at occasional residues. Based on the results obtained from this table the K_d values were measured for those residues which had detectable CSP variations. Table 3.3 shows individual K_d s for each residue of ubiquitin and, the average K_d between ubiquitin and p62 (P392L; 341-440) was compared to the K_d between p62 (WT; 341-440) and ubiquitin.

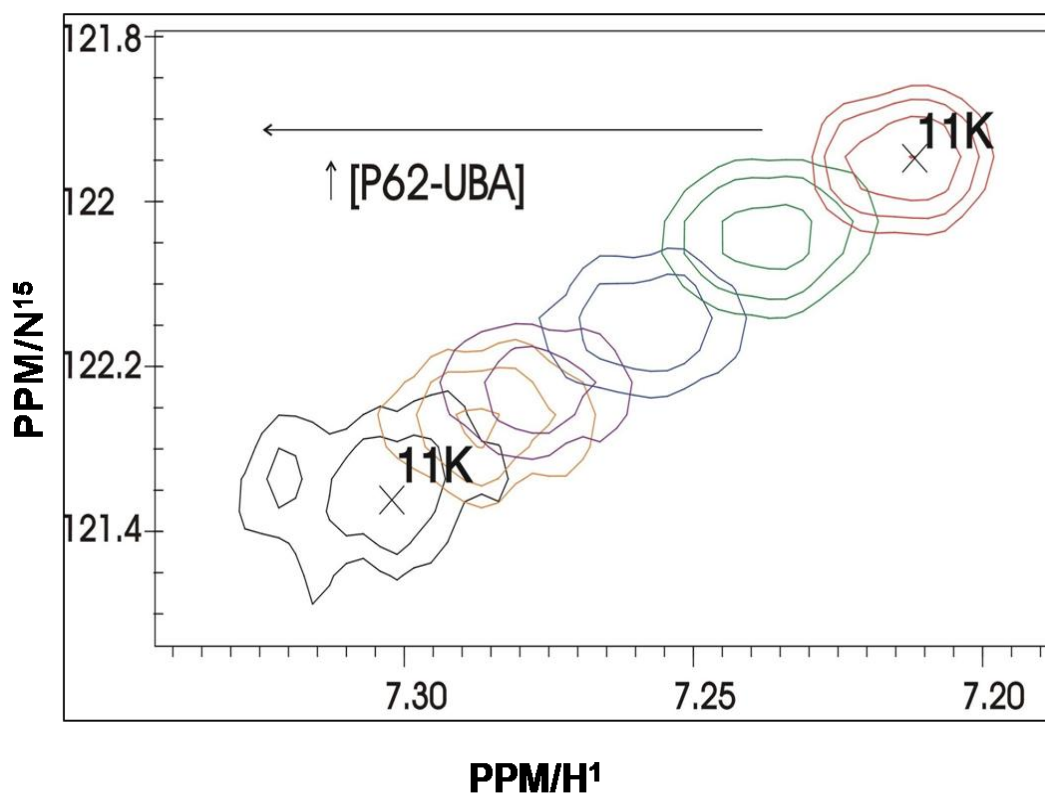


Figure 3.18: Detailed (^{15}N , ^1H) 2D HSQC NMR spectra for K11 of ubiquitin

This spectrum shows a detailed illustration of chemical shift dynamics for one ubiquitin residue. The chemical shift for K11 of ^{15}N -ubiquitin was measured in the absence (red) and after titration with different concentrations of p62 (P392L; 341-440) (black) using an NMR spectrometer. Using a constant concentration of ubiquitin (1mM) the chemical shifts were measured after the addition of different concentrations of p62 (P392L; 341-440) up to a 1:6 molar ratio. The spectrum was collected at 298K (25°C), pH7 using a Bruker Avance 600MHz NMR spectrometer. In the absence of p62 (P392L; 341-440), the N-H shift from K11 of ubiquitin is at 7.21 PPM/ ^1H and 121.95 PPM/ ^{15}N . As the concentration of p62 (P392L; 341-440) increases the residue shifts from its starting position to 7.30 PPM/ ^1H and ~ 122.375 PPM/ ^{15}N , indicating changes in the chemical environment of ubiquitin at that residue.

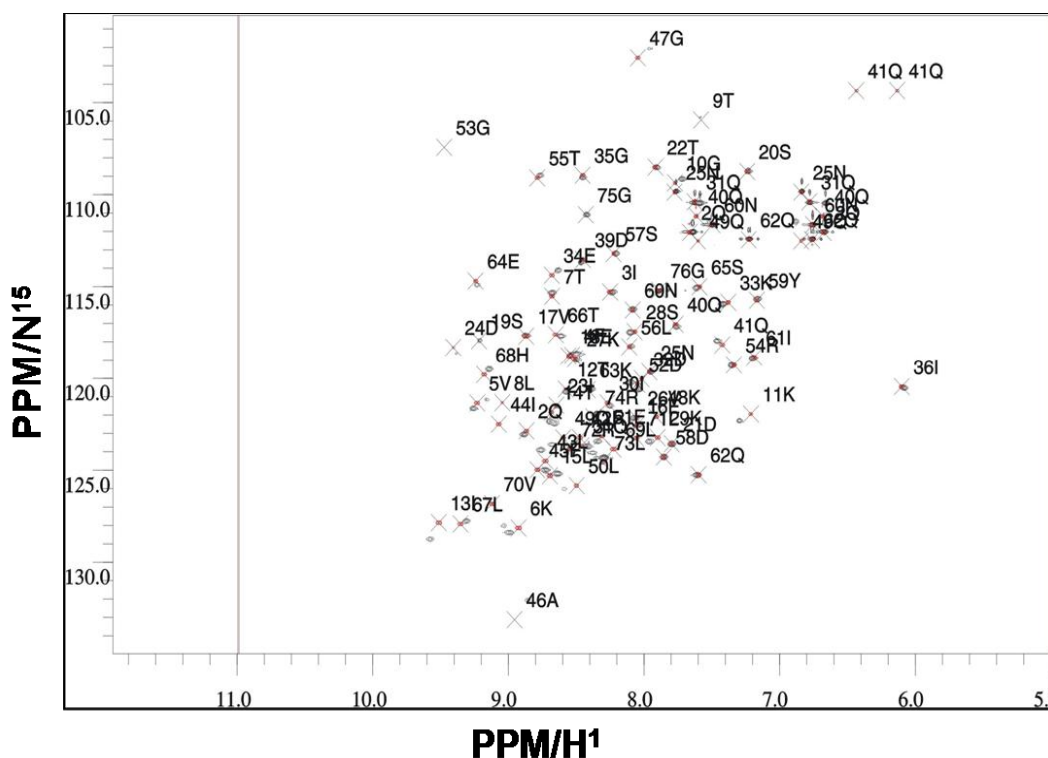


Figure 3.19: (^{15}N , ^1H) 2D HSQC NMR spectra of ubiquitin's interaction with p62 (P392L; 341-440) labelling shifts from each residue of ubiquitin

Chemical shifts for ^{15}N labelled ubiquitin's residues were measured in the absence (red) and after titration with p62 (P392L; 341-440) (black) using a constant concentration of ubiquitin (1mM). The chemical shifts were measured after the addition of p62 (P392L; 341-440) using a range of molar ratios (Table 3.3). The resultant chemical shifts of some of the residues show slight changes in their PPM, while the majority of the residues were superimposed indicating slight change in the chemical environment around the residues i.e. weak interaction. A Bruker Avance 600MHz NMR spectrometer was used and the spectra was collected at 298K (25°C), pH7. CSP values were fitted to Equation (3) using Igor Pro 5.0.5.7 software (Figure 3.21). A clearer graph is illustrated next page to show degree of CSP of bound and unbound residues. The chemical shifts are displayed at saturation.

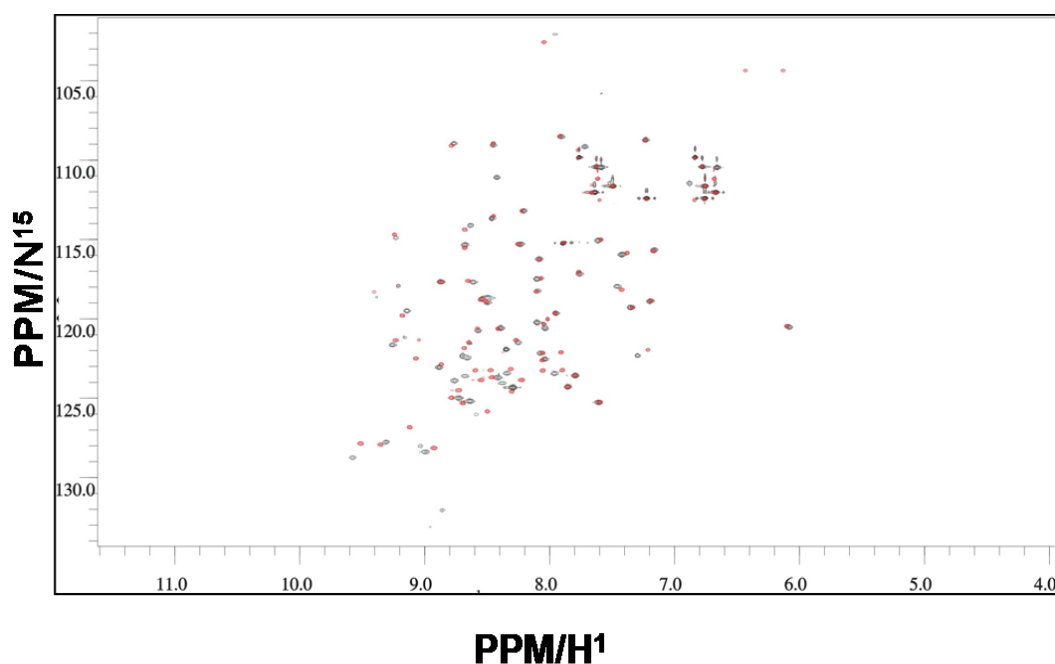


Figure 3.20: (^{15}N , ^1H) 2D HSQC NMR spectra of ^{15}N -ubiquitin's interaction with p62 (P392L; 341-440)

Chemical shifts for ^{15}N labelled ubiquitin's residues were measured in the absence (red) and after titration with p62 (P392L; 341-440) (black) using a constant concentration of ubiquitin (1mM). The chemical shifts were measured after the addition of different concentrations of p62 (P392L; 341-440). The resultant CSPs of some of the residues showed slight changes in their PPM, while the majority of the residues are superimposed indicating minor changes in the chemical environment around the residues i.e. weak interaction. A Bruker Avance 600MHz NMR spectrometer was used and the spectra was collected at 298K (25°C), pH7. The chemical shifts are displayed at saturation. CSP values were fitted to Equation (3) using Igor Pro 5.0.5.7 software (Figure 3.21).

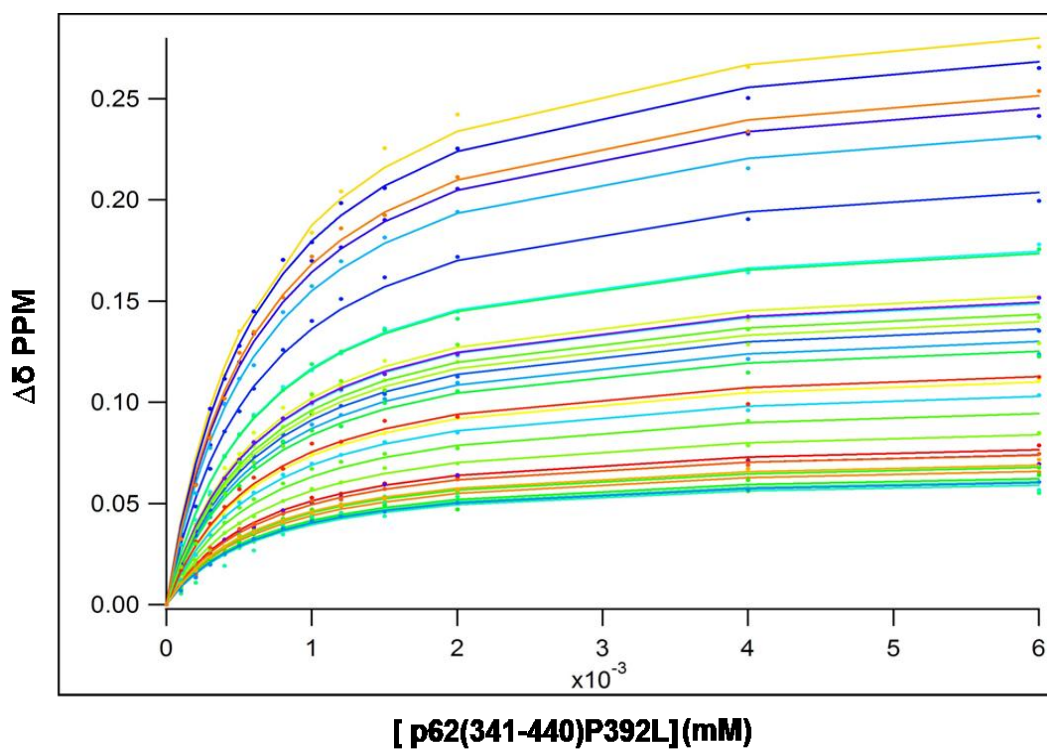


Figure 3.21: Binding curves for p62 (P392L; 341-440) and ubiquitin

Each curve represents the chemical shift of different residues of ubiquitin as they were titrated with different concentration of p62 (P392L; 341-440). Based on Equation (3) the curves were plotted using Igor Pro 5.0.5.7 software which calculates the K_a between ubiquitin and p62 (P392L; 341-440), the plateau represents the saturation of the interactions between the proteins, and CSPmax was obtained from the concentration where the chemical shifts start to plateau.

CSP Value	P62 (P392L; 341-440)	p62 (WT; 341-440)
0.05-0.1	2,5,6,9,10,15,24,29,34,41,45,51,52,67,68,73	2,5,6,9,10,15,24,29,33,41,45,39,51,52,64,66,67,68,73
0.1-0.15	8,11,14,32,43,47,50,41b	32,34,43,50,
0.15-0.2	13,49,69, 72, 40a, 40b,	8,69,72,SC40a,SC40b,SC41b, <i>13,53</i>
0.2-0.25	46, SC49a <i>48</i>	46, 49, SC49a, <i>48</i>
>0.25	44, 70, SC49b , <i>42, 71</i>	44, SC49b, <i>70, 42 ,71</i>

Table 3.2: CSP values for selected ubiquitin residues as they interact with p62 (WT; 341-440) and p62 (P392L; 341-440)

The table shows that similar residues of p62 (P392L; 341-440) and p62 (WT; 341-440) undergo chemical shifts as they interact with ¹⁵N-ubiquitin. The "CSP values" are used as a guide to detect those residues which undergo highest CPS variations and are used for subsequent analyses. SC indicates 'side chains', a and b represents two different ¹H atoms attached to the ¹⁵N of the same group (Figure 3.13). Italics are for minimum CSP predicted values for broadened residues from CSP at 0.1.

Ubiquitin Residue Number	K _a (P392L)	K _a (WT)	Ubiquitin Residue Number	K _a (P392L)	K _a (WT)
5	1444.4±53.5	2183.5±147	46	1529.5±54.5	1859.4±112
6	1804.9±149	2183.4±232	47	1739.9 ±131	-
8	1737.1 ±73	2247.5±173	*49	1459.7±44.8	2267.8 ±133
10	1482.9±66.5	1863.8±198	50	1758.2 ±104	2210.6 ±201
11	1658.3±82.7	2243.4±176	51	1638.6±80.4	2328.5 ±183
13	1516.8±72.4	-	52	1472 ±61.5	1983.1 ±122
14	1383.4±40.1	-	68	1388.1±41.6	2066.3 ±130
15	1285.6±138	2294.2±185	69	1434.6±59.8	1703.1 ±140
24	1580.8±106	1608.5±144	70	1573.1±59.9	-
29	1441.6±62.3	2046.6±120	72	1628.3±79.1	2125.5 ±173
32	1524.8±52.9	2545.1±189	SC40a	1465 ±28.2	2278.6 ±114
34	1520.4±93.3	2631.9±197	SC40b	1465.7±28.7	2279.4 ±121
41	1797.4±139	1745.5±115	SC41a	1385.5 ±133	1731.2 ±142
43	1572.3±33.5	2165.2±145	SC49a	1521.2±55.1	1639.8 ±154
44	1411.8±88.8	1896.2±176	SC49b	1488.4±58.6	1626.1 ±173
45	1539.5±184	2646.2±254	**Average K ^a (K ^d)	1537.09M ⁻¹ K _d (654μM)	2088.904M ⁻¹ K _d (479μM)

Table 3.3: Comparison of K_a between ¹⁵N-ubiquitin interaction with p62 (P392L; 341-440) versus p62 (WT; 341-440) The K_a values were calculated from the CSP of selected residues measured by NMR spectroscopy (Figure 3.19) with each value calculated from the binding curves (Figure 3.21) and an average K_a (K_d) was calculated (and is highlighted). '-' represents disappearing residues on the spectrum, ± represents average difference between the calculated fit line and the experimental data point. *The binding curve for residue 49 of ubiquitin is shown in (Figure 3.22). ** After fitting the data to global fitting curves the average K_ds for p62 (P392L; 341-440) and p62 (WT; 341-440) was 658± 22μM and 501±34μM respectively.

The average calculated K_d s were $501 \pm 34 \mu\text{M}$ for p62 (WT; 341-440) and $658 \pm 22 \mu\text{M}$ for p62 (P392L; 341-440). These values indicate that p62 (WT; 341-440) may bind slightly more strongly to ubiquitin than p62 (P392L; 341-440), although the difference was marginal and in terms of NMR analyses is negligible and unlikely to be significant. Indeed to emphasise the similarity of the values, the CSP of residue number 49 of ubiquitin as it interacts with both p62 constructs is illustrated in Figure 3.22; at different concentrations of p62 protein, the changes in CSP values are virtually indistinguishable (and in fact overlay) for titrations with p62 (P392L; 341-440) and p62 (WT; 341-440). Thus, we conclude that this approach cannot reliably detect significant differences in binding affinity between p62 (WT; 341-440) and p62 (P392L; 341-440).

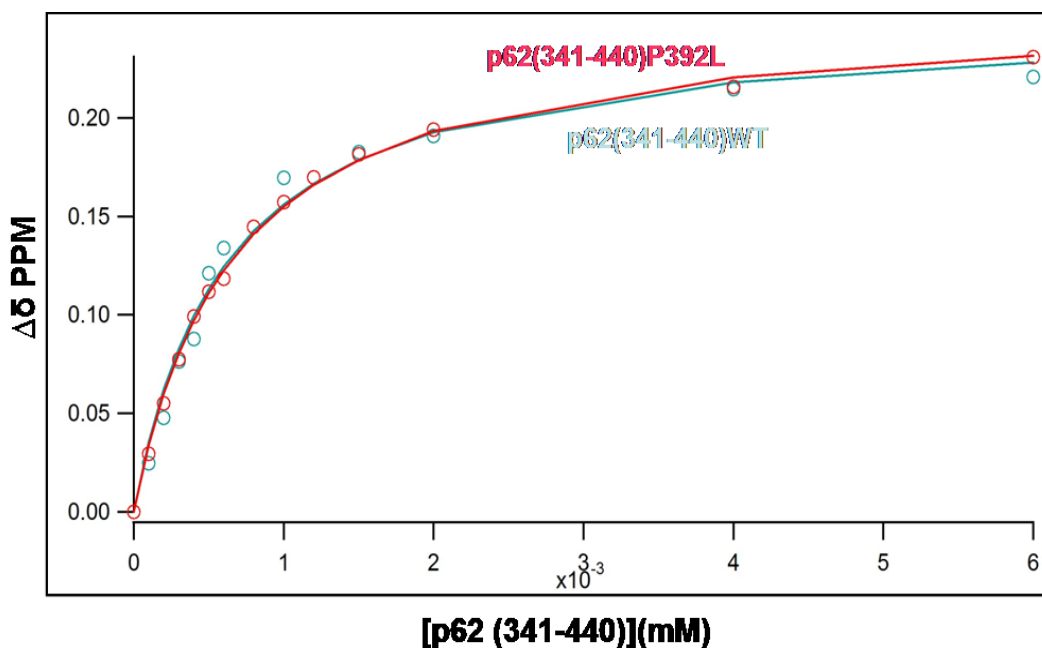


Figure 3.22: Comparison of the chemical shift for residue number 49 of ¹⁵N- ubiquitin (side chain NH₂) resultant from titration of ubiquitin with p62 (WT; 341-440) and p62 (P392L; 341-440)

Each curve represents the chemical shift of residue 49 of ubiquitin upon titration with different concentration of WT and p62 (P392L; 341-440). Based on Equation (3) the curves were plotted using Igor Pro 5.0.5.7 software. Note the curves virtually overlay and differences in chemical shifts appear negligible, consistent with identical binding affinities.

3.10 Discussion

The majority of PDB-associated p62 mutations investigated to date are located within the UBA domain and result in impairment of the ubiquitin-binding properties of the p62 protein. Here we investigated a new hypothesis that non-UBA domain mutations (A381V, D335E and Δ 351-388) might similarly affect the ubiquitin-binding properties of p62.

The A381V mutant p62 retained its ubiquitin-binding function at pH7.5 in pull-down assays, but interestingly showed reduced ubiquitin-binding in a mildly acidic environment. This pH-dependent variation of the ubiquitin-binding properties of the A381V mutant cannot be rationalised simply, but it is notable that an acidic environment exists inside autophagosomes in which p62 and ubiquitinated proteins are degraded by the autophagy machinery (Biørkøy *et al.*, 2005; Pankiv *et al.*, 2007). The effects of PDB mutations on p62-mediated autophagy have not been assessed to date.

The p62 deletion mutant Δ 351-388, which notably removes A381, also reduced ubiquitin-binding relative to wild type p62 and consistent with original findings of Vadlamudi and co-workers related to the function of p62 (Vadlamudi *et al.*, 1996), which noted two p62 internal deletion constructs (Δ 368-391 and Δ 391-440) exhibited partial loss of ubiquitin-binding. Based on these observations it was proposed that p62 might have two ubiquitin-binding regions, or that ubiquitin has more than one binding site with p62 (Vadlamudi *et al.*, 1996). Interestingly, our own co-workers also noted a correlation between the length of UBA domain constructs with increasingly extended N-terminal sequences and ubiquitin-binding ability in pull-down assays; as the N-terminus of the UBA domain was progressively extended the binding affinity of p62 to ubiquitin increased, indicating that multiple regions of

p62 affect the interaction with ubiquitin (Najat *et al.*, 2009). Further, quantitative analyses showed that the longer (341-440) UBA construct bound ubiquitin more tightly than the UBA domain alone (387-436), with respective K_d 's of $710 \pm 10\mu\text{M}$ (387-436) and $501\mu\text{M} \pm 34\mu\text{M}$ (341-440) (Tom Gallagher, School of chemistry, University of Nottingham, personal communication).

Previous structural analyses give few clues to rationalise the effects of A381V and Δ 351-388 non-UBA domain mutations on the ubiquitin-binding affinity of the UBA domain, nor how non-UBA sequences contribute to binding affinity. The A381V mutation is located within a region of p62 (341-386) which precedes the UBA domain and through a combination of NMR spectroscopy and circular dichroism (CD) analysis it was shown that this region is unstructured (Figure 3.23) (Najat *et al.*, 2009). P387L, a missense mutation previously shown to result in a partial loss of ubiquitin-binding function is located on a potential hinge region of p62 immediately before the UBA domain and it was initially suggested that this region adopts a flexible α -helix conformation and might be recruited to form a stable structure that binds ubiquitin (Cavey *et al.*, 2006). However, a structural investigation of the longer p62 UBA construct (341-440) using NMR did not support this hypothesis, providing no evidence for additional secondary structure with the UBA domain (Najat *et al.*, 2009). Collectively, these results indicate that although our observations support the important role of non-UBA domain sequences in regulating binding affinity, more research is needed to understand the mechanism of ubiquitin recognition by p62.

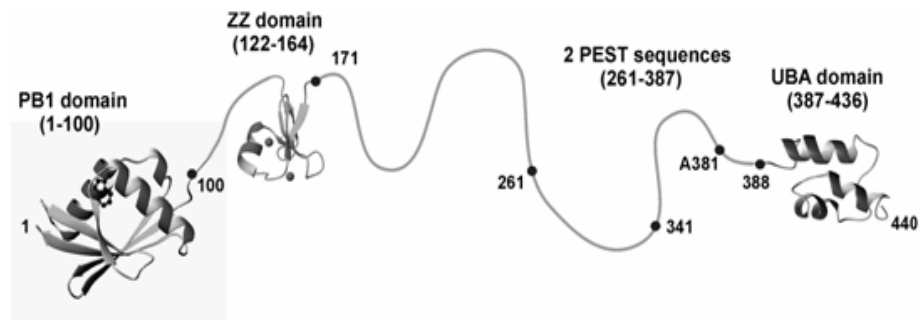


Figure 3.23: Proposed tertiary structure of the p62 protein.

The A381V mutation affects a region of p62 predicted to be unstructured and some eleven residues from the start (P392) of the structured UBA domain. The N-terminal PB1 domain which adopts ubiquitin-like fold is shown (in this case the PB1 and ZZ domains of other proteins are presented). Numbering relates to the positions of specific residues in the 440 amino acid sequence. Residues 351-388 are removed in a predicted product of the G1205C splice-site mutation. From (Najat *et al.*, 2009)

In contrast to the other non-UBA domain mutants, the D335E mutant p62 protein retained ubiquitin-binding function at both pH7.5 and pH6.5. This is perhaps not surprising as D335E is a conservative mutation involving a substitution of an acidic side chain with another acidic side chain; alternatively, D335E may simply represent a rare polymorphism. Further, a recent study noted that P364S, another 'new' non-UBA domain mutation, also had no effect on ubiquitin-binding properties of p62 at both pH7.5 and pH 6.5 (Rea *et al.*, 2009). Together, these data suggest that as the p62 mutations are located further from the UBA domain, their effects on ubiquitin-binding (at least in our *in vitro* pull-down assays) become less pronounced. One interpretation of these observations is that loss of p62's ubiquitin-binding function may not be important in PDB aetiology. Alternatively, non-UBA domain regions of p62 may be involved in additional interactions with its ubiquitinated substrates (most likely other components of the RANK-NF- κ B signalling pathway). In other words non-UBA domain mutations might cause reduced binding to ubiquitinated substrates of p62 but, in contrast to UBA domain mutations, might specifically impair interaction with the substrate proteins rather than the ubiquitin modification. Such effects would not be evident in our *in vitro* assays. To further investigate the effects of the D335E mutation on then biological functions of p62, we went on to use immunofluorescence confocal microscopy to study the interaction between the D335E mutant and LC3 (see section 4.6.1). LC3 is an autophagic marker and notably the D335E change is located within the middle of LC3-interacting region (LIR) of p62 (321-342).

There remains ongoing debate as to whether PDB is caused by viral infections or genetic factors, whilst a few groups have suggested that combination of these two factors may be important. Since some *SQSTM1* mutations appear to have an incomplete penetrance, it is difficult to conclude whether genetic

variants play a causal role in PDB or simply increase the susceptibility to the disease. Correlations between disease severity in patients with *SQSTM1* mutations, and ubiquitin-binding properties of corresponding mutant p62 proteins, would provide strong evidence that the mutations play a central role in PDB aetiology. In 2004 Hocking *et al.* proposed that in some cases PDB disease severity might be correlated to the ubiquitin-binding properties of p62, based on the notion that a p62 truncating mutation (E396X) lost its ubiquitin-binding function completely in *in vitro* pull-down assay and the patient carriers of this mutation had the most extensive disease phenotypes compared to other PDB mutations (Table 3.4).

We also attempted to correlate the ubiquitin-binding properties of p62 carrying the double UBA domain mutation S399P/P392L, and individual P392L or S399P mutants, to disease phenotype. P392L/S399P mutant p62 showed complete loss of ubiquitin-binding function in our *in vitro* pull-down binding assay at room temperature, and was associated with a particularly severe disease phenotype (Eekhoff *et al.*, 2004) (Table 3.4). In contrast individual P392L and S399P mutations had less obvious effects on the ubiquitin-binding function of p62, and are reported to be associated with milder disease phenotypes than the double mutation S399P/P392L (Eekhoff *et al.*, 2004). This indicates that the double mutation appeared to have an additive effect both on protein function and disease phenotype, providing support for the relationship between disease severity and the ubiquitin-binding properties of PDB-mutant p62 proteins. However, as these proposals are based on phenotypic descriptions of only single S399P and P392L/S399P carriers, in the future more investigations are needed to derive robust conclusions about this relationship.

Mutation type	Mutation	Age at diagnosis	Bones involved	No. of patients	Patient phenotypes and notes	Ref.
No p62 mutation	—	61 ± 11.63	2.6 ± 1.6	65	N.A	(1)
Truncating mutation	E396X	47 ± 3.9	6.2 ± 2.8	14	Severe disease phenotypes having highest number of bones involved and significantly earlier age of onset	(1)
Point mutation	P392L	55 ± 2.4	3.6 ± 2.5	23	This is the most common mutation in PDB patients had a mild phenotype	(1)
Point mutation	S399P	N.A	N.A	1	Had less severe phenotypes than the double mutation P392L/S399P	(2)
Double mutation	P392L/S399P	N.A	N.A	1	This patient had nearly all his skeleton affected which caused pronounced deformities of the extremities, spine and his skull.	(2)

Table 3.4: Selected PDB-associated p62 mutations and their phenotypes; some of the mutations have limited data therefore the corresponding fields are denoted as N.A. (not available). Reference 1: (Hocking *et al.*, 2004), Reference 2: (Eekhoff *et al.*, 2004).

In our study, we initially assessed the ubiquitin-binding properties of p62 proteins mutations by subjective visual assessments of western blots of the *in vitro* pull-down assays. Although attempts were made to generate semi-quantitative binding data by densitometric analyses of blots, this was on the whole found to be unreliable. In addition, within the binding assays themselves some limitations were noted; for example, difficulty arose in pipetting equal amounts of the Sepharose beads, which varied slightly between the experiments or within the same experiment, because Sepharose beads tend to stick to pipette tips. Further, maintaining constant temperatures (especially 37°C) throughout the binding/washing stages of the pull-down assay was difficult. Consequently, better methods to quantify the ubiquitin-binding properties of p62 were sought; specifically, we decided to measure the dissociation constant (K_d) for interactions between p62 (residues 341-440) and ubiquitin using 2D-HSQC NMR, as such measurements represent a more accurate quantitative assessment of protein binding affinities.

The ultimate goal of our experiments was to measure K_d values for the interactions between wild type/A381V mutant p62 and ubiquitin using 2D-HSQC NMR, in order to try to confirm subtle effects of the A381V mutation on the ubiquitin-binding properties of p62 noted in our pull-down assays. In an extension, it would also have been desirable to collect K_d values for all PDB mutations. However, we concluded that this approach is not optimal to study the interaction between ubiquitin and p62 for several reasons. Firstly, we began by analysing a well characterised PDB mutation known to be associated with loss of ubiquitin-binding function in pull down assays (P392L), but noted that the K_d value for the interaction of p62 (P392L; 341-440) with ubiquitin was not significantly different than that of p62 (WT; 341-440). This indicates that the K_d values were broadly inconsistent with the *in vitro* ubiquitin-binding results, and that protein NMR would not be able to detect the even more

subtle changes in protein function exerted by other PDB-associated p62 mutations. However, the experimental parameters were unavoidably different between the two methods (pull-down and protein NMR). A pH of 7.5 and 37°C was used in the *in vitro* pull-down assays, whilst the NMR experiments were performed at a pH7 and 25°C, as raising the temperature to greater than 25°C can lead to protein denaturation over the time scale of the NMR analyses; protein chemical shifts are also very sensitive to slight changes in the pH, temperature or environmental changes (Vaynberg *et al.*, 2008). In hindsight a PDB-associated mutation which was not associated with significant increases in ubiquitin-binding affinity in pull-down assays at temperatures below 37°C (e.g. G425R) may also have been a better choice of mutation to initially analyse by protein NMR. A further limitation we noted is that the protein NMR technique required expression of >40 litres of culture of *E. coli* expressing the GST-p62 (341-440) proteins to obtain sufficient (~40mg) protein for analysis; hence this method of protein preparation was labour intensive, time consuming, and costly. In the future other biophysical approaches, such as ITC (isothermal titration calorimetry) and SPR (surface plasmon resonance) which rely on less sample should be considered to quantify p62-ubiquitin interaction.

In summary, work in this chapter showed that some (A381V, Δ351-388) but not all (D335E) non-UBA domain PDB-associated mutations are associated with reduced p62 ubiquitin-binding function in pull-down assays; provided support for the proposed relationship between (mutant) p62 ubiquitin-binding function and disease severity in patients; and indicated that protein NMR was not optimal to quantitatively assess the interaction between p62 and ubiquitin *in vitro*.

Subsequent chapters describe work to develop approaches to investigate interactions between wild type and PDB-mutant p62 and ubiquitin in a more physiologically relevant and functional context.

CHAPTER 4

Cellular phenotypes of PDB mutant p62 proteins

Chapter 4: Cellular phenotypes of PDB mutant p62 proteins

4.1 Introduction

Following our initial analyses of the ubiquitin-binding properties of p62 proteins using *in vitro* binding assays and protein NMR (Chapter 3), we extended our study to examine the interaction of p62 and certain PDB mutants with ubiquitin in a cellular context. In particular, it was hoped that these experiments could provide further support for the partial loss of ubiquitin-binding function associated with the A381V mutation suggested from the pull-down assays (Chapter 3).

For these studies, we took advantage of earlier published work which showed that when transfected into mammalian cells, p62 forms cytoplasmic bodies containing ubiquitin, and that a 'functional' UBA domain of p62 is required for the formation of these structures (Biørkøy *et al.*, 2005) consistent with the p62-ubiquitin interaction being central to their biogenesis. Although not fully characterised, some of these structures are presumed to represent membrane-confined autophagosomes and a role for p62 in autophagic protein clearance (as well as turnover of p62 via autophagy) of ubiquitinated proteins has recently been suggested (Pankiv *et al.*, 2007; Komatsu *et al.*, 2007). Another group previously investigated the subcellular localisation of two PDB-associated missense p62 mutants (P392L, P387L) in HEK293 cells (Biørkøy *et al.*, 2005). Their study concluded that both mutant proteins formed larger cytoplasmic bodies (possibly also equivalent to non-membrane-confined p62 protein aggregates as well as autophagosomes) than wild type p62, although co-localisation of ubiquitin with these mutant proteins was not investigated (Leach *et al.*, 2006).

In addition, studies have shown that transfected p62 exhibits similar cellular phenotypes in a wide range of cell lines, including human HEK293 and U2OS cells (Biørkøy *et al.*, 2005), and since U2OS cells are osteosarcoma-derived (i.e. bone-derived) we selected this line for our studies.

Specifically, we used indirect immunofluorescence staining and confocal microscopy to study the effects of selected PDB mutations on (i) p62 subcellular localisation and (ii) co-localisation of p62 with ubiquitin, with the assumption being that the latter may act as a 'surrogate' of the ubiquitin-binding function of p62. The experiments were performed by transfecting polyHis-FLAG-tagged p62 constructs both without and with HA-tagged ubiquitin, followed by immunofluorescence staining and protein visualisation using 2D confocal laser scanning microscopy. In these experiments, image analysis software was used to quantify the sizes of p62 cytoplasmic bodies and the degree of co-localisation between p62 and ubiquitin. This is because often co-localisation measurements depend on visual assessment of a digital image with a mixed colour resultant from overlaying two different colours, and such an assessment is subjective and qualitative with a high degree of variability (French *et al.*, 2008).

In addition, we went on to further characterise the nature of p62 cytoplasmic bodies and noted like others (Biørkøy *et al.*, 2005; Pankiv *et al.*, 2007) co-localisation of transfected p62 with transfected LC3. LC3 (Light Chain 3) is a mammalian homologue to Atg8 in yeast (Kabeya *et al.*, 2000). Cleavage of LC3 at its C-terminus forms cytosolic LC3 (LC3-I). LC3-I is converted to LC3-II through conjugation of phosphatidylethanolamine (PE) to an exposed glycine residue of LC3-I. LC3-II is the autophagosome membrane-associated type of LC3 (Pankiv *et al.*, 2007) and since bound LC3-II on the inner membrane of autophagosomes together with the sequestered materials will be degraded at

the late stages of autophagy, LC3-II is commonly used as an autophagic marker (Kabeya *et al.*, 2000; Koamtsu *et al.*, 2007). As the p62-LC3 interaction is central to autophagosome formation (Biørkøy *et al.*, 2005; Pankiv *et al.*, 2007), we also tested the hypothesis that the PDB-associated D335E mutant of p62 which is located within the LC3-binding region of p62 (Pankiv *et al.*, 2007), may manifest its effects by disrupting this interaction and colocalisation.

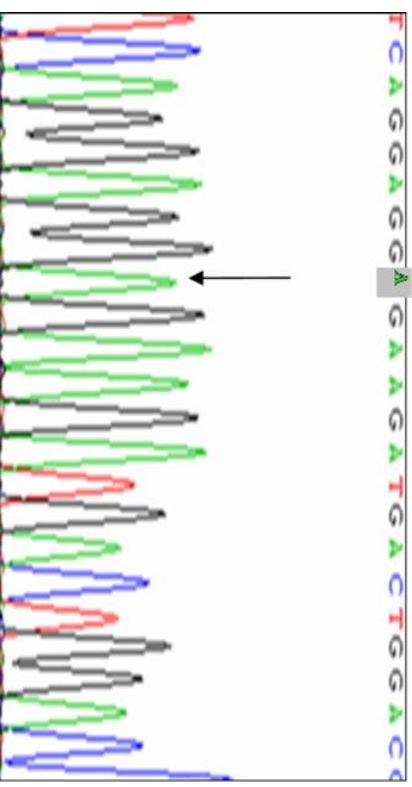
4.2 Generation of eukaryotic expression constructs for PDB mutant p62 proteins

Previously in the lab, a construct allowing expression of polyHis-FLAG tagged wild type human p62 in mammalian cells was prepared by introducing the p62 cDNA sequence into the pcDNA3.1 plasmid (Invitrogen). The D335E and A381V mutations were introduced separately into the wild type pcDNA3.1-p62 sequence by site-directed mutagenesis following the instructions of QuikChange® Site-Directed Mutagenesis kit (Stratagene; see Materials and Methods). Each mutant plasmid was analysed by DNA sequencing and resulting chromatograms were viewed using ChromasLite2 software (Figures 4.1). The mutations were confirmed by sequence alignment with the wild type p62 sequence using ClustalW2.

Since three well characterised PDB-associated p62 mutants (E396X, G425R and P392L), each associated with significant impairment of ubiquitin-binding function, were used as controls for the *in vitro* ubiquitin-binding assays (Chapter 3), these same mutants were used as controls in our cellular studies. These mutants were generated from the wild type pcDNA3.1-p62 construct, previously in the lab; the P392L/S399P double mutant and Δ 351-388 splice

site mutant (Chapter 3) were not analysed further in these experiments. The HA-ubiquitin expression vector (kindly provided by T. Hagen, University of Nottingham) was generated by PCR amplification from the human ubiquitin C IMAGE clone 4076286, including an *XhoI* site, an HA tag in the 5' PCR primer, and a *KpnI* site in the 3' primer, and ligation into the pcDNA3.1myc/his (2) plasmid (Invitrogen). The pcDNA3.1 construct for expression of LC3 as a fusion with tdTomato (tdTomato-LC3), a red fluorescent protein (Biørkøy *et al.*, 2005), was kindly provided by T. Johansen, University of Tromsø, Norway.

(D335E)
T>A



A381V
C>T

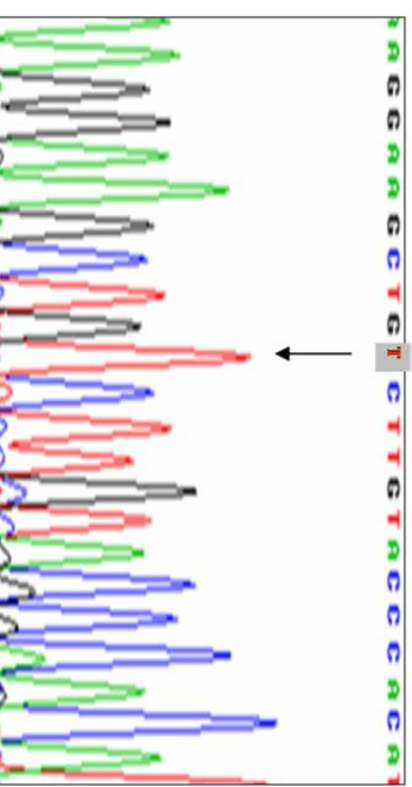


Figure 4.1: DNA sequencing of polyHis-FLAG-p62 expression constructs containing PDB mutations D335E or A381V.

Each of the mutations was introduced to the wild type polyHis-FLAG-p62 sequence by site-directed mutagenesis. Arrows indicate the sites of each mutation, with the bases changes shown above.

4.3 Method development

The principle of indirect immunofluorescence staining depends on laser excitation of a fluorescent dye linked to specific secondary antibodies (in complex with primary antibodies bound to antigens within the sample under investigation), followed by detecting the emitted light by confocal microscopy. In this case, a wavelength of 568nm (green-yellow) is used for the excitation of the fluorescent secondary antibody directed against one of the protein targets to be detected, resulting in the emission of red light. At the same time, a wavelength of 488nm (red) is used for the excitation of the fluorescent secondary antibody directed against the other target, resulting in the emission of green light. In addition, to facilitate efficient location and shape of the cells, the nucleus is stained with another fluorescent dye, in this case Hoescht 32258, which emits a blue light upon UV-excitation (Suzuki *et al.*, 1992; Kuroiwa *et al.*, 1982). This approach is sensitive to several experimental variables, which can result in poor image quality and non-reproducible results; therefore, we first optimised the detection protocols prior to detailed co-localisation studies. Some of the experimental variables investigated as part of method development are described below.

4.3.1 Localisation of endogenous p62 and ubiquitin in U2OS cells

Prior to detailed analyses of the co-localisation of transfected polyHis-FLAG-tagged p62 and HA-tagged ubiquitin in U2OS cells, the expression and subcellular localisation of endogenous proteins (i.e. at normal physiological expression levels) was first investigated. This was important to ensure that the subsequent expression of transfected proteins was associated with cellular phenotypes that were physiologically relevant. U2OS cells without ectopic expression of p62/ubiquitin were fixed (in this case using formaldehyde) and

immunoprobed with anti-ubiquitin and anti-p62 antibodies, to detect endogenous ubiquitin and p62 proteins, respectively. Endogenous ubiquitin staining was diffuse throughout the cytoplasm and nucleus, whilst endogenous p62 staining was noted as small cytoplasmic bodies (as previously reported (Biørkøy *et al.*, 2005)); limited overlap of staining of the endogenous p62 and ubiquitin proteins was noted (Figure 4.2).

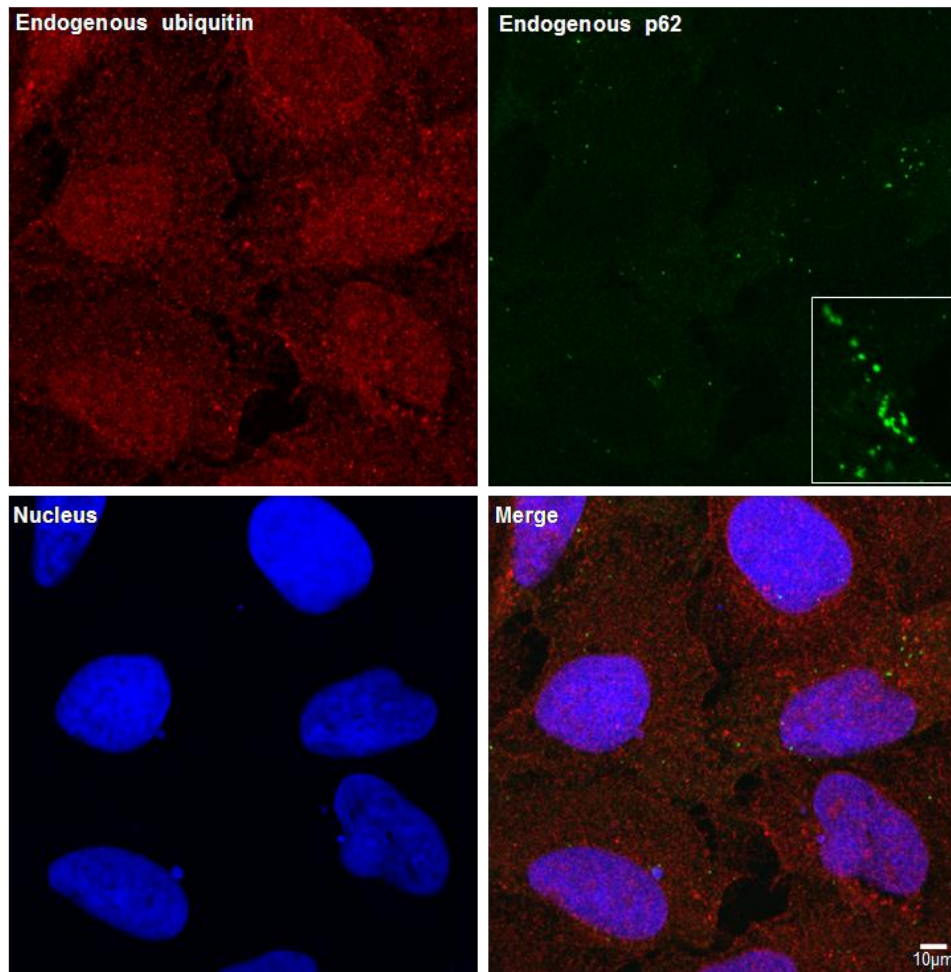


Figure 4.2: Localisation of endogenous p62 and ubiquitin in U2OS cells

U2OS cells fixed with formaldehyde were probed using mouse anti-p62 as primary antibody and stained green using anti-mouse Alexafluor 488 as secondary antibody. Rabbit anti-ubiquitin was used as primary antibody to detect endogenous ubiquitin and anti-rabbit Alexafluor 568 is used as secondary antibody (red). Hoescht 32258 was used for nuclear staining. On analysis by confocal microscopy, endogenous ubiquitin showed a diffuse pattern in the cytoplasm and the nucleus, whilst endogenous p62 staining was localised to small cytoplasmic vesicle-like structures (a higher magnification and staining intensity image of p62 is included). All images were collected with a 63X objective lens, with scale bar as indicated.

4.3.2 Comparison between different chemical fixatives

Processing of samples for analysis by indirect immunofluorescence staining and confocal microscopy begins with fixation. A fixation method must balance the preservation of cellular morphology with access to antigenic sites. Initially methanol-acetone (50:50) was used to fix the U2OS cells singly transfected with polyHis-FLAG-tagged wild type p62 prior to immunostaining, however later the cells were fixed with formaldehyde. In both cases p62 staining was found to be similar (Figure 4.3), with cellular phenotypes that appeared to be exaggerated forms of those noted for the endogenous protein i.e. distinct cytoplasmic bodies; in some cases these were noted to be perinuclear. Although the methanol-acetone mixture gave encouraging initial results, overall formaldehyde gave more reproducible and higher quality images upon confocal microscopic analysis (Figure 4.3). Therefore, formaldehyde fixative was chosen to fix U2OS cells for subsequent experiments.

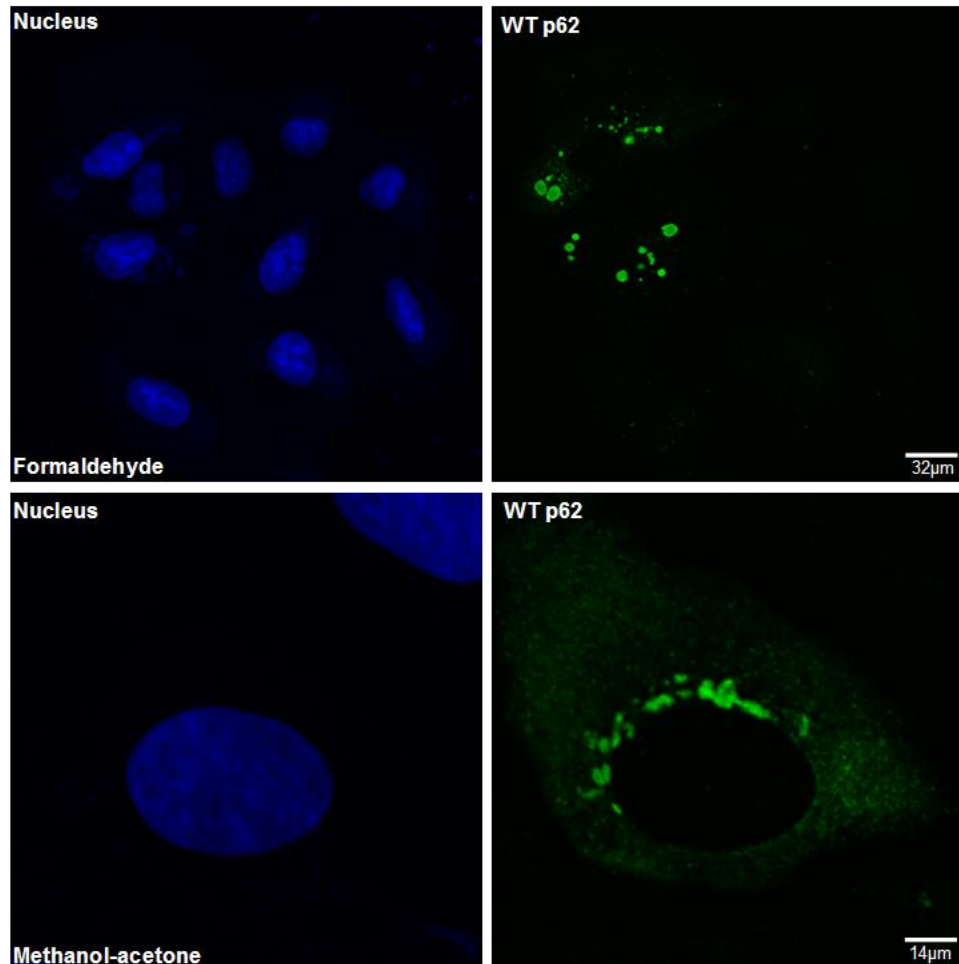


Figure 4.3: Comparison between different chemical fixatives

Wild type polyHis-FLAG-p62 was transfected in to U2OS cells which after ~40 hours were fixed as indicated. Detection of p62 was using mouse anti-p62 as primary antibody and anti-mouse Alexafluor 488 as secondary antibody. Hoescht 32258 was used for staining of nuclei. Confocal microscopy images were collected at 63X objective lens, with scale bar as indicated. Overall formaldehyde fixation was judged to produce more reproducible and higher quality images.

4.3.3 Optimisation of polyHis-FLAG-tagged p62 plasmid concentration for transfections

To determine the optimum concentration of plasmids to use in subsequent experiments, two different concentrations of wild type polyHis-FLAG-tagged p62 plasmid were selected and transfected into U20S cells. Approximately 40 hours after transfection, cells were fixed and transfected. p62 was detected by immunoprobng with anti-p62 antibodies and visualisation by confocal microscopy analysis. At the two different plasmid concentrations used (0.15µg/ml and 0.5µg/ml) p62 staining was similar (Figure 4.4), with cellular phenotypes that again appeared to be exaggerated forms of those noted for the endogenous protein i.e. cytoplasmic bodies. These observations indicate that formation of p62 cytoplasmic bodies was not plasmid concentration-dependent in our cells, opposing previous reports which suggested that p62 'aggregate' formation was proportional to plasmid concentration in transfection experiments (Paine *et al.*, 2005). However, it should be noted that we used a different experimental method to investigate the optimum plasmid concentration; we used confocal microscopy whilst Paine *et al.* used SDS-PAGE analysis.

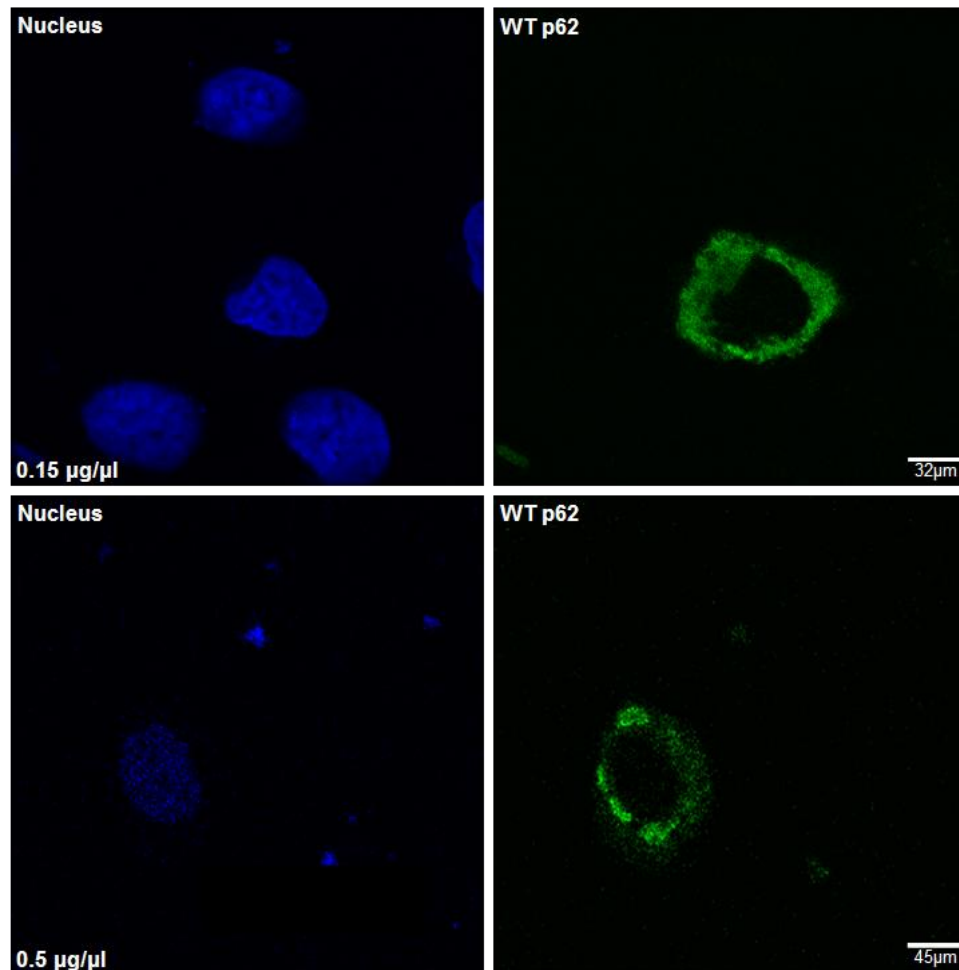


Figure 4.4: Optimisation of polyHis-FLAG-tagged p62 plasmid concentration for transfections

Two different concentrations of wild type polyHis-FLAG-tagged p62 plasmid, 0.15 µg/ml and 0.5 µg/ml, were transfected into U2OS cells, which after ~40 hours were fixed with formaldehyde. p62 was detected using mouse anti-p62 as primary antibody and stained green using anti-mouse Alexafluor 488 as secondary antibody. Hoescht 32258 was used for nucleus staining. All images were collected at 63X objective lens. Transfected p62 showed broadly similar localization and staining in U2OS cells at the two different plasmid concentrations.

4.3.4 Optimisation of time of transfection

Previous studies reported that the formation of p62 cytoplasmic bodies/aggregates is proportional to incubation time of the plasmids after transfection (Paine *et al.*, 2005). To test this in our U2OS cells, we transfected cells with polyHis-FLAG tagged p62 for different time intervals prior to immunostaining and confocal microscopy analysis (Figure 4.5). After 56 hours of transfection, cells showed a significant proportion of large p62-positive cytoplasmic bodies. At approximately 36-40 hours transfection, p62 still formed cytoplasmic bodies, but in general these were judged to be smaller than at the longer incubation times with a cellular phenotype closer to that of non-transfected cells, consistent with the earlier observations of Paine *et al.* Consequently, 36-40 hours was chosen as the optimum transfection time for subsequent experiments.

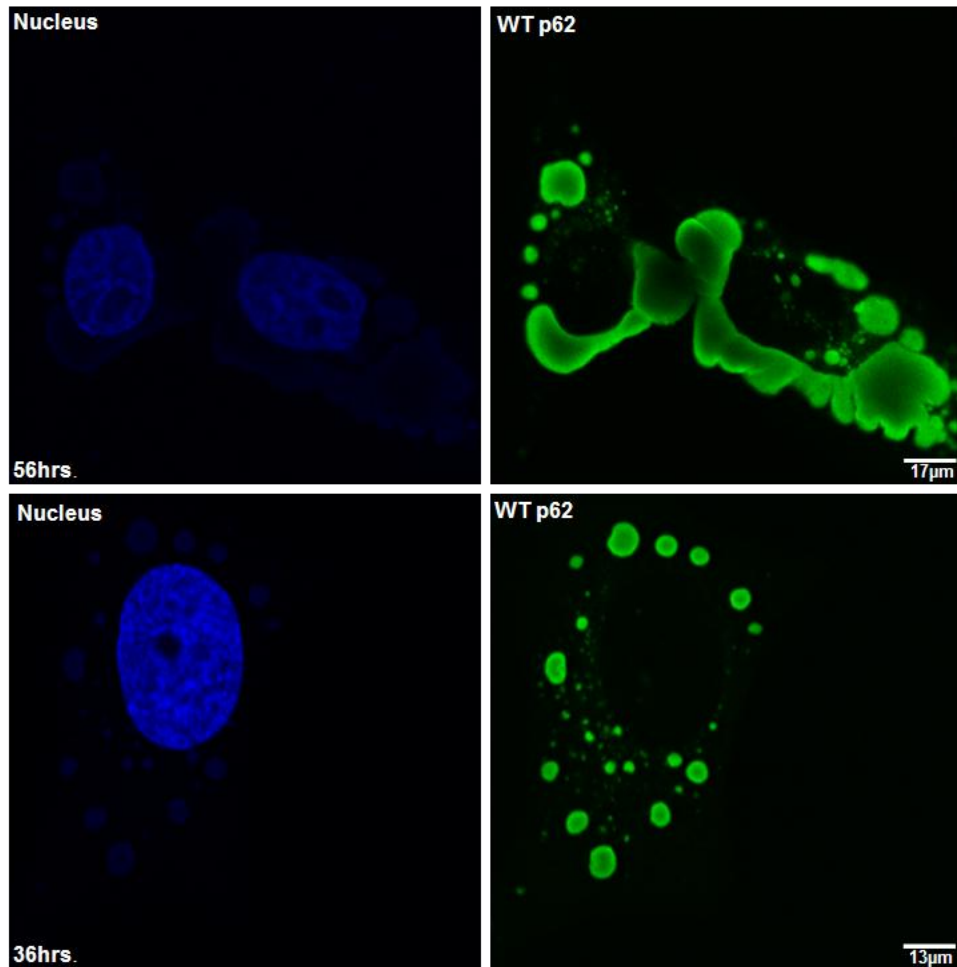


Figure 4.5: Optimisation of time of transfection

U2OS cells were transfected with polyHis-FLAG tagged p62 for different time intervals prior to fixing the cells with formaldehyde. p62 was detected using mouse anti-p62 as primary antibody and stained green using anti-mouse Alexafluor 488 as secondary antibody. Hoescht 32258 was used for nucleus staining. All images were collected at 63X objective lens. After 56 hours of transfection, cells showed a significant proportion of large p62-positive cytoplasmic bodies. At approximately 36-40 hours transfection, p62 still formed cytoplasmic bodies, but in general these were judged to be smaller than at the than longer incubation times with a cellular phenotype closer to that of non-transfected cells, as a result we chose approximately 36 hours as optimum transfection time.

4.3.5 Co-transfection of polyHis-FLAG-p62 and HA-ubiquitin, and comparison of staining of different primary antibodies

To begin to investigate interactions between p62 and ubiquitin in transfected cells, U20S were co-transfected with wild type polyHis-FLAG-tagged p62 and HA-ubiquitin plasmids, using conditions established in 4.3.2 and 4.3.4 (cell fixation with formaldehyde; transfection for ~36-40 hours). As p62 cytoplasmic body formation did not seem to be sensitive to amount of p62 plasmid in the range we tested (4.3.3), a concentration of 0.5 μ g/ml was selected for the transfected plasmids (both polyHis-FLAG-p62 and HA-ubiquitin). In addition, two different primary antibodies were assessed for detecting p62 and ubiquitin after transfection. p62 was detected with anti-FLAG and anti-p62, the latter of which was judged to show more robust and clearer staining upon confocal microscopy analysis. For ubiquitin detection, anti-ubiquitin and anti-HA was compared and again the latter was judged to show better staining (Figure 4.6). Upon co-transfection with ubiquitin, p62 staining was broadly similar to that noted in single transfections of p62 only, with cytoplasmic bodies still clearly visible, and significant co-localisation of wild type poly-His-FLAG-p62 and HA-ubiquitin was noted (see 4.3.8 for a more detailed analysis).

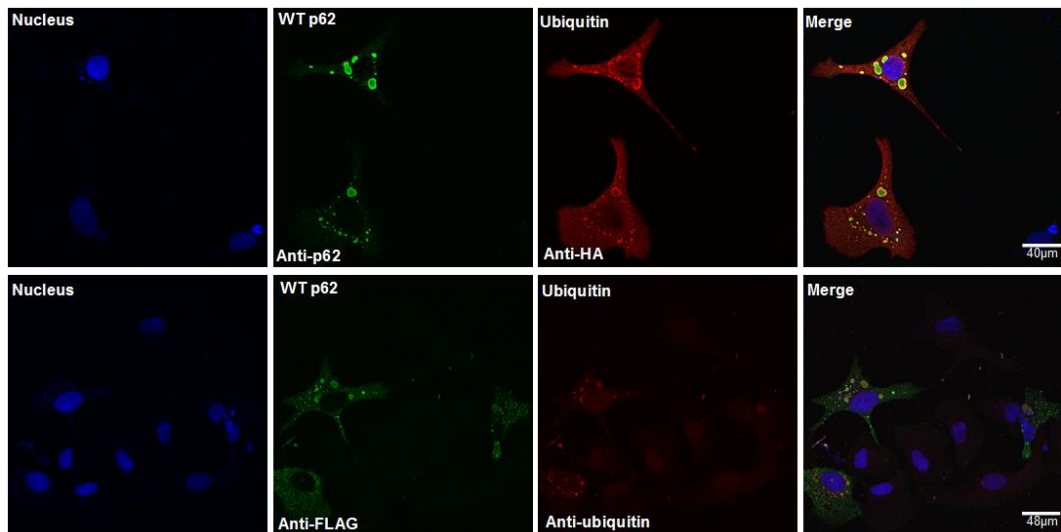


Figure 4.6: Co-transfection of polyHis-FLAG-p62 and HA-ubiquitin, and comparison of staining of different primary antibodies

Wild type polyHis-FLAG-tagged p62 plasmid and HA-ubiquitin were co-transfected into U2OS cells, which after ~40 hours were fixed with formaldehyde. p62 was detected using two different primary antibodies as indicated and stained green using anti-mouse Alexafluor 488 as secondary antibody. Ubiquitin was also detected with two different primary antibodies as indicated and stained red using anti-rabbit Alexafluor 568 as secondary antibody. Hoescht 32258 was used for nuclear staining. Confocal microscopy images were collected at 63X objective lens, with scale bar as indicated. Overall anti-p62 and anti-HA primary antibodies were assessed to produce clearer staining and more reproducible results.

4.3.6 Comparison of different staining colours for p62 and ubiquitin

Two different colours (secondary antibodies) were tested to stain for co-transfected wild type polyHis-FLAG-p62 and HA-ubiquitin in U2OS cells. After immunoprobng for p62 with mouse anti-p62 and for ubiquitin with rabbit anti-HA (as established in 4.3.5), p62 was stained green with anti-mouse Alexafluor 488 and ubiquitin stained red with anti-rabbit Alexafluor 568; alternatively, p62 was stained red with anti-mouse Alexafluor 568 and ubiquitin stained green with anti-rabbit Alexafluor 488. The staining patterns of the interchanged antibodies were similar. However, since ubiquitin has a wider distribution in the cytoplasm and the nucleus of the cells than p62, and based on our visual preferences, we subsequently stained ubiquitin as red and p62 as green (Figure 4.7).

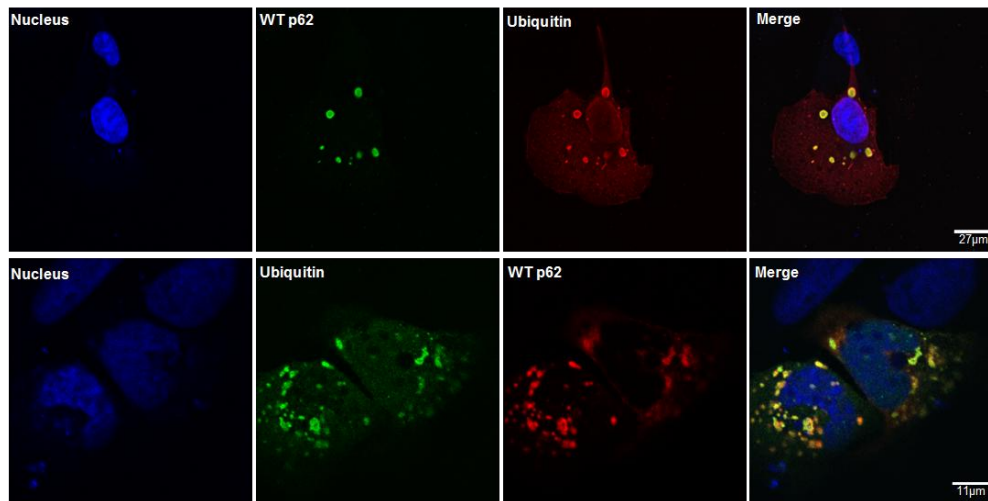


Figure 4.7: Comparison of different staining colours for p62 and ubiquitin

Wild type polyHis-FLAG-tagged p62 plasmid and HA-ubiquitin were co-transfected in to U2OS cells, which after ~40 hours were fixed with formaldehyde. p62 was detected using mouse anti-p62 as primary antibody and ubiquitin was detected using rabbit anti-HA as primary antibody. The secondary antibodies (anti-mouse Alexafluor 488 and anti-rabbit Alexafluor 568) were used to stain p62 and ubiquitin interchangeably. Hoescht 32258 was used for nuclear staining. Confocal microscopy images were collected at 63X objective lens, with scale bar as indicated. Based on visual preference we decided to subsequently stain p62 as green and ubiquitin as red.

4.3.7 Specificity of secondary antibodies

As a final control, the specificity of the secondary antibodies was investigated after co-transfection of U2OS cells with wild type polyHis-FLAG-p62 and HA-ubiquitin for ~40 hours. Transfected cells were treated with a mixture of secondary antibodies (anti-mouse Alexafluor 488 and anti-rabbit Alexafluor 568), whilst primary antibodies were omitted. Both red and green channels of the collected images showed no evidence of non-specific binding of secondary antibodies (Figure 4.8).

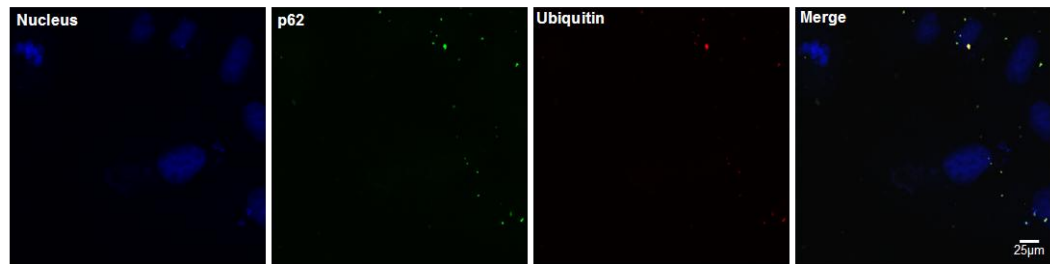


Figure 4.8: Specificity of secondary antibodies

U2OS cells co-transfected with wild type polyHis-FLAG-tagged p62 plasmid and HA-ubiquitin for ~40 hours were fixed with formaldehyde. Cells were treated with a mixture of secondary antibodies (anti-mouse Alexafluor 488 and anti-rabbit Alexafluor 568), whilst primary antibodies were omitted. Hoescht 32258 was used for nuclear staining. All images were collected with a 63X objective lens, with scale bar as indicated. Both red and green channels of the collected images showed no evidence of non-specific binding of secondary antibodies.

4.3.8 Cellular phenotypes of transfected wild type polyHis-FLAG-p62 and selected PDB mutants in U2OS cells

Prior to the detailed co-localisation studies between wild type and PDB mutant p62 and ubiquitin, p62 localisation (in the absence of transfected HA-ubiquitin) in U2OS cells was investigated to evaluate any effects of selected PDB mutations (A381V, D335E, E396X) on cellular phenotype. U2OS cells were transiently transfected with polyHis-FLAG-p62 for ~40 hours and fixed with formaldehyde. Mouse anti-p62 was used as a primary antibody for probing p62 and then anti-mouse Alexafluor 488 was used as a secondary antibody. Wild type p62 and the missense mutations showed cytoplasmic bodies varying in their size and shape (investigated in detail in sections 4.4; 4.5), whilst in contrast the E396X mutant showed diffuse staining throughout the cytoplasm (Figure 4.9).

To confirm that the observed phenotypes (in particular that of the E396X mutant) were not resultant from variable expression levels of the ectopic proteins, the expression levels of each p62 construct in U2OS cells were detected with western-blotting after ~40 hours transfection (using anti-p62). The blots confirmed similar p62 expression levels for the wild type protein and its mutants (Figure 4.10).

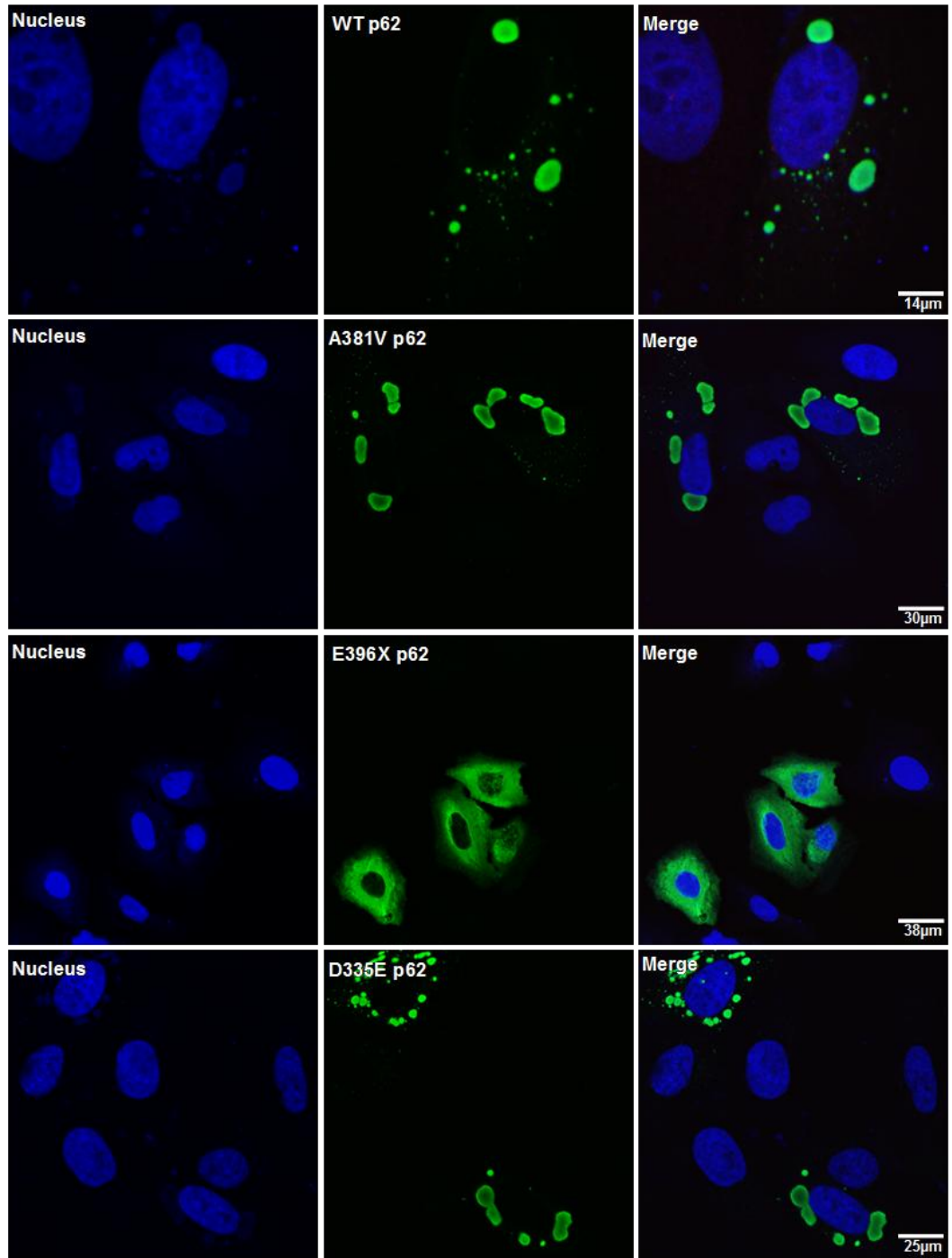


Figure 4.9: Representative examples of wild type and PDB mutant polyHis-FLAG-p62 localisation in U2OS cells (previous page)

Wild type or PDB mutant (as indicated) polyHis-FLAG-p62 was transfected in to U2OS cells, which after ~40 hours were fixed with formaldehyde. Detection of p62 was using mouse anti-p62 as primary antibody and anti-mouse Alexafluor 488 as secondary antibody. Hoescht 32258 was used for staining of nuclei. Confocal microscopy images were collected at 63X objective lens, with scale bars as indicated. Wild type p62 and the A381V or D335E missense mutants formed cytoplasmic bodies, however the E396X mutant exhibited diffuse staining throughout the cytoplasm.

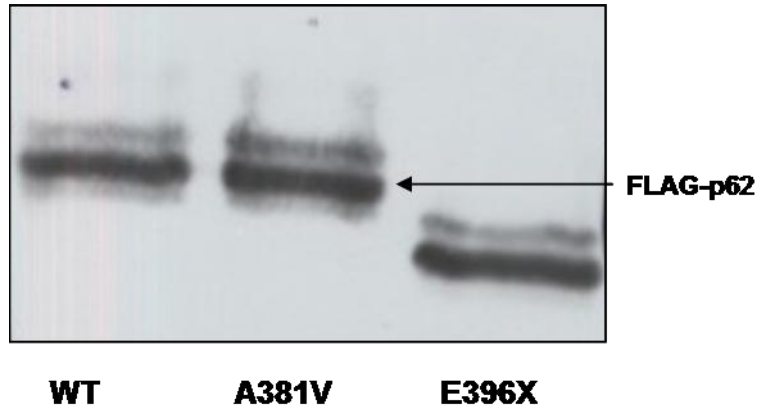


Figure 4.10: Immunoblot of ectopic expression levels of polyHis-FLAG-p62 constructs in U2OS cells

Equal numbers of U2OS cells were transiently transfected with polyHis-FLAG-p62 constructs as indicated. After ~40 hours cells were washed and then solubilised with gel loading buffer; equal volumes of resulting lysates were resolved by SDS PAGE and analysed by western blotting (anti-p62). The blot shows approximately equal expression levels of transfected wild type and A381V or E396X mutant p62. The D335E mutant similarly showed comparable expression levels to the wild type (data not shown).

4.3.9 Cellular phenotypes of transfected HA-ubiquitin in U2OS cells

Prior to the detailed co-localisation studies between wild type and PDB mutant p62 and ubiquitin, transfected HA-ubiquitin cellular localisation (in the absence of transfected polyHis-FLAG-p62) in U2OS cells was also first investigated.

U2OS cells were transiently transfected with HA-ubiquitin for ~40 hours and fixed with formaldehyde. Rabbit anti-HA was used as a primary antibody to detect ubiquitin and then anti-rabbit Alexafluor 568 was used as a secondary antibody. Transfected HA-ubiquitin showed a diffuse distribution in the cytoplasm as well as in the nucleus (Figure 4.11), comparable with the staining pattern of the endogenous protein (Figure 4.2).

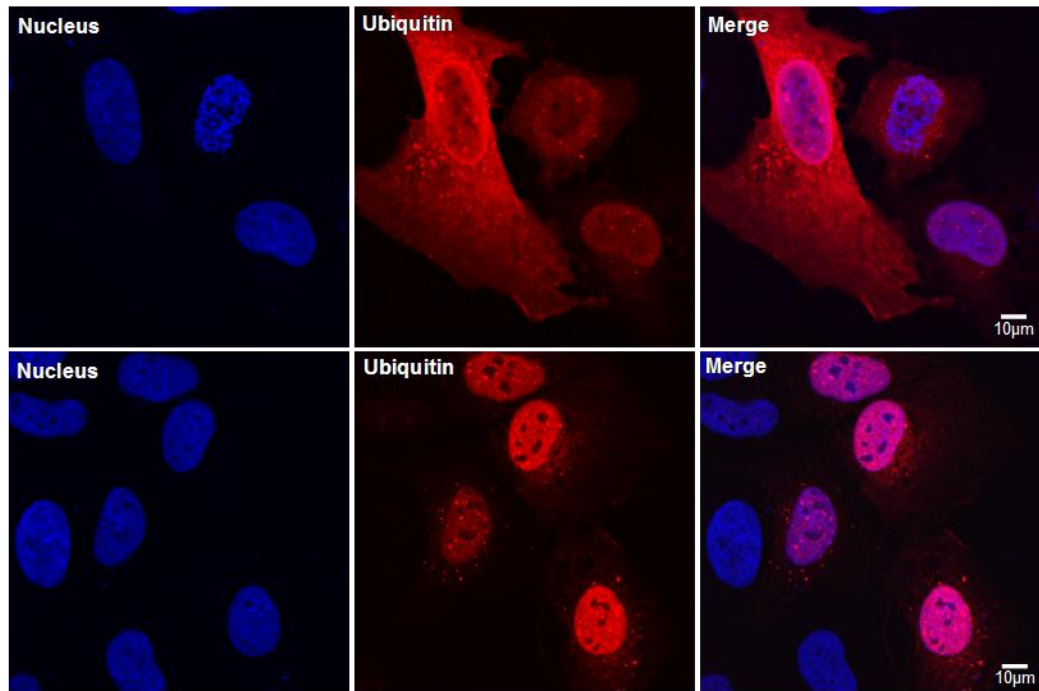


Figure 4.11: Localisation of transfected HA-ubiquitin in U2OS cells

HA-ubiquitin was transfected into U2OS cells, which after ~40 hours were fixed with formaldehyde. Detection of ubiquitin was using rabbit anti-HA as primary antibody and anti-rabbit Alexafluor 568 as secondary antibody. Hoescht 32258 was used for staining of nuclei. Confocal microscopy images were collected at 63X objective lens, with scale bar as indicated. Transfected ubiquitin exhibited a diffused staining pattern, and was distributed evenly in the cytoplasm or in the nucleus.

4.4 Co-localisation of wild type and PDB mutant polyHis-FLAG-p62 with HA-ubiquitin

Previous studies showed strong co-localisation between wild type p62 and ubiquitin co-transfected in mammalian cells (Biørkøy *et al.*, 2005). Therefore, we decided to assess the effects of PDB-associated mutations on the interaction of p62 with ubiquitin by examining co-localisation patterns in U2OS cells. In particular, it was hoped that these experiments may provide support for the marginal loss of ubiquitin-binding function associated with the A381V mutant noted in the pull-down assays, and would provide an alternative method to 2D-HSQC NMR for examining p62-ubiquitin interactions (Chapter 3).

U2OS cells were transiently co-transfected with p62 and ubiquitin for ~40 hours and the cells were fixed with formaldehyde. p62 was detected with anti-p62 and ubiquitin with anti-HA. The secondary antibodies were a mixture of Alexafluor 488 and Alexafluor 568.

To obtain accurate co-localisation measurements, the confocal microscope was adjusted to its optimum settings, as confocal microscopes have several technical limitations. One of the limitations of confocal microscopes is "cross talk" phenomenon, which is caused by the overlap of the emission and excitation spectra of the fluorophores of the secondary antibodies. The fluorophores usually have emission or excitation spectra that are close together or partially overlapping, thereby the wavelength selected to excite the first fluorophore might excite the second fluorophore at the same time, causing false co-localisation intensities (French *et al.*, 2008). To avoid the cross talk phenomenon, the spectra of the fluorophores must be separated as far as possible, and a narrow detection band for the emitted light should be

used (French *et al.*, 2008). Also, collecting the images with sequential scanning decreases background and cross talk emission by reducing the overlap between the two emission spectra of the fluorophores.

After setting the microscope to its optimum setting, the slides were scanned. Wild type polyHis-FLAG-p62 co-localised strongly with HA-ubiquitin (Figure 4.12, 4.13). Notably, upon co-transfection with HA-ubiquitin wild type polyHis-FLAG-p62 showed similar cellular phenotypes to singly transfected p62 protein. In contrast, transfected HA-ubiquitin changed its morphology from a diffuse pattern and became incorporated within cytoplasmic bodies, which mimicked the cytoplasmic bodies of polyHis-FLAG-p62. As a result, it was concluded that transfected polyHis-FLAG-p62 appears to recruit HA-ubiquitin in to the cytoplasmic bodies, which were later shown to contain an autophagosome marker (see section 4.6).

The E396X mutant did not co-localise when co-transfected with HA-ubiquitin (Figure 4.14). Each of the p62 missense mutants A381V, P392L and D335E retained their co-localisation with ubiquitin and on first inspection their co-localisation patterns were subjectively indistinguishable from those of wild type polyHis-FLAG-p62 with HA-ubiquitin (Figures 4.17-4.20). Hence, minor defects in the ubiquitin-binding function associated with the A381V mutant noted in the pull-down assays (Chapter 3) did not appear to manifest as obvious differences in co-localisation of transfected proteins, nor did more severe effects on ubiquitin-binding function previously noted for the P392L mutant (Cavey *et al.*, 2005). Notably, the G425R mutant was the only missense mutant that occasionally showed reduced co-localisation with ubiquitin (Figure 4.16); this mutant was associated with significant impairment of ubiquitin-binding *in vitro* (Cavey *et al.*, 2005).

Assessing the images visually, we noted that transfected wild type polyHis-FLAG-p62 appeared to form two distinct major cellular phenotypes, based on their morphology. The first group was denoted *common rounded and semi-rounded cytoplasmic bodies*, and was further subdivided to three types (Figure 4.12):

A - Small rounded cytoplasmic bodies.

B - Medium rounded cytoplasmic bodies.

C - Large semi-rounded cytoplasmic bodies.

The second group was denoted *rarer irregular cytoplasmic structures*, and was also further subdivided to three types (Figure 4.13):

D - Perinuclear structures.

E - Multiple connected bodies.

F - Diffuse structures.

To ensure the results were consistent, the experiment was repeated several times and on each occasion, all of the above cellular phenotypes were noted.

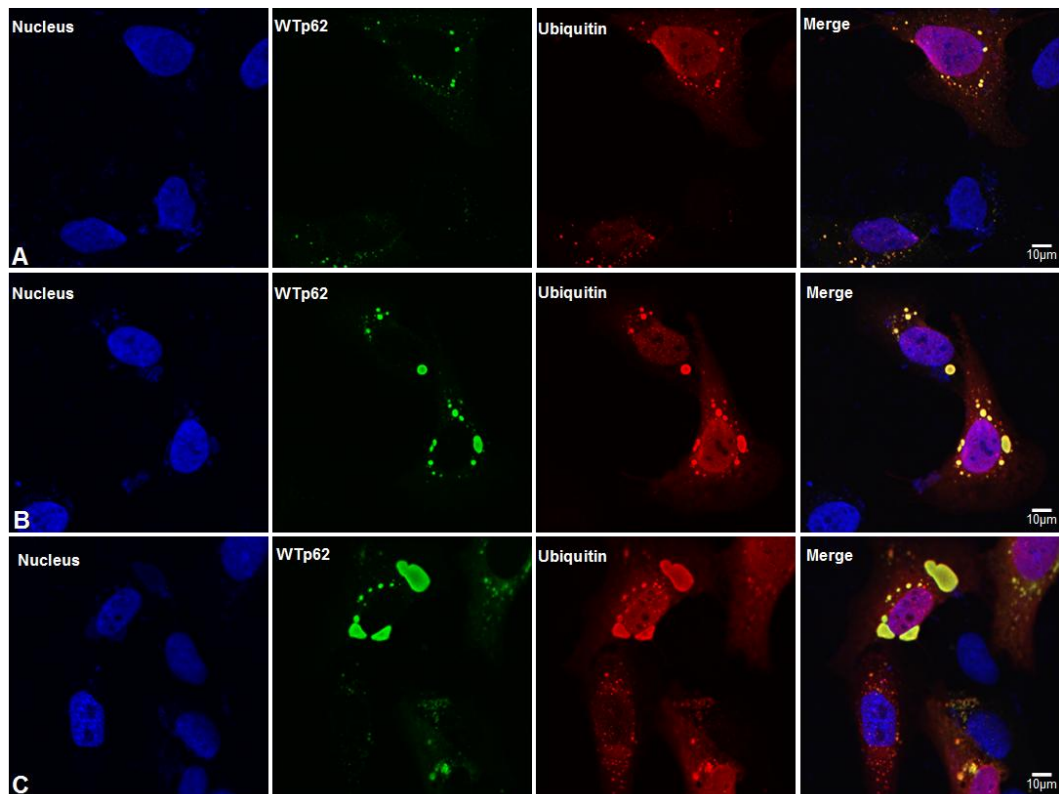


Figure 4.12: Co-localisation of wild type polyHis-FLAG-p62 and HA-ubiquitin in U2OS cells and their cellular phenotypes (part 1)

Wild type polyHis-FLAG-p62 and HA-ubiquitin were co-transfected into U2OS cells, which after ~40 hours were fixed with formaldehyde. p62 was detected using mouse anti-p62 as primary antibody and stained green using anti-mouse Alexafluor 488 as secondary antibody. Ubiquitin was detected using rabbit anti-HA primary antibody and stained red using anti-rabbit Alexafluor 568 as secondary antibody. Hoescht 32258 was used for staining nuclei. Confocal microscopy images were collected at 63X objective lens, with scale bars as indicated. Wild type polyHis-FLAG-p62 co-localised strongly with HA-ubiquitin.

Three major cellular phenotypes, *common rounded and semi-rounded cytoplasmic bodies*, were observed to be associated wild type polyHis-FLAG-p62:

- A) Small rounded cytoplasmic bodies.
- B) Medium rounded cytoplasmic bodies.
- C) Large semi-rounded cytoplasmic bodies.

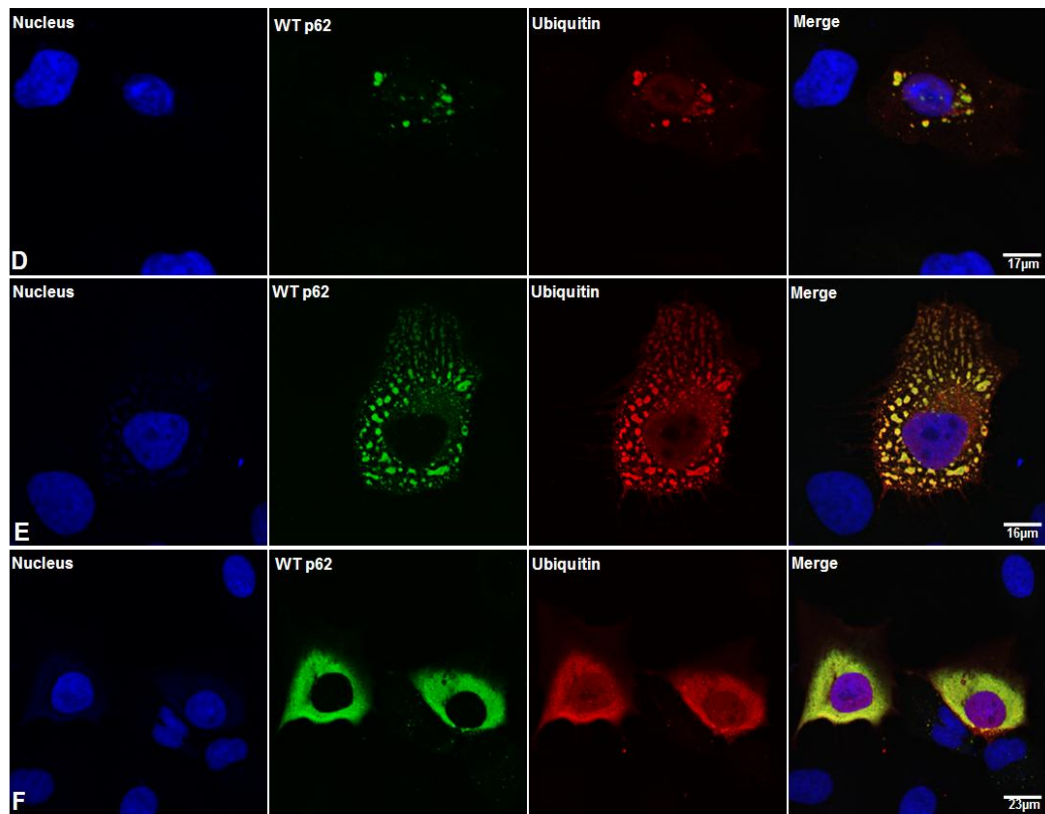


Figure 4.13: Co-localisation of wild type polyHis-FLAG-p62 and HA-ubiquitin in U2OS cells and their cellular phenotypes (part 2)

Wild type polyHis-FLAG-p62 and HA-ubiquitin were co-transfected into U2OS cells, which after ~40 hours were fixed with formaldehyde. p62 was detected using mouse anti-p62 as primary antibody and stained green using anti-mouse Alexafluor 488 as secondary antibody. Ubiquitin was detected using rabbit anti-HA primary antibody and stained red using anti-rabbit Alexafluor 568 as secondary antibody. Hoescht 32258 was used for staining nuclei. Confocal microscopy images were collected at 63X objective lens, with scale bars as indicated. Wild type polyHis-FLAG-p62 co-localised strongly with HA-ubiquitin.

Three *rarer irregular cytoplasmic structures* observed for wild type polyHis-FLAG-p62 were:

- D) Perinuclear structures.
- E) Multiple connected bodies.
- F) Diffuse staining (similar to E396X diffuse staining phenotype).

The cellular phenotypes of cells co-transfected with E396X mutant polyHis-FLAG-p62 and HA-ubiquitin were not comparable to the rest of the p62 constructs, as this mutant commonly showed diffuse staining as opposed to cellular bodies/perinuclear staining. Very rarely miniature cytoplasmic bodies were also noted for this mutant (Figure 4.14, 4.15). The G425R mutant exhibited similarities to the cellular phenotypes of wild type polyHis-FLAG-p62, although occasionally this mutant also showed distinct 'semi-diffuse' structures, which were not observed to be associated with other PDB-associated mutants (Figure 4.16). The P392L mutant also exhibited very similar cytoplasmic bodies to wild type polyHis-FLAG-p62 (Figure 4.17). Figures 4.16 and 4.17 show some common cellular phenotypes associated with the G425R and P392L mutants, although other cellular phenotypes equivalent to those noted for wild type polyHis-FLAG-p62 were also evident for these mutants (data not shown).

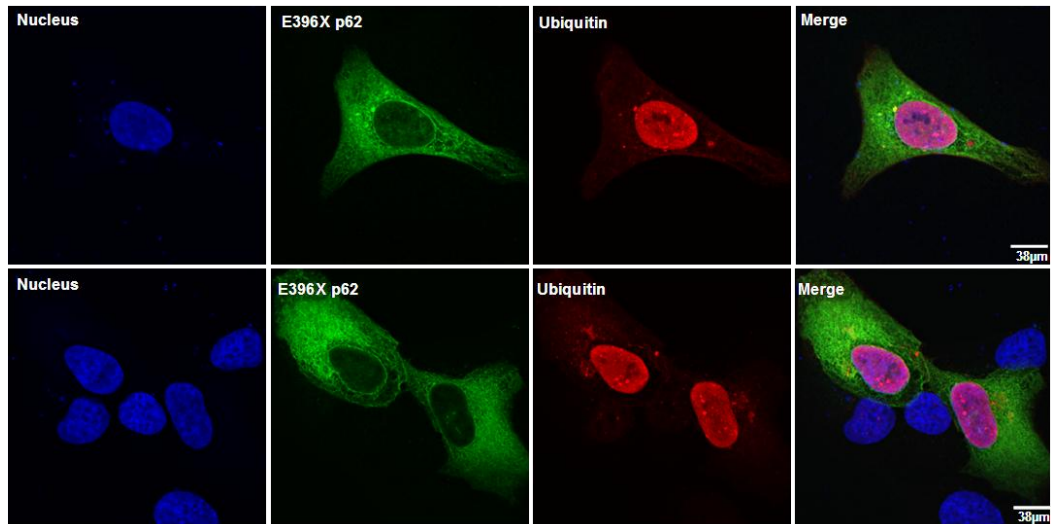


Figure 4.14: Co-localisation of E396X mutant polyHis-FLAG-p62 and HA-ubiquitin in U2OS cells and their cellular phenotypes (part 1)

E396X mutant polyHis-FLAG-p62 and HA-ubiquitin were co-transfected into U2OS cells, which after ~40 hours were fixed with formaldehyde. p62 was detected using mouse anti-p62 as primary antibody and stained green using anti-mouse Alexafluor 488 as secondary antibody. Ubiquitin was detected using rabbit anti-HA primary antibody and stained red using anti-rabbit Alexafluor 568 as secondary antibody. Hoescht 32258 was used for staining nuclei. Confocal microscopy images were collected at 63X objective lens, with scale bars as indicated. Transfected E396X mutant commonly showed a diffuse staining pattern which did not co-localise with ubiquitin. Rarely cytoplasmic bodies were also observed for E396X mutant polyHis-FLAG-p62, as shown in Figure 4.15.

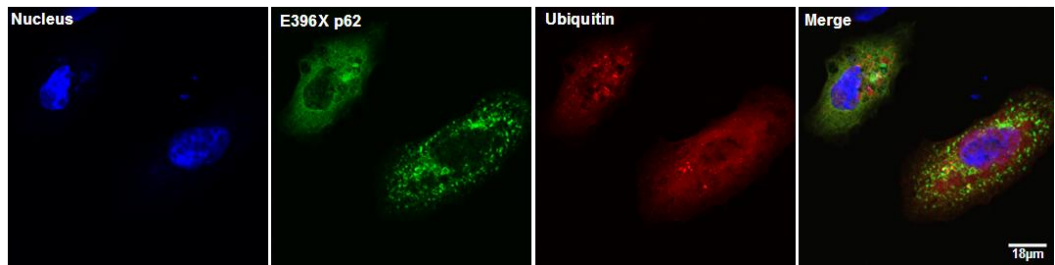


Figure 4.15: Co-localisation of E396X mutant polyHis-FLAG-p62 and HA-ubiquitin in U2OS cells and their cellular phenotypes (part 2)

E396X mutant polyHis-FLAG-p62 and HA-ubiquitin were co-transfected into U2OS cells, which after ~40 hours were fixed with formaldehyde. p62 was detected using mouse anti-p62 as primary antibody and stained green using anti-mouse Alexafluor 488 as secondary antibody. Ubiquitin was detected using rabbit anti-HA primary antibody and stained red using anti-rabbit Alexafluor 568 as secondary antibody. Hoescht 32258 was used for staining nuclei. Confocal microscopy images were collected at 63X objective lens, with scale bars as indicated. This rare cellular phenotype involved miniature cytoplasmic bodies but only very occasionally, which did not co-localise with ubiquitin.

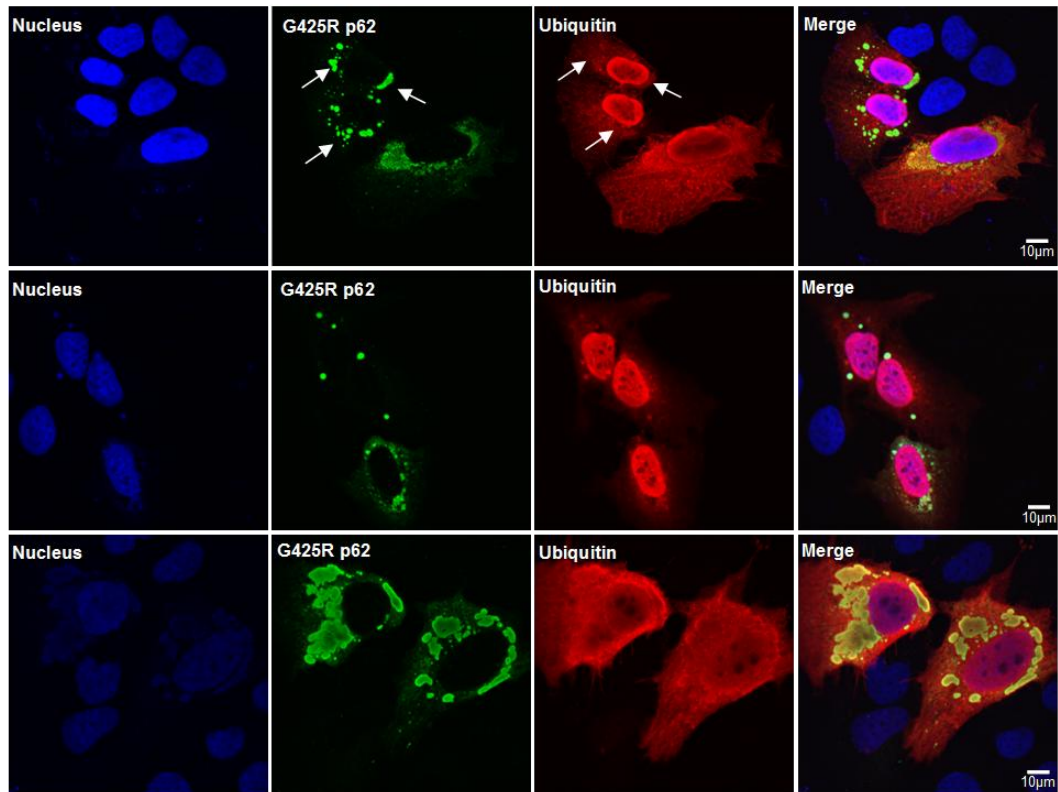


Figure 4.16: Co-localisation of G425R mutant polyHis-FLAG-p62 and HA-ubiquitin in U2OS cells and their cellular phenotypes

G425R mutant polyHis-FLAG-p62 and HA-ubiquitin were co-transfected into U2OS cells, which after ~40 hours were fixed with formaldehyde. p62 was detected using mouse anti-p62 as primary antibody and stained green using anti-mouse Alexafluor 488 as secondary antibody. Ubiquitin was detected using rabbit anti-HA primary antibody and stained red using anti-rabbit Alexafluor 568 as secondary antibody. Hoescht 32258 was used for staining nuclei. Confocal microscopy images were collected at 63X objective lens, with scale bars as indicated. The G425R mutant showed co-localisation with ubiquitin in some cells, although reduced co-localised with ubiquitin (relative to wild type) was also sometimes noted as indicated by the arrows of the first row of the images. In general G425R mutant polyHis-FLAG-p62 exhibited similar cellular phenotypes to wild type p62 (in this figure medium and large cytoplasmic bodies are shown but the other cellular phenotypes were also evident). This mutant also exhibited a semi-diffuse staining pattern in a few cells as evident from the images of the first and third rows.

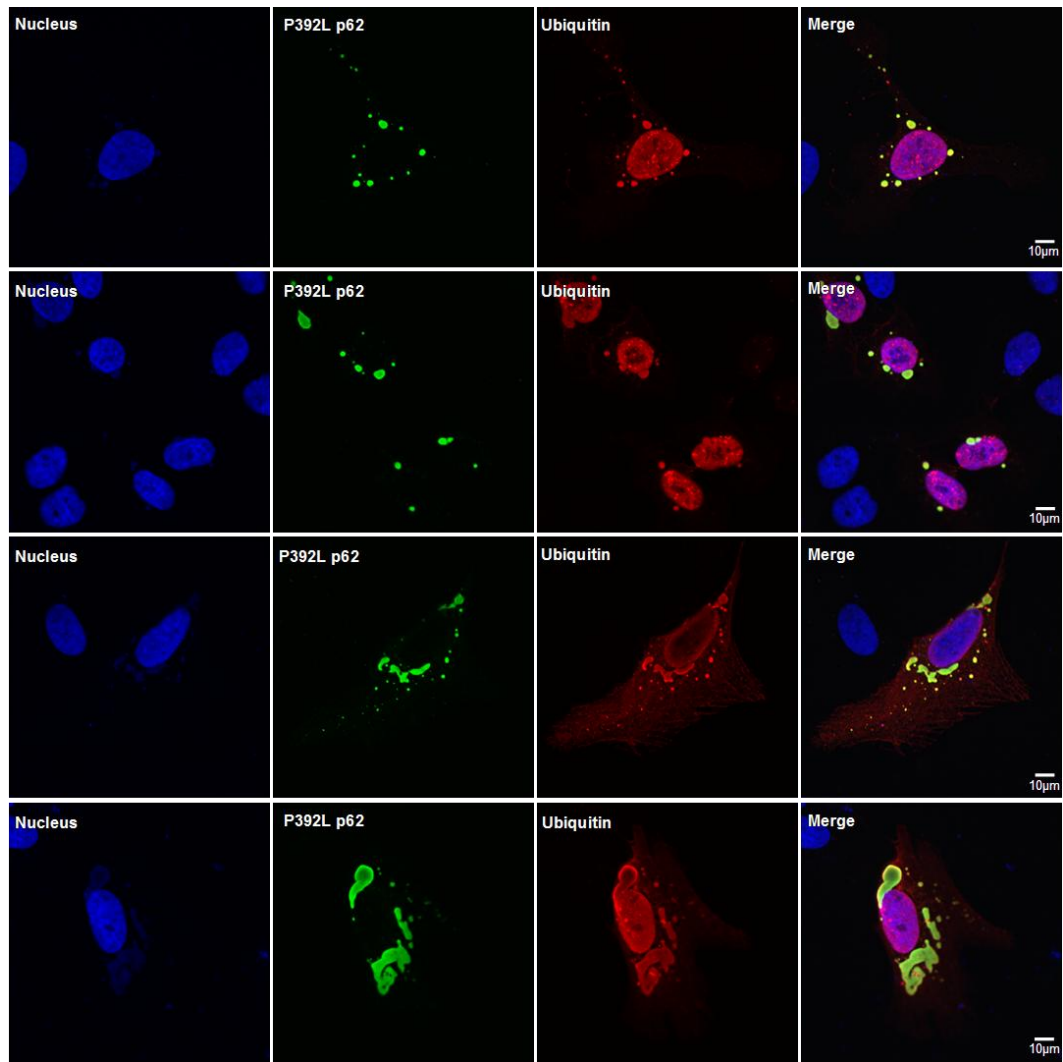


Figure 4.17: Co-localisation of P392L mutant polyHis-FLAG-p62 and HA-ubiquitin in U2OS cells and their cellular phenotypes

P392L mutant polyHis-FLAG-p62 and HA-ubiquitin were co-transfected into U2OS cells, which after ~40 hours were fixed with formaldehyde. p62 was detected using mouse anti-p62 as primary antibody and stained green using anti-mouse Alexafluor 488 as secondary antibody. Ubiquitin was detected using rabbit anti-HA primary antibody and stained red using anti-rabbit Alexafluor 568 as secondary antibody. Hoescht 32258 was used for staining nuclei. Confocal microscopy images were collected at 63X objective lens, with scale bars as indicated. P392L mutant polyHis-FLAG-p62 strongly co-localised with HA-ubiquitin. This mutant exhibited very similar cellular phenotypes to wild type p62 (in this figure, medium and large cytoplasmic bodies are shown, but the other cellular phenotypes were also evident).

The various cellular phenotypes of cells co-transfected with A381V mutant polyHis-FLAG-p62 and HA-ubiquitin were very similar to those associated with wild type p62 (Figures 4.18 and 4.19), with strong co-localisation of staining. However, more detailed visual assessments suggested that larger cytoplasmic bodies may be more commonly associated with the A381V mutant than the wild type sequence, which would be consistent with earlier investigations which concluded that P392L and P387L mutants formed larger cytoplasmic bodies than wild type p62 (Leach *et al.*, 2006); this is investigated further in Section 4.5.

The D335E mutant also showed similar cellular phenotypes to those of wild type p62, although notably few very large cytoplasmic bodies were observed, with infrequent observation of the rare phenotypes associated with the wild type sequence (Figure 4.20). Again, strong co-localisation of p62 and ubiquitin staining was noted.

Notably, all transfected cells that contained smaller cytoplasmic bodies ($\leq 5\mu\text{m}^2$), regardless of p62 sequence, were noted to contain more rounded bodies than cells with larger cytoplasmic bodies.

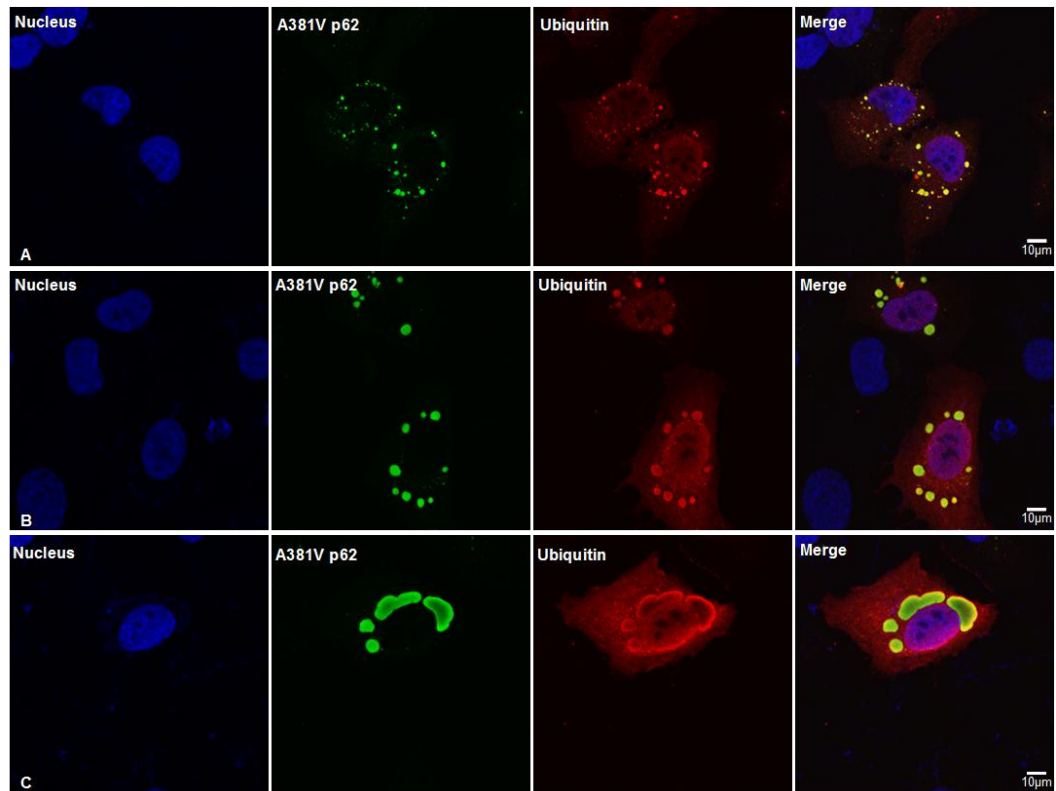


Figure 4.18: Co-localisation of A381V mutant polyHis-FLAG-p62 and HA-ubiquitin in U2OS cells and their cellular phenotypes (part 1)

A381V mutant polyHis-FLAG-p62 and HA-ubiquitin were transfected into U2OS cells, which after ~40 hours were fixed with formaldehyde. p62 was detected using mouse anti-p62 as primary antibody and stained green using anti-mouse Alexafluor 488 as secondary antibody. Ubiquitin was detected using rabbit anti-HA primary antibody and stained red using anti-rabbit Alexafluor 568 as secondary antibody. Hoescht 32258 was used for staining nuclei. Confocal microscopy images were collected at 63X objective lens, with scale bars as indicated. A381V mutant polyHis-FLAG-p62 co-localised strongly with HA-ubiquitin.

Similar to the wild type sequence, three major cellular phenotypes were observed to be associated A381V mutant polyHis-FLAG-p62:

- A) Small rounded cytoplasmic bodies.
- B) Medium rounded cytoplasmic bodies.
- C) Large semi-rounded cytoplasmic bodies.

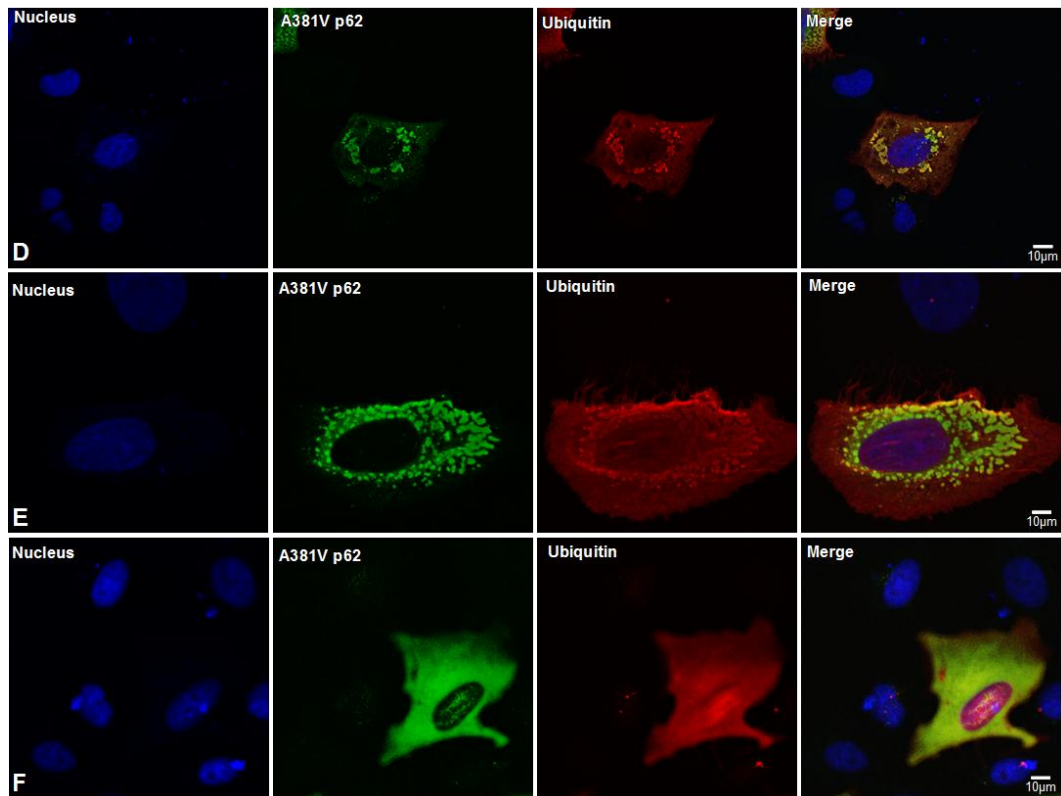


Figure 4.19: Co-localisation of A381V mutant polyHis-FLAG-p62 and HA-ubiquitin in U2OS cells and their cellular phenotypes (part 2)

A381V mutant polyHis-FLAG-p62 and HA-ubiquitin were transfected into U2OS cells, which after ~40 hours were fixed with formaldehyde. p62 was detected using mouse anti-p62 as primary antibody and stained green using anti-mouse Alexafluor 488 as secondary antibody. Ubiquitin was detected using rabbit anti-HA primary antibody and stained red using anti-rabbit Alexafluor 568 as secondary antibody. Hoescht 32258 was used for staining nuclei. Confocal microscopy images were collected at 63X objective lens, with scale bars as indicated. A381V mutant polyHis-FLAG-p62 co-localised strongly with HA-ubiquitin.

Similar to the wild type sequence, three rarer irregular cytoplasmic structures observed for A381V mutant polyHis-FLAG-p62 were:

- D) Perinuclear structures.
- E) Multiple connected bodies.
- F) Diffuse staining.

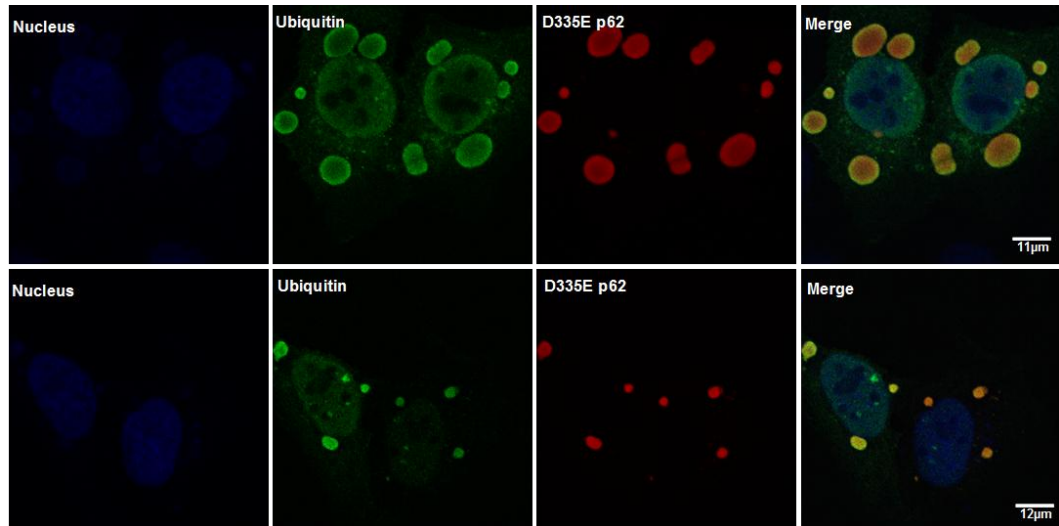


Figure 4.20: Co-localisation of D335E mutant polyHis-FLAG-p62 and HA-ubiquitin in U2OS cells and their cellular phenotypes

D335E mutant polyHis-FLAG-p62 and HA-ubiquitin were co-transfected into U2OS cells, which after ~40 hours were fixed with formaldehyde. p62 was detected using mouse anti-p62 as primary antibody and stained red using anti-mouse Alexafluor 568 as secondary antibody. Ubiquitin was detected using rabbit anti-HA primary antibody and stained green using anti-rabbit Alexafluor 488 as secondary antibody. Hoescht 32258 was used for staining nuclei. Confocal microscopy images were collected at 63X objective lens, with scale bars as indicated. D335E mutant polyHis-FLAG-p62 strongly co-localised with HA-ubiquitin. This mutant displayed a similar range of cellular phenotypes to the wild type protein (in this figure medium and large cytoplasmic bodies are shown, but the other cellular phenotypes were also evident). Although the D355E mutant showed both the common and rarer p62 cellular phenotypes associated with wild type sequence, medium rounded cytoplasmic bodies were the predominant phenotype.

Finally, co-transfected HA-Ubiquitin with polyHis-FLAG-p62 in U2OS cells was also analysed using western blotting. Following transfection of cells for ~40 hours, HA-ubiquitin was detected by western blotting with rabbit anti-HA. The immunoreactivity was associated with high molecular weight smears, consistent with covalent conjugation of HA-ubiquitin to other cellular proteins (Figure 4.21).

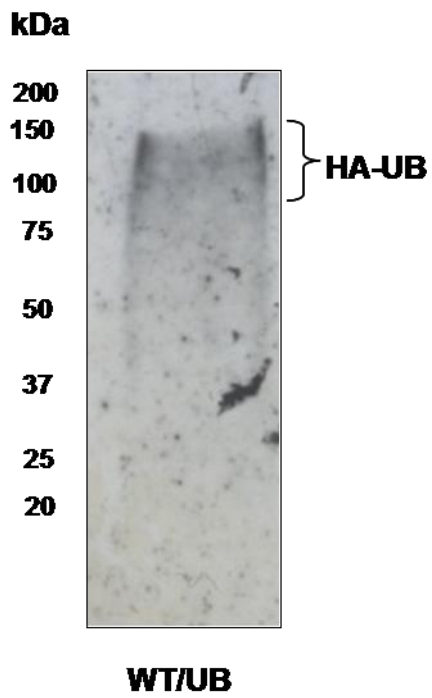


Figure 4.21: Immunoblot of HA-ubiquitin in U2OS cells

U2OS cells were transiently co-transfected with polyHis-FLAG-p62 and HA-Ubiquitin. After ~40 hours incubation cells were washed and then solubilised with gel loading buffer; resulting lysate was resolved by SDS PAGE and analysed by western blotting (anti-HA). The immunoreactivity is associated with high molecular weight smears, consistent with covalent conjugation of HA-ubiquitin to other cellular proteins.

4.5 Quantification of the size of p62-positive and ubiquitin-positive cytoplasmic bodies

Co-localisation analyses of proteins using confocal microscopy involves selection of two different coloured fluorescent probes and detection of the emission spectra of these probes in two different channels of a digital imager. Then a merged image, which forms a mixed colour, is used to assess the degree of the co-localisation by evaluating the brightness of the resultant mixed colour.

In confocal microscopy, visual assessment is used commonly to compare the degree of co-localisation between proteins (French *et al.*, 2008) but, visual assessment is highly subjective. Random co-localisation of two proteins in the same compartment does not imply actual co-localisation, because the compartments are not well separated spatially (Costes *et al.*, 2004), which is caused by the limitation of the microscopes resolution and zooming levels. In addition, sometimes the signals might originate from outside the plane of interest (French *et al.*, 2008), causing false co-localisation intensities.

Considering these caveats, we initially tried to objectively quantify co-localisation of polyHis-FLAG-p62 and HA-ubiquitin, using Volocity confocal imaging software from Improvision (version 4.2.0). However, we noted that the co-localisation measurements also resulted in considerable variation using this approach (the same images, analysed on different occasions, resulted in differing results). Subsequently, we sought alternative ways to analyse the polyHis-FLAG-p62 cytoplasmic bodies without considering the intensity of the co-localised fluorophores. This was best achieved using Leica confocal microscopy software to simply measure the area of p62 cytoplasmic bodies in confocal images of cells transfected with wild type or mutant polyHis-FLAG-

p62. The areas of p62 structures were measured by drawing a polygram around a selected structure, which is defined as ROI: region of interest. These area measurements gave reproducible results (not shown) and allowed us to accurately determine if any of the p62 mutants were associated with more extensive cytoplasmic bodies than wild type p62, as indicated in other studies (Leach *et al.*, 2006).

The *common rounded and semi-rounded cytoplasmic bodies* (section 4.4) could now be classified based on their areas, as follows:

- A) Small rounded cytoplasmic bodies, having an area ranging from detection limit of the microscope to $5\mu\text{m}^2$.
- B) Medium rounded cytoplasmic bodies, having an average area from 5- $40\mu\text{m}^2$.
- C) Large semi-rounded cytoplasmic bodies, having an average area of $40\mu\text{m}^2$ or greater.

The *rarer irregular cytoplasmic structures* had more irregular shapes, therefore it was difficult to calculate their areas accurately, as calculations require drawing a continuous line around the area to be measured. Therefore, we omitted calculating the areas of these cellular phenotypes.

Figure 4.22 is a representative example of area measurements of cytoplasmic bodies of wild type polyHis-FLAG-p62 and a selected PDB-associated mutant (A381V). Similar analyses were performed on the rest of the selected PDB-associated mutants (P392L, G425R, D335E), in which they showed similar ranges of cellular phenotypes to the wild type sequence (not shown). Each of the missense mutations also previously noted to show similar ranges of cellular phenotypes to the wild type sequence (section 4.4).

In summary, our analyses confirmed that the polyHis-FLAG-p62 cytoplasmic bodies representing common cellular phenotypes associated with the selected PDB-associated missense mutations (A381V, P392L, G425R, D335E) had comparable areas to the cytoplasmic bodies formed by the wild type p62 sequence.

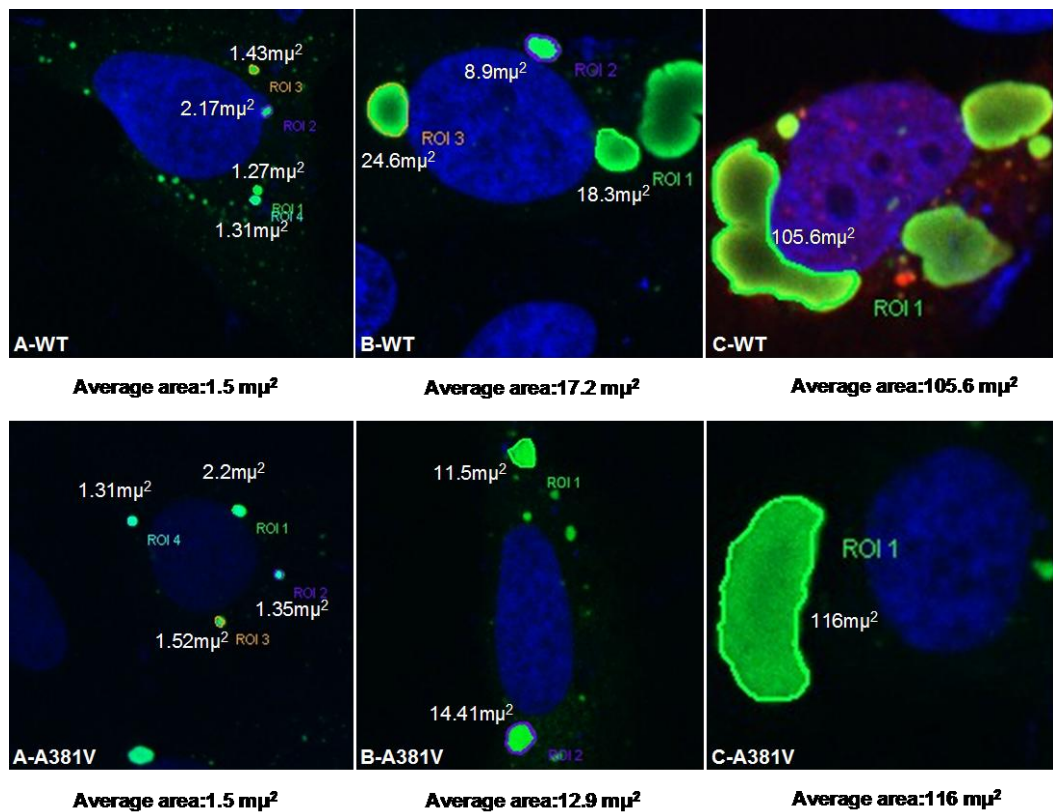


Figure 4.22: Area calculations of cytoplasmic bodies associated with wild type and A381V polyHis-FLAG-p62

Leica confocal software was used to calculate the areas of wild type and A381V polyHis-FLAG-p62 cytoplasmic bodies in U2OS cells co-transfected with HA-ubiquitin by drawing polygons matching the shapes of the p62 structures using a mouse and cursor (although the images were taken from cells co-transfected with polyHis-FLAG-p62 with HA-ubiquitin, ubiquitin is omitted in the images, because the red colour of ubiquitin obscured the borders of the cytoplasmic bodies). All the images were taken at a fixed scanning zoom (2.3). Calculated areas for different regions of interest (ROI; separate medium rounded bodies) as indicated are presented, along with average areas. A, B and C represents small, medium and large p62 cytoplasmic bodies respectively as described in page 178.

4.6 Further analysis of polyHis-FLAG-p62 cytoplasmic bodies

As all of the polyHis-FLAG-p62 constructs (except the E396X mutant) formed various cytoplasmic bodies when transfected in U2OS cells, attempts were made to further characterise these structures in order to understand their physiological significance.

Earlier investigations of transfected p62 proteins showed that ectopic expression of p62 resulted in numerous rounded cytoplasmic bodies in the perinuclear region of human HeLa cells (Lamark *et al.*, 2003; Biørkøy *et al.*, 2005). These p62 cytoplasmic bodies were classified to two populations: large immobile cytoplasmic bodies ($>0.5\mu\text{m}$) that were membrane-free structures and not related to endocytic vesicles (Biørkøy *et al.*, 2005); and small rounded highly mobile cytoplasmic bodies ($<0.3\mu\text{m}$), which were suggested to be late endosomes or lysosomes. In addition, the larger p62 bodies were also rarely observed in the nucleus (Biørkøy *et al.*, 2005). Notably, all these p62 bodies were ubiquitin-positive, consistent with the interaction of ubiquitin and p62 through its UBA domain (Biørkøy *et al.*, 2005).

Both PB1 and UBA domains of p62 were reported to be required for the formation of these cytoplasmic bodies (Biørkøy *et al.*, 2005) and absence of either of the domains resulted in diffuse p62 localisation. Interestingly, a p62 construct containing a fusion of only the two domains (PB1 and UBA) was still able to form the regular cytoplasmic bodies, which were indistinguishable from the cytoplasmic bodies formed by full length p62 constructs (Biørkøy *et al.*, 2005). Further, a significant portion of p62's cytoplasmic structures (the smaller rounded highly mobile cytoplasmic bodies) were shown to represent autophagosomes or autolysosomes (Biørkøy *et al.*, 2005). Aggregates containing ubiquitin and p62 (e.g. the large immobile membrane-free

cytoplasmic bodies) might also occasionally be engulfed in autophagosomes without delivery to the lysosomes, indicating a possible protective role of autophagy for these aggregates (Shvets *et al.*, 2008).

Indeed more detailed analyses revealed that cytoplasmic p62 might be either part of membrane-free aggregates called "sequestosomes" or double membrane structures, which were indicative of autophagosomes (Biørkøy *et al.*, 2005). Interestingly, p62 is also itself degraded by autophagy (Biørkøy *et al.*, 2005) and autophagic degradation of polyubiquitylated proteins is dependent on p62 interaction with polyubiquitylated proteins via the UBA domain of p62, self oligomerisation of p62 through its PB1 domain and further interaction of p62 with LC3 (Biørkøy *et al.*, 2005; Pankiv *et al.*, 2007). Notably, the interaction between p62 and LC3 is direct, involving the LC3-interaction region (LIR), and although a conservative change, the D335E missense mutation is located within the LIR.

As an extension of Biørkøy's study we also investigated the role of polyHis-FLAG-p62-containing cytoplasmic bodies in autophagy and studied the interaction of transfected proteins with co-transfected tdTomato-LC3 using confocal microscopy. Here, tdTomato-LC3 is used as an autophagic marker: this autophagic marker is the LC3-II form, which is tightly associated with the autophagosomal membrane (Biørkøy *et al.*, 2005) and detection is achieved with the red fluorescent tdTomato protein. These co-localisation studies also allowed us to investigate effects of the D335E mutation on the recruitment of p62 to LC3-positive autophagosomes.

Before investigating the co-localisation between wild type polyHis-FLAG-p62 and tdTomato-LC3, subcellular localisation of the latter alone was first investigated in U2OS cells. tdTomato-LC3 was transiently transfected into

U2OS cells, which were fixed after ~40 hours with formaldehyde, then the cells were visualised using a Leica confocal microscope. Singly transfected tdTomato-LC3 showed a diffuse phenotype in U2OS cells and distributed evenly in the cytoplasm and the nucleus (Figure 4.23).

Later, we investigated the co-localisation of wild type polyHis-FLAG-p62 and tdTomato-LC3. U2OS cells were transiently co-transfected with wild type polyHis-FLAG-p62 and tdTomato-LC3 and fixed after ~40 hours with formaldehyde. Mouse anti-p62 was used as a primary antibody for probing p62 and anti-mouse Alexafluor 488 was used as a secondary antibody. Endogenous fluorescence of tdTomato was directly detected. Wild type polyHis-FLAG-p62 co-localised strongly with tdTomato-LC3 (Figure 4.24) and co-transfection of polyHis-FLAG-p62 with tdTomato-LC3 changed the LC3's cellular phenotype from a diffuse pattern to rounded cytoplasmic bodies, suggesting that the p62 and ubiquitin-positive structures previously noted (Section 4.4) are likely to represent autophagosomes. Occasionally, wild type polyHis-FLAG-p62 formed a shell surrounding tdTomato-LC3 structures, consistent with previous reports (Pankive *et al.*, 2007) and with p62's role in autophagosome formation.

Another possibility to explain the formation of p62/LC3-containing cytoplasmic bodies is that p62 polymerisation, through its PB1 domain, with other p62 monomers (or with other proteins containing PB1 domain), produces polymers structured in a 'back to front' manner (Wilson *et al.*, 2003). Therefore, we checked that the observed p62 cytoplasmic bodies were not simply aggregates of p62 polymers. Interestingly, although the UBA domain of p62 is not required for p62 polymerisation (Leach *et al.*, 2006) the E396X deletion mutant (which lacks the whole UBA domain but contains the LIR) was still unable to form p62/LC3-containing cytoplasmic bodies, thereby confirming

that the observed polyHis-FLAG-p62 cytoplasmic bodies were not simply p62 polymers.

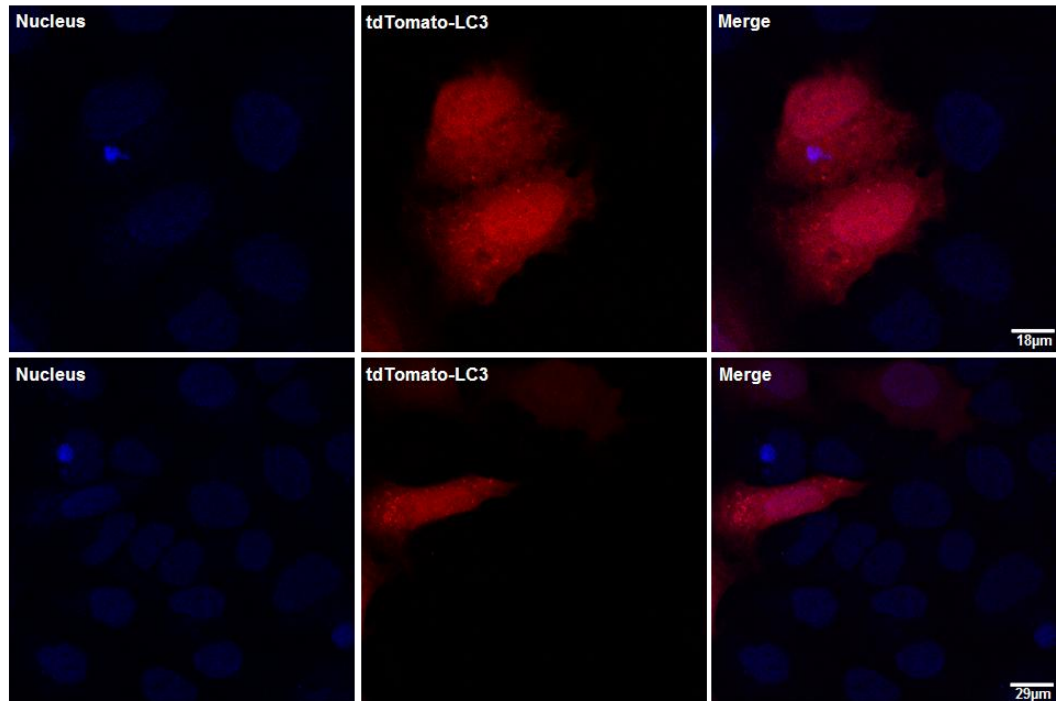


Figure 4.23: tdTomato-LC3 localisation in U2OS cells

tdTomato-LC3 was transfected into U2OS cells, which after ~40 hours were fixed with formaldehyde. tdTomato is a red fluorescent protein and endogenous fluorescence was detected directly. Hoescht 32258 was used for staining nuclei. Confocal microscopy images were collected at 63X objective lens, with scale bars as indicated. tdTomato-LC3 showed a diffuse staining pattern with even distribution in the cytoplasm as well as in the nucleus. Small rounded dot-like structures are likely to represent autophagosomes.

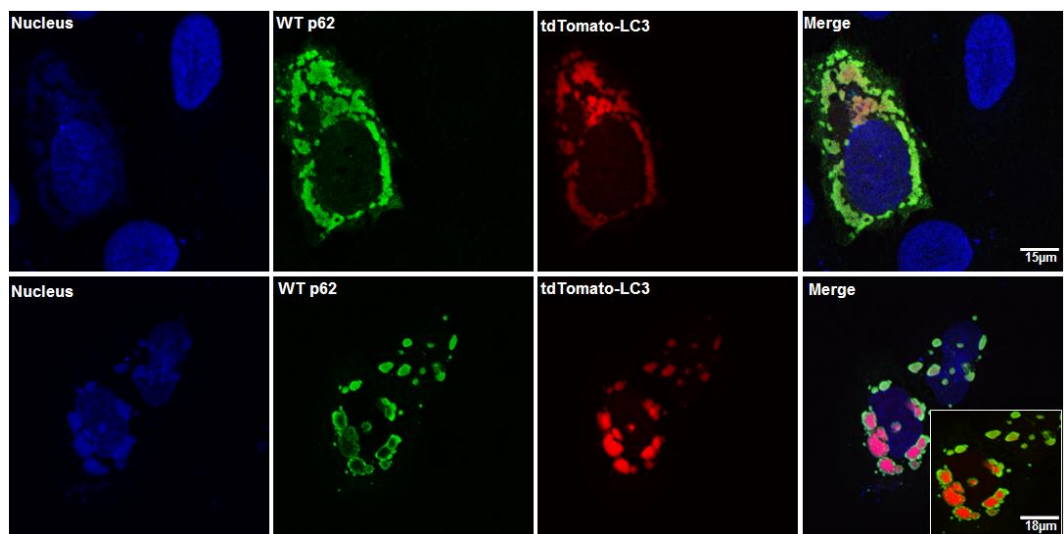


Figure 4.24: Co-localisation of tdTomato-LC3 and with wild type polyHis-FLAG-p62 in U2OS cells

Wild type polyHis-FLAG-p62 and tdTomato-LC3 were co-transfected into U2OS cells, which after ~40 hours were fixed with formaldehyde. p62 was detected using mouse anti-p62 as primary antibody and stained green using anti-mouse Alexafluor 488 as secondary antibody. Endogenous fluorescence of tdTomato was detected directly. Hoescht 32258 was used for staining nuclei. Confocal microscopy images were collected at 63X objective lens, with scale bars as indicated. Wild type polyHis-FLAG-p62 co-localised strongly with tdTomato-LC3. Occasionally, wild type polyHis-FLAG-p62 formed a shell surrounding tdTomato-LC3-containing structures. The embedded square of the last image is presented without nuclear staining for improved visualisation.

4.6.1 Co-localisation studies of D335E mutant polyHis-FLAG-p62 with tdTomato-LC3 in U2OS cells

In our *in vitro* ubiquitin-binding assays (Chapter 3), the PDB-associated D335E mutant of p62 retained its full ubiquitin-binding activity at both pH7.5 and pH6.5. Studying the effects of this mutation on other cellular functions of p62 may provide further clues to whether the D335E substitution is a *bona fide* mutation or a rare polymorphism. Since D335 is located within the LIR of p62 (residues 321-342) (Pankiv *et al.*, 2007), we speculated that the D335E change may affect the interaction between p62 and LC3.

Accordingly, we studied the co-localisation patterns between D335E mutant polyHis-FLAG-p62 and tdTomato-LC3. U2OS cells were transiently co-transfected with D335E mutant polyHis-FLAG-p62 and tdTomato-LC3, and fixed with formaldehyde. Mouse anti-p62 was used as a primary antibody for probing p62 and then anti-mouse Alexafluor 488 was used as a secondary antibody; tdTomato fluorescence was detected directly.

D335E mutant polyHis-FLAG-p62 co-localised with tdTomato-LC3 and exhibited similar co-localisation patterns to wild type polyHis-FLAG-p62 and tdTomato-LC3. Both p62 constructs (wild type and D335E) co-localised with LC3, suggesting that the D335E variant was still able to produce autophagosomes, and the change did not affect the normal co-localisation patterns between p62 and LC3. Occasionally the D335E mutant, like wild type p62, formed a shell around the LC3-containing structures (Figure 4.25).

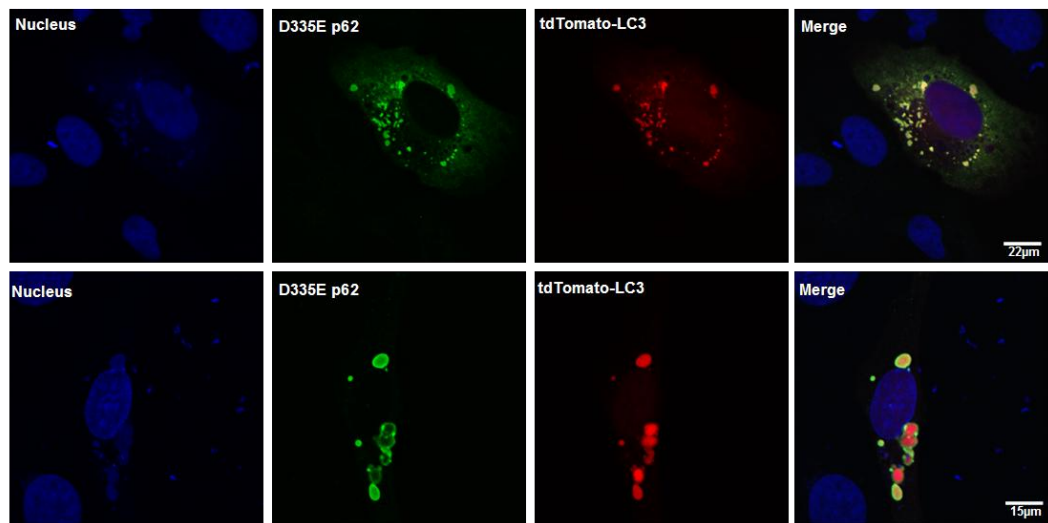


Figure 4.25 Co-localisation of tdTomato-LC3 and with D335E mutant polyHis-FLAG-p62 in U2OS cells

D335E mutant polyHis-FLAG-p62 and tdTomato-LC3 were co-transfected into U2OS cells, which after ~40 hours were fixed with formaldehyde. p62 was detected using mouse anti-p62 as primary antibody and stained green using anti-mouse Alexafluor 488 as secondary antibody. Endogenous fluorescence of tdTomato was detected directly. Hoescht 32258 was used for staining nuclei. Confocal microscopy images were collected at 63X objective lens, with scale bars as indicated. D335E mutant polyHis-FLAG-p62 co-localised strongly with tdTomato-LC3, showing a similar co-localisation pattern to wild type p62 and tdTomato-LC3. Occasionally, D335E mutant polyHis-FLAG-p62 formed a shell surrounding tdTomato-LC3-containing structures.

4.7 Discussion

Earlier studies showed that transfected wild type p62 co-localised strongly with ubiquitin in HEK293 cells (Biørkøy *et al.*, 2005); therefore, we sought to extend these studies and investigate the co-localisation of selected PDB-associated p62 mutants and ubiquitin. In addition, we hoped to develop a more physiologically relevant (cell-based) model to study p62-ubiquitin interactions, in improvement to our *in vitro* ubiquitin-binding assays (Chapter 3).

In our study, wild type polyHis-FLAG- p62 was found to co-localise with HA-ubiquitin, consistent with the *in vitro* binding data, whilst the E396X truncating mutant showed little or no co-localisation with ubiquitin, consistent with earlier studies that showed a requirement for the UBA domain to achieve co-localisation in cells (Biørkøy *et al.*, 2005). The remainder of the PDB-associated p62 mutations analysed - P392L, A381V, D335E - also showed strong co-localisation with ubiquitin, with the exception of the G425R mutant, which showed reduced co-localisation with ubiquitin.

These co-localisation patterns between the various p62 constructs and ubiquitin indicate that there is no simple correlation between the *in vitro* ubiquitin-binding assay and co-localisation of p62/ubiquitin in transiently transfected cells. For example, in contrast to our *in vitro* ubiquitin-binding assay, in which the G425R, P392L and A381V mutants all showed impaired ubiquitin-binding function (albeit only partial loss at pH6.5 for the A381V mutant), these selected mutants retained strong co-localisation with ubiquitin in transfected cells. In contrast, the co-localisation patterns of the D335E and E396X PDB-associated p62 mutants and ubiquitin were consistent with their ubiquitin-binding properties obtained from *in vitro* ubiquitin-binding assay, in

which the former retained full ubiquitin-binding, whilst the latter showed complete loss of ubiquitin-binding. This inconsistency between the two assays may in part be caused by experimental limitations associated with the confocal microscopy studies (see Section 4.7.1). To remove bias from subjective visual assessment in confocal microscopy, we attempted to quantify co-localisation of the fluorophores of p62 and ubiquitin, but these results were also variable probably due to uncontrollable factors within the confocal analysis (see section 4.7.1).

Following our failure to quantify the co-localisation intensities between p62 and ubiquitin staining, we further investigated the various cellular phenotypes associated by both wild type polyHis-FLAG-p62 and the selected PDB-associated mutants. In summary, the PDB-associated mutants showed a similar subcellular localisation to the wild type sequence, with the exception of the E396X mutant which had a diffuse staining pattern, indicating that the presence of a UBA domain (be it functional or defective with respect to ubiquitin-binding) is required for the formation of p62-containing cytoplasmic bodies.

We went on to classify the different phenotypes of these p62 cellular bodies into two types: first, *common rounded and semi-rounded cytoplasmic bodies*, which in turn were subdivided to three subgroups ranging in their average area from the detection limit of the microscope to $40\mu\text{m}^2$ or greater; and second, *rarer irregular cytoplasmic structures*, which again could be divided to three subgroups (perinuclear structures, multiple connected bodies and diffuse structures).

In contrast to a study by Leach *et al.*, we could not confirm that the A381V mutant nor the selected PDB-associated p62 missense mutants analysed

formed larger cytoplasmic bodies than the wild type sequence. Several experimental differences might account for the discrepancies between our results and those of the Leach study, as they used a different cell line (HEK293), and an EGFP-tagged protein. In addition, certain experimental conditions, which are important in the formation of p62-containing cytoplasmic bodies, such as time of transfection, plasmid concentration, relative protein expression levels, and method of quantification of the cytoplasmic bodies were disregarded or not reported in their study.

Interestingly, our results were also in opposition to the observation that ubiquitin-binding of p62 is required for the formation of its cytoplasmic bodies (Biørkøy *et al.*, 2005), as the P392L and G425R mutants impaired ubiquitin-binding *in vitro* ((Cavey *et al.*, 2005) and confirmed in Chapter 3) however, these two missense mutants still formed various cytoplasmic bodies; notably, only the truncated UBA domain mutant of p62 (E396X) did not form cytoplasmic bodies in our experiments. However, it should be noted that although the P392L and G425R mutants present as complete loss of binding function in *in vitro* pull-down assays, in fact in reality they do retain some ubiquitin-binding activity (including *in vivo*) at a level (K_d) that is undetectable in the assays. Overall these results indicate the requirement of UBA domain, but not necessarily ubiquitin-binding, for the formation of p62-containing cytoplasmic bodies. In addition, it should be considered that p62, through its UBA domain, would interact with non-ubiquitin partners, which might be required for the formation of p62's cytoplasmic bodies, and these interactions could be maintained in G425R and P392L mutants (Najat *et al.*, 2009).

We presume that some of the p62-containing cytoplasmic bodies observed in our cells represent autophagosomes, as wild type polyHis-FLAG-p62 co-localised with LC3, consistent with autophagic clearance of p62 along with

polyubiquitylated proteins (Biørkøy *et al.*, 2005). Notably, other studies using live cell imaging indicate these cytoplasmic bodies appear to grow by fusion, and the various sizes of p62-containing cytoplasmic bodies might represent accumulated proteins associated with different components/stages of autophagy machinery (Waters *et al.*, 2009). Although the exact relationship between autophagy and bone remodelling has not been investigated yet, these results indicate a possible role of autophagy in PDB, obviously, further research is needed in this area (Najat *et al.*, 2009).

The PDB-associated D335E variant of p62, which is located within the LIR, did not appear to disturb the interaction between p62 and LC3 (at least in transfected cells), as this mutant showed strong co-localisation with LC3. Using the *in vitro* ubiquitin-binding assay (Chapter 3), the D335E mutant retained its ubiquitin-binding function. Collectively these data suggest that the D335E variant did not affect two functionally-relevant cellular interactions of p62, which might be because the D335E change is conservative, substituting one acidic side chain for another, thereby only causing weak effects on the overall binding between p62 and LC3. Another possibility is that D335E may represent a rare polymorphism rather than disease-associated mutations, as this change was found only in one Italian patient.

In summary, the selected PDB-associated p62 mutants (except E396X) were indistinguishable from wild type p62 in our co-transfection experiments, as they in general co-localised with ubiquitin in a similar manner to the wild type protein, and also formed various cytoplasmic bodies with similar cellular phenotypes/sizes to wild type p62. Interestingly, the p62 cytoplasmic bodies were presumed to be autophagosomes, which was supported by the co-localisation of wild type p62 with LC3.

Since the confocal analyses did not provide further support for the partial loss of ubiquitin-binding function associated with the A381V mutation suggested from the *in vitro* pull down assays (Chapter 3), we moved on to study the functional effects of this mutation on NF- κ B signalling (Chapter 5).

4.7.1 Limitations of indirect immunofluorescence and 2D confocal laser scanning microscopy

This approach has several limitations, because it depends on measuring the intensity of the emitted light from a fluorescent source, which in turn is dependent on several factors such as: labelling methods, sample preparation, washing stages, laser stability and the way the samples and the images were collected. These factors are difficult to control, especially between independent experiments, even with samples prepared in the same day (Alan R.Hibbs 1st Ed.).

Technical limitations within the confocal microscope can also cause false co-localisation results. For example, if the zoom level and the resolution of the scanning images are decreased the fluorescence might appear falsely co-localised, because the imaging systems of the microscope cannot resolve small distances between very closely co-localised proteins (French *et al.*, 2008). Another limitation is if the fluorophore is exposed to the laser for too long, bleaching can occur, although the exposure time can be decreased by collecting the images with less optical slices, or with a single optical slice. However, a single optical slice is thin and causes false labelling levels, therefore it is advisable to collect confocal images by comparing areas of a specimen as quickly as possible with smallest number of optical slices (Alan R.Hibbs 1st Ed.).

Obviously, co-localisation analyses of fluorophores using this approach can be misleading, and it was suggested that quantification of the fluorophore signals could give better estimation of the intensity of the co-localised fluorophores using commercial (Volocity) image analysis software. Unfortunately the intensity of the co-localised fluorophores was also found to be inconsistent in this case, consistent with previous studies on the quantification software (French *et al.*, 2008). It is possible that the variability observed was caused by the software design, as Volocity depends on producing a scatter plot for a merged image composed of red, green and yellow pixels. Volocity calculates the co-localisation intensities by defining a colour threshold manually with a regular computer mouse, and this technique inevitably causes pixel loss. Despite these limitations and caveats, a semi-quantitative analysis was achieved, and work is still ongoing to improve the available quantification software (French *et al.*, 2008) (Alan R.Hibbs 1st Ed.).

In the future, other protein interaction methods should be used to obtain definitive measurements of the ubiquitin-binding properties of p62. For example, studying protein interaction with Fluorescence resonance energy transfer (FRET) might overcome the limitations of confocal microscopes, as FRET investigates two molecules within several nanometres, which is sufficient to evaluate physical molecular interactions.

CHAPTER 5

Effects of PDB-mutant p62 proteins on NF- κ B signalling

Chapter 5: Effects of PDB-mutant p62 proteins on NF- κ B signalling

5.1 Overview

Earlier attempts in our study to investigate the changes exerted by the non-UBA domain A381V mutation on the ubiquitin-binding properties of p62 were inconclusive. For example, using *in vitro* ubiquitin-binding assays the A381V mutation was found to be associated with only very subtle changes in p62's ubiquitin-binding properties (Chapter 3), and the co-localisation pattern of transfected A381V mutant p62 with ubiquitin was indistinguishable to that of wild type p62 in U2OS cells (Chapter 4). A further sensitive method for studying protein-protein interactions, 2D-HSQC NMR, proved to have limited utility for studying the effects of the A381V mutation on protein function (Chapter 3).

As investigations have shown that other PDB-associated p62 mutations known to be associated with loss of ubiquitin-binding function result in increased (relative to wild type sequence) NF- κ B activation and osteoclast activity *in vitro* (Yip *et al.*, 2006; Rea *et al.*, 2006), and that selective inhibition of NF- κ B signalling inhibits osteoclastogenesis (Jimi *et al.*, 2004), we sought to study the effects of the A381V mutation (and other selected PDB-associated mutations) on NF- κ B signalling as a surrogate of protein function. Specifically, we used three different approaches to investigate the effects of p62 (and its mutation) on NF- κ B signalling. Initially, luciferase reporter assays were chosen to investigate the gross functional effects of the A381V mutation on basal and induced p62-dependent NF- κ B signalling in HEK293 cells.

p62 has been reported to negatively regulate NF- κ B signalling through its UBA domain-dependent interaction with TRAF6 (Xu *et al.*, 2008) and wild type p62 repressed NF- κ B activation relative to empty vector controls in reporter assays

(Rea *et al.*, 2006). However, the precise mechanism by which p62 exerts its effects on NF- κ B pathway is still not clear, and interaction of p62 with other elements of the RANK/NF- κ B pathway might contribute to this negative regulatory function (Figure 5.1). Indeed, another protein (CYLD), which is a deubiquitinating (DUB) enzyme, negatively regulates NF- κ B signalling through deubiquitylation of TRAF6 (Jin *et al.*, 2008) (Figure 5.1.1). Interestingly, p62 mediates the interaction of CYLD with TRAF6 and notably, a p62 construct lacking the UBA domain failed to interact with CYLD (Wei *et al.*, 2008). Therefore, we used indirect immunofluorescence staining and confocal microscopy to study the effects of the A381V mutation (and other PDB-associated mutations) on the p62-CYLD interaction in transfected cells.

Finally, since p62 has been shown to form a complex with IKK (Zhang *et al.*, 2005) a downstream effector of RANK, and may also regulate the ubiquitination of IKK γ (NEMO), a component of the IKK complex (Martin *et al.*, 2006), we also investigated the effects of p62 (and its mutation) on the p62-NEMO interaction. Here, we tested the speculative hypothesis that PDB-associated p62 mutations might disturb autophagic degradation of NEMO, as NEMO is degraded by autophagy (Li *et al.*, 2006), and p62 mediates autophagic degradation of ubiquitylated proteins (Biørkøy *et al.*, 2005) (Figure 5.1.2). Specifically the hypothesis was tested by assessing the effects of ectopic p62 expression in U2OS cells on the expression levels of endogenous NEMO.

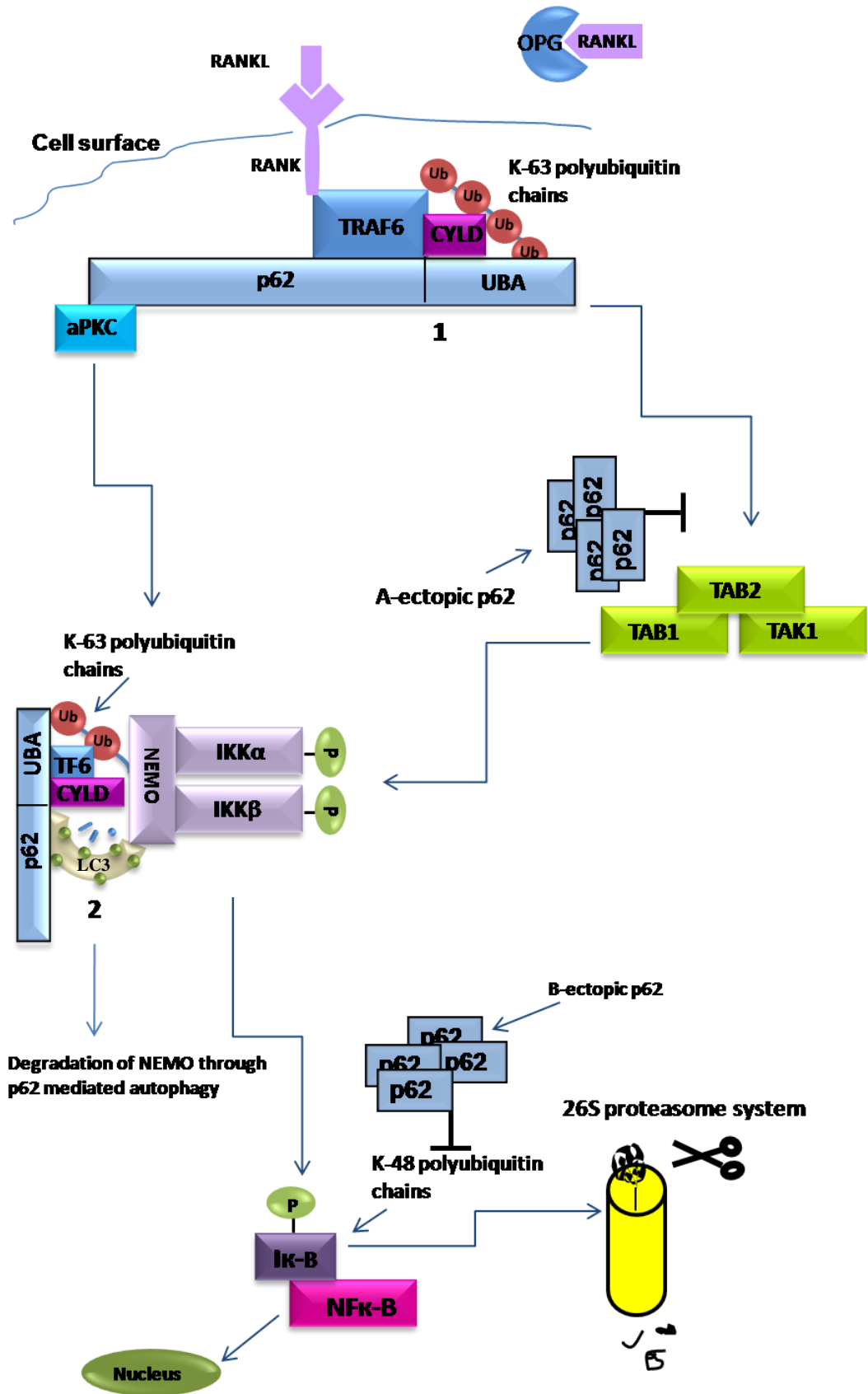


Figure 5.1: Overview of the RANK-NF- κ B signalling pathway

In osteoclasts NF- κ B signalling is activated by RANK-L and antagonised by OPG. Normally, I- κ B sequesters NF- κ B in the cytoplasm and upon phosphorylation (and degradation of I- κ B) NF- κ B is released to the nucleus to activate gene expression. I- κ B degradation is triggered by the activated IKK complex (composed of IKK α , IKK β and IKK γ [NEMO]), which in turn is activated by two different complexes, the first of which is composed of TAB1-TAB2-TAK1 and the second composed of p62-aPKC-TRAF6. Ubiquitylation is required at various stages for NF- κ B activation. CYLD deubiquitylates K63-linked polyubiquitylated proteins in the pathway (e.g. TRAF6, NEMO) and hence negatively regulates NF- κ B signalling. A and B represent ectopic p62 (as in reporter assays) expression, which might cause competition for ubiquitin and hence inhibiting the NF- κ B pathway. The IKK complex (including NEMO) is selectively degraded by autophagy (Qing *et al.*, 2006). LC3 (light chain 3) is an autophagic marker.

*1 and 2 are illustrated in more detail in Figures 5.1.1 and 5.1.2 respectively.

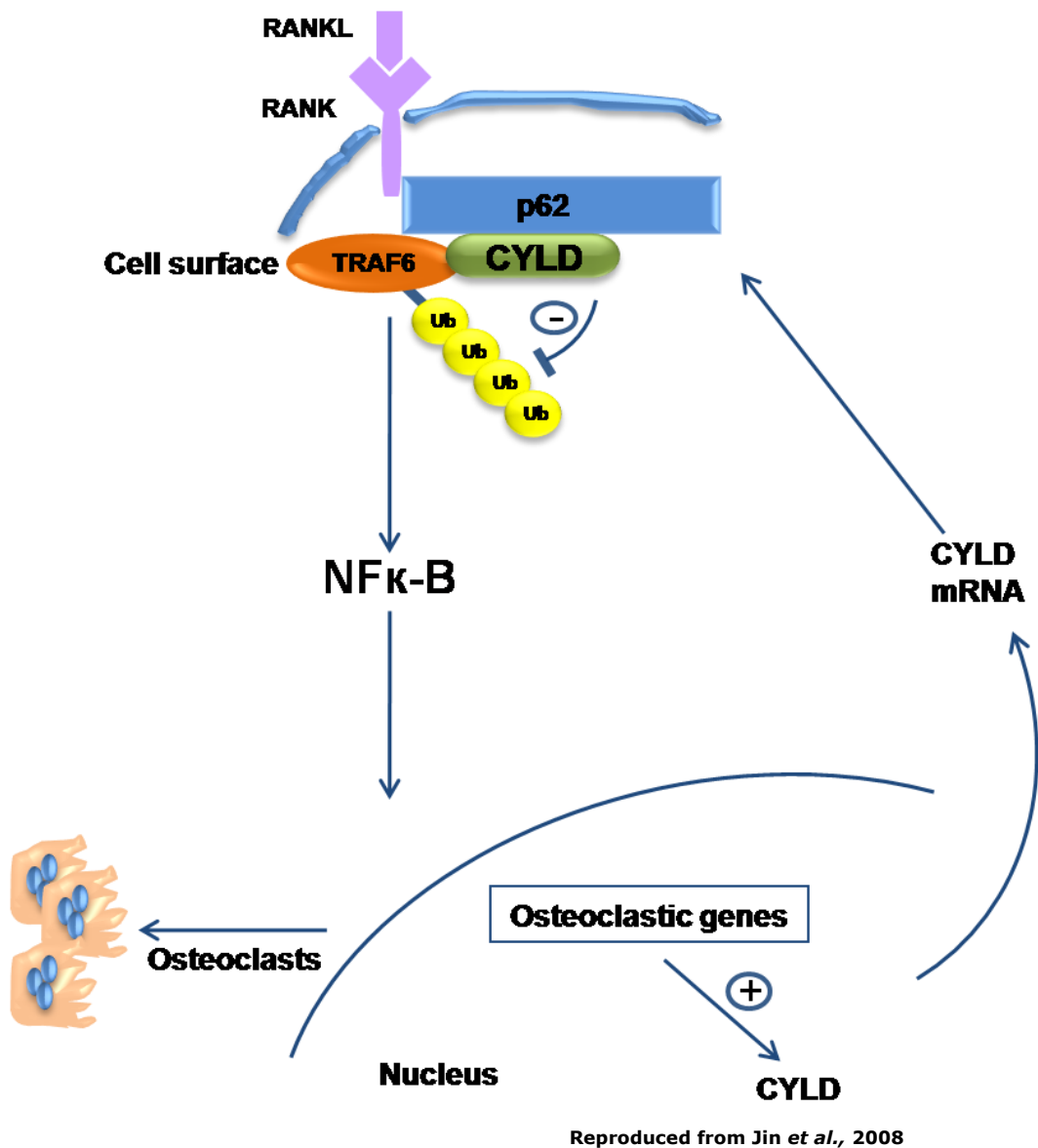


Figure 5.1.1: Negative regulation of NF-κB signalling by CYLD

Interaction of RANK-L with RANK induces K63-linked polyubiquitylation of TRAF6, causing induction of NF-κB and expression of genes required for osteoclastogenesis/osteoclast activity. p62 and CYLD also regulate RANK-L signalling as they control ubiquitylation of TRAF6. CYLD deubiquitylates TRAF6 and p62 scaffolds this process, hence CYLD negatively regulate RANK-NF-κB signalling. CYLD expression is also induced by NF-κB in a feedback loop.

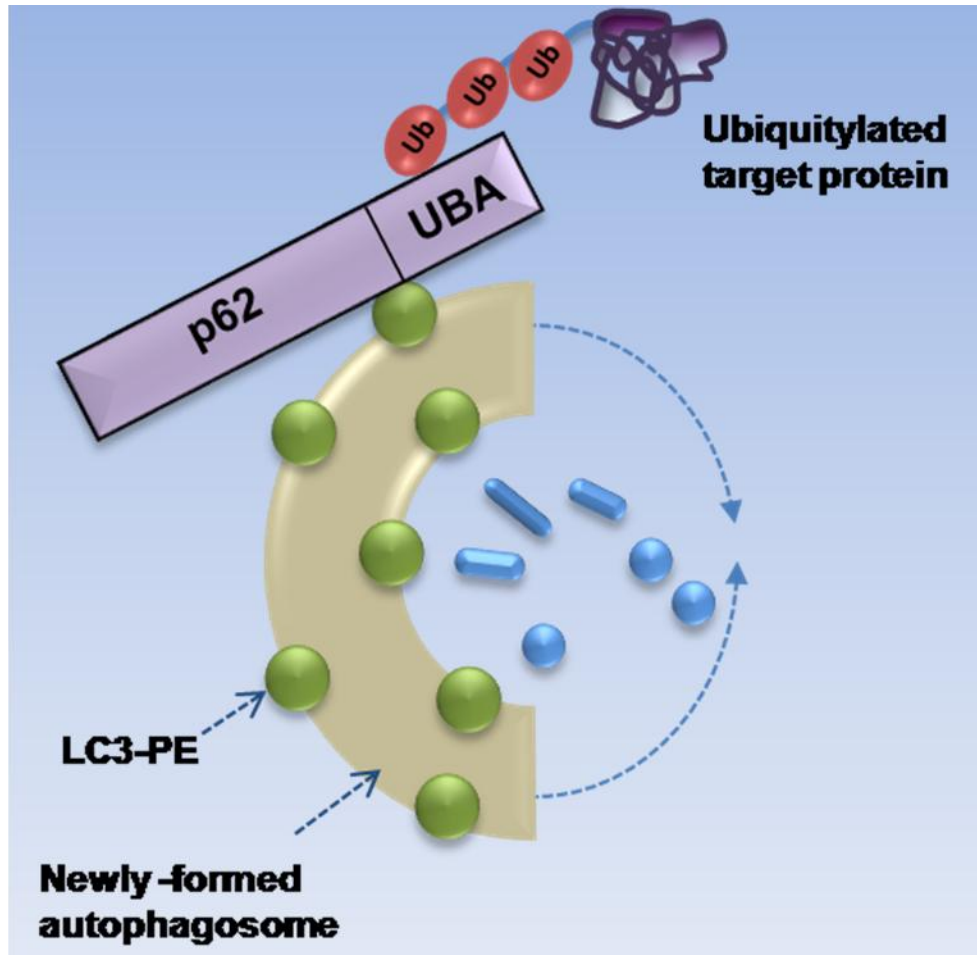


Figure 5.1.2: p62-dependent autophagic degradation of ubiquitylated proteins

Autophagy starts with isolation and formation of a double membrane structure (autophagosome) which engulfs the materials for degradation. Ubiquitylated proteins (such as NEMO) may be delivered to the autophagy machinery by p62 to be degraded at the later steps of autophagy, through fusion of the autophagosomes with lysosomes. p62 interacts with LC3-PE through its LIR (residues 321-342).

PE: Phosphatidylethanolamine (lipid modification of LC3 which anchors the protein to the autophagosome)

Chapter 5 - Part I

**Investigation of regulation of NF- κ B activation by
PDB-mutant p62 proteins using luciferase
reporter assays**

5.2 Investigation of regulation of NF- κ B activation by PDB-mutant p62 proteins using luciferase reporter assays

5.2.1 Introduction

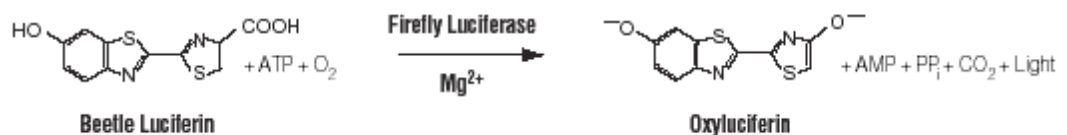
Several previous studies investigated the effects of transfecting different p62 constructs on NF- κ B activation using cell-based luciferase reporter assays (e.g. Rea *et al.*, 2006) and concluded that certain PDB-associated p62 mutations (all associated with loss of ubiquitin-binding function) increased NF- κ B activation relative to wild type p62, and wild type p62 repressed NF- κ B activation relative to empty vector controls. We extended these reporter assay studies to determine the effect of the A381V non-UBA domain mutation (and other PDB mutations) on NF- κ B activation.

Reporter assays have been used widely to monitor transcriptional activities, because they are relatively easy to perform and give accurate results. A reporter gene is a recombinant gene, which is placed downstream of the promoter region of an expression vector. An ideal reporter gene is not expressed endogenously by the selected cell type of the study.

In our study the expression vector was pGL2 (Promega), the promoter was composed of a consensus sequence (IL8) which is recognized by NF- κ B transcription factors. The structural gene region of the pGL2 expression vector encodes the firefly luciferase enzyme and hence expression of luciferase is regulated by the IL8 promoter; therefore, the amount of luciferase enzyme is proportional to the activity of the IL8 promoter in the fused gene. Upon over-expression of p62 constructs along with the reporter gene in HEK293 cells, NF- κ B will be de-activated and prevented from interacting with the IL8 promoter in the reporter gene, which in turn leads to reduced expression of luciferase;

this technique serves as an indirect method to measure the activation levels of NF- κ B by p62 variants.

In the luciferase reporter assay, a chemiluminescent reaction results from mixing a luciferase substrate (Luciferin) with cell extracts containing luciferase expressed from the reporter. The amount of the emitted light is measured quantitatively with a luminometer (Reaction 1). The amount of the light produced from the reaction is directly proportional to the amount of luciferase enzyme produced by the cells, which in turn is regulated by the transcriptional activity of the gene of interest.



Reaction 1: Monooxygenation of Luciferin (provided within the assay kit) is catalyzed by the enzyme (firefly) luciferase, which is expressed from HEK293 cell lysates, and in the presence of magnesium ions, oxygen and excess ATP.

5.2.2 Measurements of basal NF- κ B activation using luciferase reporter assays

HEK293 cells were cultured in 12-well plates and co-transfected with 0.3 μ g per well of NF- κ B firefly luciferase reporter construct and 0.2 μ g of wild type or various PDB mutant polyHis-FLAG-p62 pCDNA3.1 constructs (produced in Chapter 4), or empty pCDNA3.1 vector control. Luciferase activity was measured ~30 hours after co-transfection of the plasmids, using the Steady-Glo luciferase assay system (Promega) and according to the manufacturer's instructions.

In this study, the E396X and P392L mutants were used as controls for the A381V mutant, as they both showed significant loss of ubiquitin-binding function when investigated with *in vitro* ubiquitin-binding assays (Chapter 3 and (Cavey *et al.*, 2005)). In addition, the P392L mutant was investigated in similar reporter assays in a previous study (Rea *et al.*, 2006)

Because the absolute luminescent signal is variable between independent experiments (although maximum care is taken to replicate the experiments with the same conditions small changes were inevitable such as in cell growth rate and temperature) an empty vector is used for the assay as a control, to normalise the results obtained from different experiments. In addition, to determine the transfection efficiency, in some experiments, cells were co-transfected with 0.1 μ g of Renilla luciferase control plasmid (pRL-CMV; Promega) and the firefly and Renilla luciferase activities were measured using the dual luciferase reporter assay system. There was no significant difference in the Renilla luciferase activity with the various p62 constructs; therefore, all results were expressed as percentage firefly luciferase activity compared with the empty vector control.

The A381V, P392L and E396X mutants were all found to be associated with increased basal NF- κ B activation, relative to wild type p62, although all constructs decreased NF- κ B activation compared to the empty vector control (consistent with previous findings). The E396X truncating mutation was associated with the greatest level of NF- κ B activation although both missense mutations (P392L and A381V) also appeared to be associated with a greater signalling potential than wild type p62. Each experiment was performed in duplicate and the assay was repeated in three different occasions; the values obtained from the luminometer were expressed as percentage firefly luciferase activity compared to the empty vector control, then the data were transformed to [log₁₀ %] data (as % data is not normally distributed). To determine if there was a statistical significance in the differences in NF- κ B activation between wild type p62 and PDB mutants, statistical tests was performed using a one way ANOVA with Dunnett's test using Prism software (version 4). The statistical analysis was performed by selecting a 95% confidence limit. Data for the E396X mutant showed $P < 0.01$, and for the A381V and P392L mutants $P < 0.05$, confirming the difference between the activation of basal NF- κ B signalling for each mutant relative to wild type p62 was statistically significant (Figure 5.2).

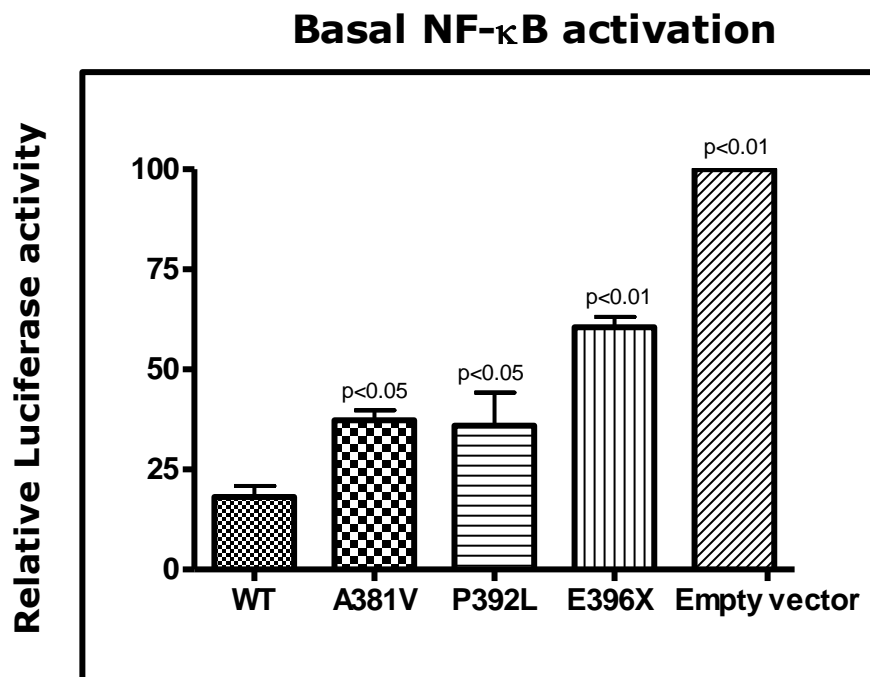


Figure 5.2: Effects of PDB-mutant p62 proteins on basal NF- κ B signalling

The effects of transfection of different polyHis-FLAG-p62 constructs with indicated PDB mutations on basal NF- κ B signalling in HEK293 cells were assessed using luciferase reporter assays. Note that although PDB mutant p62 constructs (including the A381V mutant) activated NF- κ B signalling more efficiently than wild type (WT), compared with empty vector control all p62 constructs showed reduced activation, suggesting the mutations may be diminishing a repressive function of p62 with respect to NF- κ B signalling. Experiments were performed in duplicate, and assays were repeated on three independent occasions. Data are presented as mean values \pm SE, with p values indicating significance difference compared with WT.

5.2.3 Measurements of TNF- α induced NF- κ B activation using luciferase reporter assays

Effects of the p62 constructs on induced NF- κ B activation was measured using the same protocol for basal NF- κ B activation (see 5.2.2) but with addition of 25ng/ml of TNF- α to the HEK293 cells 7 hours after co-transfection of the cells for 23 hours (again 0.3 μ g NF- κ B firefly luciferase reporter construct and 0.2 μ g of wild type or PDB-mutant p62 pCDNA3.1 construct, or empty pCDNA3.1 control, was used). As for basal signalling, transfection of wild type p62 and the PDB mutants (A381V, P392L, E396X) suppressed NF- κ B activation relative to the empty vector control. To compare the statistical significance of the changes exerted by each mutation relative to wild type p62, the results were analysed with one way ANOVA by choosing Dunnett's statistical test and using Prism software (version4). The statistical analysis was performed by selecting a 95% confidence limit (Figure 5.3).

Data for the P392L and E396X mutants showed P values were <0.05, confirming the difference between the activation of induced NF- κ B signalling for each of these mutant (relative to wild type p62) was statistically significant. However, data for the A381V mutant showed a P value >0.05, indicating in this case the increase in NF- κ B activation (relative to wild type) was not statistically significant.

TNF- α induced NF- κ B activation

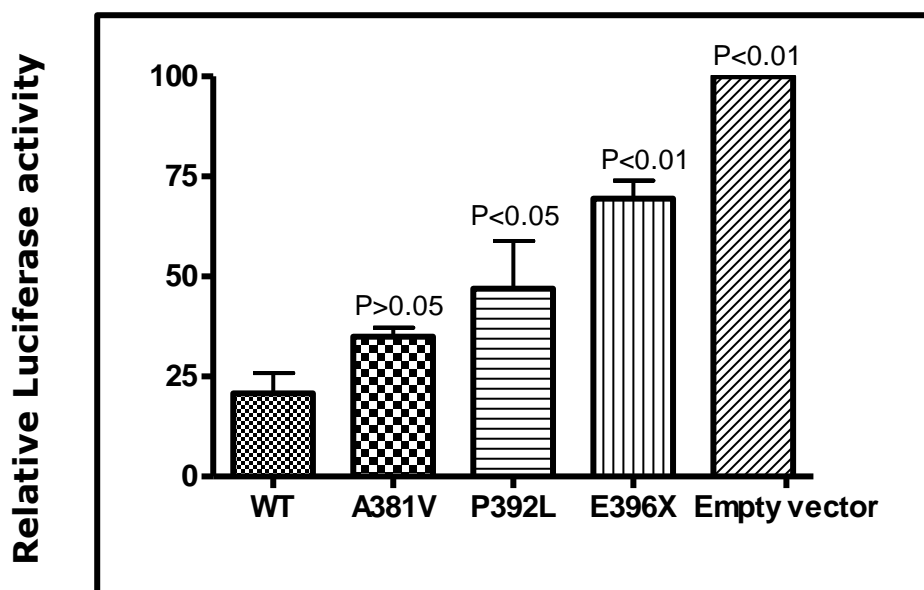


Figure 5.3: Effects of PDB-mutant p62 proteins on TNF- α induced NF- κ B signalling

The effects of transfection of different polyHis-FLAG-p62 constructs with indicated PDB mutations on TNF- α induced NF- κ B signalling in HEK293 cells were assessed using luciferase reporter assays. The P392L and E396X mutants showed a statistically significant increase in their efficiency of activating NF- κ B signalling, relative to wild type (WT), although the increase for the A381V mutant was not statistically significant. Experiments were performed in duplicate, and assays were repeated on three independent occasions. Data are presented as mean values \pm SE, with p values indicating significance difference compared with WT.

5.2.4 polyHis-FLAG-p62 expression levels in luciferase reporter assays

To confirm that changes in NF- κ B activation associated with different p62 constructs noted in the luciferase reporter assays was not caused by variations in ectopic p62 expression levels, lysates of HEK293 cells (used in the reporter assays) were analysed with western blotting (anti-FLAG), which confirmed relatively equal expression levels for the p62 variants (Figure 5.4).

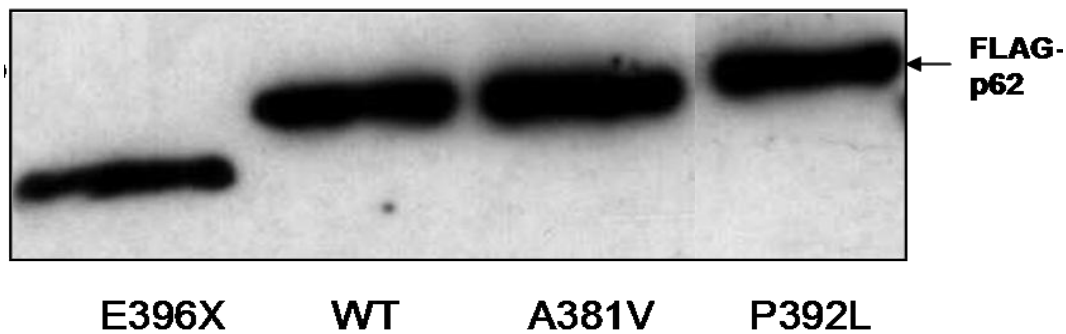


Figure 5.4: Ectopic expression levels of polyHis-FLAG-p62 in HEK293 cell lysates analysed in luciferase reporter assays

HEK293 cells were co-transfected with polyHis-FLAG-p62 and NF- κ B firefly luciferase reporter constructs for ~24 hours, then the cells were lysed according to the manufacturer's instructions in the Steady-Glo luciferase assay system. Equal volumes of cell lysate were then analysed by western blotting (anti-FLAG). Representative blot (in this case from a basal signalling assay) indicates that the cell lysates show relatively similar expression levels of different p62 variants.

Chapter 5 - Part II

Interaction of PDB-mutant p62 proteins and CYLD

5.3 Interaction of PDB-mutant p62 proteins and CYLD

5.3.1 Introduction

In certain contexts, p62 also appear to function as a positive regulator of RANK-NF- κ B signalling through regulation of a cascade that leads to phosphorylation and degradation of I- κ B, thereby releasing NF- κ B from the cytoplasm to the nucleus (Scheidereit, *et al.*, 2006). However, in addition to its positive role, p62 also appears to have a negative role in regulating RANK-NF- κ B signalling demonstrated in earlier work on the function of p62 (Rea *et al.*, 2006). In addition, we confirmed in the previous section (see 5.2) that although transfected PDB-associated p62 mutants (A381V, P392L, E396X) activated basal NF- κ B signalling relative to the wild type sequence, in fact all constructs analysed repressed signaling relative to empty vector controls. Although the mechanism of this negative regulation is poorly understood, it may involve interaction of p62 with negative regulators of NF- κ B signalling (Wei *et al.*, 2008). One of these negative regulators of NF- κ B signalling is a DUB enzyme, CYLD, which appears to exert its effects through interactions with TRAF6, TRAF2 and NEMO (Kovalenco *et al.*, 2003). Interestingly, p62 through its C-terminal mediates the interaction between CYLD and TRAF6 (Wei *et al.*, 2008); indeed co-immunoprecipitation assays showed that p62 deletion mutants lacking the UBA domain could not physically interact with CYLD (Wei *et al.*, 2008). CYLD might specifically mediate the negative signalling function of p62 in the RANK-NF- κ B pathway by deubiquitylating K63-polyubiquitylated TRAF6 (Wei *et al.*, 2008) (Figure 5.1.1), thereby causing deactivation of signaling (Trompouki *et al.*, 2003). Notably, the interaction between p62 and TRAF6 is not affected by expression levels of CYLD, and CYLD itself seems to be induced by NF- κ B expression as part of a feedback loop (Jono *et al.*, 2004) (Figure 5.1.1).

Based on these observations we attempted to assess the impact of PDB-associated mutations on the p62-CYLD interaction using indirect immunofluorescence staining and confocal microscopy, with the rationale that mutant p62 may be less able to recruit CYLD to (ubiquitylated) TRAF6 and thus may account for its reduced ability to repress NF- κ B signalling in reporter assays.

5.3.2 Co-localisation studies of wild type and PDB mutant polyHis-FLAG-p62 with HA-CYLD

To assess the effects of PDB-associated mutations on the interaction of p62 and CYLD, co-localisation of co-transfected proteins in U2OS cells was investigated using indirect immunofluorescence staining and confocal microscopy (in a similar manner to Chapter 4 where p62-ubiquitin interactions in transfected cells were investigated). For these experiments, polyHis-FLAG-p62 and HA-CYLD constructs (the latter kindly provided by Dr. SC Sun, Houston) were used. Prior to the detailed co-localisation studies between p62 and CYLD, transfected CYLD localisation alone (in the absence of transfected FLAG-p62) in U2OS cells was investigated to evaluate any effects of the selected PDB mutations on cellular phenotype. U2OS cells were transiently transfected with HA-CYLD for ~48 hours and fixed with formaldehyde. Rabbit anti-HA was used as a primary antibody for probing CYLD and then anti-rabbit Alexafluor 568 was used as a secondary antibody. Transfected HA-CYLD showed a diffuse distribution pattern in U2OS cells, and localised mainly in the cytoplasm, perinuclear area and occasionally in the nucleus (Figure 5.5).

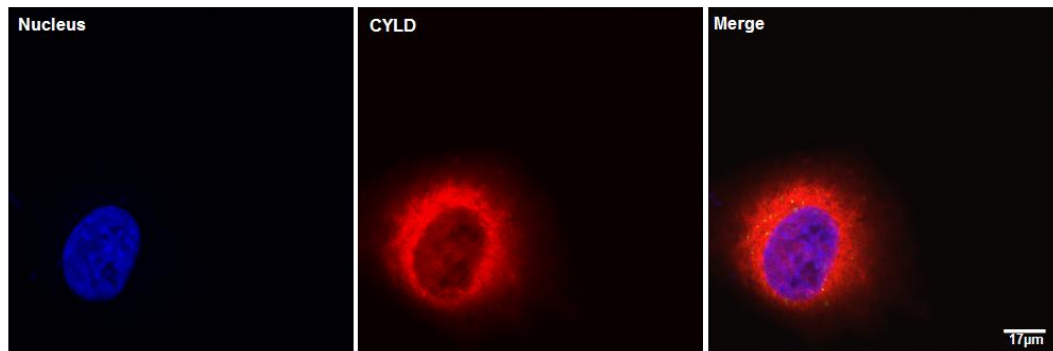


Figure 5.5: Subcellular localisation of transfected HA-CYLD in U2OS cells

U2OS cells were transiently transfected with a plasmid encoding HA-CYLD. After ~48 hours incubation the cells were fixed with formaldehyde. Transfected CYLD was probed using rabbit anti-HA as primary antibody and stained red using anti-rabbit Alexaflour568 as secondary antibody. Hoescht 32258 was used for staining nuclei. The images were collected at 40X objective lens with scale bar as indicated. HA-CYLD showed a diffuse staining pattern in the cytoplasm and perinuclear region, and occasionally the nucleus (as in this representative image).

Next, HA-CYLD and polyHis-FLAG-p62 constructs were transiently co-transfected in U2OS cells. p62 was probed with mouse anti-p62 as primary antibody and stained green using anti-mouse Alexafluor 488 as secondary antibody. CYLD was probed using rabbit anti-HA as primary antibody and stained red using anti-rabbit Alexafluor 568 as secondary antibody. Transfected CYLD showed some overlap of staining with each of the different p62 constructs tested (wild type, A381V, P392L and E396X mutants). However, in complete contrast to the findings in Chapter 4, when co-transfected with CYLD all of the regular cytoplasmic p62 bodies were lost and instead p62 staining was consistently of a diffuse nature (Figure 5.6). Thus, these experiments revealed that CYLD expression appears to abrogate the formation of p62 cytoplasmic bodies, and therefore interaction of p62 with CYLD could not be compared to the common p62 cytoplasmic bodies.

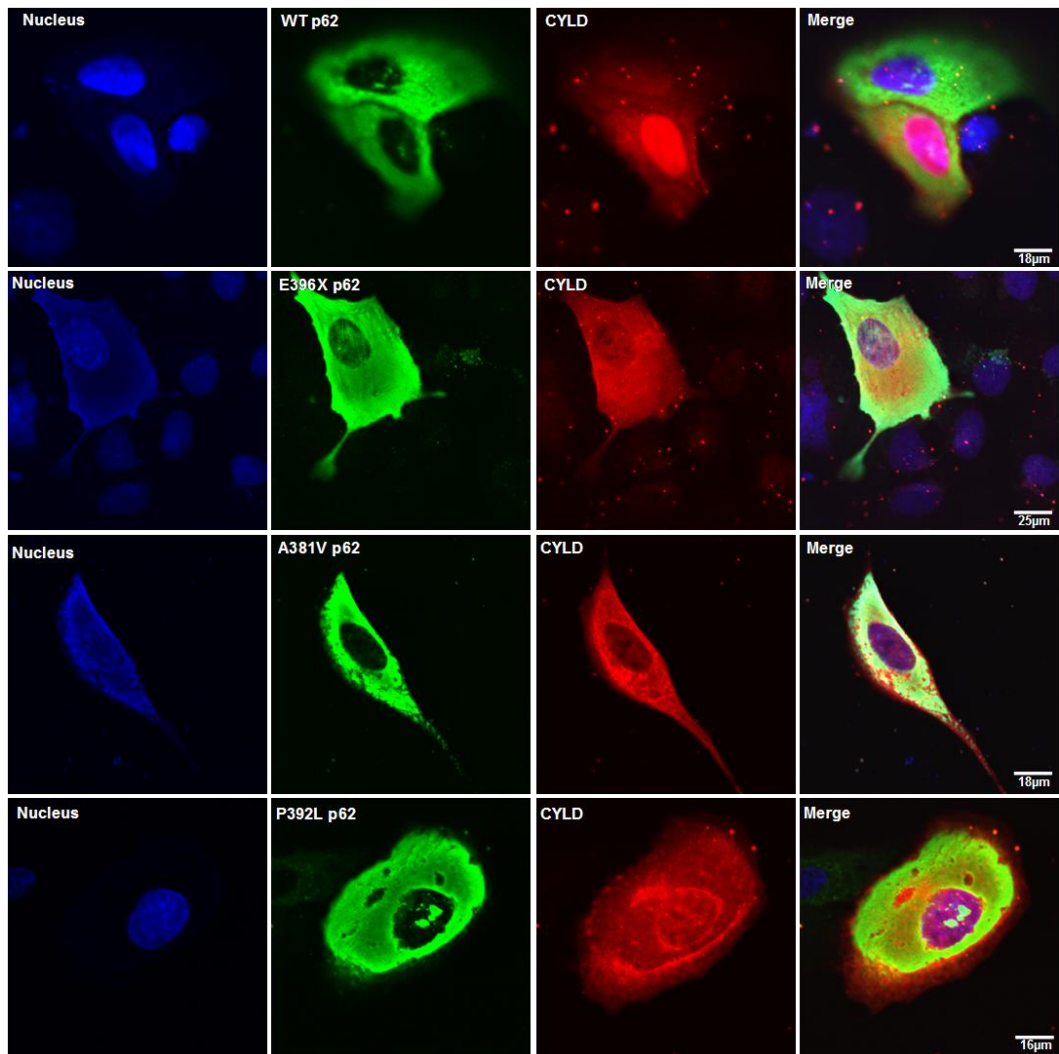


Figure 5.6: Co-localisation of HA-CYLD with polyHis-FLAG-p62 in U2OS cells

polyHis-FLAG-p62 constructs as indicated were transiently co-transfected with HA-CYLD in U2OS cells. After ~48 hours cells were fixed with formaldehyde; p62 were probed using mouse anti-p62 as primary antibody and stained green using anti-mouse Alexafluor488 as secondary antibody. CYLD was probed using rabbit anti-HA as primary antibody and stained red using anti-rabbit Alexafluor568 as secondary antibody. Hoescht 32258 was used for staining nuclei. The images were collected at 40X objective lens with scale bars as indicated. In all transfected cells both p62 and CYLD had a diffuse staining pattern, CYLD was distributed in the cytoplasm and the nucleus, and p62 cytoplasmic bodies were not evident.

Since CYLD expression appeared to abrogate the formation of p62 cytoplasmic bodies, structures that were commonly found to be ubiquitin-positive (Chapter 4), we reasoned that protein ubiquitination may be required for the formation of these cytoplasmic bodies and that changes in cellular ubiquitination following CYLD transfection may be sufficient to prevent cytoplasmic body formation. To investigate this idea further, whole cell lysates of U2OS cells which have been transiently co-transfected with HA-CYLD and polyHis-FLAG-p62 constructs were western blotted with anti-ubiquitin antibodies (Figure 5.7). Endogenous ubiquitin showed a conjugated staining pattern (Figure 5.7) even when CYLD was expressed, suggesting that CYLD does not exert its effects on p62 cytoplasmic body formation by grossly affecting protein ubiquitination, but instead must manifest more subtle effects. The same blot was re-probed with anti- β -actin, (Figure 5.7), in order to confirm equal loading of the U2OS cell lysates.

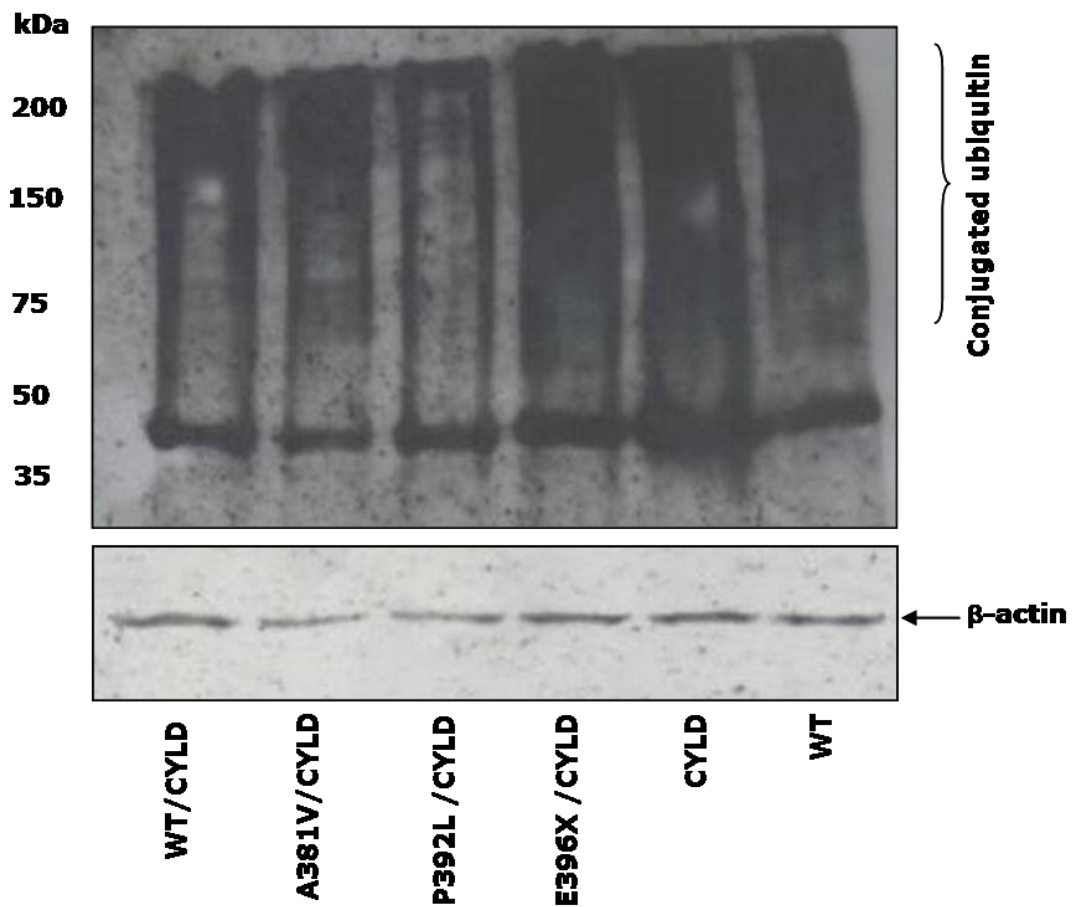


Figure 5.7: Detection of endogenous conjugated ubiquitin in U2OS cells co-transfected with polyHis-FLAG p62 and HA-CYLD

U2OS cells were transiently co-transfected with polyHis-FLAG-p62 constructs as indicated (WT = wild type and A381V, P392L and E396X mutants) and HA-CYLD for \sim 48hours, followed by subjecting whole cells lysates to SDS-PAGE and immunoblotting with anti-ubiquitin antibodies. Ubiquitin showed a characteristic conjugated staining pattern which was not significantly affected by CYLD expression.

The bottom blot shows detection of endogenous β -actin in U2OS cells co-transfected with polyHis-FLAG-p62 and HA-CYLD. The blot, used to detect conjugated ubiquitin in U2OS cells co-transfected with polyHis-FLAG-p62 and HA-CYLD, was re-probed with mouse anti- β -actin antibodies confirming approximately equal loading of cell lysates.

Chapter 5 - Part III

Interaction of PDB-mutant p62 proteins and NEMO

5.4 Interaction of PDB-mutant p62 proteins and NEMO

5.4.1 Introduction

In part I of this Chapter, changes in NF- κ B activation associated with PDB mutants of p62 were studied using luciferase reporter assays. These experiments showed that wild type p62 suppressed the activation of NF- κ B compared to empty vector controls indicating that p62 may function as a negative regulator of NF- κ B signalling, and that certain PDB mutants (A381V, P392L, E396X) exerted less of a repressive effect on signalling than wild type p62. As CYLD is a negative regulator of NF- κ B signalling and interacts with p62's C-terminus (containing the UBA domain), we then studied the effects of PDB mutations on the CYLD-p62 interaction (Chapter 5, Part II). However, unexpectedly we found that CYLD expression altered the cellular phenotype of p62-transfected cells such that p62 cytoplasmic bodies were no longer formed; consequently interaction of p62 with CYLD could not be reliably assessed using confocal microscopy.

Therefore, in a final attempt to investigate the molecular mechanism by which p62 (and its PDB mutants) exerts its effects on NF- κ B signalling pathways we examined interactions with another important regulator of NF- κ B signalling, NEMO. NEMO /IKK γ is part of the IkappaB kinase (IKK) complex, which is composed of two catalytic subunits (IKK α , IKK β) and one regulatory subunit, NEMO. NEMO binds to IKK β , which is necessary to activate NF- κ B (Scheidereit, *et al.*, 2006).

We selected NEMO specifically for this study because previous work showed that p62 is part of a complex composed of TRAF6, aPKC and IKK (Zhang *et al.*,

2005) and p62 interacts with NEMO and mediates its K63-linked polyubiquitylation through TRAF6 (Figure 5.1) (Martin *et al.*, 2005). In addition, CYLD also regulates the K63-linked polyubiquitylation of NEMO (Kovalenko *et al.*, 2003) and also interacts with NEMO as well as p62 (Figure 5.1) (Courtious *et al.*, 2008; Trompouki *et al.*, 2003). Hence, we sought to assess the effects of PDB-associated mutations on the interaction of p62 constructs with endogenous NEMO, using co-localisation of co-transfected proteins in U2OS cells with immunofluorescence staining and confocal microscopy.

A further way to study the effects of PDB-associated p62 mutations on NEMO homeostasis relates to the autophagic degradation of NEMO. IKK (including NEMO) is selectively degraded by autophagy and not through the proteasome system (Li *et al.*, 2006) and since p62 is part of the autophagy machinery (Bjørkøy *et al.*, 2005) we speculated that one role of p62 may be to recruit NEMO to the autophagic machinery mediating its degradation. Our proposal was that PDB mutant p62 may be less efficient than wild type at recruiting NEMO to autophagosomes, thereby resulting in defective autophagic degradation of NEMO and hence a net activation of the IKK complex and NF- κ B signalling. Specifically, we initially sought to examine any effects of ectopic p62 expression on levels of endogenous NEMO in U2OS cells.

5.4.2 Effects of expression of polyHis-FLAG-p62 on levels of endogenous NEMO in U2OS cells

In these experiments ectopic expression of polyHis-FLAG-p62 in U2OS cells was used to test the hypothesis that NEMO is degraded by p62-mediated autophagy and that PDB mutant p62 is less efficient in promoting this process. U2OS cells were transfected with different p62 constructs (wild type p62, A381V and E396X mutants) and incubated for ~48 hours, then cell lysates were immunoblotted for both transfected p62 and endogenous NEMO/IKK γ . The NEMO blots showed that U2OS cells expressing different p62 constructs contained equal levels of endogenous NEMO protein (Figure 5.8), suggesting that expression of PDB mutants did not alter rates of NEMO degradation. Approximately equal expression of p62 variants was confirmed by re-probing the blots with anti-FLAG antibodies (not shown).

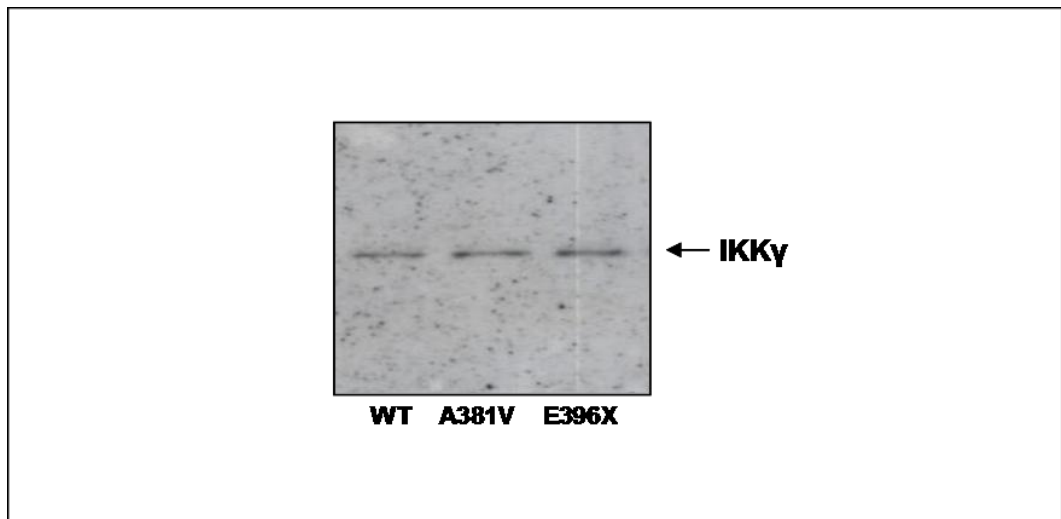


Figure 5.8: NEMO (IKK γ) protein levels in U2OS cells transfected with polyHis-FLAG-p62 constructs

U2OS cells transiently transfected with polyHis-FLAG-p62 constructs as indicated were incubated for ~48 hours. The cells were lysed with SDS PAGE loading buffer and lysates were analysed by western blotting (anti-NEMO) to detect endogenous NEMO/IKK γ . The representative blot shows approximately equal levels of NEMO protein in cells transfected with different p62 constructs.

5.4.3 Co-localisation studies of wild type and PDB mutant polyHis-FLAG-p62 with endogenous NEMO

Prior to the detailed co-localisation studies between wild type and PDB mutant p62 and NEMO, endogenous NEMO localisation (in the absence of transfected polyHis-FLAG-p62) in U2OS cells was investigated to evaluate any effects of p62 expression on cellular phenotype.

Non-transfected U2OS cells were incubated for ~40 hours after splitting into 12-well plates. Cells were stained with anti-NEMO and analysed by confocal microscopy as described earlier. Endogenous NEMO was distributed in U2OS cells in a diffuse pattern, mainly around the nucleus and the cytoplasm (Figure 5.9).

U2OS cells were then transiently transfected with various polyHis-FLAG-p62 constructs (wild type, and A381V, P392L, E396X mutants). Mouse anti-p62 was used as a primary antibody to detect p62 and then anti-mouse Alexafluor 488 used as a secondary antibody. Rabbit anti-NEMO was used as a primary antibody to detect endogenous NEMO and then anti-rabbit Alexafluor 568 is used as a secondary antibody.

Ectopic expression of wild type p62 had an obvious effect on the phenotype of endogenous NEMO in U2OS cells, as NEMO was recruited to cytoplasmic bodies similar to the previously characterised p62 cytoplasmic bodies (Figure 5.10) presumed to represent autophagosomes. Indeed transfected wild type p62 and endogenous NEMO showed strong co-localisation. Although the E396X mutant of p62 again failed to form cytoplasmic bodies (and co-localise with NEMO), the A381V and P392L mutants retained this property and consistently recruited endogenous NEMO to these structures. Thus, PDB-associated

mutants of p62 did not appear to be associated with a generalised loss of co-localisation (and presumably interaction) with NEMO.

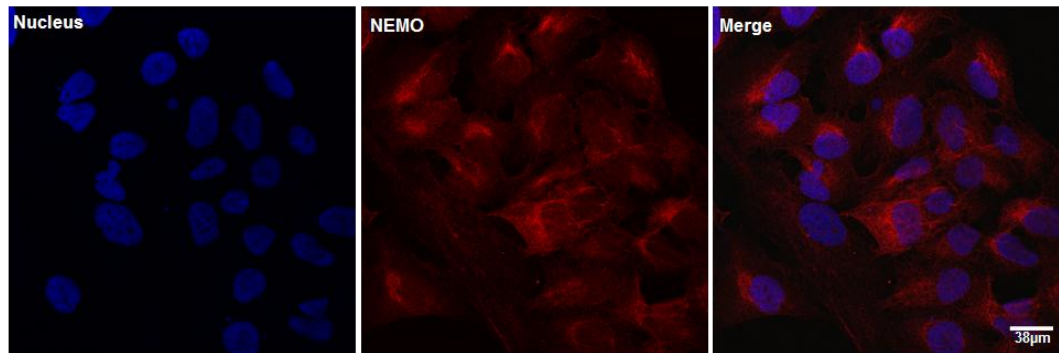


Figure 5.9: Subcellular localisation of endogenous NEMO in U2OS cells

U2OS cells were incubated for ~40 hours after splitting without ectopic protein expression. The cells were fixed with formaldehyde. Endogenous NEMO was probed using rabbit anti-NEMO as primary antibody and stained red using anti-rabbit Alexaflour568 as secondary antibody. Hoescht 32258 was used for staining nuclei. All images were collected at 63X objective lens with scale bar as indicated. Endogenous NEMO showed a diffuse staining pattern and was not able to form cytoplasmic structures in the absence of ectopic p62 (compare to Figure 5.10).

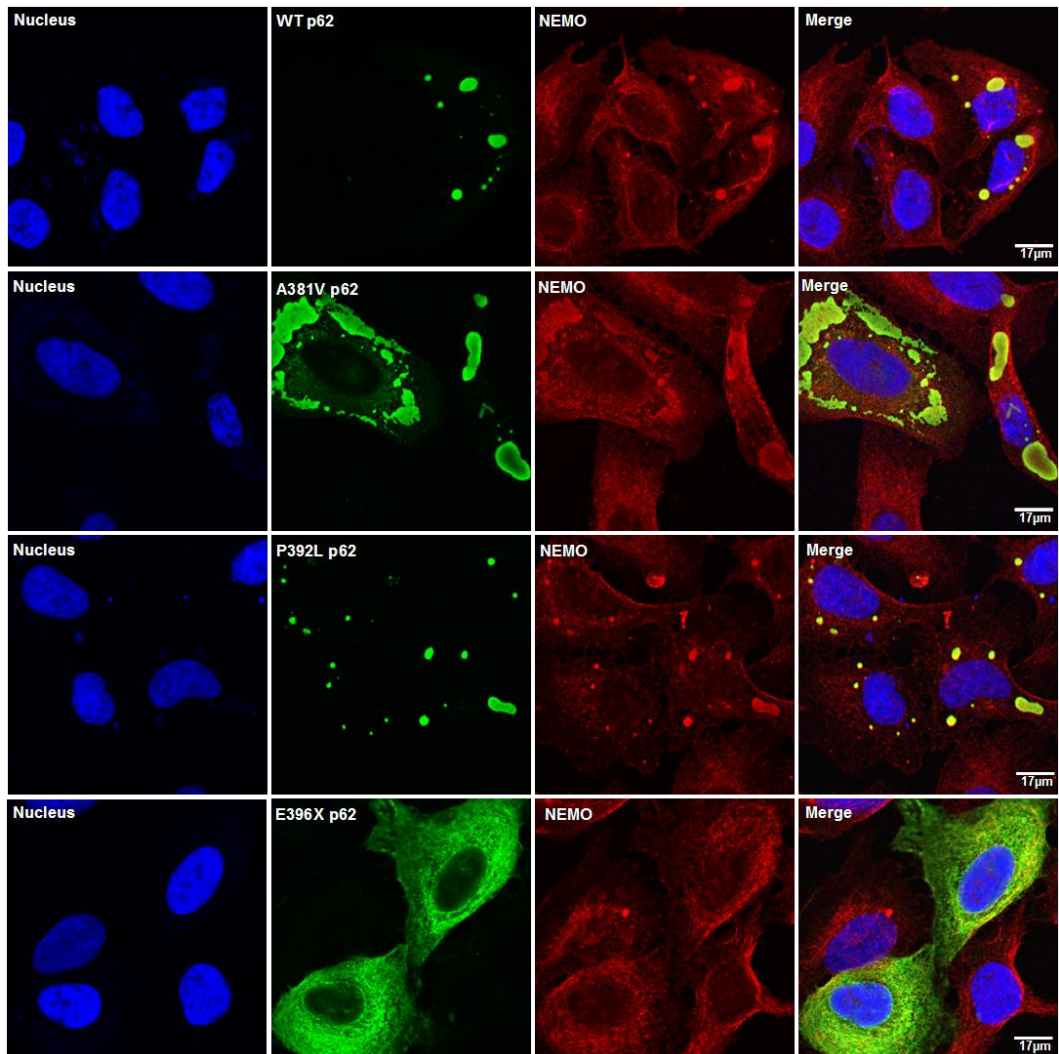


Figure 5.10: Co-localisation of endogenous NEMO and polyHis-FLAG-p62 in U2OS cells

polyHis-FLAG-p62 constructs as indicated were transiently transfected in U2OS cells. After ~48 hours incubation the cells were fixed with formaldehyde. p62 was probed using mouse anti-p62 as primary antibody and stained green using anti-mouse Alexafluor488 as secondary antibody. Endogenous NEMO was probed using rabbit anti-NEMO as primary antibody and stained red using anti-rabbit Alexafluor568 as secondary antibody. Hoescht 32258 was used for staining nuclei. All images were collected at 63X objective lens with scale bars as indicated. p62 cytoplasmic bodies (wild type, A381V, P392L but not present in E396X) showed a general co-localisation with endogenous NEMO.

5.5 Discussion

Earlier we used several protein interaction methods to study the ubiquitin-binding properties of p62 and its PDB-associated mutants, including the non-UBA domain A381V mutant. Using *in vitro* ubiquitin-binding assays, the A381V mutant showed subtle changes in its ubiquitin-binding properties compared to wild type p62 (Chapter 3) but confocal microscopy studies of transfected cells failed to distinguish the co-localisation of the mutant p62 and ubiquitin with that observed for the wild type. Therefore, in this chapter we went on to study the functional effects of the A381V mutation on NF- κ B signalling, initially using cell-based luciferase reporter assays.

The selected PDB-associated p62 mutants including A381V (as well as P392L and E396X) all increased basal NF- κ B signalling relative to wild type p62, despite the fact that the A381V variant had only minimal effects on the ubiquitin-binding properties of p62. In contrast to basal NF- κ B activation, the A381V mutant did not significantly activate TNF- α induced signalling, although the control mutants (P392L and E396X) were associated with a statistically significant increase (relative to wild type). The high P value for the A381V mutant (>0.05) may be due to the experimental limitations of the luciferase reporter assay (see Section 5.5.2).

Compared with previous studies, our results were consistent with those observed by Rea *et al.*, in which both E396X and (K378X) deletion mutants increased NF- κ B activation relative to wild type. In contrast, Wooten *et al.* reported that a UBA-domain deletion construct of p62 (Δ 385-440) decreased NF- κ B activation compared to wild type (Wooten *et al.*, 2005). This discrepancy might arise from different experimental conditions of the assays, as the luciferase reporter assay is sensitive to many experimental variables.

Nevertheless, in general experimental evidence from several different studies suggests that UBA domain deletion mutants are associated with increased rather than decreased NF- κ B activity, relative to wild type p62. For example, another p62 UBA-domain deletion mutant (Δ 371-442) was found to increase RANK-L induced NF- κ B activation relative to wild type (Xu *et al.*, 2008).

Our results were also consistent with a recent study of another novel non-UBA domain mutation, P364S, which was found to increase NF- κ B signalling relative to wild type despite retaining its full ubiquitin-binding function at both pH7.5 and pH6.5 (Rea *et al.*, 2009). Together these results imply that the ubiquitin-binding properties of p62 proteins do not simply correlate with the activation of NF- κ B signalling, and suggest other components of the NF- κ B signalling axis might be involved in the regulation of this pathway (Rea *et al.*, 2009) (Najat *et al.*, 2009).

In conclusion, our data showed that in reporter assays wild type p62 inhibited NF- κ B signalling and that PDB-associated mutations increase NF- κ B activation relative to wild type. However, the precise physiological significance of the apparent repression of signalling by p62 is still unclear (Layfield *et al.*, 2007) (see Section 5.5.1 for detailed discussion).

To further examine the function of p62 in the regulation of NF- κ B signalling we went on to determine possible effects of PDB-associated mutations on the p62-CYLD interaction. Interestingly, we were unable to conduct detailed co-localisation studies (by confocal microscopy) because CYLD expression changed the sub-cellular localisation of p62 in U2OS cells, resulting in the loss of the common p62 cytoplasmic bodies (see Section 4.6) previously shown to be ubiquitin-positive and associated with wild type, A381V and P392L p62 mutants. Notably, the diffuse p62 staining pattern observed for these

constructs when co-transfected with CYLD was very similar to the diffuse phenotype normally observed for the E396X mutant (when transfected both without and with ubiquitin). The cellular phenotype of the E396X mutant of p62, which lacks almost the entire UBA domain (and is unable to bind ubiquitin) may provide some clues to explain the diffuse staining pattern noted when the other p62 constructs were co-transfected with CYLD. One possibility is that full length p62, regardless of whether it is wild type or mutant, through its UBA domain interacts with transfected CYLD and this competes with other interactions required for the formation of p62 cytoplasmic bodies/autophagosomes (which cannot be formed by the E396X mutant). Another possible explanation is that since CYLD is a DUB, full length p62 constructs could not form their regular phenotypes, because of a lack of cellular conjugated ubiquitin normally required for cytoplasmic body/autophagosome formation when CYLD is expressed at high levels. However, immunoblotting of U2OS cells transfected with CYLD could not demonstrate gross changes in cellular ubiquitylation. Moreover, it remains a possibility that CYLD selectively deubiquitylates only certain cellular proteins, the ubiquitylation of which regulates p62 cytoplasmic body/autophagosome formation.

Finally, we went on to study the interaction of p62 (and its PDB mutants) with another important regulator of NF- κ B signalling, IKK γ /NEMO. We concluded that NEMO appeared to be recruited to p62-positive cytoplasmic bodies (as some of these cytoplasmic bodies interacted with the autophagic marker, LC3) regardless of the mutation status of p62, which may be indicative of its delivery to autophagosomes for degradation. However, despite the findings of earlier studies, which showed that the IKK complex (including NEMO) is selectively degraded by autophagy (Qing *et al.*, 2006), ectopic expression of p62 (wild type or mutant) did not appear to accelerate the degradation of

NEMO, as assessed by western blotting. Nevertheless these contradicting results may be rationalised, as we speculate that NEMO might be stably recruited to p62-positive autophagosomes but only degraded in a signal induced manner (our transfected cells were unstimulated). Clearly further research is needed to understand the role of PDB-associated p62 mutations in the disruption of NEMO-mediated NF- κ B signalling. A final possibility is that p62 might not recruit NEMO to the autophagy machinery at all and that the p62-positive structures in our cells might not all be autophagosomes, as p62 and LC3 are able to interact within aggregates that are independent from autophagy pathway (Shvetz *et al.*, 2008); again further studies in this area will be informative.

In conclusion, our results show that the non-UBA domain A381V PDB-associated mutation of p62, although having only minimal effects on ubiquitin-binding *in vitro*, is (like other PDB mutations) associated with increased basal NF- κ B activation relative to wild type. We concluded that wild type and PDB-mutant p62 proteins are capable of recruiting NEMO to cytoplasmic bodies which may represent autophagosomes, but do not appear to accelerate its degradation. Finally, we found that CYLD expression appears to abrogate the formation of p62 cytoplasmic bodies, although not through gross changes in protein ubiquitination; mutations in CYLD might have subtle roles in PDB development and further work is clearly needed to investigate possible genetic abnormalities in other genes of the of RANK/NF- κ B signalling axis in PDB patients.

5.5.1 p62 positively and negatively regulates RANK-NF- κ B signalling

Earlier studies demonstrated that p62 is central to RANK-NF- κ B signalling and osteoclastogenesis, but the exact role of p62 *in vivo* is still poorly characterised (Layfield *et al.*, 2007). NF- κ B is a transcription factor which is

normally sequestered by I- κ B in the cytoplasm, and a series of signalling cascades mediated by p62-mediated ubiquitylation ultimately leads to degradation of I- κ B and subsequent release of NF- κ B to the nucleus (Figure 5.1). Specifically p62 appears to regulate the K63-linked polyubiquitylation of NEMO (which is a regulatory subunit of the IKK complex) through TRAF6, and this process causes phosphorylation of NEMO and subsequent K48-linked polyubiquitylation of I- κ B, which serves as a tag for its degradation by the 26S proteasome system causing the release of NF- κ B to the nucleus (Zhang *et al.*, 2005). One of the cascades that lead to NF- κ B activation is through activation of IKK complex, the activation of which is regulated by two different signalling complexes, which both depend on ubiquitylation (Figure 5.1). The first complex comprises TAB1-TAB2-TAK1, and K63-linked polyubiquitylation of TRAF6 mediates its recruitment to TAB2-TAK1 through binding of K63-polyubiquitin chains to TAB2 (TRAF6 may also bind to TAB2 without the involvement of K63-polyubiquitin chains). The interaction between TRAF6 and TAB2 activates TAK1, which then phosphorylates IKK β , which in turn activates the IKK complex and ultimately NF- κ B (Chen *et al.*, 2005).

The second complex, which results in IKK activation, is composed of p62-aPKC-TRAF6 (Duran *et al.*, 2004), and functions in a similar manner to the TAB2-TAK1 complex (Chen *et al.*, 2005). Upon various stimuli (including RANK activation by RANK-L) the complex will form, in which p62 bridges aPKCs to TRAF6; this complex activates IKK and subsequently causes activation of NF- κ B (Jin *et al.*, 2008). This signalling system illustrates a positive role of p62 in NF- κ B activation; experimental models also support the importance of p62 in osteoclast NF- κ B activation, as p62 knockout mice show defective NF- κ B signalling and osteoclastogenesis upon stimulation with parathyroid hormone related protein, although basal osteoclastogenesis was not affected in these animals (Duran *et al.*, 2004).

Based on these data one might expect that ectopic expression of wild type p62 in U2OS cells would activate NF- κ B signalling, whilst the PDB mutants might decrease NF- κ B activation relative to wild type as they (in general) bind more weakly to ubiquitin than the wild type protein. However, despite this notion, differences in p62 expression levels appear to be associated with different effects on NF- κ B activity. For example, in our reporter assays (and previous studies) where p62 is expressed at relatively high levels, wild type and mutant constructs in fact repress NF- κ B activation compared to empty vector controls, and PDB mutants are associated with increased signalling compared to wild type (Figure 5.2). These results indicate that at these expression levels wild type p62 has a repressive function with respect to NF- κ B signalling and that PDB-associated mutants diminish this repressive function (Rea *et al.*, 2006). Previously such results were interpreted that p62 is in fact normally a negative regulator of NF- κ B signalling but of course this proposal contradicts the defective NF- κ B signalling noted in the p62 knock out mice. The most feasible explanation for the repressive effects of ectopic p62 expression on NF- κ B activation is that since p62 is an ubiquitin-binding protein, over-expression of the protein may lead to competition with other ubiquitin-binding proteins in the NF- κ B pathway disturbing their ubiquitin-dependent functions. Hence, we speculate that in our luciferase reporter assay, the repression of signalling observed might represent an 'artefact' of high p62 expression levels above normal physiological levels of p62 in cells. For example, ectopic p62 might compete with TAB2 for binding polyubiquitin, hence deactivating the TAB1-TAB2-TAK1 complex and causing subsequent deactivation of IKK and NF- κ B (Figure 5.1 (A)). Further, p62 might also compete ubiquitylated I- κ B binding to the 26S proteasome, thus inhibiting I- κ B degradation and presenting as a repression of NF- κ B activation (Figure 5.1 (B)). In this regard, it could be argued that in the reporter assays the effects of PDB-associated p62 mutants

that do not repress signalling to the level of wild type p62, simply result from differences in the ability of the transfected proteins to compete in these ubiquitin-dependent interactions.

Interestingly, this competition mechanism of p62 binding to ubiquitin can be compared to a parallel signalling system, which involves another polyubiquitin-binding protein, AWP1, which also normally positively regulates NF- κ B signalling. Over expression of AWP1 repressed NF- κ B signalling in reporter assays, and it was suggested that ectopic AWP1 would compete with NEMO for K63-polyubiquitin chains, thereby repressing NF- κ B (Fenner *et al.*, 2009).

Another possible explanation for the negative regulation of NF- κ B signalling by p62 over-expression in reporter assays is as a result of interactions with the DUB enzyme CYLD. CYLD interacts with p62 through the UBA domain and specifically negatively regulates NF- κ B signalling by the deubiquitylation of K63-linked polyubiquitylated chains assembled by TRAF6 (Jin *et al.*, 2008). In addition, CYLD might deubiquitylate several other proteins in the NF- κ B pathway, as previous reports showed that CYLD suppresses NF- κ B activation upstream of IKK (Chen *et al.*, 2005); since IKK activation requires ubiquitylation, a reversible covalent process, it was suggested that IKK also is regulated by deubiquitylation (Chen *et al.*, 2005). These studies collectively confirm that proteins modified with or that can bind to K63-linked polyubiquitin play important roles in the regulation of NF- κ B signalling.

Following on from the proposed theories of p62s role in the regulation of NF- κ B signalling, many questions remain unanswered and obviously more research is required. One of these questions is why the E396X truncating mutant, which loses most of its UBA domain and has no ubiquitin-binding ability *in vitro*, still appears to activate the NF- κ B activity relative to wild type

p62 *in vitro* (in fact this could equally be viewed as repression of signalling, relative to the empty vector control) (Figures 5.2 and 5.3). This observation suggests that other domains of p62 must also contribute to the regulation of NF- κ B signalling.

In summary, all the data available to date suggests that p62 may be able to both positively and negatively regulate NF- κ B signalling, and further research is necessary to understand how defective p62-mediated signalling contributes to the pagetic phenotype.

5.5.2 Limitations of the luciferase reporter assay

The luciferase reporter assays were repeated at least three times and although care was taken to use the same experimental conditions, such as temperature and media composition, variability was still observed for this assay. Of note, the P392L mutant gave a great degree of variability in results when compared to the other p62 sequences, and this variation was even apparent for the duplicates of the same experiment performed in the same day with the same transfected cell samples.

Interestingly, another group noted the same variability associated with the P392L mutant in luciferase reporter assays (S Rea, personal communication). One possibility is that this variation may arise because P392L is a temperature-sensitive mutation (Cavey *et al.*, 2005) and small differences in temperature when incubating the cultured cells could translate to differences in ubiquitin-binding affinities of the transfected P392L-p62 protein.

The statistical analyses also contribute to the limitation of the reporter assay, because the high standard deviation of P392L data affected the individual P values for the other mutations; for example by running the ANOVA (Dunnett's

test) without considering P392L data, the P value associated with the data for the A381V mutant (relative to wild type) changed from non-significant to significant in the TNF- α induced signalling assays. These results show the importance of precision in statistical analyses. Obviously, a more robust result requires more than three repeats, which is the minimum number of replicates required to run a Dunnett's test.

CHAPTER 6

General discussion

Chapter 6: General Discussion

6.1 General Discussion

In recent years there has been substantial research and conflicting theories related to the pathogenesis of PDB (Roodman *et al.*, 2005). The most important breakthrough in bone remodelling was the identification of the osteoclastic regulatory signalling axis comprising OPG/RANKL/RANK (Khosla *et al.*, 2001). Several therapies of pathological bone conditions subsequently emerged based on the regulation of this axis, however direct and precise manipulation is difficult, as this may cause unwanted side effects (Boyle *et al.*, 2003).

Several mutated genes were identified in PDB patients and those with related syndromes in recent years, many of which were found to be important regulators of osteoclastogenesis, therefore extensive recent research has focused on the role of genetic factors in osteoclastogenesis and their subsequent effects on bone remodelling in bone diseases (Roodman *et al.*, 2005).

In this study we extended a proposal by Cavey *et al.* that all of the *SQSTM1* mutations associated with PDB manifest as loss of or impaired ubiquitin-binding function of the p62 protein (Cavey *et al.*, 2006). Specifically, we investigated newly identified and previously uncharacterised PDB-associated non-UBA domain mutations of p62, hoping to understand the effects of these mutations on ubiquitin-binding function of p62 and on RANKL-NF- κ B signalling. Two of the non-UBA domain PDB-associated mutations analysed in this study (A381V, Δ 351-388) resulted in subtle reductions in ubiquitin-binding function of p62 in pull-down assays, although notably the A381V mutant only showed

reductions in its ubiquitin-binding function in pull-down assays under acidic conditions; we correlated this finding with the notion that p62-bound ubiquitylated proteins are shuttled to autophagosomes, which themselves operate at an acidic pH. Our findings were consistent with a previously studied artificial deletion construct of p62 (368-391), which showed impaired ubiquitin-binding properties (Vadlamudi *et al.*, 1996). Structural analyses of p62 may provide some clues to the role of the non-UBA domain mutations in regulating the ubiquitin-binding function of p62; indeed it was found through structural analysis that the region of p62 which immediately precedes the UBA-domain and contains A381V (residues 341-386) is not significantly structured. Further, this region contributes to a small enhancement of ubiquitin-binding affinity of the p62 UBA domain (Najat *et al.*, 2009). Notably however, another novel non-UBA domain mutation tested in a parallel study (P364S) retained its ubiquitin-binding function at both pH7.5 and pH6.5 (Rea *et al.*, 2009). Based on these data we speculated that missense mutations located further from the UBA domain have less pronounced effects on ubiquitin-binding function of p62. In combination, these observations can be rationalised by the notion that impaired ubiquitin-binding function of p62 *per se* is not directly required for PDB pathogenesis, or more likely that non-UBA domain regions of p62 contribute to additional interactions of p62 with ubiquitylated proteins (including protein members of the RANK signalling pathway). In other words, non-UBA domain mutations might cause reduced interaction with previously ubiquitylated substrates of p62, rather than directly with the ubiquitin modification as is the case for UBA domain mutations (Najat *et al.*, 2009). In conclusion, our results indicate that non-UBA domain sequences play an important role in regulating binding affinity of p62, but their exact contribution to p62-ubiquitin recognition is still unclear. Further research is clearly needed in this area.

A previous study by Hocking *et al.* highlighted a possible correlation between the ubiquitin-binding properties of p62 and disease severity in PDB patients with the corresponding mutations. Most interestingly, patients with truncating UBA domain mutants had the most severe disease phenotypes, changes associated with a complete loss of ubiquitin-binding function of p62 *in vitro*. Therefore, we used a double p62 mutation (P392L/S399P on the same allele) to further test the hypothesis of a relationship between (mutant) protein function and disease phenotype. The P392L/S399P double mutation had an additive effect both on p62 protein function and disease phenotype, as the mutant p62 protein showed complete loss of ubiquitin-binding function in our *in vitro* pull-down binding assay at room temperature where individual mutations retained some binding. The ubiquitin-binding function of these mutations correlated with disease severity in patients with the double mutation, who were described to have particularly severe disease phenotypes, whilst carriers of the individual mutations had milder disease phenotypes (Eekhoff *et al.*, 2004). These observations further support the original proposal of a possible correlation between disease severity and the ubiquitin-binding properties of mutant p62 (Hocking *et al.*, 2004). However, the proposal has some limitations and extensive research is needed to draw robust conclusions, and in light of our other findings it should be considered that this proposal may only be relevant to UBA domain mutations (Najat *et al.*, 2009).

Based on these results, it was deemed necessary to quantify using biophysical approaches the interaction properties of p62 and ubiquitin, to more rigorously support the previous proposal. However using 2D-HSQC protein NMR we found that it is not feasible to easily study the interaction constants (K_a and K_d) between p62 and ubiquitin, and in the future using other quantitative methods such as surface plasmon resonance, may provide better quantitative results.

Following our failure to study the interaction constants between mutant p62 and ubiquitin using protein NMR, we sought a more physiologically relevant (cell based) model to investigate the ubiquitin-binding properties of p62. Our cell based confocal microscopy analyses, involving co-transfection of p62 and ubiquitin proteins, provided no advantage over pull-down assays in distinguishing the function of wild type p62 from several PDB-associated mutants (except for the E396X truncating mutant), as all the missense mutations studied co-localised with ubiquitin in a similar manner to wild type p62. In addition, sizes of cytoplasmic bodies formed by the p62 mutants could not be used to distinguish them from wild type p62, contradicting earlier proposals that missense PDB-associated mutants produce larger cytoplasmic bodies than the wild type p62 in transfected cells (Leach *et al.*, 2006). The co-localisation patterns between various p62 constructs (wild type and PDB-mutant) and ubiquitin indicated that there is no simple correlation between the *in vitro* ubiquitin-binding assay and co-localisation of p62/ubiquitin in transiently transfected cells. Previous studies and some of our own observations showed that a functional UBA domain (with respect to ubiquitin-binding) is required for the formation of ubiquitin-positive and p62-positive cytoplasmic bodies, however analyses of other mutations, such as P392L (which impaired ubiquitin-binding of p62 *in vitro*) contradicted this notion, as the P392L mutant readily formed regular p62/ubiquitin positive cytoplasmic bodies in transfected cells. In contrast, the E396X mutant did not form cytoplasmic bodies; these contradicting observations might be because the UBA domain interacts with other substrate proteins (in addition to ubiquitin), which are required for the formation of p62 bodies and that the A381V and P392L mutants maintain these interactions (Najat *et al.*, 2009).

Interestingly, and similar to previous studies, we found that some of the p62-positive cytoplasmic bodies may be autophagosomes, as they co-localised with the autophagic marker LC3. Another non-UBA domain mutant, D335E, was investigated in this study and it did not affect two functionally-relevant cellular interactions of p62; the D335E mutant retained its ubiquitin-binding function in the *in vitro* ubiquitin-binding assays, and this mutant also co-localised strongly with LC3 in transfected U2OS cells. These observations may be rationalised by the fact that the D335E change is conservative, substituting one acidic side chain for another, or since this change was found only in one Italian patient, D335E may represent a rare polymorphism rather than a disease-associated mutation.

Since the partial loss of ubiquitin-binding function of the A381V mutant of p62 could not be investigated further with confocal microscopy analyses, we studied the effects of this mutation on cellular functions of p62, first determining the functional effects of the mutation on NF- κ B signalling. Our results showed that this non-UBA domain PDB-associated mutation, although having only minimal effects on ubiquitin-binding *in vitro*, is (like other PDB mutations) associated with increased basal NF- κ B activation relative to wild type in luciferase reporter assays. Interestingly another novel non-UBA domain, P364S, has also recently been reported to show increased NF- κ B signalling potential relative to wild type p62, and this mutation retained its full ubiquitin-binding function at both pH7.5 and pH6.5 (Rea *et al.*, 2009). Together these results imply that the ubiquitin-binding properties of p62 proteins do not simply correlate with the activation of NF- κ B signalling, although defective NF- κ B signalling may still be a major cause of disrupted bone remodelling. Further these results suggest that dysregulation of other components of the NF- κ B signalling axis might be involved in PDB aetiology (Rea *et al.*, 2009; Najat *et al.*, 2009).

The NF- κ B luciferase reporter assays also showed that p62 mutants (like wild type sequence) have a repressive function in NF- κ B signalling relative to empty vector controls, which might indicate that p62 has a role in negative regulation of NF- κ B pathway (diminished when p62 is mutant). To further investigate this hypothesis, we examined the interaction properties of PDB-associated p62 mutants with a negative regulator of the NF- κ B pathway, the DUB enzyme CYLD. CYLD co-transfection with p62 in U2OS cells resulted in a loss of the formation of p62 cytoplasmic bodies, therefore we could not investigate the effects of p62 mutants on p62-CYLD interactions using this approach; however, this result does not exclude the possibility that the p62-CYLD interaction might still have important roles in PDB pathogenesis and in NF- κ B regulation.

Finally, we studied the effects of selected PDB mutations on the interaction properties of p62 and NEMO, which is an important regulator of NF- κ B pathway. Our western blot analyses suggested that ectopic expression of p62 (wild type or mutant) did not facilitate the degradation of NEMO, regardless of the confocal analyses results, which indicated that NEMO was recruited to p62-positive cytoplasmic bodies (which we presumed were autophagosomes) formed by both wild type p62 and selected PDB-associated p62 mutants. Obviously more detailed investigation is needed to understand the potential role of PDB-associated p62 mutations in the disruption of NEMO-mediated NF- κ B signalling.

Based on our results and current research on PDB pathogenesis, more detailed investigations are necessary to understand the molecular basis of PDB, in order to develop specific therapeutic targets for the disease. Previously, it was proposed that bisphosphonates can be used to control the extent of PDB; however a recent clinical trial of intensive bisphosphonate treatment versus

symptomatic management of PDB showed that no significant differences in the pain or quality of life between the two groups (Langston *et al.*, 2009). In particular, extensive research is needed to understand the functional role of p62 and its mutations on RANKL-NF- κ B pathway. Also, other genes associated with PDB might give important clues to the disease pathogenesis (Goode *et al.*, 2009).

Our results (together with previous studies) suggested that in reporter assays overexpressed p62 functions as a negative regulator of the NF- κ B pathway. But, based on the recent emerging links between autophagy and the ubiquitin-proteasome system, in which autophagy inhibition resulted in delays in shuttling p62 ubiquitylated proteins to the proteasome system further causing aggregation of p62 (Korolchuk *et al.*, 2009), it is more logical to speculate that p62 is not a normal physiological negative regulator of the NF- κ B pathway, but rather p62 accumulation (resulting from defective autophagy) causes defective degradation of ubiquitylated proteins (such as I- κ B) by the proteasome systems (Goode *et al.*, 2009). Obviously, defective autophagy may effect the signalling proteins downstream the RANKL-NF- κ B signalling pathway, but it should be considered that current investigations suggest that defective autophagy and dysregulated NF- κ B signalling in PDB may not necessarily be mutually exclusive (Goode *et al.*, 2009).

The role of p62 in autophagy might introduce another important cellular degradation system in bone remodelling and bone diseases, although there is not any investigation to date on the link between autophagy and osteoclasts. It would certainly be interesting to investigate the role of autophagy in PDB, as potentially autophagy could be used as an alternative therapeutic target for pathological bone conditions, because autophagy is relatively easily pharmacologically manipulated *in vivo* (Goode *et al.*, 2009).

Finally, the role of viruses and other environmental factors in PDB should not be disregarded, in order to draw a combined theory for the disease aetiology, (Goode *et al.*, 2009) as for example there is an emerging realisation that many viruses in fact target mammalian autophagic systems (Taylor *et al.*, 2009).

References

References

- Albagha, OME, Visconti, MR, Alonso, N et al. 2009. Identification of novel genetic variants that predispose to Paget's disease of bone by genome wide association. *Bone* 2: 224-5
- Aono, J, Yanagawa, T, Itoh, K, Li, B, Yoshida, H et al. 2003. Activation of Nrf2 and accumulation of ubiquitinated A170 by arsenic in osteoblasts. *Biochem. Biophys. Res. Commun.* 305: 271-77
- Barker, DJ. 1984. The epidemiology of Paget's disease of bone. *Br. Med. Bull.* 40: 396-400
- Bellu, AR, Komori, M, van der Klei, IJ, Kiel, JAKW, Veenhuis, M. 2001. Peroxisome Biogenesis and Selective Degradation Converge at Pex14p. *Journal of Biological Chemistry* 276: 44570-74
- Bersano, A, Del Bo, R, Lamperti, C, Ghezzi, S, Fagiolari, G et al. 2009. Inclusion body myopathy and frontotemporal dementia caused by a novel VCP mutation. *Neurobiol. Aging* 30: 752-58
- Beyens, G, Wuyts, W, Cleiren, E, de Freitas, F, Tiegs, R, Van Hul, W. 2006. Identification and molecular characterization of a novel splice-site mutation (G1205C) in the SQSTM1 gene causing Paget's disease of bone in an extended American family. *Calcif. Tissue Int.* 79: 281-88
- Beyens, G, Daroszewska, A, de Freitas, F, Franssen, E, Vanhoenacker, F et al. 2007. Identification of sex-specific associations between polymorphisms of the osteoprotegerin gene, TNFRSF11B, and Paget's disease of bone. *J Bone Miner. Res.* 22: 1062-71
- Bharti, AC, Aggarwal, BB. 2004. Ranking the role of RANK ligand in apoptosis. *Apoptosis* 9: 677-90
- Bignell, GR, Warren, W, Seal, S, Takahashi, M, Rapley, E et al. 2000. Identification of the familial cylindromatosis tumour-suppressor gene. *Nat. Genet.* 25: 160-65
- Bjorkoy, G, Lamark, T, Brech, A, Outzen, H, Perander, M et al. 2005. p62/SQSTM1 forms protein aggregates degraded by autophagy and has a protective effect on huntingtin-induced cell death. *J. Cell Biol.* 171: 603-14
- Bolland, MJ, Tong, PC, Naot, D, Callon, KE, Wattie, DJ et al. 2007. Delayed development of Paget's disease in offspring inheriting SQSTM1 mutations. *J Bone Miner. Res.* 22: 411-15
- Bonizzi, G, Karin, M. 2004. The two NF-kappaB activation pathways and their role in innate and adaptive immunity. *Trends Immunol.* 25: 280-88
- Boyle, WJ, Simonet, WS, Lacey, DL. 2003. Osteoclast differentiation and activation. *Nature* 423: 337-42
- Cavey, JR, Ralston, SH, Hocking, LJ, Sheppard, PW, Ciani, B et al. 2005. Loss of ubiquitin-binding associated with Paget's disease of bone p62 (SQSTM1) mutations. *J Bone Miner. Res.* 20: 619-24

- Cavey, JR, Ralston, SH, Sheppard, PW, Ciani, B, Gallagher, TR et al. 2006. Loss of ubiquitin binding is a unifying mechanism by which mutations of SQSTM1 cause Paget's disease of bone. *Calcif. Tissue Int.* 78: 271-77
- Cecconi, F, Levine, B. 2008. The role of autophagy in mammalian development: cell makeover rather than cell death. *Dev. Cell* 15: 344-57
- Chan, NL, Hill, CP. 2001. Defining polyubiquitin chain topology. *Nat. Struct. Biol.* 8: 650-52
- Chau, V, Tobias, JW, Bachmair, A, Marriott, D, Ecker, DJ et al. 1989. A multiubiquitin chain is confined to specific lysine in a targeted short-lived protein. *Science* 243: 1576-83
- Chen, ZJ. 2005. Ubiquitin signalling in the NF-kappaB pathway. *Nat. Cell Biol.* 7: 758-65
- Ciani, B, Layfield, R, Cavey, JR, Sheppard, PW, Searle, MS. 2003. Structure of the ubiquitin-associated domain of p62 (SQSTM1) and implications for mutations that cause Paget's disease of bone. *J. Biol. Chem.* 278: 37409-12
- Cody, JD, Singer, FR, Roodman, GD, Otterund, B, Lewis, TB et al. 1997. Genetic linkage of Paget disease of the bone to chromosome 18q. *Am. J Hum. Genet.* 61: 1117-22
- Collet, C, Michou, L, Audran, M, Chasseigneaux, S, Hilliquin, P et al. 2007. Paget's disease of bone in the French population: novel SQSTM1 mutations, functional analysis, and genotype-phenotype correlations. *J Bone Miner. Res.* 22: 310-17
- Cooper, C, Dennison, E, Schafheutle, K, Kellingray, S, Guyer, P, Barker, D. 1999. Epidemiology of Paget's disease of bone. *Bone* 24: 3S-5S
- Cooper, C, Harvey, NC, Dennison, EM, van Staa, TP. 2006. Update on the epidemiology of Paget's disease of bone. *J Bone Miner. Res.* 21 Suppl 2: 3-8
- Costes, SV, Daelemans, D, Cho, EH, Dobbin, Z, Pavlakis, G, Lockett, S. 2004. Automatic and quantitative measurement of protein-protein colocalization in live cells. *Biophys. J* 86: 3993-4003
- Courtois, G. 2008. Tumor suppressor CYLD: negative regulation of NF-kappaB signaling and more. *Cell Mol. Life Sci* 65: 1123-32
- Cuervo, AM. 2004. Autophagy: in sickness and in health. *Trends Cell Biol.* 14: 70-77
- Cundy, T, McAnulty, K, Wattie, D, Gamble, G, Rutland, M, Ibbertson, HK. 1997. Evidence for secular change in Paget's disease. *Bone* 20: 69-71
- Cundy, T. 2006. Is the prevalence of Paget's disease of bone decreasing? *J Bone Miner. Res.* 21 Suppl 2: 9-13
- Cundy, T, Bolland, M. 2008. Paget disease of bone. *Trends Endocrinol. Metab* 19: 246-53
- Dai, RM, Chen, E, Longo, DL, Gorbea, CM, Li, CC. 1998. Involvement of valosin-containing protein, an ATPase Co-purified with IkappaBalpha and 26 S

proteasome, in ubiquitin-proteasome-mediated degradation of IkappaBalpha. *J Biol.Chem.* 273: 3562-73

Daroszewska,A, Hocking,LJ, McGuigan,FE, Langdahl,B, Stone,MD et al. 2004. Susceptibility to Paget's disease of bone is influenced by a common polymorphic variant of osteoprotegerin. *J Bone Miner.Res.* 19: 1506-11

Daroszewska,A, Ralston,SH. 2005. Genetics of Paget's disease of bone. *Clin.Sci.* 109: 257-63

Deng,L, Wang,C, Spencer,E, Yang,L, Braun,A et al. 2000. Activation of the IkappaB kinase complex by TRAF6 requires a dimeric ubiquitin-conjugating enzyme complex and a unique polyubiquitin chain. *Cell* 103: 351-61

Ding,WX, Ni,HM, Gao,W, Yoshimori,T, Stolz,DB et al. 2007. Linking of autophagy to ubiquitin-proteasome system is important for the regulation of endoplasmic reticulum stress and cell viability. *Am.J Pathol.* 171: 513-24

Doherty,FJ, Dawson,S, Mayer,RJ. 2002. The ubiquitin-proteasome pathway of intracellular proteolysis. *Essays Biochem.* 38: 51-63

Duran,A, Serrano,M, Leitges,M, Flores,JM, Picard,S et al. 2004. The atypical PKC-interacting protein p62 is an important mediator of RANK-activated osteoclastogenesis. *Dev.Cell* 6: 303-09

Eekhoff,EW, Karperien,M, Houtsma,D, Zwinderman,AH, Dragoiescu,C et al. 2004. Familial Paget's disease in The Netherlands: occurrence, identification of new mutations in the sequestosome 1 gene, and their clinical associations. *Arthritis Rheum.* 50: 1650-54

Elmore,SP, Qian,T, Grissom,SF, Lemasters,JJ. 2001. The mitochondrial permeability transition initiates autophagy in rat hepatocytes. *FASEB J* 15: 2286-87

Erickson,SL, de Sauvage,FJ, Kikly,K, Carver-Moore,K, Pitts-Meek,S et al. 1994. Decreased sensitivity to tumour-necrosis factor but normal T-cell development in TNF receptor-2-deficient mice. *Nature* 372: 560-63

Falchetti,A, Di Stefano,M, Marini,F, Del Monte,F, Mavilia,C et al. 2004. Two novel mutations at exon 8 of the Sequestosome 1 (SQSTM1) gene in an Italian series of patients affected by Paget's disease of bone (PDB). *J.Bone Miner.Res.* 19: 1013-17

Falchetti,A, Di Stefano,M, Marini,F, Ortolani,S, Olivieri,MF et al. 2009. Genetic epidemiology of Paget's disease of bone in Italy: sequestosome1/p62 gene mutational test and haplotype analysis at 5q35 in a large representative series of sporadic and familial Italian cases of Paget's disease of bone. *Calcif.Tissue Int.* 84: 20-37

Farley,JR, Hall,SL, Tanner,MA, Wergedal,JE. 1994. Specific activity of skeletal alkaline phosphatase in human osteoblast-line cells regulated by phosphate, phosphate esters, and phosphate analogs and release of alkaline phosphatase activity inversely regulated by calcium. *J Bone Miner.Res.* 9: 497-508

Fenner,BJ, Scannell,M, Prehn,JH. 2009. Identification of polyubiquitin binding proteins involved in NF-kappaB signaling using protein arrays. *Biochim.Biophys.Acta* 1794: 1010-16

- Filimonenko,M, Stuffers,S, Raiborg,C, Yamamoto,A, Malerod,L et al. 2007. Functional multivesicular bodies are required for autophagic clearance of protein aggregates associated with neurodegenerative disease. *J.Cell Biol.* 179: 485-500
- Fotino,M, Haymovits,A, Falk,CT. 1977. Evidence for linkage between HLA and Paget's disease. *Transplant.Proc.* 9: 1867-68
- Franzoso,G, Carlson,L, Xing,L, Poljak,L, Shores,EW et al. 1997. Requirement for NF-kappaB in osteoclast and B-cell development. *Genes Dev.* 11: 3482-96
- French,AP, Mills,S, Swarup,R, Bennett,MJ, Pridmore,TP. 2008. Colocalization of fluorescent markers in confocal microscope images of plant cells. *Nat.Protoc.* 3: 619-28
- FRIEDRICH,WE, REDDY,SV, BRUDER,JM, CUNDY,TIM, CORNISH,JILL et al. 2002. Sequence Analysis of Measles Virus Nucleocapsid Transcripts in Patients with Paget's Disease. *Journal of Bone and Mineral Research* 17: 145-51
- Fukunaga,M, Sone,T. 2001. [Bone metabolic markers and diagnosis of abnormal bone and calcium metabolism]. *Clin.Calcium* 11: 856-62
- Galan,JM, Haguenaer-Tsapis,R. 1997. Ubiquitin lys63 is involved in ubiquitination of a yeast plasma membrane protein. *EMBO J* 16: 5847-54
- Galibert,L, Tometsko,ME, Anderson,DM, Cosman,D, Dougall,WC. 1998. The involvement of multiple tumor necrosis factor receptor (TNFR)-associated factors in the signaling mechanisms of receptor activator of NF-kappaB, a member of the TNFR superfamily. *J Biol.Chem.* 273: 34120-27
- Gardner,MJ, Guyer,PB, Barker,DJ. 1978. Radiological prevalence of Paget's disease of bone in British migrants to Australia. *Br.Med.J* 1: 1655-57
- Geetha,T, Wooten,MW. 2002. Structure and functional properties of the ubiquitin binding protein p62. *FEBS Lett.* 512: 19-24
- Gennari,L, Merlotti,D, Martini,G, Nuti,R. 2006. Paget's disease of bone in Italy. *J Bone Miner.Res.* 21 Suppl 2: 14-21
- Gherardi,G, Lo,C, V, Bonucci,E. 1980. Fine structure of nuclei and cytoplasm of osteoclasts in Paget's disease of bone. *Histopathology* 4: 63-74
- Ghosh,S, Karin,M. 2002. Missing pieces in the NF-kappaB puzzle. *Cell* 109 Suppl: S81-S96
- Good,DA, Busfield,F, Fletcher,BH, Duffy,DL, Kesting,JB et al. 2002. Linkage of Paget disease of bone to a novel region on human chromosome 18q23. *Am.J Hum.Genet.* 70: 517-25
- Good,DA, Busfield,F, Fletcher,BH, Lovelock,PK, Duffy,DL et al. 2004. Identification of SQSTM1 mutations in familial Paget's disease in Australian pedigrees. *Bone* 35: 277-82
- Goode,A, Layfield,R. 2009. Recent advances in understanding the molecular basis of Paget's disease of bone. *J Clin Pathol*

- Gozuacik,D, Kimchi,A. 2004. Autophagy as a cell death and tumor suppressor mechanism. *Oncogene* 23: 2891-906
- Haglund,K, Di Fiore,PP, Dikic,I. 2003. Distinct monoubiquitin signals in receptor endocytosis. *Trends Biochem.Sci* 28: 598-603
- Haglund,K, Dikic,I. 2005. Ubiquitylation and cell signaling. *EMBO J* 24: 3353-59
- Harinck,HI, Bijvoet,OL, Vellenga,CJ, Blanksma,HJ, Frijlink,WB. 1986. Relation between signs and symptoms in Paget's disease of bone. *Q.J Med.* 58: 133-51
- Harris,H. 1990. The human alkaline phosphatases: what we know and what we don't know. *Clin.Chim.Acta* 186: 133-50
- Harvey,L, Gray,T, Beneton,MN, Douglas,DL, Kanis,JA, Russell,RG. 1982. Ultrastructural features of the osteoclasts from Paget's disease of bone in relation to a viral aetiology. *J Clin Pathol* 35: 771-79
- Haslam,SI, Van Hul,W, Morales-Piga,A, Balemans,W, San Millan,JL et al. 1998. Paget's disease of bone: evidence for a susceptibility locus on chromosome 18q and for genetic heterogeneity. *J Bone Miner.Res.* 13: 911-17
- Helfrich,MH, Hobson,RP, Grabowski,PS, Zurbriggen,A, Cosby,SL et al. 2000. A negative search for a paramyxoviral etiology of Paget's disease of bone: molecular, immunological, and ultrastructural studies in UK patients. *J Bone Miner.Res.* 15: 2315-29
- Helfrich,MH, Hocking,LJ. 2008. Genetics and aetiology of Pagetic disorders of bone. *Arch.Biochem.Biophys.* 473: 172-82
- Hershko,A, Ciechanover,A. 1998. The ubiquitin system. *Annu.Rev Biochem.* 67: 425-79
- Hiruma,Y, Kurihara,N, Subler,MA, Zhou,H, Boykin,CS et al. 2008. A SQSTM1/p62 mutation linked to Paget's disease increases the osteoclastogenic potential of the bone microenvironment. *Hum.Mol.Genet.* 17: 3708-19
- Hocking,LJ, Herbert,CA, Nicholls,RK, Williams,F, Bennett,ST et al. 2001. Genomewide search in familial Paget disease of bone shows evidence of genetic heterogeneity with candidate loci on chromosomes 2q36, 10p13, and 5q35. *Am.J Hum.Genet.* 69: 1055-61
- Hocking,LJ, Lucas,GJ, Daroszewska,A, Mangion,J, Olavesen,M et al. 2002. Domain-specific mutations in sequestosome 1 (SQSTM1) cause familial and sporadic Paget's disease. *Hum.Mol Genet.* 11: 2735-39
- Hocking,LJ, Lucas,GJ, Daroszewska,A, Cundy,T, Nicholson,GC et al. 2004. Novel UBA domain mutations of SQSTM1 in Paget's disease of bone: genotype phenotype correlation, functional analysis, and structural consequences. *J Bone Miner.Res.* 19: 1122-27
- Hoffman,L, Rechsteiner,M. 1996. Nucleotidase activities of the 26 S proteasome and its regulatory complex. *J Biol.Chem.* 271: 32538-45

- Hosking,D, Lyles,K, Brown,JP, Fraser,WD, Miller,P et al. 2007. Long-Term Control of Bone Turnover in Paget's Disease With Zoledronic Acid and Risedronate. *Journal of Bone and Mineral Research* 22: 142-48
- Hubbers,CU, Clemen,CS, Kesper,K, Boddich,A, Hofmann,A et al. 2007. Pathological consequences of VCP mutations on human striated muscle. *Brain* 130: 381-93
- Hughes,AE, Shearman,AM, Weber,JL, Barr,RJ, Wallace,RG et al. 1994. Genetic linkage of familial expansile osteolysis to chromosome 18q. *Hum.Mol.Genet.* 3: 359-61
- Hughes,AE, Ralston,SH, Marken,J, Bell,C, MacPherson,H et al. 2000. Mutations in TNFRSF11A, affecting the signal peptide of RANK, cause familial expansile osteolysis. *Nat Genet.* 24: 45-48
- Huvos,AG. 1986. Osteogenic sarcoma of bones and soft tissues in older persons. A clinicopathologic analysis of 117 patients older than 60 years. *Cancer* 57: 1442-49
- Ichimura,Y, Kominami,E, Tanaka,K, Komatsu,M. 2008. Selective turnover of p62/A170/SQSTM1 by autophagy. *Autophagy.* 4: 1063-66
- Iotsova,V, Caamano,J, Loy,J, Yang,Y, Lewin,A, Bravo,R. 1997. Osteopetrosis in mice lacking NF-kappaB1 and NF-kappaB2. *Nat.Med.* 3: 1285-89
- Ishii,T, Yanagawa,T, Kawane,T, Yuki,K, Seita,J et al. 1996. Murine peritoneal macrophages induce a novel 60-kDa protein with structural similarity to a tyrosine kinase p56lck-associated protein in response to oxidative stress. *Biochem.Biophys.Res.Comm.* 226: 456-60
- Iwata,J, Ezaki,J, Komatsu,M, Yokota,S, Ueno,T et al. 2006. Excess peroxisomes are degraded by autophagic machinery in mammals. *J Biol.Chem.* 281: 4035-41
- Jimi,E, Aoki,K, Saito,H, D'Acquisto,F, May,MJ et al. 2004. Selective inhibition of NF-kappa B blocks osteoclastogenesis and prevents inflammatory bone destruction in vivo. *Nat.Med.* 10: 617-24
- Jin,DY, Giordano,V, Kibler,KV, Nakano,H, Jeang,KT. 1999. Role of adapter function in oncoprotein-mediated activation of NF-kappaB. Human T-cell leukemia virus type I Tax interacts directly with IkappaB kinase gamma. *J Biol.Chem.* 274: 17402-05
- Jin,W, Chang,M, Paul,EM, Babu,G, Lee,AJ et al. 2008. Deubiquitinating enzyme CYLD negatively regulates RANK signaling and osteoclastogenesis in mice. *J Clin.Invest* 118: 1858-66
- Johnson-Pais,TL, Wisdom,JH, Weldon,KS, Cody,JD, Hansen,MF et al. 2003. Three novel mutations in SQSTM1 identified in familial Paget's disease of bone. *J Bone Miner.Res.* 18: 1748-53
- Johnson,ES, Ma,PC, Ota,IM, Varshavsky,A. 1995. A proteolytic pathway that recognizes ubiquitin as a degradation signal. *J Biol Chem.* 270: 17442-56
- Jono,H, Lim,JH, Chen,LF, Xu,H, Trompouki,E et al. 2004. NF-kappaB is essential for induction of CYLD, the negative regulator of NF-kappaB: evidence

for a novel inducible autoregulatory feedback pathway. *J Biol.Chem.* 279: 36171-74

Joshi,SR, Ambhore,S, Butala,N, Patwardhan,M, Kulkarni,M et al. 2006. Paget's disease from Western India. *J Assoc.Physicians India* 54: 535-38

Joung,I, Strominger,JL, Shin,J. 1996. Molecular cloning of a phosphotyrosine-independent ligand of the p56lck SH2 domain. *Proc.Natl.Acad.Sci.U.S.A* 93: 5991-95

Kabeya,Y, Mizushima,N, Ueno,T, Yamamoto,A, Kirisako,T et al. 2000. LC3, a mammalian homologue of yeast Apg8p, is localized in autophagosome membranes after processing. *EMBO J* 19: 5720-28

Karin,M, Greten,FR. 2005. NF-kappaB: linking inflammation and immunity to cancer development and progression. *Nat.Rev.Immunol.* 5: 749-59

Khosla,S. 2001. Minireview: the OPG/RANKL/RANK system. *Endocrinology* 142: 5050-55

Kirkin,V, McEwan,DG, Novak,I, Dikic,I. 2009. A role for ubiquitin in selective autophagy. *Mol.Cell* 34: 259-69

Kitamura,H, Torigoe,T, Asanuma,H, Hisasue,SI, Suzuki,K et al. 2006. Cytosolic overexpression of p62 sequestosome 1 in neoplastic prostate tissue. *Histopathology* 48: 157-61

Komatsu,M, Waguri,S, Koike,M, Sou,YS, Ueno,T et al. 2007. Homeostatic levels of p62 control cytoplasmic inclusion body formation in autophagy-deficient mice. *Cell* 131: 1149-63

Kong,YY, Yoshida,H, Sarosi,I, Tan,HL, Timms,E et al. 1999. OPGL is a key regulator of osteoclastogenesis, lymphocyte development and lymph-node organogenesis. *Nature* 397: 315-23

Korolchuk,VI, Mansilla,A, Menzies,FM, Rubinsztein,DC. 2009. Autophagy inhibition compromises degradation of ubiquitin-proteasome pathway substrates. *Mol.Cell* 33: 517-27

Kovalenko,A, Chable-Bessia,C, Cantarella,G, Israel,A, Wallach,D, Courtois,G. 2003. The tumour suppressor CYLD negatively regulates NF-kappaB signalling by deubiquitination. *Nature* 424: 801-05

Kroemer,G, Jaattela,M. 2005. Lysosomes and autophagy in cell death control. *Nat.Rev.Cancer* 5: 886-97

Kurihara,N, Reddy,SV, Mena,C, Anderson,D, Roodman,GD. 2000. Osteoclasts expressing the measles virus nucleocapsid gene display a pagetic phenotype. *J Clin.Invest* 105: 607-14

Kurihara,N, Zhou,H, Reddy,SV, Garcia,P, V, Subler,MA et al. 2006. Expression of measles virus nucleocapsid protein in osteoclasts induces Paget's disease-like bone lesions in mice. *J Bone Miner.Res.* 21: 446-55

Kurihara,N, Hiruma,Y, Zhou,H, Subler,MA, Dempster,DW et al. 2007. Mutation of the sequestosome 1 (p62) gene increases osteoclastogenesis but does not induce Paget disease. *J Clin.Invest* 117: 133-42

- Kuroiwa,T, Kawano,S, Nishibayashi,S, Sato,C. 1982. Epifluorescent microscopic evidence for maternal inheritance of chloroplast DNA. *Nature* 298: 481-83
- Kuusisto,E, Salminen,A, Alafuzoff,I. 2001. Ubiquitin-binding protein p62 is present in neuronal and glial inclusions in human tauopathies and synucleinopathies. *Neuroreport* 12: 2085-90
- Kuusisto,E, Salminen,A, Alafuzoff,I. 2002. Early accumulation of p62 in neurofibrillary tangles in Alzheimer's disease: possible role in tangle formation. *Neuropathol.Appl.Neurobiol.* 28: 228-37
- Lallena,MJ, Diaz-Meco,MT, Bren,G, Paya,CV, Moscat,J. 1999. Activation of Ikappa B Kinase beta áby Protein Kinase C Isoforms. *Mol.Cell.Biol.* 19: 2180-88
- Lamark,T, Perander,M, Outzen,H, Kristiansen,K, Overvatn,A et al. 2003. Interaction codes within the family of mammalian Phox and Bem1p domain-containing proteins. *J Biol.Chem.* 278: 34568-81
- Langston,AL, Campbell,MK, Fraser,WD, Maclennan,GS, Selby,PL, Ralston,SH. 2009. Randomised Trial of Intensive Bisphosphonate Treatment Versus Symptomatic Management in Paget's Disease of Bone. *J Bone Miner.Res.*
- Laurin,N, Brown,JP, Lemainque,A, Duchesne,A, Huot,D et al. 2001. Paget disease of bone: mapping of two loci at 5q35-qter and 5q31. *Am.J Hum.Genet.* 69: 528-43
- Laurin,N, Brown,JP, Morissette,J, Raymond,V. 2002. Recurrent mutation of the gene encoding sequestosome 1 (SQSTM1/p62) in Paget disease of bone. *Am.J.Hum.Genet.* 70: 1582-88
- Layfield,R, Cavey,JR, Lowe,J. 2003. Role of ubiquitin-mediated proteolysis in the pathogenesis of neurodegenerative disorders. *Ageing Res.Rev.* 2: 343-56
- Layfield,R, Ciani,B, Ralston,SH, Hocking,LJ, Sheppard,PW et al. 2004. Structural and functional studies of mutations affecting the UBA domain of SQSTM1 (p62) which cause Paget's disease of bone. *Biochem.Soc.Trans.* 32: 728-30
- Layfield(a),R, Hocking,LJ. 2004. SQSTM1 and Paget's disease of bone. *Calcif.Tissue Int.* 75: 347-57
- Layfield,R, Cavey,JR, Najat,D, Long,J, Sheppard,PW et al. 2006. p62 mutations, ubiquitin recognition and Paget's disease of bone. *Biochem.Soc.Trans.* 34: 735-37
- Leach,RJ, Singer,FR, Ench,Y, Wisdom,JH, Pina,DS, Johnson-Pais,TL. 2006. Clinical and cellular phenotypes associated with sequestosome 1 (SQSTM1) mutations. *J Bone Miner.Res.* 21 Suppl 2: 45-50
- Lemasters,JJ. 2005. Selective mitochondrial autophagy, or mitophagy, as a targeted defense against oxidative stress, mitochondrial dysfunction, and aging. *Rejuvenation.Res.* 8: 3-5

- Lenkinski,RE, Chen,DM, Glickson,JD, Goldstein,G. 1977. Nuclear magnetic resonance studies of the denaturation of ubiquitin. *Biochimica et Biophysica Acta (BBA) - Protein Structure* 494: 126-30
- Leung,KS, Fung,KP, Liu,PPL, Lee,KM. 1995. Bone-specific alkaline phosphatase activities in plasma and callus during callotaxis in rabbits. *Life Sciences* 57: 637-43
- Lever,JH. 2002. Paget's disease of bone in Lancashire and arsenic pesticide in cotton mill wastewater: a speculative hypothesis. *Bone* 31: 434-36
- Levine,B, Yuan,J. 2005. Autophagy in cell death: an innocent convict? *J Clin.Invest* 115: 2679-88
- Li,D. 2006. Selective degradation of the IkappaB kinase (IKK) by autophagy. *Cell Res.* 16: 855-56
- Li,Q, Verma,IM. 2002. NF-kappaB regulation in the immune system. *Nat Rev Immunol.* 2: 725-34
- Long,J, Gallagher,TR, Cavey,JR, Sheppard,PW, Ralston,SH et al. 2008. Ubiquitin recognition by the ubiquitin-associated domain of p62 involves a novel conformational switch. *J Biol.Chem.* 283: 5427-40
- Lopez-Abente,G, Morales-Piga,A, Bachiller-Corral,FJ, Illera-Martin,O, Martin-Domenech,R, Abraira,V. 2003. Identification of possible areas of high prevalence of Paget's disease of bone in Spain. *Clin.Exp.Rheumatol.* 21: 635-38
- Lucas,GJ, Hocking,LJ, Daroszewska,A, Cundy,T, Nicholson,GC et al. 2005. Ubiquitin-associated domain mutations of SQSTM1 in Paget's disease of bone: evidence for a founder effect in patients of British descent. *J Bone Miner.Res.* 20: 227-31
- Lucas,GJ, Riches,PL, Hocking,LJ, Cundy,T, Nicholson,GC et al. 2008. Identification of a major locus for Paget's disease on chromosome 10p13 in families of British descent. *J Bone Miner.Res.* 23: 58-63
- Maiuri,MC, Zalckvar,E, Kimchi,A, Kroemer,G. 2007. Self-eating and self-killing: crosstalk between autophagy and apoptosis. *Nat Rev Mol Cell Biol* 8: 741-52
- Martin,P, Diaz-Meco,MT, Moscat,J. 2006. The signaling adapter p62 is an important mediator of T helper 2 cell function and allergic airway inflammation. *EMBO J* 25: 3524-33
- Matthews,BG, Afzal,MA, Minor,PD, Bava,U, Callon,KE et al. 2008. Failure to detect measles virus ribonucleic acid in bone cells from patients with Paget's disease. *J Clin.Endocrinol.Metab* 93: 1398-401
- Menaa,C, Devlin,RD, Reddy,SV, Gazitt,Y, Choi,SJ, Roodman,GD. 1999. Annexin II increases osteoclast formation by stimulating the proliferation of osteoclast precursors in human marrow cultures. *J Clin.Invest* 103: 1605-13
- Menaa,C, Reddy,SV, Kurihara,N, Maeda,H, Anderson,D et al. 2000. Enhanced RANK ligand expression and responsivity of bone marrow cells in Paget's disease of bone. *J Clin.Invest* 105: 1833-38

- Michou,L, Collet,C, Laplanche,JL, Orcel,P, Cornelis,F. 2006. Genetics of Paget's disease of bone. *Joint Bone Spine* 73: 243-48
- Miller,PD, Brown,JP, Siris,ES, Hoseyni,MS, Axelrod,DW, Bekker,PJ. 1999. A randomized, double-blind comparison of risedronate and etidronate in the treatment of Paget's disease of bone. Paget's Risedronate/Etidronate Study Group. *Am.J Med.* 106: 513-20
- Mills,BG, Singer,FR. 1976. Nuclear inclusions in Paget's disease of bone. *Science* 194: 201-02
- Mills,BG, Yabe,H, Singer,FR. 1988. Osteoclasts in human osteopetrosis contain viral-nucleocapsid-like nuclear inclusions. *J Bone Miner.Res.* 3: 101-06
- Mizushima,N, Yamamoto,A, Matsui,M, Yoshimori,T, Ohsumi,Y. 2004. In vivo analysis of autophagy in response to nutrient starvation using transgenic mice expressing a fluorescent autophagosome marker. *Mol Biol Cell* 15: 1101-11
- Mizushima,N. 2007. Autophagy: process and function. *Genes Dev.* 21: 2861-73
- Morales-Piga,AA, Rey-Rey,JS, Corres-Gonzalez,J, Garcia-Sagredo,JM, Lopez-Abente,G. 1995. Frequency and characteristics of familial aggregation of Paget's disease of bone. *J Bone Miner.Res.* 10: 663-70
- Morales-Piga,AA, Bachiller-Corral,FJ, Abraira,V, Beltran,J, Rapado,A. 2002. Is clinical expressiveness of Paget's disease of bone decreasing? *Bone* 30: 399-403
- Morissette,J, Laurin,N, Brown,JP. 2006. Sequestosome 1: mutation frequencies, haplotypes, and phenotypes in familial Paget's disease of bone. *J Bone Miner.Res.* 21 Suppl 2: 38-44
- Moscat,J, Diaz-Meco,MT. 2002. The atypical PKC scaffold protein P62 is a novel target for anti-inflammatory and anti-cancer therapies. *Adv.Enzyme Regul.* 42: 173-79
- Mundy,GR. 1999. Cellular and molecular regulation of bone turnover. *Bone* 24: 35S-8S
- Nagaoka,U, Kim,K, Jana,NR, Doi,H, Maruyama,M et al. 2004. Increased expression of p62 in expanded polyglutamine-expressing cells and its association with polyglutamine inclusions. *J Neurochem.* 91: 57-68
- Najat,D, Garner,T, Hagen,T, Shaw,B, Sheppard,PW et al. 2009. Characterization of a non-UBA domain missense mutation of sequestosome 1 (SQSTM1) in Paget's disease of bone. *J Bone Miner.Res.* 24: 632-42
- Naot,D, Bava,U, Matthews,B, Callon,KE, Gamble,GD et al. 2007. Differential Gene Expression in Cultured Osteoblasts and Bone Marrow Stromal Cells From Patients With Paget's Disease of Bone. *Journal of Bone and Mineral Research* 22: 298-309
- O'Driscoll,JB, Anderson,DC. 1985. Past pets and Paget's disease. *Lancet* 2: 919-21

- Okazaki,M, Ito,S, Kawakita,K, Takeshita,S, Kawai,S et al. 1999. Cloning, Expression Profile, and Genomic Organization of the Mouse STAP/A170 Gene. *Genomics* 60: 87-95
- Paine,MG, Babu,JR, Seibenhener,ML, Wooten,MW. 2005. Evidence for p62 aggregate formation: role in cell survival. *FEBS Lett.* 579: 5029-34
- Pankiv,S, Clausen,TH, Lamark,T, Brech,A, Bruun,JA et al. 2007. p62/SQSTM1 binds directly to Atg8/LC3 to facilitate degradation of ubiquitinated protein aggregates by autophagy. *J Biol.Chem.* 282: 24131-45
- Park,I, Chung,J, Walsh,CT, Yun,Y, Strominger,JL, Shin,J. 1995. Phosphotyrosine-independent binding of a 62-kDa protein to the src homology 2 (SH2) domain of p56lck and its regulation by phosphorylation of Ser-59 in the lck unique N-terminal region. *Proc.Natl.Acad.Sci.U.S.A* 92: 12338-42
- Pfeilschifter,J, Chenu,C, Bird,A, Mundy,GR, Roodman,GD. 1989. Interleukin-1 and tumor necrosis factor stimulate the formation of human osteoclastlike cells in vitro. *J Bone Miner.Res.* 4: 113-18
- Ponting,CP, Blake,DJ, Davies,KE, Kendrick-Jones,J, Winder,SJ. 1996. ZZ and TAZ: new putative zinc fingers in dystrophin and other proteins. *Trends Biochem.Sci* 21: 11-13
- Prajapati,S, Gaynor,RB. 2002. Regulation of Ikappa B kinase (IKK)gamma /NEMO function by IKKbeta -mediated phosphorylation. *J Biol.Chem.* 277: 24331-39
- Puls,A, Schmidt,S, Grawe,F, Stabel,S. 1997. Interaction of protein kinase C zeta with ZIP, a novel protein kinase C-binding protein. *Proc.Natl Acad.Sci U.S.A* 94: 6191-96
- Qing,G, Yan,P, Xiao,G. 2006. Hsp90 inhibition results in autophagy-mediated proteasome-independent degradation of IkappaB kinase (IKK). *Cell Res.* 16: 895-901
- Rahighi,S, Ikeda,F, Kawasaki,M, Akutsu,M, Suzuki,N et al. 2009. Specific recognition of linear ubiquitin chains by NEMO is important for NF-kappaB activation. *Cell* 136: 1098-109
- Ralston,SH, Digiovine,FS, Gallacher,SJ, Boyle,IT, Duff,GW. 1991. Failure to detect paramyxovirus sequences in Paget's disease of bone using the polymerase chain reaction. *J Bone Miner.Res.* 6: 1243-48
- Ralston,SH. 1993. Paget's disease of bone. *BMJ* 306: 332-33
- Ralston,SH, Afzal,MA, Helfrich,MH, Fraser,WD, Gallagher,JA et al. 2007. Multicenter blinded analysis of RT-PCR detection methods for paramyxoviruses in relation to Paget's disease of bone. *J Bone Miner.Res.* 22: 569-77
- Ralston(a),SH, Langston,AL, Reid,IR. 2008. Pathogenesis and management of Paget's disease of bone. *Lancet* 372: 155-63
- Ralston(b),SH. 2008. Juvenile Paget's disease, familial expansile osteolysis and other genetic osteolytic disorders. *Best.Pract.Res.Clin.Rheumatol.* 22: 101-11

- Ralston,SH. 2008. Pathogenesis of Paget's disease of bone. *Bone* 43: 819-25
- Ravikumar,B, Futter,M, Jahreiss,L, Korolchuk,VI, Lichtenberg,M et al. 2009. Mammalian macroautophagy at a glance. *J Cell Sci* 122: 1707-11
- Rea,SL, Walsh,JP, Ward,L, Yip,K, Ward,BK et al. 2006. A novel mutation (K378X) in the sequestosome 1 gene associated with increased NF-kappaB signaling and Paget's disease of bone with a severe phenotype. *J Bone Miner.Res.* 21: 1136-45
- Rea,SL, Walsh,JP, Ward,L, Magno,AL, Ward,BK et al. 2009. Sequestosome 1 mutations in Paget's disease of bone in Australia: prevalence, genotype/phenotype correlation, and a novel non-UBA domain mutation (P364S) associated with increased NF-kappaB signaling without loss of ubiquitin binding. *J Bone Miner.Res.* 24: 1216-23
- Rechsteiner,M, Rogers,SW. 1996. PEST sequences and regulation by proteolysis. *Trends Biochem.Sci* 21: 267-71
- Reddy(a),SV, Menaa,C, Singer,FR, Cundy,T, Cornish,J et al. 1999. Measles virus nucleocapsid transcript expression is not restricted to the osteoclast lineage in patients with Paget's disease of bone. *Exp.Hematol.* 27: 1528-32
- Reddy,SV, Menaa,C, Singer,FR, Demulder,A, Roodman,GD. 1999. Cell biology of Paget's disease. *J Bone Miner.Res.* 14 Suppl 2: 3-8
- Reddy,SV, Kurihara,N, Menaa,C, Roodman,GD. 2001. Paget's disease of bone: a disease of the osteoclast. *Rev.Endocr.Metab Disord.* 2: 195-201
- Reid,IR, Miller,P, Lyles,K, Fraser,W, Brown,JP et al. 2005. Comparison of a single infusion of zoledronic acid with risedronate for Paget's disease. *N.Engl.J Med.* 353: 898-908
- Rhodes,EC, Johnson-Pais,TL, Singer,FR, Ankerst,DP, Bruder,JM et al. 2008. Sequestosome 1 (SQSTM1) mutations in Paget's disease of bone from the United States. *Calcif.Tissue Int.* 82: 271-77
- Rodriguez,A, Duran,A, Selloum,M, Champy,MF, Diez-Guerra,FJ et al. 2006. Mature-onset obesity and insulin resistance in mice deficient in the signaling adapter p62. *Cell Metab* 3: 211-22
- Roodman,GD, Kurihara,N, Ohsaki,Y, Kukita,A, Hosking,D et al. 1992. Interleukin 6. A potential autocrine/paracrine factor in Paget's disease of bone. *J Clin.Invest* 89: 46-52
- Roodman,GD. 1996. Advances in bone biology: the osteoclast. *Endocr.Rev.* 17: 308-32
- Roodman,GD. 1998. Osteoclast differentiation and activity. *Biochem.Soc.Trans.* 26: 7-13
- Roodman,GD, Windle,JJ. 2005. Paget disease of bone. *J Clin.Invest* 115: 200-08
- Sanz,L, Sanchez,P, Lallena,MJ, Diaz-Meco,MT, Moscat,J. 1999. The interaction of p62 with RIP links the atypical PKCs to NF-kappaB activation. *EMBO J.* 18: 3044-53

- Sanz,L, Diaz-Meco,MT, Nakano,H, Moscat,J. 2000. The atypical PKC-interacting protein p62 channels NF-kappaB activation by the IL-1-TRAF6 pathway. *EMBO J* 19: 1576-86
- Scheidereit,C. 2006. IkappaB kinase complexes: gateways to NF-kappaB activation and transcription. *Oncogene* 25: 6685-705
- SCHLESINGER,DH, GOLDSTEIN,GIDE. 1975. Molecular conservation of 74 amino acid sequence of ubiquitin between cattle and man. *Nature* 255: 423-24
- Schneider,D, Hofmann,MT, Peterson,JA. 2002. Diagnosis and treatment of Paget's disease of bone. *Am.Fam.Physician* 65: 2069-72
- Sebban-Benin,H, Pescatore,A, Fusco,F, Pascuale,V, Gautheron,J et al. 2007. Identification of TRAF6-dependent NEMO polyubiquitination sites through analysis of a new NEMO mutation causing incontinentia pigmenti. *Hum.Mol.Genet.* 16: 2805-15
- Seibenhener,ML, Babu,JR, Geetha,T, Wong,HC, Krishna,NR, Wooten,MW. 2004. Sequestosome 1/p62 Is a Polyubiquitin Chain Binding Protein Involved in Ubiquitin Proteasome Degradation. *Mol.Cell.Biol.* 24: 8055-68
- Selby,PL, Davie,MW, Ralston,SH, Stone,MD. 2002. Guidelines on the management of Paget's disease of bone. *Bone* 31: 366-73
- Selby,PL, Davies,M, Mee,AP. 2006. Canine distemper virus induces human osteoclastogenesis through NF-kappaB and sequestosome 1/P62 activation. *J Bone Miner.Res.* 21: 1750-56
- Shankar,S, Hosking,DJ. 2006. Biochemical assessment of Paget's disease of bone. *J Bone Miner.Res.* 21 Suppl 2: 22-27
- Shin,J. 1998. P62 and the sequestosome, a novel mechanism for protein metabolism. *Archives of Pharmacal Research* 21: 629-33
- Shvets,E, Fass,E, Scherz-Shouval,R, Elazar,Z. 2008. The N-terminus and Phe52 residue of LC3 recruit p62/SQSTM1 into autophagosomes. *J Cell Sci* 121: 2685-95
- Simonet,WS, Lacey,DL, Dunstan,CR, Kelley,M, Chang,MS et al. 1997. Osteoprotegerin: a novel secreted protein involved in the regulation of bone density. *Cell* 89: 309-19
- Siris,ES, Ottman,R, Flaster,E, Kelsey,JL. 1991. Familial aggregation of Paget's disease of bone. *J Bone Miner.Res.* 6: 495-500
- Sofaer,JA, Holloway,SM, Emery,AE. 1983. A family study of Paget's disease of bone. *J Epidemiol.Community Health* 37: 226-31
- Suzuki,T, Kawano,S, Sakai,A, Fujie,M, Kuroiwa,H et al. 1992. Preferential mitochondrial and plastid DNA synthesis before multiple cell divisions in *Nicotiana tabacum*. *J Cell Sci* 103: 831-37
- Suzuki,T, Fujikura,K, Higashiyama,T, Takata,K. 1997. DNA Staining for Fluorescence and Laser Confocal Microscopy. *J.Histochem.Cytochem.* 45: 49-54

- Takata,S, Hashimoto,J, Nakatsuka,K, Yoshimura,N, Yoh,K et al. 2006. Guidelines for diagnosis and management of Paget's disease of bone in Japan. *J Bone Miner.Metab* 24: 359-67
- Taylor,MP, Jackson,WT. 2009. Viruses and arrested autophagosome development. *Autophagy*. 5: 870-71
- Thompson,HG, Harris,JW, Wold,BJ, Lin,F, Brody,JP. 2003. p62 overexpression in breast tumors and regulation by prostate-derived Ets factor in breast cancer cells. *Oncogene* 22: 2322-33
- Thrower,JS, Hoffman,L, Rechsteiner,M, Pickart,CM. 2000. Recognition of the polyubiquitin proteolytic signal. *EMBO J* 19: 94-102
- Tilyard,MW, Gardner,RJ, Milligan,L, Cleary,TA, Stewart,RD. 1982. A probable linkage between familial Paget's disease and the HLA loci. *Aust.N.Z.J Med*. 12: 498-500
- Trompouki,E, Hatzivassiliou,E, Tschritzis,T, Farmer,H, Ashworth,A, Mosialos,G. 2003. CYLD is a deubiquitinating enzyme that negatively regulates NF-kappaB activation by TNFR family members. *Nature* 424: 793-96
- Vadlamudi,RK, Joung,I, Strominger,JL, Shin,J. 1996. p62, a phosphotyrosine-independent ligand of the SH2 domain of p56lck, belongs to a new class of ubiquitin-binding proteins. *J.Biol.Chem*. 271: 20235-37
- Vadlamudi,RK, Shin,J. 1998. Genomic structure and promoter analysis of the p62 gene encoding a non-proteasomal multiubiquitin chain binding protein. *FEBS Lett*. 435: 138-42
- van Staa,TP, Selby,P, Leufkens,HG, Lyles,K, Sprafka,JM, Cooper,C. 2002. Incidence and natural history of Paget's disease of bone in England and Wales. *J Bone Miner.Res*. 17: 465-71
- Vaynberg,J, Qin,J. 2006. Weak protein-protein interactions as probed by NMR spectroscopy. *Trends in Biotechnology* 24: 22-27
- Wada,T, Nakashima,T, Hiroshi,N, Penninger,JM. 2006. RANKL-RANK signaling in osteoclastogenesis and bone disease. *Trends Mol.Med*. 12: 17-25
- Wallace,RG, Barr,RJ, Osterberg,PH, Mollan,RA. 1989. Familial expansile osteolysis. *Clin Orthop.Relat Res*. 265-77
- Wang,C, Deng,L, Hong,M, Akkaraju,GR, Inoue,J, Chen,ZJ. 2001. TAK1 is a ubiquitin-dependent kinase of MKK and IKK. *Nature* 412: 346-51
- Waters,S, Marchbank,K, Solomon,E, Whitehouse,C, Gautel,M. 2009. Interactions with LC3 and polyubiquitin chains link nbr1 to autophagic protein turnover. *FEBS Letters* 583: 1846-52
- Watts,GD, Thomasova,D, Ramdeen,SK, Fulchiero,EC, Mehta,SG et al. 2007. Novel VCP mutations in inclusion body myopathy associated with Paget disease of bone and frontotemporal dementia. *Clin.Genet*. 72: 420-26
- Wileman,T. 2007. Aggresomes and pericentriolar sites of virus assembly: cellular defense or viral design? *Annu.Rev Microbiol*. 61: 149-67

Wilson,MI, Gill,DJ, Perisic,O, Quinn,MT, Williams,RL. 2003. PB1 domain-mediated heterodimerization in NADPH oxidase and signaling complexes of atypical protein kinase C with Par6 and p62. *Mol.Cell* 12: 39-50

Wooten,MW, Seibenhener,ML, Mamidipudi,V, Diaz-Meco,MT, Barker,PA, Moscat,J. 2001. The atypical protein kinase C-interacting protein p62 is a scaffold for NF-kappaB activation by nerve growth factor. *J.Biol.Chem.* 276: 7709-12

Wooten,MW, Geetha,T, Seibenhener,ML, Babu,JR, Diaz-Meco,MT, Moscat,J. 2005. The p62 scaffold regulates nerve growth factor-induced NF-kappaB activation by influencing TRAF6 polyubiquitination. *J Biol.Chem.* 280: 35625-29

Wuyts,W, Van Wesenbeeck,L, Morales-Piga,A, Ralston,S, Hocking,L et al. 2001. Evaluation of the role of RANK and OPG genes in Paget's disease of bone. *Bone* 28: 104-07

Xu,J, Wu,HF, Ang,ES, Yip,K, Woloszyn,M et al. 2009. NF-kappaB modulators in osteolytic bone diseases. *Cytokine Growth Factor Rev.* 20: 7-17

Yip,KH, Feng,H, Pavlos,NJ, Zheng,MH, Xu,J. 2006. p62 ubiquitin binding-associated domain mediated the receptor activator of nuclear factor-kappaB ligand-induced osteoclast formation: a new insight into the pathogenesis of Paget's disease of bone. *Am.J Pathol.* 169: 503-14

Zatloukal,K, Stumptner,C, Fuchsbichler,A, Heid,H, Schnoelzer,M et al. 2002. p62 Is a common component of cytoplasmic inclusions in protein aggregation diseases. *Am.J.Pathol.* 160: 255-63

Zhang,P, Chan,J, Dragoi,AM, Gong,X, Ivanov,S et al. 2005. Activation of IKK by thymosin alpha1 requires the TRAF6 signalling pathway. *EMBO Rep.* 6: 531-37

Crockett,JC, Helfrich,M, Greenhorn,J, Scott,DI, Duthie,A, Ralston,SH, Rogers,MJ et al. 2007. Disease-associated mutations in the signal peptide of RANK alter RANK localisation and downstream activation of NF-κB. *Calcif Tissue Int.* 81:145–151 "Abstract".

E. Corral Moro, Corral Gudino,L, García Aparicio,J, Ciria Abad,S, Alonso López,N, del Pino Montes,J, González Sarmiento,R et al. 2005. Mutations of the sequestosome 1 gene associated with Paget's disease in patients from salamanca, spain. *Calcif Tissue Int.* 76: 466-482 "Abstract".

Alan R.Hibbs, Confocal microscopy for biologist, Springer, 1st edition, 2004.

Branden and Tooze, Introduction to Protein Structure, Garland Science, 2nd editdion, 1999.

Harrison's Principles of Internal Medicine by Dennis L. Kasper, McGraw-Hill Professional, 16th edition, 2004.

Robert A. Alberty, Physical Chemistry, Wiley, 2th edition, 1996.

R, Rubin, David S Strayer Rubin's Pathology: Clinicopathologic Foundations of Medicine, Lippincott Williams & Wilkins, 5th edition, 2007.

Kanis JA, Pathophysiology and treatment of Paget's disease of bone, 1st edition. London: Martin Dunitz, 1992.

Whyte MP. Hypophosphatasia. Favus MJ, ed. Primer on the Metabolic Bone Diseases and Disorders of Mineral Metabolism, 3rd edition. New York, NY: Lippincott, 288-290; 1993,

Web resources: (The websites were accessed in 25-09-09)

<http://stud.chem.uni.wroc.pl/users/lucek/JAREMKO/ubiquitin.htm>

<http://www.paget.org.uk>

Leach 2004: http://www.pathology.vcu.edu/news/22_Oct_2004.pdf

List of publications resulted from the thesis:

- **Najat,D**, Garner,T, Hagen,T, Shaw,B, Sheppard,PW et al. 2009. Characterization of a non-UBA domain missense mutation of sequestosome 1 (SQSTM1) in Paget's disease of bone. *J Bone Miner.Res.* 24: 632-42
- Layfield,R, Cavey,JR, **Najat,D**, Long,J, Sheppard,PW et al. 2006. p62 mutations, ubiquitin recognition and Paget's disease of bone. *Biochem.Soc.Trans.* 34: 735-37

Abstracts presented at meetings

- **Biochemistry society Meeting Glasgow, 23-27 July 2006**
Testing the hypothesis of a unifying disease mechanism in Paget's disease of bone with p62/SQSTM1 mutations
D. Najat, B. Shaw, A. Larder, M. Searle, A. Falchetti, F. Marini, M.L. Brandi, J.R. Cavey and R. Layfield.
- **International Symposium on Paget's Disease of bone, 12-13 July 2007**
Effects of Paget's disease of bone mutations on the ubiquitin-binding function of SQSTM1.
D Najat, L Bradley, K Brownless, S Martin, A Falchetti, F Marini, M L Brandi, B Shaw, J R Cavey, R Layfield. *Calcif Tissue Int* (2007) 81:145-151.

APPENDIX

Appendix: vector maps

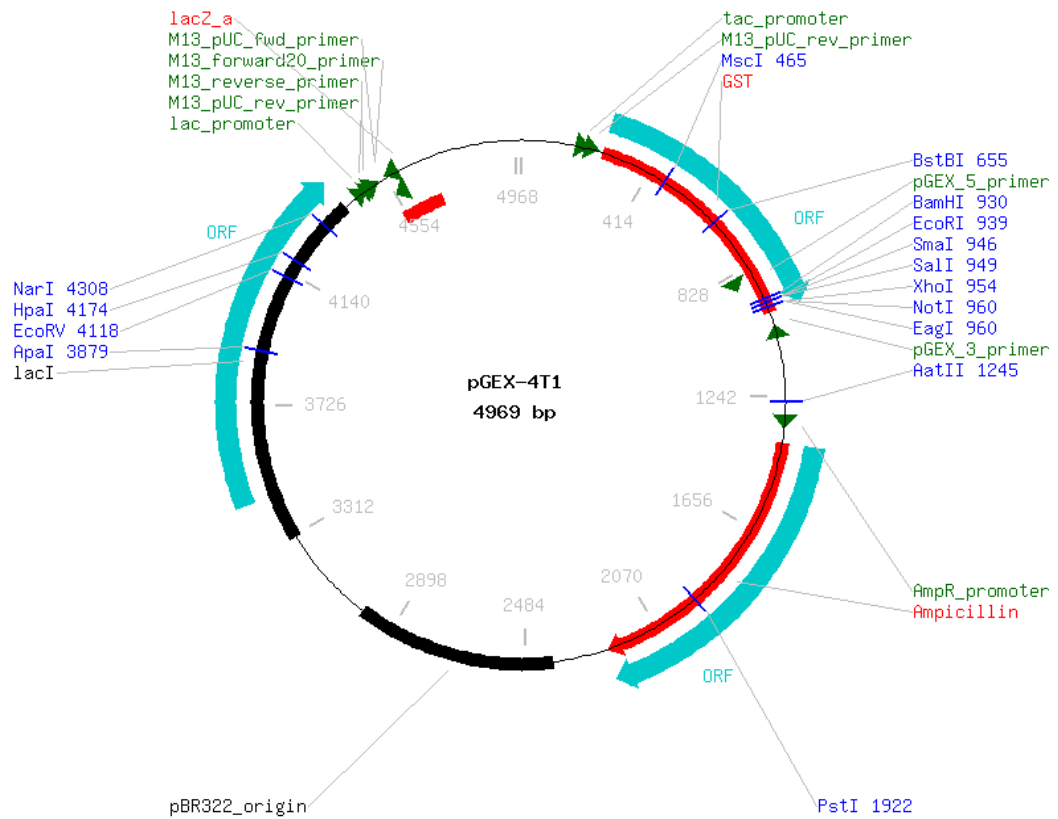


Figure A.1: Empty pGEX-4T1 (Amersham Biosciences). pGEX-4T1-WT-p62 was generated by introducing cDNA encoding the complete p62 protein (IMAGE clone 2906264) to the *EcoRI/XhoI* restriction sites of the pGEX-4T-1 plasmid.

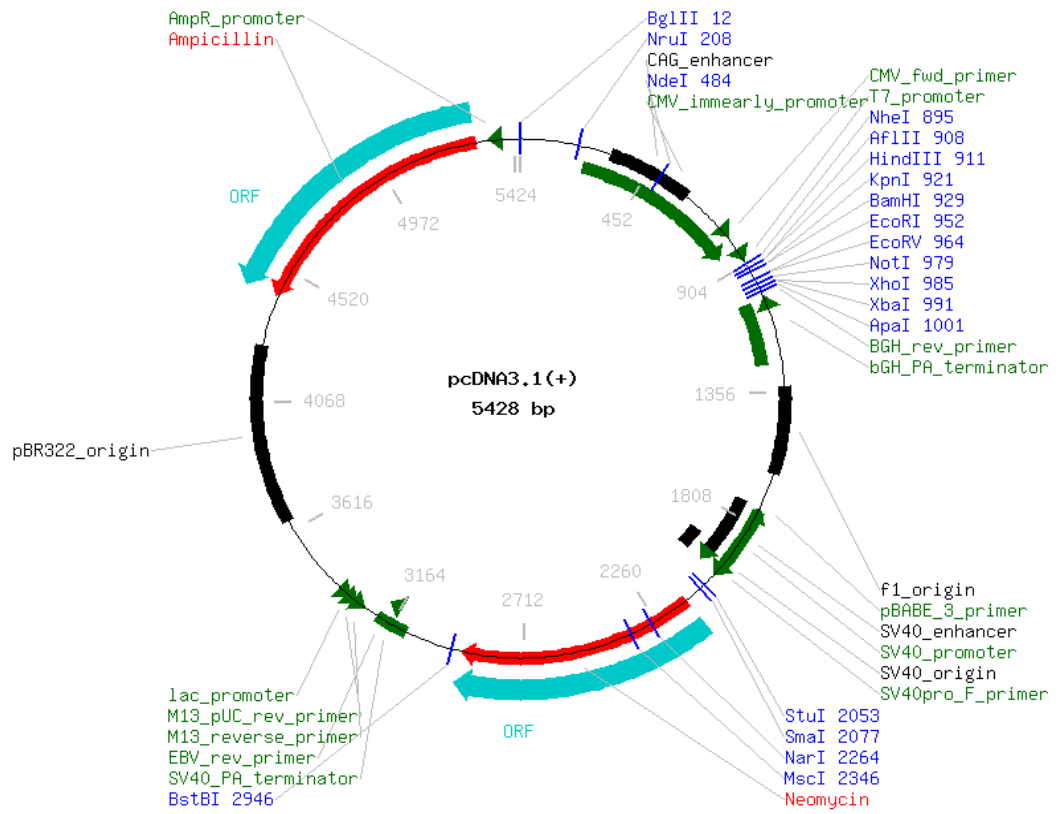


Figure A.2: Empty pDNA3.1 (+)(Invitrogen). pcDNA3.1 (+)-WT-p62 was generated by PCR amplification of the wildtype p62 cDNA, and ligation into the *NotI* restriction site of a pcDNA3.1.

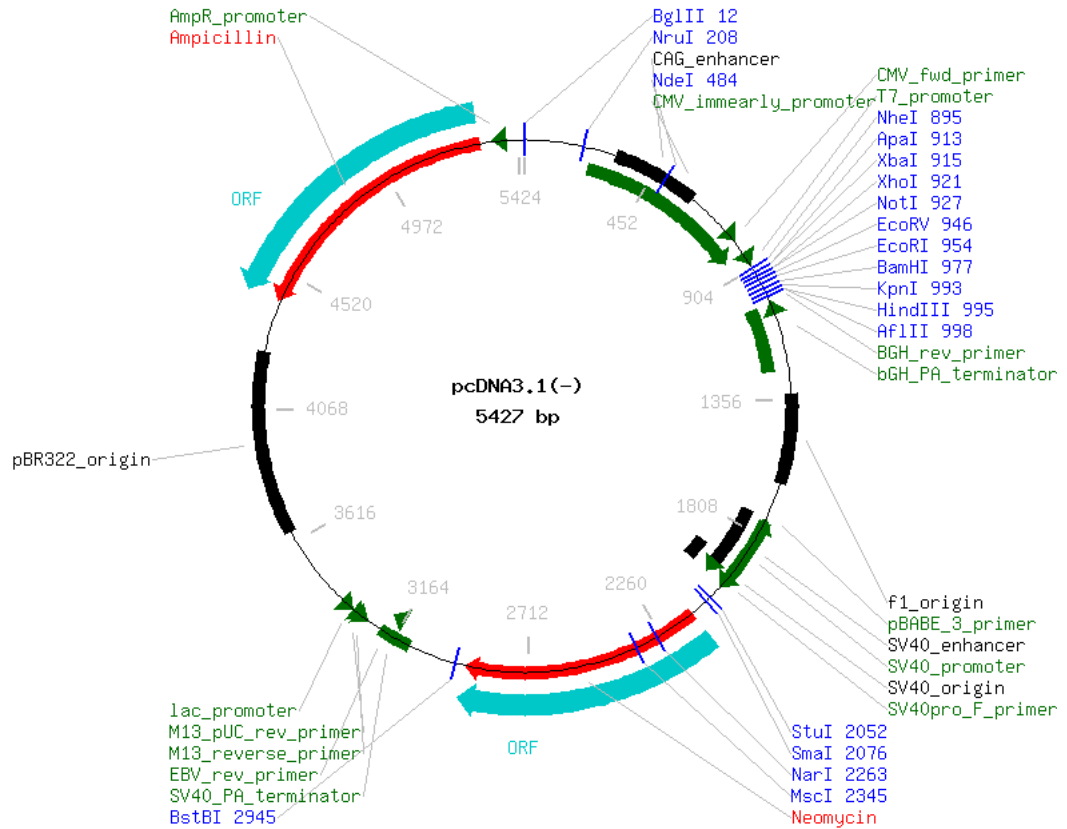


Figure A.3: Empty pcDNA3.1(-) (Invitrogen). HA-Ub-pcDNA3.1(-) was generated by PCR amplification from the human ubiquitin C IMAGE clone 4076286, including an *XhoI* site, an HA tag in the 5' PCR primer, and a *KpnI* site in the 3' primer, and ligation into the pcDNA3.1 (-) plasmid.

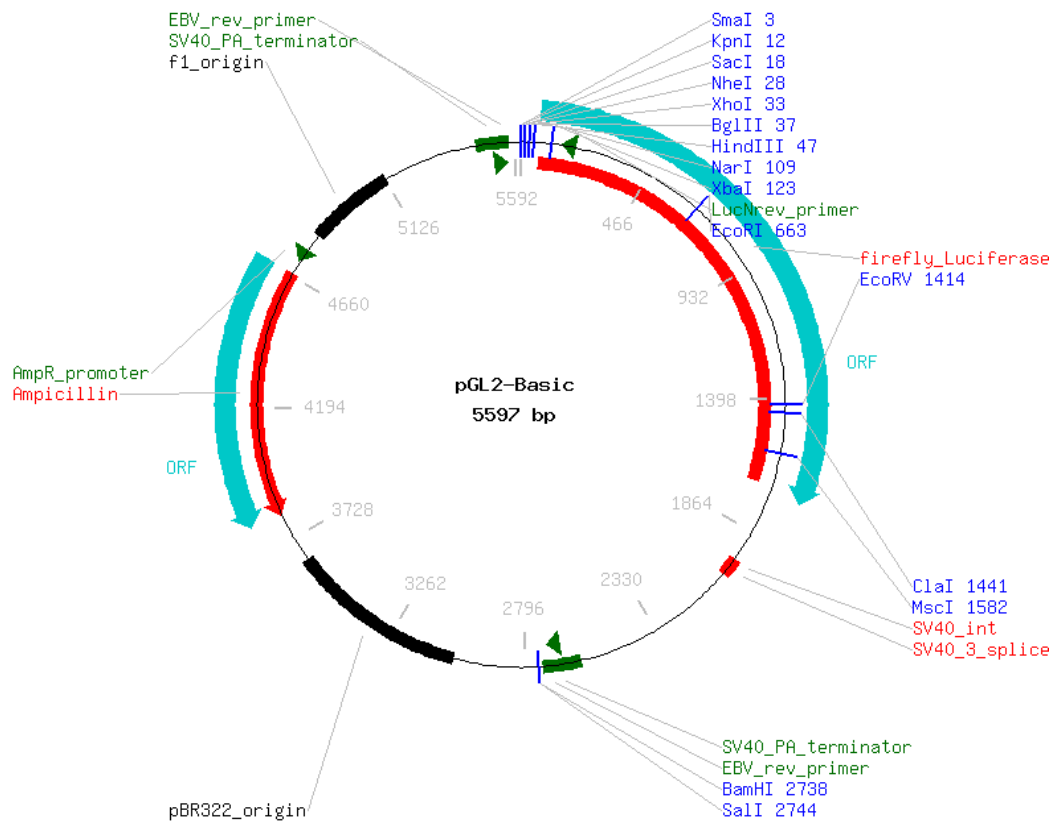


Figure A.4: Empty pGL2 (Promega). The NF- κ B reporter construct contained the -2415/-293 fragment of the human IL8 promoter cloned into the *KpnI* and *HindIII* restriction sites of the pGL2 plasmid.

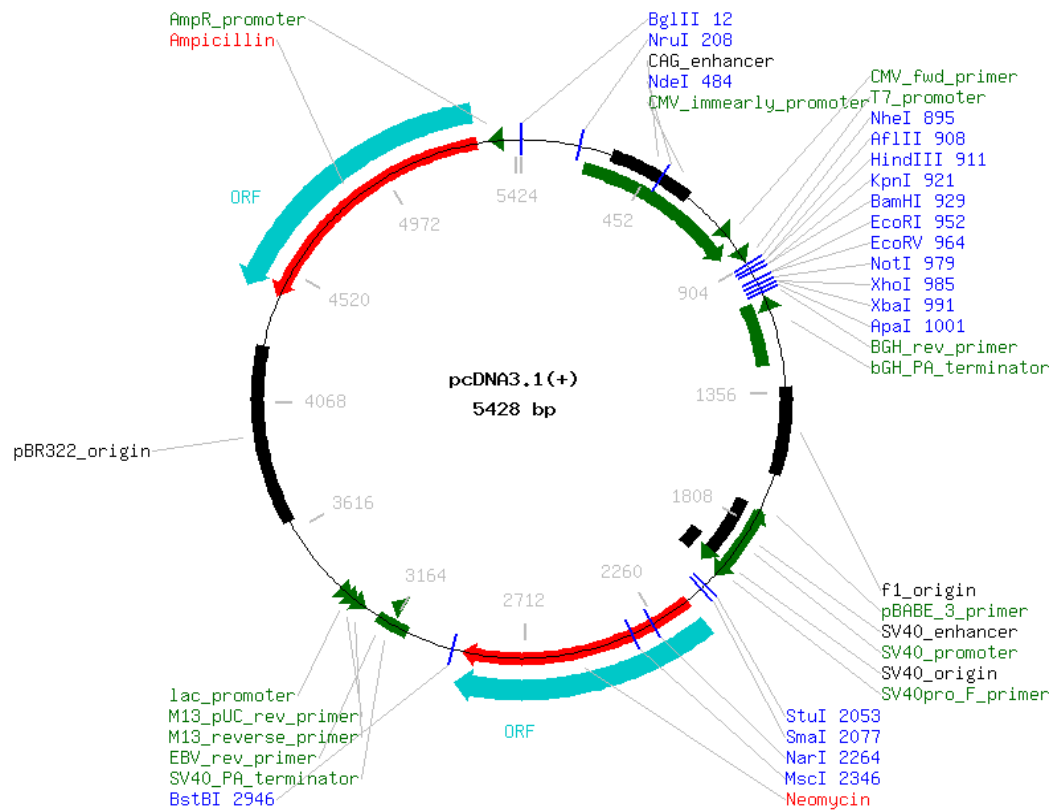


Figure A.5: Empty pcDNA3.1(+)(Invitrogen). pcDNA3.1-HA-CYLD was generated by isolating human CYLD by RT-PCR using SCSH1122/1123 primers, cut with *ClaI/SpeI* and ligated into the *ClaI/XbaI* sites in the pcDNA-HA vector.

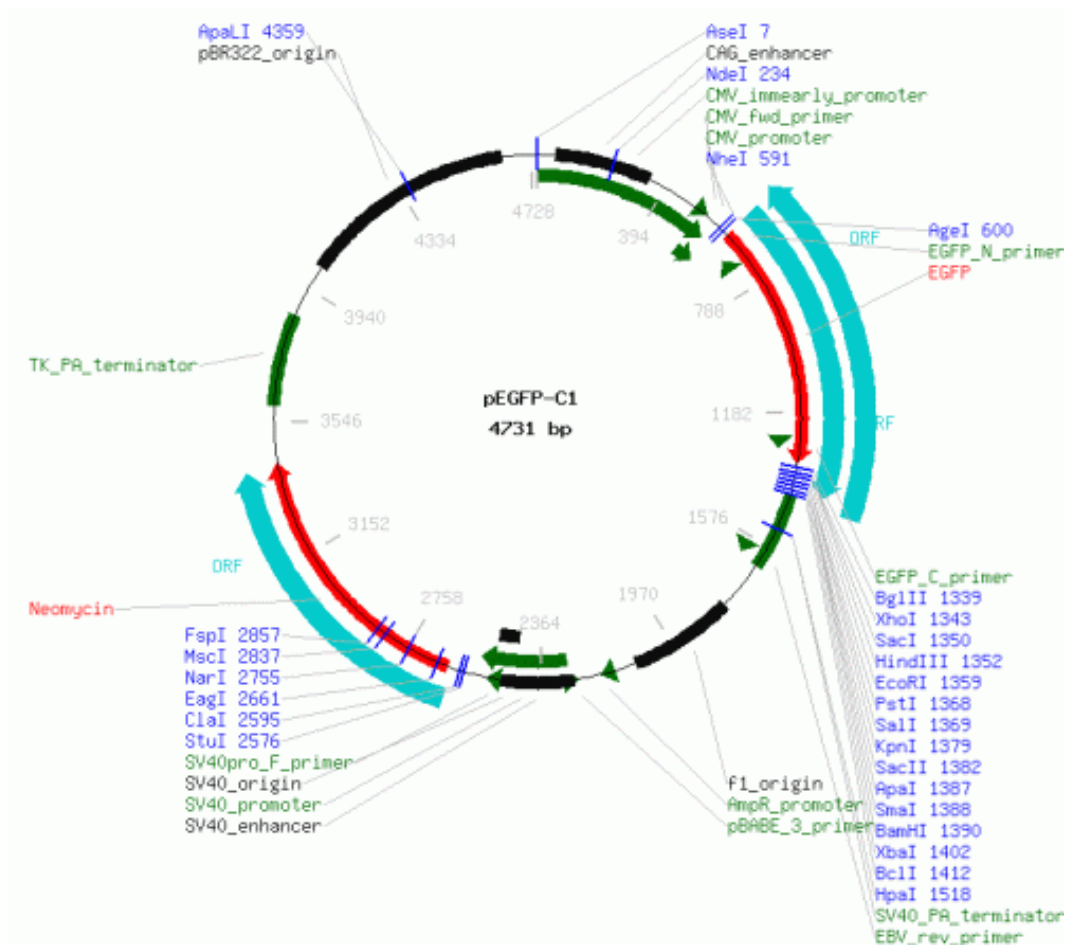


Figure A.6: Empty pEGFP-C1 (Clontech Laboratories). tdtomato-LC3 was generated through two steps. First, to obtain pGFP-LC3 (pEGFP-C1-LC3) (Figure A.6.1), LC3 cDNA was inserted into the *BgIII* and *EcoRI* sites of pEGFP-C1, then ptdTomato-LC3 was made by inserting a 400-bp *EcoRI*-*BamHI* fragment from pEGFP-C1-LC3 (Clontech Laboratories) into ptdTomato-C1 (Figure A.6.2) (Clontech Laboratories) cut with the same enzymes.

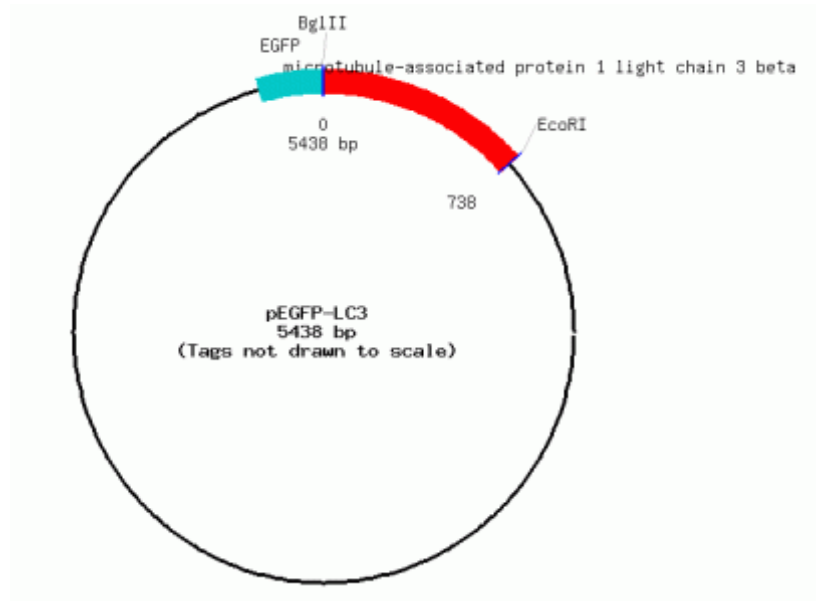


Figure A.6.1: Empty pGFP-LC3 (pEGFP-C1-LC3) (Clontech Laboratories).

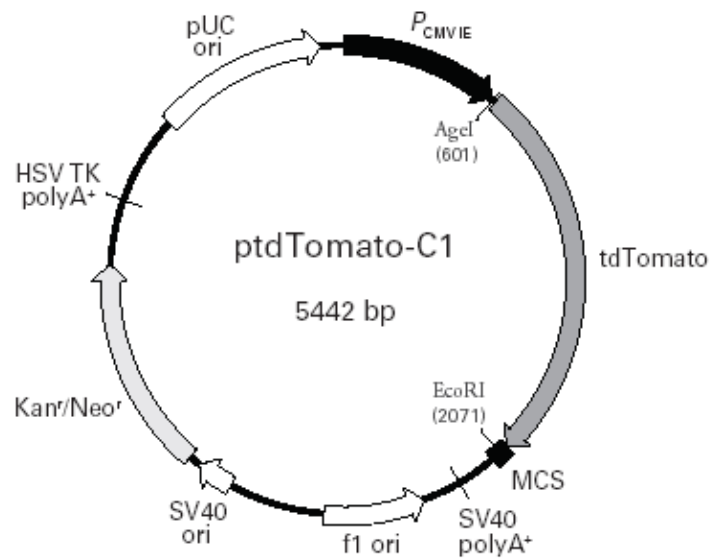


Figure A.6.2: Empty ptdTomato-C1 (Clontech Laboratories originally from Tsiens lab).